

**Pedro Filipe Castela Horta**

**Design and synthesis of novel quinolones directed  
to the *Plasmodium falciparum* bc<sub>1</sub> protein complex**



**UNIVERSIDADE DO ALGARVE**  
FACULDADE DE CIÊNCIAS E TECNOLOGIA  
DEPARTAMENTO DE QUÍMICA E FARMÁCIA

Doutoramento em Química, Química Orgânica

**2016**



**Pedro Filipe Castela Horta**

**Design and synthesis of novel quinolones directed  
to the *Plasmodium falciparum* *bc*<sub>1</sub> protein complex**

Tese elaborada para a obtenção do grau de Doutor no ramo de  
Química, especialidade de Química Orgânica

**Trabalho efectuado sob a orientação de :**

Maria de Lurdes dos Santos Cristiano (Universidade do Algarve) – orientadora

Paul Michael O'Neill (University of Liverpool, UK) – co-orientador



**UNIVERSIDADE DO ALGARVE**  
FACULDADE DE CIÊNCIAS E TECNOLOGIA  
DEPARTAMENTO DE QUÍMICA E FARMÁCIA

**Faro (2016)**



# **Design and synthesis of novel quinolones directed to the *Plasmodium falciparum* bc<sub>1</sub> protein complex**

Doutoramento em Química, especialidade de Química Orgânica

## **Declaração de Autoria do Trabalho**

Declaro ser o autor deste trabalho, que é original e inédito. Autores e trabalhos consultados estão devidamente citados no texto e constam da listagem de referências incluídas.

Pedro Filipe Castela Horta

.....

## **Direitos de cópia ou Copyright**

© Copyright: Pedro Filipe Castela Horta.

A Universidade do Algarve reserva para si o direito, em conformidade com o disposto no Código de Direito de Autor e dos Direitos Conexos, de arquivar, reproduzir e publicar a obra, independentemente do meio utilizado, bem como de a divulgar através de repositórios científicos e de admitir a sua cópia e distribuição para fins meramente educacionais ou de investigação e não comerciais, conquanto seja dado o devido crédito ao autor e editor respectivos.



*To my family,*

*To you*





---

## *Acknowledgments*

---

This thesis represents the culmination of four years of study, research, work, inspiration, patience and persistence. During this doctoral program I benefited from the help, guidance and support of supervisors, laboratory's team, friends and family.

First and foremost I would like to express my gratitude to my supervisor Professor Maria de Lurdes Cristiano for her help, support, leadership and encouragement throughout our project. Thank you for all the knowledge, experience, motivation and courage that you have passed to me over the years. Together, we worked a lot, fought against all adversity and broke the stone to find the large diamond that the science (chemistry) is. There are no words to acknowledge everything that you have done for me, for our work and for our laboratory.

To Professor Paul O'Neill I thank for the opportunity to carry out a part of this project at the University of Liverpool. Knowing a new reality, in a different country, with characteristic weather, food, habits and customs, made me grow up professionally and personally.

I express my gratitude for the support in the synthesis and docking studies provided at Liverpool, by Dr Neil Berry, Dr David Hong, Dr Paul Stocks and Dr Chandra Pidathala.

Special thanks are due to my fellow lab members and friends, Amin Ismael and Lília Cabral (PhD team). Without you, none of this would have been possible. I cannot describe how your presence was crucial for all this research. I will never forget our discussions, lunches, coffee breaks and free times. You are part of this thesis, this thesis is partly yours.

To my Italian colleagues and friends, Miriam Polletta, Paolo Sangiorgi and Alessandro Andreani. Thank you so much for your friendship, lunch break conversations (mixing three languages: Portuguese, Italian and English) and for helping me to feel like in my country.

I also owe my thankfulness to Rosário Lopes and Catarina Sebastião (Departamento de Química e Farmácia at the Universidade do Algarve) for helping us achieving the best possible scenery concerning logistic and chemical materials.

Huge thanks are due to Department of Chemistry (University of Liverpool) and REQUIMTE (Rede de Química e Tecnologia – Universidade Nova de Lisboa) for providing facilities for compounds characterization, namely mass spectrometry, NMR and elemental analysis. The NMR spectrometers at REQUIMTE are part of The National NMR Facility, supported by Fundação para a Ciência e Tecnologia (RECI/BBB-BQB/0230/2012).

To the staff of Liverpool School of Tropical Medicine and Instituto de Higiene e Medicina Tropical (Dr Fátima Nogueira, Lis Coelho and Fernanda Murtinheira), I would like to acknowledge for conducting the biological assays to my compounds. CQC (Departamento de Química, Universidade de Coimbra) and CFisUC (Departamento de Física, Universidade de Coimbra), more exactly to Professor Rui Fausto, Dr Nihal Kuş, Professor José António Paixão and Marta Henriques, for all the collaboration and availability in matrix isolation and X-ray facilities. Jointly, we achieved better science.

A gigantic acknowledgement to Fundação para a Ciência e Tecnologia (FCT – Portugal) and CCMAR for generous financial support, especially within the framework of the FCT doctoral grant SFRH/BD/81821/2011 and the project UID/Multi/04326/2013 (Centro de Ciências do Mar, CCMAR).

And last, but not least, I would like to (and must) express my love and my gratitude to my family. Thank you for believing in me and for all the love and support that you have ever transmitted. More than family, you are friends, you are my people, the reason of my life. Mother, Father, Sister, Brother, Catarina, João, Fernando, Zé, Dorys, Sammy, Ricardo... I love you. As NGC 7023 (a star cluster), you are my brightness, my strength, my inspiration. I am very lucky to have you all.

(“Finalmente, mas o mais importante, eu gostaria, e tenho de expressar o meu amor e gratidão à minha família. Obrigado por acreditarem em mim, por todo o amor e suporte que sempre me transmitem. Mais do que família, vocês são os meus amigos, vocês são as pessoas, a razão da minha vida. Mãe, Pai, Mana, Mano, Catarina, João, Fernando, Zé, Dorys, Sammy, Ricardo... Amo-vos.”)

---

## *Statement*

---

O presente trabalho foi desenvolvido sob a orientação científica da Professora Doutora Maria de Lurdes dos Santos Cristiano e coorientação do Professor Doutor Paul O'Neill. O trabalho foi elaborado em Portugal, na Universidade do Algarve (Faculdade de Ciências e Tecnologia, Departamento de Química e Farmácia), e em Inglaterra, na University of Liverpool (Faculty of Science, Department of Chemistry). Este trabalho foi financiado pela Fundação para a Ciência e Tecnologia, através de uma bolsa individual de doutoramento com a referência **SFRH/BD/81821/2011**.

This work was developed under scientific supervision of Professor Maria de Lurdes dos Santos Cristiano and co-supervision of Professor Paul O'Neill. This work was conducted in Portugal, at the Universidade do Algarve (Faculdade de Ciências e Tecnologia, Departamento de Química e Farmácia), and in England, at the University of Liverpool (Faculty of Science, Department of Chemistry). The work was financially supported by Fundação para a Ciência e Tecnologia, through the doctoral grant **SFRH/BD/81821/2011**.



---

## *Publications*

---

Part of the original work described in this thesis has been included in the following publications or communications.

### **Research articles published in peer reviewed journals:**

**1** - Nixon, G. L.; Gibbons, P. D.; Leung, S. C.; Hong, W. D.; Amewu, R.; Stocks, P. A.; Stachulski, A.; Horta, P.; Cristiano, M. L. S.; Shone, A. E.; Moss, D.; Ardrey, A.; Sharma, R.; Warman, A. J.; Bedingfield, P.; Fisher, N. E.; Aljayyousi, G.; Mead, S.; Caws, M.; Berry, N. G.; Ward, S. A.; Biagini, G. A.; O'Neill, P. M.: "Rational design, synthesis and biological evaluation of heterocyclic quinolones; targeting the respiratory chain of *Mycobacterium Tuberculosis*", submitted to **J. Med. Chem.**, 2016 (April);

**2** - Horta, P.; Kuş, N.; Henriques, M. S.; Paixão, J. A.; Coelho, L.; Nogueira, F.; O'Neill, P. M.; Fausto, R.; Cristiano, M. L.: "Quinolone-hydroxyquinoline tautomerism in quinolone 3-esters; preserving the 4-oxoquinoline structure to retain antimalarial activity", **J. Org. Chem.**, 2015 (November), 80 (24), 12244-12257 – DOI: 10.1021/acs.joc.5b02169;

**3** - Horta, P. C.; Henriques, M. S. C.; Kuş, N.; Paixão, J. A.; O'Neill, P. M.; Cristiano, M. L. S.; Fausto, R.: "Synthesis, structural and conformational analysis, and IR spectra of ethyl 4-chloro-7-iodoquinoline-3-carboxylate", **Tetrahedron**, 2015 (August), 71 (40), 7583-7592 – DOI: 10.1016/j.tet.2015.07.076;

### **Abstracts published in peer reviewed journals:**

**4** - Horta, P.; O'Neill, P. M.; Cristiano, M. L. S.: "Design and synthesis of quinolones targeting plasmodial cytochrome *bc*<sub>1</sub> and/or *Pf*NDH2", Abstract, **ChemMedChem**, Wiley Online Library, EFMC-ISMIC 2014, 183-184;

### **Oral presentations in international conferences:**

5 - Cristiano, M. L. S.; Kuş, N.; Henriques, M.; Paixão, J.; O'Neill, P.; Fausto, R.; and Horta, P.: "Tautomerism in quinolone 3-esters targeting the  $bc_1$  complex of *P. falciparum*: implications in product selectivity and activity", European Symposium on Organic Reactivity, Kiel (September 2015), Germany;

### **Oral communications in private meetings:**

6 - Horta, P.: "Docking simulation - Antimalarial quinolones binding to the  $Q_i$  site of cytochrome  $bc_1$  complex", Group Meeting (Medicinal Chemistry and Organic Reactivity Group), Faro (March 2016), Portugal;

7 - Horta, P.: "Structural studies, CLogP calculations and antimalarial activity evaluation of selected quinolones, considering quinolone-hydroxyquinoline tautomerism", Group Meeting (Medicinal Chemistry and Organic Reactivity Group), Faro (October 2015), Portugal;

8 - Horta, P.: "Synthesis and study of quinolones targeting plasmodial  $bc_1$  protein complex", Research Seminars of Doctoral Program, Faro (September 2015), Portugal;

9 - Horta, P.: "Design and synthesis of quinolones directed to the *Plasmodium falciparum*  $bc_1$  protein complex", Group Meeting (Medicinal Chemistry and Organic Reactivity Group), Faro (May 2014), Portugal;

10 - Horta, P.: "Design and synthesis of small-molecules (quinazolines) with potential activity against *Mycobacterium tuberculosis*", Group Meeting (Medicinal Chemistry and Organic Reactivity Group), Faro (March 2014), Portugal;

11 - Horta, P.: "Inhibiting  $bc_1$  protein complex: synthesis of novel quinolones", Group Meeting (Medicinal Chemistry and Organic Reactivity Group), Faro (January 2014), Portugal;

### Poster presentations in international conferences:

**12** - Henriques, M. S. C.; Kuş, N.; Horta, P.; Cristiano, M. L. S.; Paixão, J. A.; Fausto, R.: "Synthesis, structural and conformational analysis, and IR spectra of ethyl 4-chloro-7-iodoquinoline-3-carboxylate", Colloquium Spectroscopicum Internationale XXXIX, Figueira da Foz, Coimbra (September 2015), Portugal;

**13** - Horta, P.; Kuş, N.; Henriques, M. S. C.; Paixão, J. A.; O' Neill, P. M.; Berry, N.; Fausto, R.; Cristiano, M. L. S.: "Synthesis and structure of ethyl 4-chloro-7-iodoquinoline-3-carboxylate, a versatile building block for the preparation of inhibitors targeting the *bc*<sub>1</sub> complex of *Plasmodium falciparum*", 19<sup>th</sup> European Symposium on Organic Chemistry, Lisbon (July 2015), Portugal;

**14** - Horta, P.; Kuş, N.; Henriques, M. S. C.; Paixão, J. A.; O' Neill, P. M.; Fausto, R.; Cristiano, M. L. S.: "Synthesis of quinolone 3-esters targeting *bc*<sub>1</sub> complex of *P. falciparum*: Implications of tautomerism in selectivity", 7th Spanish-Portuguese-Japanese Organic Chemistry Symposium, Seville (June 2015), Spain;

**15** - Horta, P.; O' Neill, P. M.; Cristiano, M. L. S.: "Design and synthesis of quinolones targeting plasmodial cytochrome *bc*<sub>1</sub> and/or *Pf*NDH2", International Symposium on Medicinal Chemistry, Lisbon (September 2014), Portugal;

**16** - Kuş, N.; Horta, P.; Cristiano, M. L. S.; Fausto, R.: "Matrix-isolation FTIR study of the chromogenic 3-ethylcarboxy-4-hydroxy-6-methyl substituted", 1st International Caparica Conference on Chromogenic and Emissive Materials, Costa de Caparica (September 2014), Portugal.





---

## *Resumo*

---

**Nome:** Pedro Filipe Castela Horta

**Universidade:** Universidade do Algarve

**Faculdade:** Faculdade de Ciências e Tecnologia, Departamento de Química e Farmácia

**Orientadora:** Professora Maria de Lurdes dos Santos Cristiano (Universidade do Algarve)

**Co-orientador:** Professor Paul O'Neill (University of Liverpool)

**Título da tese:** “Desenho e síntese de novas quinolonas direccionadas para o complexo  $bc_1$  de *Plasmodium falciparum*”

**Data:** 2012-2016

Apesar dos intensos esforços para controlo da malária, esta doença parasítica milenar permanece como uma das doenças infecciosas conducentes a maiores taxas de mortalidade no mundo. É transmitida pela picada de um mosquito infectado do género *Anopheles* (apenas a fêmea transmite a doença) e causada por um parasita do género *Plasmodium*. *P. falciparum* é a mais prevalente de entre as cinco estirpes de *Plasmodium* que afectam o homem e é também a mais mortal, sendo responsável por cerca de 90% do número total de óbitos por malária registados anualmente. Actualmente, a Organização Mundial de Saúde estima que cerca de 40% da população mundial está em risco de contrair a infecção e que, anualmente, cerca de 600 000 pessoas morrem devido a esta doença. O rápido desenvolvimento de resistência por parte de *P. falciparum* a pelo menos um dos fármacos antimaláricos convencionais de primeira linha e a terapias baseadas em artemisinina e seus derivados, estimula enormemente a comunidade científica e médica, convocando-a para a investigação e desenvolvimento de novos fármacos antimaláricos eficazes, seguros, acessíveis e fáceis de administrar, preferencialmente direccionados para novos alvos terapêuticos.

A combinação farmacológica designada por Malarone® foi lançada pela GlaxoSmithKline para o tratamento e prevenção de malária causada por estirpes multi-

resistentes. Este medicamento resulta da combinação de dois fármacos antimaláricos: atovaquona e proguanil. A atovaquona é um competidor da ubiquinona, inibindo especificamente o complexo  $bc_1$  de *P. falciparum* através da sua ligação ao sítio  $Q_o$  deste complexo. O complexo  $bc_1$  é essencialmente responsável pela transferência de electrões e translocação de prótons ao longo da membrana mitocondrial, formando um potencial de membrana. A sua inibição leva à perda da função mitocondrial (relevante para o fornecimento de intermediários para a síntese de ATP e pirimidina), colapso do potencial electroquímico transmembranar e, finalmente, morte do parasita, validando este complexo como um potencial novo alvo terapêutico para o desenvolvimento de novos fármacos.

Além de ser o local de ação da atovaquona, o sítio  $Q_o$  é também conhecido como o local de ação da estigmatelina (composto natural) e da endoquina (um dos primeiros antimaláricos sintéticos). A endoquina serviu como modelo para o desenvolvimento de análogos (ELQ) que mantiveram o núcleo quinolínico na sua estrutura.

Além da sua potencial utilização na quimioterapia da malária, a versatilidade do quimiotipo quinolona tem atraído intensa investigação, originando principalmente 4-oxo-quinolinas com propriedades farmacológicas melhoradas e com potencial aplicação terapêutica noutras áreas, como no tratamento de cancro, hepatite B, hepatite C, SIDA, herpes, infeções fúngicas ou tuberculose. A utilização das quinolonas como agentes antibacterianos teve início em 1963 com a descoberta do ácido nalidíxico. Muitos outros derivados quinolínicos com propriedades farmacológicas foram entretanto sintetizados, destacando-se as fluoroquinolonas norfloxacin, ciprofloxacina e levofloxacina.

Nos últimos anos têm surgido publicações que reportam uma grande variedade de compostos 4-oxo-quinolínicos com grupos éster em posição 3 que demonstram atividade antimalárica em concentrações que se situam na gama nanomolar baixa, atuando por inibição do complexo  $bc_1$  plasmodial. No entanto, devido à existência de algumas fragilidades nestes compostos, de que se destacam a fraca solubilidade em meio aquoso e baixa biodisponibilidade oral, esta classe de compostos requer optimização.

O projecto de investigação descrito nesta tese foca-se no desenho, síntese e estudo estrutural de uma biblioteca de novas 3-etiléster-4-oxo-quinolinas (quinolonas), introduzindo diversidade química, essencialmente, nas posições 6 e/ou 7 da quinolona.

Estudos de docking realizados *in silico* no sítio  $Q_o$  do complexo  $bc_1$  (de levedura - *yeast*) sugerem um papel importante dos resíduos His182 e Glu272 no reconhecimento de potentes inibidores. Os mesmos estudos também indicam a importância da presença

do grupo carbonilo e do grupo N-H do núcleo quinolónico na formação de ligações por pontes de hidrogénio com os resíduos proteicos His182 e Glu272, respectivamente. Deste modo, a possibilidade de tautomerismo entre as formas 4-oxo-quinolina e 4-hidroxi-quinolina não deve ser negligenciada, no contexto do desenvolvimento desta classe para terapia antimalárica.

Esta tese está organizada em 5 capítulos. No **capítulo 1** faz-se uma apresentação sobre a malária, bem como sobre os fármacos antimaláricos existentes, seu modo de ação e alvos terapêuticos moleculares. Os fármacos que atuam por inibição do complexo *bc<sub>1</sub>* plasmoidal e o uso e síntese de quinolonas em química medicinal também são abordados nesta secção.

No **capítulo 2** são descritas as abordagens sintéticas e a otimização das condições reacionais seguidas no desenvolvimento de quinolonas selecionadas. De uma forma geral, ao longo deste projecto de doutoramento, as quinolonas foram sintetizadas utilizando a metodologia de Gould-Jacobs. De acordo com esta metodologia ocorre ciclização térmica de um composto  $\alpha,\beta$ -insaturado, derivado de uma anilina. Alternativamente, em algumas situações recorreu-se a uma outra estratégia utilizando o oxicloreto de fósforo.

No decorrer destas sínteses, mais especificamente na etapa de ciclização, por vezes obtiveram-se alguns produtos inesperados relacionados com o padrão de substituição aromática decorrente da ciclização térmica e com a possibilidade de tautomerismo ceto-enólico.

A possibilidade de tautomerismo entre as formas 4-oxo-quinolina e 4-hidroxi-quinolina suscitou questões do ponto de vista mecanístico e estrutural que são aqui especialmente relevantes, tendo em conta a sua eventual repercussão no perfil farmacodinâmico dos compostos. Assim, foi conduzida uma investigação estrutural detalhada em alguns compostos, de forma a melhor compreender a atividade e reactividade química de derivados de quinolonas, descrita no **capítulo 3**. Os resultados obtidos com base em estudos de cristalografia de raio X, espectroscopia FTIR acoplada com isolamento em matriz criogénica e cálculos teóricos são apresentados e discutidos, e indicam que, em derivados quinolónicos com um grupo éster em posição 3, a forma enólica (4-hidroxi-quinolina) é mais favorável do que a forma ceto (4-oxo-quinolina).

O tautomerismo poderá traduzir-se em alterações nas propriedades químicas e físicas dos compostos, com possíveis implicações nos perfis farmacocinéticos e farmacodinâmicos dos mesmos. Os compostos sintetizados neste projecto foram testados *in vitro* contra estirpes sensíveis e resistentes de *P. falciparum*. Os resultados destes

estudos, juntamente com estudos de avaliação da lipofilicidade/solubilidade de alguns compostos, são descritos e discutidos no **capítulo 4**.

Tendo em conta os resultados de atividade biológica obtidos para alguns compostos e o facto de alguns estudos demonstrarem que certas quinolonas conseguem ultrapassar, embora parcialmente, os fenómenos de resistência à atovaquona, neste projecto de investigação estudou-se a possibilidade de ligação de potenciais fármacos a sítios alternativos e diferentes do sítio  $Q_o$  do complexo  $bc_1$ . Assim, foram efectuados estudos de simulação por docking no sítio  $Q_i$  do complexo  $bc_1$ , estando os resultados também descritos e discutidos no **capítulo 4**.

Adicionalmente, foram sintetizadas algumas quinolonas substituídas com grupos arilo nas posições 2 e 3 que foram testadas contra estirpes de *Mycobacterium tuberculosis*, o agente responsável pelo desenvolvimento da tuberculose, cuja infeção é muitas vezes concomitante com a infeção pelo parasita da malária. A descrição e discussão deste trabalho é apresentada no **capítulo 5**.

Para finalizar, e numa secção à parte, serão apresentadas as conclusões e considerações finais sobre o trabalho desenvolvido bem como algumas perspectivas para trabalho futuro.

**Termos chave:** malária, quimioterapia antimalárica, descoberta de fármacos, quinolonas, inibidores do complexo  $bc_1$  de *P. falciparum*, tautomeria 4-oxo-quinolina/4-hidroxi-quinolina

---

## *Abstract*

---

Malaria remains one of the most deadly infectious diseases. The growing spread of resistance by *P. falciparum*, the most prevalent strain affecting mankind, against conventional antimalarial drugs, urges the search for novel chemotherapeutics directed to new targets. The approval of Malarone<sup>®</sup> (combination of atovaquone and proguanil) for treatment and prevention of multidrug resistant malaria validated the *P. falciparum* *bc*<sub>1</sub> complex as target for new antimalarials. Inhibition of *bc*<sub>1</sub> leads to loss of mitochondrial function (relevant to provide intermediates for pyrimidine and ATP synthesis), collapse of the transmembrane electrochemical potential and, ultimately, parasite death.

The versatility of the quinolone chemotype has attracted intense research, yielding mainly 4-oxo-quinolines with improved pharmacological properties, targeting a variety of applications, *e.g.*, cancer, hepatitis, HIV, tuberculosis or malaria.

Recent publications report on the high activity of some quinolone 3-esters against the plasmodial *bc*<sub>1</sub> protein complex. However, due to some liabilities (*e.g.* poor solubility and low oral bioavailability), this class requires optimization.

The research described within this thesis focus on the design, synthesis, structure and properties of a library of new 4-oxo-quinoline 3-esters substituted at positions 6 and/or 7 of the quinolone pharmacophore.

**Chapter one** presents an introduction to malaria and antimalarial drugs. Other topics in this chapter are the plasmodial *bc*<sub>1</sub> protein complex, the use of quinolones as inhibitors of this drug target and the synthetic routes to quinolones. In **chapter two**, synthetic approaches and conditions followed in the preparation of our library of quinolones, are described. For a better understanding of chemical reactivity and activity, a detailed structural investigation was undertaken on selected compounds, described in **chapter three**. Compounds synthesized in this project have been tested *in vitro* against *P. falciparum*. The results are discussed in **chapter four**, jointly with studies of lipophilicity/solubility evaluation and docking simulations. Additionally, selected quinolones were prepared and tested against *Mycobacterium tuberculosis* (**chapter five**). Conclusions and prospects for future work are presented in a final section.

**Keywords:** malaria, antimalarial chemotherapy, drug discovery, quinolone 3-esters, inhibitors of *P. falciparum*  $bc_1$  complex, 4-oxo-quinoline/4-hydroxy-quinoline tautomerism

---

# *Table of Contents*

---

Acknowledgments.....	iii
Statement .....	v
Publications.....	vii
Resumo .....	xi
Abstract.....	xv
Table of Contents.....	xvii
List of Figures .....	xxi
List of Tables .....	xxv
List of Schemes.....	xxvii
List of Charts.....	xxix
Abbreviations.....	xxxii
Scope of this thesis.....	xxxv
<b>CHAPTER ONE - INTRODUCTION.....</b>	<b>1</b>
<b>1.1. Malaria.....</b>	<b>3</b>
1.1.1. History.....	3
1.1.2. Epidemiology .....	4
1.1.3. Transmission .....	5
1.1.4. Apicomplexa, Sporozoa, <i>Plasmodium</i> .....	6
1.1.5. Parasite life cycle.....	7
1.1.6. Immune response to <i>Plasmodium</i> .....	10
1.1.7. Symptomatology.....	11
1.1.8. Diagnosis.....	14
1.1.9. Preventing and control of malaria.....	16
<b>1.2. Chemotherapy .....</b>	<b>19</b>
1.2.1. Inhibitors of haemozoin formation (quinolines) .....	21
1.2.2. Folate antagonists .....	25
1.2.3. Protein synthesis inhibitors.....	27
1.2.4. Precursors of free radicals .....	27
1.2.5. Other approaches and emerging chemotherapeutic tools against malaria .....	30
<b>1.3. Mitochondria – an essential organelle.....</b>	<b>33</b>
1.3.1. The mitochondrial electron transport chain of <i>P. falciparum</i> .....	33
1.3.2. Cytochrome <i>bc</i> <sub>1</sub> protein complex (Complex III).....	35

1.3.2.1. Protonmotive Q-cycle .....	36
1.3.3. Inhibition of the cytochrome <i>bc</i> <sub>1</sub> .....	37
1.3.4. Atovaquone .....	39
1.3.4.1. Atovaquone binding at Q <sub>o</sub> .....	40
1.3.4.2. Atovaquone and selection for resistance .....	42
1.3.5. Other antimalarial compounds targeting cytochrome <i>bc</i> <sub>1</sub> protein complex.....	43
1.3.5.1. Atovaquone analogues (1,4-naphthoquinones).....	44
1.3.5.2. 4(1H)-pyridones .....	45
1.3.5.3. Acridinediones and acridones.....	46
1.3.5.4. Quinolones .....	47
<b>1.4. Quinolones in medicinal chemistry .....</b>	<b>49</b>
1.4.1. From antibacterial to antimalarial agents .....	49
1.4.2. State of the art: endochin and endochin like quinolones (ELQ).....	51
1.4.3. Synthetic routes to the 4-oxo-quinoline core .....	56
1.4.3.1. Cyclisation of ortho-COR-substituted aromatic amines .....	57
1.4.3.2. Camps cyclisation .....	58
1.4.3.3. Niementowski quinoline synthesis .....	58
1.4.3.4. Cyclisation from a Michael-type addition product .....	59
1.4.3.5. Conrad-Limpach synthesis .....	59
1.4.3.6. Cyclisation by formation of bond <i>E</i> (multistage reactions) .....	60
<b>1.5. PhD project's presentation .....</b>	<b>61</b>

## CHAPTER TWO – RESULTS AND DISCUSSION

<b>Synthesis of quinolone 3-esters with potential activity against <i>P. falciparum</i> .....</b>	<b>63</b>
2.1. General synthetic approach .....	65
2.1.1. Reduction of nitro aromatic compounds to aniline derivatives .....	65
2.1.2. Coupling of the aniline derivative with DEEMM and Gould-Jacobs cyclisation .....	66
2.2. Exploring position 7 – modifying O-link.....	68
2.2.1. Preparation of 4-oxo-quinolines with ester or ether linkage at position 7 .....	68
2.2.2. Preparation of 4-oxo-quinolines with an heterocyclic group as substituent in position 7.....	73
2.3. Exploring position 7 – from nucleophilic aromatic substitution .....	80
2.4. Exploring positions 6 and 7 – the issue of isomeric mixture.....	88
2.5. Cyclisation by using phosphorus oxychloride .....	91
2.6. Synthesis of 4-oxo-quinoline.....	93
2.7. Summary, conclusions and future work.....	94
2.8. Experimental .....	96



## CHAPTER THREE – RESULTS AND DISCUSSION

<b>Structural investigation of selected quinolone 3-esters</b> .....	127
3.1. Structural, conformational and vibrational analysis of ethyl 4-chloro-7-iodoquinoline-3-carboxylate ( <b>56</b> ).....	129
3.1.1. Theoretical calculations .....	129
3.1.2. Matrix isolation - Infrared spectroscopy studies .....	131
3.1.3. Single crystal X-ray .....	134
3.2. Investigation of the 4-oxo/4-hydroxy-quinoline tautomerism in quinolone 3-esters.	136
3.2.1. Single crystal X-ray of <b>82b.HCl</b> .....	137
3.2.2. NMR and FTIR spectroscopy .....	138
3.2.3. Theoretical calculations – Molecular structure, potential energy and aromaticity.....	141
3.2.4. Matrix-isolation - IR spectroscopy and photostability studies .....	146
3.2.5. Evaluation of photostability; UV-induced photochemistry of matrix-isolated <b>82b</b> .....	148
3.3. Investigation of 4-oxo/4-hydroxy-quinoline tautomerism using the unsubstituted 4-oxo-quinoline ( <b>92a</b> ) as model.....	149
3.4. Summary and conclusions .....	151
3.5. Experimental .....	153

## CHAPTER FOUR – RESULTS AND DISCUSSION

<b>Docking studies, CLogP calculations and evaluation of antimalarial activity</b> .....	155
4.1. Lipophilicity/solubility evaluation – CLogP calculation .....	157
4.1.1. Evaluation of CLogP .....	158
4.2. Biological activity .....	160
4.3. Docking simulations – binding of 4-oxo-quinolines to the Q <sub>i</sub> site of cytochrome <i>bc</i> <sub>1</sub> complex.....	166
4.3.1. Software available for protein-ligand docking .....	167
4.3.2. Protein – Co-crystallized structure of bovine <i>bc</i> <sub>1</sub> .....	168
4.3.3. Binding of pyridone <b>GSK932121</b> to the Q <sub>i</sub> site of cytochrome <i>bc</i> <sub>1</sub> .....	168
4.3.4. Selection of quinolone ligands .....	169
4.3.5. Docking of selected compounds – GoldScore vs IC <sub>50</sub> correlation.....	173
4.3.6. Docking pose of selected quinolones in the Q <sub>i</sub> site .....	176
4.4. Summary, conclusions and future work.....	182
4.5. Experimental .....	184

## CHAPTER FIVE – RESULTS AND DISCUSSION

### Synthesis of selected quinolone derivatives and evaluation of activity against *M.*

<i>tuberculosis</i> .....	185
5.1. Tuberculosis and malaria co-infection.....	187
5.2. Quinolones with potential antituberculosis activity .....	188
5.2.1. Synthesis of quinolone <b>128</b> and of its prodrug <b>129</b> .....	188
5.2.2. Investigation of antituberculous activity.....	192
5.3. Summary, conclusions and future work.....	199
5.4. Experimental .....	200
<b>Conclusions</b> .....	207
<b>References</b> .....	213
<b>Appendix</b> .....	223
Appendix – List of Figures and Tables.....	225
Appendix 1 - Chemical structures .....	227
Appendix 2 – Chemical characterization of compounds synthesized in this project and described in Chapter two.....	243
Appendix 3 – Structural investigation of selected quinolone derivatives, as discussed in Chapter three .....	249

---

## List of Figures

---

<b>Figure 1.1</b> – Global status of mortality by malaria per 100 000 population in 2013 .....	5
<b>Figure 1.2</b> - <i>Plasmodium falciparum</i> merozoite in an electron micrograph and as schematic images .....	6
<b>Figure 1.3</b> - <i>Plasmodium falciparum</i> life cycle.....	7
<b>Figure 1.4</b> - Diagram of a <i>Plasmodium falciparum</i> trophozoite residing in an erythrocyte, highlighting the targets of current antimalarials and of new targets that are under investigation.....	20
<b>Figure 1.5</b> - Sketch of Cinchona tree .....	21
<b>Figure 1.6</b> – Structural representation of <b>quinine, quinidine</b> and <b>methylene blue</b> .....	22
<b>Figure 1.7</b> – Structural representation of <b>pamaquine</b> and <b>mepacrine</b> .....	22
<b>Figure 1.8</b> – Structural representation of <b>chloroquine</b> and <b>hydroxychloroquine</b> .....	23
<b>Figure 1.9</b> – Structural representation of the antimalarial drugs with historical and/or current importance.....	24
<b>Figure 1.10</b> - Folate pathway in <i>Plasmodium</i> parasites .....	25
<b>Figure 1.11</b> – Structural representation of the established folate antagonists .....	26
<b>Figure 1.12</b> – Structural representation of the antibiotics with antimalarial activity.....	27
<b>Figure 1.13</b> – Structural representation of <b>artemisinin</b> and its derivatives ( <b>artemisinins</b> ) .....	28
<b>Figure 1.14</b> – Structural representation of <b>OZ277</b> and <b>OZ439</b> (1,2,4-trioxolanes) and <b>RKA182</b> (1,2,4,5-tetraoxane) .....	29
<b>Figure 1.15</b> – Structural representation of <b>glyphosate</b> and <b>fosmidomycin</b> .....	32
<b>Figure 1.16</b> – Representative diagram of <i>Plasmodium</i> mitochondrial electron transport chain .	34
<b>Figure 1.17</b> – Representative diagram of the reactions held in complex III (Protonmotive Q-cycle) .....	36
<b>Figure 1.18</b> – Representation of structural changes from ubiquinone to ubiquinol (at Q <sub>i</sub> site) and from ubiquinol to ubiquinone (at Q <sub>o</sub> site).....	37
<b>Figure 1.19</b> – Structural representation of <b>myxothiazol, stigmatellin</b> and <b>UHDBT</b> .....	38
<b>Figure 1.20</b> – Structural representation of <b>antimycin A</b> .....	38
<b>Figure 1.21</b> – Structural representation of the active compounds of the Malarone® ( <b>atovaquone</b> and <b>proguanil</b> ).....	40
<b>Figure 1.22</b> - <i>In silico</i> docking results for atovaquone binding in the ubiquinol oxidation pocket at center P of the yeast <i>bc</i> <sub>1</sub> complex .....	41
<b>Figure 1.23</b> – Representation of the core structure of 1,4-naphthoquinone class; structures of naphthoquinones studied as antimalarials .....	44
<b>Figure 1.24</b> – Structural representation of <b>clopidol</b> and other pyridone-based compounds with antimalarial properties.....	45
<b>Figure 1.25</b> – Structural representation of the acridinedione ring system, of <b>floxacrine</b> and of <b>WR249685</b> .....	46
<b>Figure 1.26</b> – Structural representation of the acridone ring system and of antimalarially active 3-ether derivatives .....	47
<b>Figure 1.27</b> – Structural representation of the quinolone scaffold .....	47
<b>Figure 1.28</b> – Structural representation of classic examples of the quinolone group .....	49
<b>Figure 1.29</b> – Structural representation of quinolones used as antibacterial agents .....	50
<b>Figure 1.30</b> - Structural representation of <b>endochin</b> and quinolone 3-esters .....	52

<b>Figure 1.31</b> – Structural representation of <b>endochin</b> and of ELQs .....	53
<b>Figure 1.32</b> – Structural representation of <b>ELQ-300</b> (a preclinical candidate), its precursor <b>ELQ-271</b> and the analogue <b>P4Q-391</b> .....	54
<b>Figure 1.33</b> – Structural representation of <b>decoquinatate</b> and <b>RCQ</b> .....	55
<b>Figure 1.34</b> – Structural representation of <b>HDQ</b> and of some quinolones substituted at positions 2 and/or 3 .....	55
<b>Figure 1.35</b> – General structure for 4-oxo-quinoline 3-esters investigated .....	61
<b>Figure 2.1</b> - <sup>1</sup> H NMR spectra showing the chemical shifts of aromatic protons (8.6-6.7 ppm), for the isomeric mixtures of <b>33a/33b</b> , <b>79a/79b</b> , <b>80a/80b</b> and <b>81a/81b</b> in D <sub>6</sub> -DMSO .....	89
<b>Figure 3.1</b> - Optimized geometries for the lower energy conformers of <b>56</b> .....	130
<b>Figure 3.2</b> - Simulated IR spectra for the most stable conformer ( <b>sa</b> ) and for the expected conformational equilibrium; observed IR spectrum of <b>56</b> , isolated in solid argon (15 K), from the vapor at room temperature (rt). .....	132
<b>Figure 3.3</b> - IR spectra of <b>56</b> obtained along the warming/cooling cycle.....	133
<b>Figure 3.4</b> - Intermolecular hydrogen-bond interactions between molecules of <b>56</b> in the same plane.....	134
<b>Figure 3.5</b> - Crystal structure of ethyl 4-hydroxy-5-methyl quinolinium chloride 3-carboxylate ( <b>82b·HCl</b> ).....	138
<b>Figure 3.6</b> - ATR-IR spectrum of crystalline <b>82b·HCl</b> and <b>82a</b> , at room temperature.....	140
<b>Figure 3.7</b> – Structural representation of the tautomers of ethyl 4-hydroxy-5-methylquinoline-3-carboxylate ( <b>82b</b> ).....	141
<b>Figure 3.8</b> – Representation of the conformers obtained for the 4-hydroxy-quinoline form of <b>82b</b> .....	142
<b>Figure 3.9</b> – Calculated relaxed potential energy profile for interconversion between conformers I and II of <b>82b</b> .....	144
<b>Figure 3.10</b> – Representation of selected (lowest energy) conformers calculated for tautomer <b>82c</b> .....	144
<b>Figure 3.11</b> – Representation of selected (lowest energy) conformers obtained for tautomer <b>82d</b> .....	145
<b>Figure 3.12</b> – IR spectrum of the as-deposited argon matrix of <b>82b</b> and calculated spectrum for conformer <b>82bI</b> . .....	147
<b>Figure 3.13</b> – Fragment of the IR spectra showing photolysis ( $\lambda > 220$ nm; 130 min) of <b>82b</b> in argon matrix .....	148
<b>Figure 3.14</b> – Structural representation of the possible tautomers of 4-oxo-quinoline ( <b>92a</b> ) considered in the theoretical investigation.....	149
<b>Figure 3.15</b> – Structural representation of the two conformational minima, <b>92b180</b> and <b>92b0</b> , calculated from the scanning for conformational evaluation of <b>92b</b> .....	149
<b>Figure 4.1</b> – Representation of the chemical structures of 4(1H)-pyridones <b>GW844520</b> and <b>GSK932121</b> .....	167
<b>Figure 4.2</b> – Representation of protein sequence alignments of bovine ( <i>B. taurus</i> ), human ( <i>H. sapiens</i> ), <i>S. cerevisiae</i> , <i>P. falciparum</i> and <i>T. gondii</i> .....	168
<b>Figure 4.3</b> – Representation of interactions between the Q <sub>i</sub> binding site and compounds <b>GSK932121</b> and <b>GW844520</b> .....	169

<b>Figure 4.4</b> - Image of the Q <sub>i</sub> site showing the highest scoring docking pose for each of the 3-aryl substituted compounds studied.....	177
<b>Figure 4.5</b> – Image representing the Q <sub>i</sub> site interactions with the quinolone core of compound <b>110</b> .....	178
<b>Figure 4.6</b> - Image representing the Q <sub>i</sub> site interactions with the quinolone core of compound <b>102</b> .....	180
<b>Figure 5.1</b> – Structural representation of quinolone derivative ( <b>130</b> ).....	193
<b>Figure 5.2</b> – Results of the MGIT assay for quinolones <b>128</b> and <b>130</b> .....	194
<b>Figure 5.3</b> – Pharmacokinetic profiles of quinolone <b>128</b> (parent quinolone) and of its acetate prodrug <b>129</b> .....	195
<b>Figure 5.4</b> – CYP3A4 inhibition assay for quinolone <b>128</b> at 0.1 μM, 1 μM and 10 μM.....	196
<b>Figure 5.5</b> – CYP3A4 inhibition assay for quinolone <b>130</b> at 0.1 μM, 1 μM and 10 μM.....	196
<b>Figure 5.6</b> – CYP2C9 inhibition assay for quinolone <b>128</b> at 0.1 μM, 1 μM and 10 μM.....	197
<b>Figure 5.7</b> – CYP2C9 inhibition assay for quinolone <b>130</b> at 0.1 μM, 1 μM and 10 μM.....	197
<b>Figure 5.8</b> – CYP2C8 inhibition assay for quinolone <b>128</b> at 1 μM, 10 μM and 100 μM, and for atovaquone (10 μM).....	198
<b>Figure 5.9</b> – CYP2C8 inhibition assay for quinolone <b>130</b> at 1 μM, 10 μM and 100 μM, and for atovaquone (10 μM).....	198



---

## *List of Tables*

---

<b>Table 3.1</b> – Calculated relative electronic energies ( $\Delta E$ ) for minima of <b>56</b> and expected room temperature gas phase populations .....	131
<b>Table 3.2</b> - Relative energies ( $\Delta E$ ) of the relevant conformers for tautomeric forms <b>82b</b> , <b>82c</b> and <b>82d</b> .....	143
<b>Table 3.3</b> – Calculated aromaticity indexes (HOMA and Bird) for tautomers <b>82b</b> , <b>82c</b> and <b>82d</b> .....	146
<b>Table 4.1</b> - CLogP values for ethyl 4-oxo-quinoline-3-carboxylates, substituted at positions 5 or 7, and for the corresponding tautomers .....	158
<b>Table 4.2</b> – Final step yield, drug-likeness properties and <i>in vitro</i> antimalarial activity for <b>chloroquine</b> and <b>mefloquine</b> and for synthesized quinolines .....	161
<b>Table 4.3</b> – Structural representations of 2-aryl substituted quinolones selected for docking and corresponding <i>in vitro</i> activities against the <i>P. falciparum</i> strains 3D7 and C2B. ....	170
<b>Table 4.4</b> - Structural representations of 3-aryl substituted quinolones selected for docking and corresponding <i>in vitro</i> activities against the <i>P. falciparum</i> strains W2 and C2B. ....	171
<b>Table 4.5</b> – GoldScore results obtained from the docking of 2-aryl substituted quinolones to the $Q_i$ site of <i>P. falciparum</i> $bc_1$ complex. ....	174
<b>Table 4.6</b> – GoldScore results obtained from the docking of 3-aryl substituted quinolones to the $Q_i$ site of <i>P. falciparum</i> $bc_1$ complex. ....	174
<b>Table 4.7</b> – Results for docking of <b>110</b> in the $Q_i$ site, expressed as GoldScore. ....	177
<b>Table 4.8</b> – Results for docking of <b>102</b> in the $Q_i$ site, expressed as GoldScore. ....	179
<b>Table 5.1</b> - <i>In vitro</i> antimalarial activities for quinolone <b>128</b> (parent quinolone) and for its acetate prodrug <b>129</b> .....	195





---

## *List of Schemes*

---

<b>Scheme 1.1</b> – Approaches to the preparation of the 4-oxo-quinoline scaffold. ....	57
<b>Scheme 1.2</b> – Schematic representation of the synthetic approach to 2,3-unsubstituted 4-oxo-quinolines, proposed by Koshinen .....	57
<b>Scheme 1.3</b> – Schematic representation of the synthetic approach to 3-ethoxycarbonyl 4-oxo-quinolines, proposed by Igglessi-Markopoulou group .....	58
<b>Scheme 1.4</b> – Schematic representation of the Camps cyclisation methodology .....	58
<b>Scheme 1.5</b> – Schematic representation of the Niementowski methodology for quinoline synthesis.....	59
<b>Scheme 1.6</b> – Schematic representation of the synthetic approach to 3-aryl 4-oxo-quinolines, proposed by Hénichart group .....	59
<b>Scheme 1.7</b> – Schematic representation of the Conrad-Limpach strategy for quinolone synthesis.....	60
<b>Scheme 1.8</b> – Schematic representation of the synthetic approach to quinolones involving cyclisation by formation of bond <i>E</i> , including multistage reactions .....	60
<b>Scheme 2.1</b> - Schematic representation of the general synthetic approach to prepare 4-oxo-quinoline 3-esters derivatives. ....	65
<b>Scheme 2.2</b> – Schematic representation of reduction pathway for conversion of nitro arenes to the corresponding anilines, via nitroso and hydroxylamine intermediates .....	66
<b>Scheme 2.3</b> – Schematic representation of the mechanism proposed for the Gould-Jacobs synthesis of 4-oxo-quinoline 3-esters .....	67
<b>Scheme 2.4</b> – General synthetic approach followed to prepare 7-ester and 7-ether substituted 4-oxo-quinoline 3-esters .....	68
<b>Scheme 2.5</b> – Esterification of 3-nitrophenol to afford 3-nitrophenyl benzoate <b>6</b> .....	69
<b>Scheme 2.6</b> – Etherification of 3-nitrophenol to afford 3-nitrophenyl benzyl ether <b>7</b> .....	69
<b>Scheme 2.7</b> – Attempted etherification of 3-nitrophenol to afford compound <b>8</b> .....	69
<b>Scheme 2.8</b> – Schematic representation of a mechanistic proposal for the triethylamine-catalysed esterification to afford 3-nitrophenyl benzoate <b>6</b> .....	70
<b>Scheme 2.9</b> – Representation of an alternative mechanistic proposal for the TEA-catalysed esterification to afford compound 3-nitrophenyl benzoate <b>6</b> .....	70
<b>Scheme 2.10</b> – Schematic representation of the mechanism proposed for the synthesis of compound <b>7</b> .....	71
<b>Scheme 2.11</b> – Schematic representation of the mechanism of elimination proposed as one possible reason for the failure of the synthesis of compound <b>8</b> .....	71
<b>Scheme 2.12</b> – Schematic representation of the general synthetic approach followed to prepare 4-oxo-quinoline 3-esters with 7-substituents susceptible to the reduction conditions .....	73
<b>Scheme 2.13</b> – Derivatization of the hydroxyl group in <b>16</b> to afford compound <b>23</b> .....	74
<b>Scheme 2.14</b> – Derivatization of the hydroxyl group in <b>16</b> to afford compound <b>24</b> .....	74
<b>Scheme 2.15</b> – Derivatization of the hydroxyl group in <b>16</b> to afford compound <b>25</b> .....	74
<b>Scheme 2.16</b> – Derivatization of the hydroxyl group in <b>16</b> to afford compound <b>26</b> .....	74
<b>Scheme 2.17</b> – Derivatization of the hydroxyl group in <b>16</b> to afford compound <b>27</b> .....	74
<b>Scheme 2.18</b> – Schematic representation of the mechanism proposed for the <i>t</i> -ButOK-catalysed esterification to afford compound <b>23</b> .....	75

<b>Scheme 2.19</b> – Schematic representation of the mechanism proposed for the synthesis of pseudo-saccharyl chloride ( <b>21</b> ).....	76
<b>Scheme 2.20</b> – Representation of the general synthetic approach followed to afford 7-substituted 4-oxo-quinoline 3-esters, using ethyl 4-chloroquinoline as intermediate compound.....	78
<b>Scheme 2.21</b> – Attempted reduction of <b>34</b> to <b>35</b> .....	80
<b>Scheme 2.22</b> – General synthetic approach followed to prepare 4-oxo-quinoline 3-esters with halide substituents at positions 6 and/or 7.....	80
<b>Scheme 2.23</b> – General synthetic approach followed to the attempted preparation of 4-oxo-quinoline 3-esters linked to tetrazole residues at position 7 ( <b>49</b> and <b>50</b> ) from <b>43</b> .....	81
<b>Scheme 2.24</b> – General synthetic approach followed for the attempted preparation of 4-oxo-quinoline 3-esters linked to a 2-methyl tetrazole residue at position 7 ( <b>54</b> ).....	82
<b>Scheme 2.25</b> – Representation of the synthetic approach followed for methylation of aminotetrazole <b>51</b> to afford <b>52</b> and <b>53</b> .....	82
<b>Scheme 2.26</b> – Schematic representation of the mechanism proposed for the mono-methylation of <b>51</b> to afford 1- and 2-methyl-5-aminotetrazoles <b>52</b> and <b>53</b> .....	83
<b>Scheme 2.27</b> – Schematic representation of the mechanism proposed for the Buchwald-Hartwig coupling.....	84
<b>Scheme 2.28</b> – Schematic representation of the mechanism proposed for the chlorination of 4-oxo-quinolines at position 4.....	85
<b>Scheme 2.29</b> – Schematic representation of the mechanism proposed for the Suzuki-Miyaura coupling reaction.....	86
<b>Scheme 2.30</b> – Representation of the synthetic approach to 7-(4-(4-morpholinomethyl)-phenyl)-4-oxo-quinoline 3-ester ( <b>60</b> ) from 7-iodo-4-chloroquinoline 3-ester ( <b>56</b> ).....	87
<b>Scheme 2.31</b> – Summary of the synthetic approach followed and results obtained for the preparation of a library of 4-oxo-quinoline 3-esters bearing substituents at positions 6 and/or 7; in some examples, a 5-substituted structural isomer was obtained upon Gould-Jacobs cyclisation.....	88
<b>Scheme 2.32</b> – Schematic representation of the mechanism proposed for the phosphorus oxychloride mediated cyclisation to afford 4-chloroquinoline-3-esters.....	91
<b>Scheme 2.33</b> – Representation of the synthetic approach followed to the unsubstituted 4-oxo-quinoline ( <b>92a</b> ).....	93
<b>Scheme 5.1</b> – Retrosynthetic analysis of quinolone derivative <b>128</b> .....	188
<b>Scheme 5.2</b> – Preparation of synthetic block 1. Representation of the synthetic approach followed to afford ketone <b>122</b> .....	189
<b>Scheme 5.3</b> – Preparation of synthetic block 2. Representation of the synthetic approach followed to afford oxazoline <b>127</b> .....	189
<b>Scheme 5.4</b> – Representation of the synthetic approach to the preparation of quinolone <b>128</b> and of its prodrug <b>129</b> .....	189
<b>Scheme 5.5</b> – Schematic representation of the mechanism proposed for the coupling reaction, following the Ullmann methodology.....	190
<b>Scheme 5.6</b> – Schematic representation of the mechanism proposed for the synthesis of ketone <b>122</b> , from the bromide derivative <b>120</b> .....	191
<b>Scheme 5.7</b> – Schematic representation of the mechanism proposed for the synthesis of isatoic anhydride <b>125</b> and for its conversion into the oxazoline derivative <b>127</b> .....	191
<b>Scheme 5.8</b> – Schematic representation of the mechanism proposed for the synthesis of quinolone derivative <b>128</b> .....	192
<b>Scheme 5.9</b> – Representation of the synthetic approach to the preparation of quinolone <b>130</b> ..	194

---

## *List of Charts*

---

**Chart 4.1** - Correlation between the GoldScore average and  $\log(1/IC_{50})$ , for 3-aryl substituted ligands selected, considering their antimalarial activities against the 3D7 strain.....175

**Chart 4.2** - Correlation between the GoldScore average and  $\log(1/IC_{50})$ , for 2-aryl substituted ligands selected, considering the antimalarial activities against the 3D7 strain .....176



---

## *Abbreviations*

---

ACT	Artemisinin combination therapy
ADME	Absorption, distribution, metabolism and excretion
ADP	Adenosine diphosphate
API	Active pharmaceutical ingredient
Ar	Aromatic group
ATP	Adenosine triphosphate
ATR	Attenuated total reflectance
bs	Broad singlet
CD4+	T helper cells
CD8+	Cytotoxic T lymphocytes
CDK	Cyclin-dependent protein kinases
CHN	Most common form of elemental analysis
CI	Chemical ionisation
CIQC	4-Chloro-7-iodo-quinoline ( <b>56</b> )
CoQ	Ubiquinone
CoQH <sub>2</sub>	Ubiquinol or dihydroubiquinone
CTL	Cytotoxic T lymphocytes
d	Doublet
dd	Doublet of doublets
DDT	Dichloro-diphenyl-trichloroethane
DEEMM	Diethyl (ethoxymethylene)malonate
DEET	<i>N,N</i> -diethyl- <i>meta</i> -toluamide
DFT	Density functional theory
DHFR	Dihydrofolate reductase
DHPS	Dihydropteroate synthase
DMF	<i>N,N</i> -dimethylformamide
DMS	Dimethyl sulfate
DMSO	Dimethyl sulfoxide
DNA	Deoxyribose nucleic acid
dq	Doublet of quartets

dt	Doublet of triplets
DTGS	Deuterated triglycine sulfate
EI	Electron impact ionisation
ELISA	Enzyme-linked immunosorbent assay
ELQ	Endochin like quinolones
ES	Electrospray ionisation
FAD	Flavin adenine dinucleotide (oxidized form)
FADH <sub>2</sub>	Flavin adenine dinucleotide (reduced form)
FAS-I	Type I fatty acid synthase
FAS-II	Type II fatty acid synthase
FeSp	Iron-sulphur subunit (Complex II)
Fp	Flavoprotein subunit (Complex II)
FTIR	Fourier-transform infrared
G6PD	Glucose-6-phosphate dehydrogenase
GA	Genetic algorithm
GCT	Gas chromatography time of flight
GOLD	Genetic Optimization for Ligand Docking
GPDH	Glycerol 3-phosphate dehydrogenase
GSK	GlaxoSmithKline
HDQ	Hydroxy-2-dodecyl-4-(1H)-quinolone
HOMA	Harmonic oscillator measure of aromaticity
HRP-2	Histidine-rich protein 2
<i>Hs</i> LDH	<i>Homo sapiens</i> lactate dehydrogenase
HSP	Heat-shock proteins
IC <sub>50</sub>	Half maximal inhibitory concentration
IFA	Indirect immunofluorescence
IgG	Immunoglobulin G
IR	Infrared
ISP	Iron-sulphur protein (Rieske iron-sulphur protein)
LCT	Liquid chromatography time of flight
LDH	Lactate dehydrogenase
m	Multiplet
MALDI	Matrix-assisted laser desorption/ionisation
MDR	Multi drug-resistant strain

MGIT	Mycobacteria growth indicator tube assay
MQO	Malate quinone oxidoreductase
MS	Mass spectrometry
mtETC	Mitochondrial electron transport chain
NAD <sup>+</sup>	Nicotinamide adenine dinucleotide (oxidized form)
NADH	Nicotinamide adenine dinucleotide (reduced form)
NK	Natural killer cells
NMR	Nuclear magnetic resonance
P	Partition coefficient
pABA	<i>Para</i> -amino benzoic acid
PCR	Polymerase chain reaction
<i>Pf</i> CRT	<i>P. falciparum</i> chloroquine resistance transporter
<i>Pf</i> DHFR	<i>P. falciparum</i> dihydrofolate reductase
<i>Pf</i> DHODH	<i>P. falciparum</i> dihydroorotate dehydrogenase
<i>Pf</i> DHPS	<i>P. falciparum</i> dihydropteroate synthase
<i>Pf</i> EMP1	<i>P. falciparum</i> erythrocyte membrane protein
<i>Pf</i> MDR1	<i>P. falciparum</i> multidrug resistance protein 1
<i>Pf</i> MRK	<i>P. falciparum</i> MO15-related protein kinase
<i>Pf</i> NDH2	<i>P. falciparum</i> Type II NADH:ubiquinone oxidoreductase
<i>Pf</i> PK5	<i>P. falciparum</i> protein kinase 5
<i>Pf</i> SUB1	<i>P. falciparum</i> subtilisin-like serine protease 1
<i>Pf</i> SUB2	<i>P. falciparum</i> subtilisin-like serine protease 2
PFT	Protein farnesyl transferase
PLDH	<i>Plasmodium</i> lactate dehydrogenase
PLP	Piecewise linear potential
q	Quartet
QTOF	Quadrupole time of flight
RDT	Rapid diagnosis test
<i>R<sub>f</sub></i>	Retention factor
RNA	Ribonucleic acid
rt	Room temperature
s	Singlet
SAR	Structure-activity relationship
SD	Standard deviation

SDH	Succinate ubiquinone oxidoreductase or Complex II
t	Triplet
TB	Tuberculosis
TCA	Tricarboxylic acid cycle
TEA	Triethylamine
TFSA	Trifluoromethanesulfonic acid
THF	Tetrahydrofuran
TLC	Thin layer chromatography
TMEDA	Tetramethylethylenediamine
TMS	Tetramethylsilane standard
TNF	Tumor necrosis factor
UHDBT	5-n-undecyl-6-hydroxy-4,7-dioxobenzothiazole
WHO	World Health Organization
XDR	Extensive drug-resistant strain
XRD	X-ray diffraction



---

## *Scope of this thesis*

---

Millions of cases of malaria occur annually and around 600 000 deaths are estimated annually. Great efforts have been undertaken to circumvent this problem, but the growing spread of resistance by *P. falciparum* to currently used antimalarial drugs, in most of the more than 100 countries where malaria is endemic, has compromised the common goal of malaria eradication or, at least, of its control.

In this scenario, the design and development of new, effective and safe chemotherapeutic agents for fighting malaria remains a major priority.

The aim of the research described within this is the design, synthesis and study the structure and properties of a chemically diverse library of new 4-oxo-quinoline 3-esters, in view of facilitating the selection of leads with improved pharmacological profile for drug development.

This PhD thesis includes five chapters:

**Chapter one** provides an introduction about malaria (history, epidemiology, symptomatology, diagnosis), *Plasmodium* (characteristics, life cycle) and antimalarial drugs or other strategies employed in the therapy, prevention and control of malaria. The role of the plasmodial *bc<sub>1</sub>* protein complex and the effects of its inhibition are also reviewed in this section, as well as some important aspects concerning the synthesis and uses of quinolone derivatives in medicinal chemistry.

**Chapter two** presents the synthetic approaches and reaction conditions followed during the preparation of our library of selected quinolones.

**Chapter three** provides results of a detailed structural investigation of representative compounds, aimed at a better understanding of their chemical reactivity and properties, including biological activity. The possibility of tautomerism was specifically addressed.

**Chapter four** presents results of *in vitro* activity tests of the synthesized compounds, against sensitive and multidrug resistant strains of *P. falciparum*. In parallel, studies for lipophilicity/solubility evaluation and docking simulations are described and explored in this section.

**Chapter five** comprises the design and synthesis of selected 2- and 3-substituted quinolones with potential activity against *Mycobacterium tuberculosis*.



---

# ***CHAPTER ONE***

---

## **INTRODUCTION**



## **1.1.Malaria**

Malaria, a parasitic disease affecting mankind, remains one of the most deadly infectious diseases in the world. It is transmitted by the bitten of an infected mosquito (*Anopheles* female) and, in the human, it is caused by parasites belonging to the genus *Plasmodium* (from the species *P. falciparum*, *P. vivax*, *P. malariae*, *P. ovale* or *P. knowlesi*).<sup>1</sup>

Considering the growing emergence of resistance, the development of adequate solutions to tackle the disease is a priority. Among the relevant approaches to this goal is the development of new, effective and safe antiplasmodial drugs.

### **1.1.1. History**

Malaria has been for long a great social, economic and health problem, specifically in the tropical areas. It was (and is) responsible for the decline of nations, forced the migration of populations, prevented the economic development and, sometimes, caused more deaths than the wars. History of malaria and its effects is as ancient as the history of civilization.

The first evidence of malaria parasites was found in mosquitoes from the Paleogene period preserved in amber, that are approximately 30-60 million years old.<sup>2</sup> These parasites have evolved and adapted to different conditions and hosts (jumped onto humans from the great apes) and, presumably, a major impact in the mankind coincided with the start of agriculture during the Neolithic revolution (about 10 thousand years ago).<sup>3</sup>

However, the first reports about malaria were found in the *Chinese Canon of Medicine* (malaria symptoms: “periodic fevers” and “enlarged spleens”), from 2700 BC. Sumerian clay tablets, Egyptian papyri and Hindu scriptures from 2000 BC to 700 BC also refer deadly “epidemic fevers” and splenomegaly, suggestive of malaria.<sup>4,5</sup>

The recognition of this infectious disease in Greece dates from 850-400 BC, being *Hippocratic corpus* the first document that correlated this “intermittent fevers” or splenic change with marshy places.<sup>5</sup>

From the first century BC, a number of Roman writers mentioned that swamps could be the cause for this disease. Considering this idea, the term “malaria” was introduced from the Italian “aria cattiva” or “mal aria” that means “bad air”.<sup>4,5</sup>

With the improvement of knowledge about microbiology the search around malaria was intensified, but in 1879 it took a wrong turn with the isolation of a microbe

from the damp soil in malarious regions, named *Bacillus malariae* speculated as the cause of malaria, by Edwin Klebs and Corrado Tommasi-Crudeli. One year after, Charles Louis Alphonse Laveran (a student of Pasteur; awarded the Nobel Prize in 1907) identified the right malaria parasite, designating it by *Oscillaria malariae* (currently *Plasmodium malariae*). In 1884 appeared the denomination for the genus *Plasmodium*, by Marchiafava and Celli. *Plasmodium vivax* and *Plasmodium falciparum*, firstly named *Haemamoeba vivax* and *Haematozoon falciparum*, were identified in 1890 (by Grassi and Feletti) and in 1897 (by William Welch), respectively. The recognition of the last malaria parasite, *Plasmodium ovale*, occurred in 1922 by John. W. Stephens.<sup>4-6</sup>

Since the ancient Hindus, the swamp theory had been questioned and, gradually, it started to crumble. Many ancient texts mentioned the possible link between malaria and mosquitoes. However, just in 1897, Ronald Ross (Nobel Prize for Medicine in 1902) found the malaria parasite while dissecting the stomach tissue of an *Anopheles* mosquito and he proved the role of this insect as vector in the transmission of malaria parasites in humans.<sup>4,6</sup>

In 1899, Bignami and Bastianelli observed the complete cycle of *P. vivax* and Grassi joined these efforts and, all together, the same feat was accomplished with *P. falciparum*.<sup>6</sup>

The genome sequences of *Anopheles gambiae*<sup>7</sup> and *Plasmodium falciparum*<sup>8</sup> were published in 2002, and those of *P. vivax*<sup>9</sup> in 2008.

### **1.1.2. Epidemiology**

Malaria and poverty are correlated, since the main focus of this disease coincides with the tropical and sub-tropical regions, affecting some of the poorest populations in the world. Besides Sub-Saharan Africa, some countries of Asia (Saudi Arabia, India, Sri Lanka, Thailand and Indonesia), Western Pacific and Latin America suffer from prevalence of malaria. Turkey, Armenia and Azerbaijan are Asian–European boundary countries where it is still possible to find malaria. Normally is not found in North America, Europe and Australia, unless the illness was contracted abroad.<sup>1,10</sup>

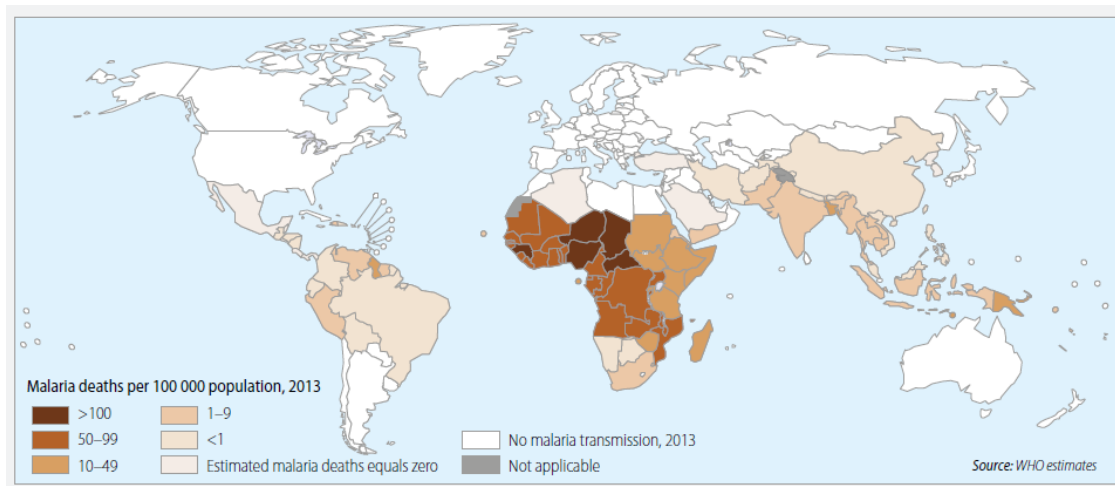


**Figure 1.1** – Global status of mortality by malaria per 100 000 population in 2013.<sup>1</sup>

Globally, World Health Organization (WHO) and current estimates place 3.2 billion people (more than 40% of the global population) at risk of malarial infection and developing disease, with 1.2 billion at high risk. In 2013 occurred 198 million cases of malaria, leading to 584 thousand of deaths, 90% of them in the African region (see Figure 1.1) and 78% in children aged under 5 years. Despite these dramatic estimates, the increase of malaria control efforts has saved more than 3 million lives, between 2000 and 2013, and the global malaria mortality rates have been reduced by 47%.

There are other infections (for example tuberculosis and human immunodeficiency virus) that demonstrate similar global distributions to malaria, exacerbating the economic problems and interfering with the fight against malaria.<sup>1</sup>

### 1.1.3. Transmission

Malaria is a vector-borne illness and can be transmitted by the bite of female *Anopheles* mosquitoes. These insects are found worldwide, in except Antarctica, and of the approximately 430 *Anopheles* species known, around 40 transmit malaria, depending on the region and the environment. In Africa, *Anopheles gambiae* is the most important as malaria vector while in Latin America is *A. darling*. Environmental changes, including deforestation, migration, new agricultural practices and climate change, may influence vector behavior.<sup>4</sup>

Others rare routes of transmission may be considered, as the exposure to infected blood or blood products, organ transplantation, use of shared infected needles and vertical transmission across the placenta (congenital infection).<sup>11</sup>

### 1.1.4. Apicomplexa, Sporozoa, *Plasmodium*

Malaria parasites are protozoa members of the Phylum Apicomplexa, characterized by the presence of a unique organelle called apical complex (see Figure 1.2).<sup>11-13</sup> *Plasmodium* (genus) parasites, responsible for malaria, do not have organelles

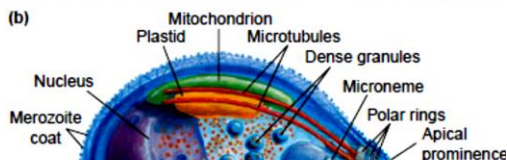
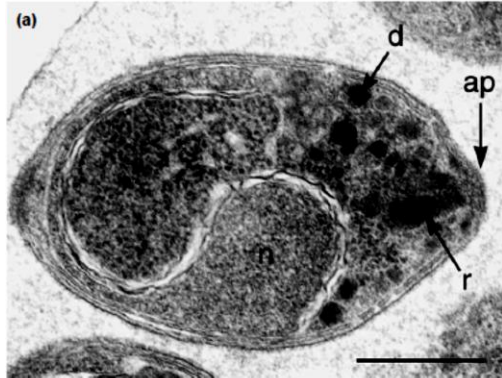


**Figure 1.2** - *Plasmodium falciparum* merozoite in an electron micrograph (a) and schematic (b) images; ap - apical prominence, d - dense granule, n - nucleus, r - rhoptry.<sup>13</sup>

of locomotion (class Sporozoa) and because of this are obligatory endoparasitic protozoa.<sup>14</sup>

Five species of *Plasmodium* are able to cause human malaria: *P. falciparum*, *P. vivax*, *P. ovale*, *P. malariae* and *P. knowlesi*. *P. falciparum* is the most lethal species (“malignant malaria”) and, at the same time, the most prevalent in the African continent and the one that develops most episodes of resistance to drugs, leading to important therapeutic problems.<sup>1</sup>

*P. vivax*, *P. ovale* and *P. malariae* cause “benign malaria” cases that rarely are

fatal. *P. vivax* is the most widely disseminated and the most prevalent parasite causing malaria in the world. However in Africa the risk of infection by *P. vivax* is quite low, essentially, because this species needs a protein to invade red blood cells that is codified by Duffy gene, and this gene is absent in many African populations. In many areas outside Africa, *P. vivax* infections are more common because *P. vivax* can survive at lower temperatures.<sup>1,14</sup>

*P. ovale* (infection least common and severe) is found in West Africa and Asia, while *P. malariae* (leads to mild or benign disease and may also affect some primates) is found in most endemic areas.<sup>11</sup>

A fifth species, *P. knowlesi*, a monkey form of malaria in macaques, is emerging as an important parasite able to cross from animals to humans (zoonosis) and infections in humans have been found in the forests of south-east Asia (especially Malaysian Borneo). Its morphology is similar to *P. malariae*, but it produces very high parasitaemias leading to severe or fatal pulmonary and hepatorenal symptoms.<sup>14</sup>



### 1.1.5. Parasite life cycle

*Plasmodium*, as most genera from the class Sporozoa, has a life cycle with both sexual (gametocyte production and sporogony) and asexual (schizogony) phases of reproduction (Figure 1.3).<sup>14</sup>

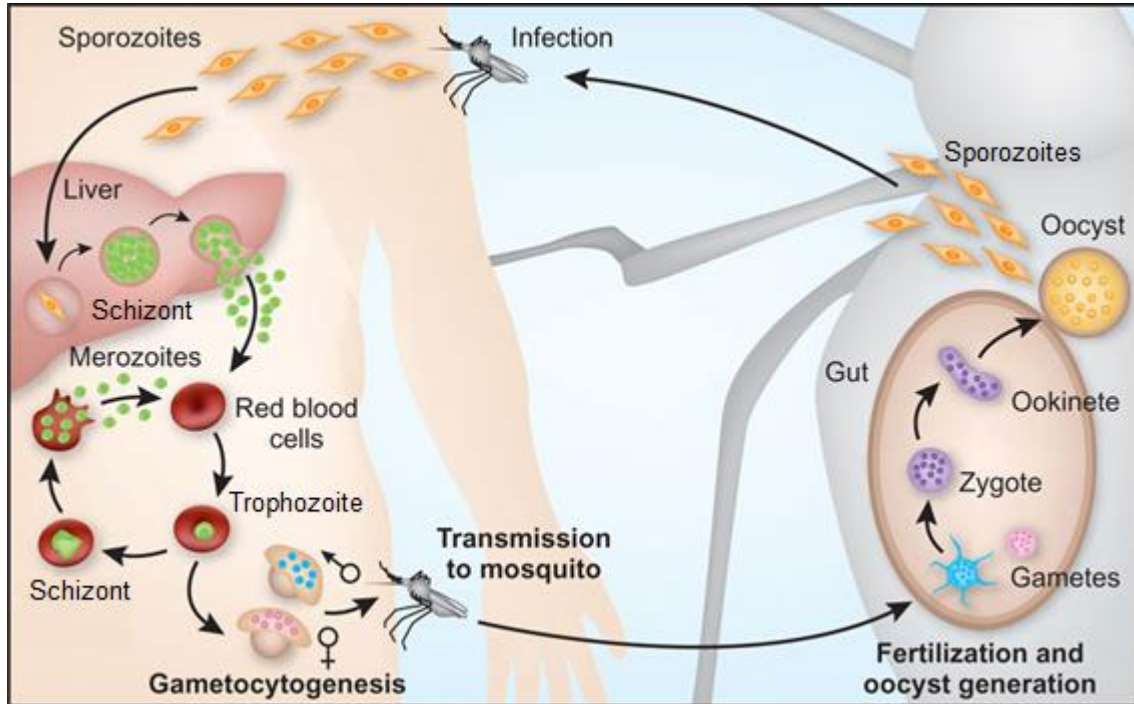


**Figure 1.3** - *Plasmodium falciparum* life cycle; female *Anopheles* mosquito-Human transmission. Adapted from Pasvol *et al.*<sup>15</sup>

Apart from the different distributions, each *Plasmodium* species may be distinguished by their morphological characteristics and their specific life cycle, responsible for the different clinical courses of the disease (incubation period, pathophysiology, morbidity and mortality associated).<sup>12</sup>

The complex life cycle of malaria parasites includes eight separate parasitic forms (or nine, if we consider hypnozoites in *P. vivax* and *P. ovale*) with different structures and metabolic processes. Then, an effective treatment, especially if acting against more than one parasite form, is difficult.<sup>6</sup>

#### A. Asexual cycle – schizogony

The asexual cycle begins with the bite of an infected female *Anopheles* mosquito (definitive host), when inoculation of infective 20-30 sporozoites and salivary anticoagulants (helping the inoculation of the parasites) from the mosquito to the human host takes place.<sup>14,15</sup>

- Primary exo-erythrocytic cycle: through the bloodstream this parasitic forms rapidly (within half an hour) reach the liver and invade hepatocytes. Each sporozoite can invade up to five hepatocytes, before setting one in which the maturation will occur. In this stage, the parasites reproduce intracellularly by asexual division and mature into schizonts (with many merozoites inside).

This asymptomatic stage is completed with the rupture of the hepatic schizonts, releasing tens of thousands of merozoites able to invade other hepatocyte and restart the cycle.

The time to complete this liver stage and the number of parasitic forms released depends on the *Plasmodium* species. *P. falciparum* species release about 40 000 parasites in 7 days, *P. vivax* release 10 000 merozoites in 6-8 days, *P. malariae* release 2000 merozoites in around 12-16 days and *P. ovale* release 15 000 merozoites in 9 days.

In *P. vivax* and *P. ovale*, a dormant parasitic form (hypnozoite) can persist in the liver, causing relapses by invading the bloodstream after weeks, months or even years later. In infections by *P. falciparum* and *P. malariae*, after the schizonts burst no parasites remain in the liver, and the liver infection ceases spontaneously in less than 4 weeks.<sup>11,14</sup>

- Erythrocytic cycle: from the rupture of the infected hepatocytes, other merozoites are released to the liver blood vessels. Once in the erythrocytic cycle, *Plasmodium* species do not reinvade the liver cells. Through the apical complex of the protozoa, the action of some proteases (e.g. *P. falciparum* subtilisin-like serine protease 1 and 2 – PfSUB1 and PfSUB2)<sup>16</sup> and by invagination with the red blood cell membrane, the merozoites invade erythrocytes.

While merozoites of *P. falciparum* are capable of infecting erythrocytes of all ages (exponential parasitaemia), those of *P. vivax* and *P. ovale* infect only reticulocytes and those of *P. malariae* just invade older red blood cells.

The binding of merozoites of *P. vivax* to erythrocyte membranes requires the presence of the Duffy blood group antigens (absent in many West African populations, thus protected from *P. vivax* infection).

In red blood cells, merozoites develop asexually forming trophozoites, which initially assume a characteristic “ring form” and then enlarge to become mature trophozoites or schizonts.<sup>11,14,15</sup>

This stage is the feeding stage of the parasite and is highly metabolically active, consuming glucose and haemoglobin from the red blood cell. With the proteolysis of haemoglobin by proteases (e.g. cysteine protease *falcipain-2* and aspartic protease

*plasmepsin* I, II and IV), in the acidic food vacuole, small globin peptides are generated and transported to the parasite cytosol where they are cleaved to obtain free amino acids for feeding parasites. At the same time, toxic products (*e.g.* haem) are released from the haemoglobin's proteolysis. To detoxify the haem group, the parasite stores it as dimers within the food vacuole and, by polymerization, a malaria pigment is obtained – haemozoin.<sup>17</sup>

By rupture, each erythrocytic schizont (in 48 hours after erythrocyte invasion in *P. falciparum*, *P. vivax* and *P. ovale*; or 72 hours for *P. malariae*) releases 16-32 merozoites that invade other red blood cells and the cell rupture is continually repeated.

Simultaneously, the contents of the parasitized erythrocyte are released into the circulation, initiating the production of cytokines that contribute to the clinical symptoms of malaria.

A parasite derived *P. falciparum* erythrocyte membrane protein (*PfEMP1*) appears on the surface of the infected erythrocyte, causing agglutination, lysis and facilitating the attachment to the vascular endothelium. Parasitic forms sequestered in the microvasculature throughout the body, including the brain, viscera and placenta, avoid the destruction by the spleen and, at the same time, the vessels become blocked, causing damage of tissues (renal, pulmonary and cerebral anoxia).<sup>11,15</sup>

### **B. Sexual cycle (gametocyte production and sporogonic cycle)**

Some merozoites (inside the erythrocytes and in a later stage of the infection) develop into microgametocytes and macrogametocytes (male and female gametocytes, respectively), by a process called gametocytogenesis. Gametocytes do not undergo further multiplication, but may survive in the peripheral blood for up to several weeks and do not cause clinical symptoms.

The sporogonic cycle begins when during a subsequent bite by a female *Anopheles*, it takes some blood and gametocytes from the infected person to its midgut. The inoculation of salivary anticoagulants secreted by the mosquito help the suction of the human blood to the *Anopheles*. Micro and macro gametes (male and female, respectively) appear from the corresponding gametocytes, a motile and elongated zygote (ookinete) is generated through fertilization, penetrates the mosquito gut wall and matures to an oocyst containing sporozoites.<sup>11,14</sup>

Oocysts grow, rupture and the sporozoites are released from the oocyst and migrate through the mosquito lymph system to the salivary glands. Inoculation of the sporozoites into a new human host perpetuates the malaria life cycle.

The vector phase takes 1 or 2 weeks to complete and can only occur where temperatures are maintained between 16°C and 33°C, and at altitudes below 2000 meters above sea level.<sup>11</sup>

#### **1.1.6. Immune response to *Plasmodium***

After a bite by an infected *Anopheles*, the main first contact between the human and the parasite is in the liver stage (within half an hour of the bite). In the hepatocyte, the merozoites are undetected by the immune system because they can modify the biology of the liver cells. These parasitic forms induce the first step of apoptosis (infected cells detach from its neighbours to move freely in the liver) but, at the same time, prevent this death process by blocking the release of Ca<sup>2+</sup> ions (calcium ions are a signal to phagocytes to engulf the dead cell). Then, the host immune system does not recognise the infected detached cell as ready to die.<sup>18</sup>

Although rarely, parasites forms in the liver may be detected by the immune system. For that, several antigens specific to the liver stage of the *Plasmodium* have been identified and by presence on the surface of infected hepatocytes lead to a recognition by cytotoxic T lymphocytes (also called as CTL, CD8+ T or Killer T; kill infected cells) and/or a stimulation of natural killer cells (NK cells) and T helper cells (CD4+) to produce interferon  $\gamma$  (triggers a cascade of reactions leading to the death of intracellular parasites).

Inside red blood cells, the merozoites modify the cell surface of the infected erythrocyte by incorporation of parasite proteins and the exposition to these antigens leads to an immune response against *Plasmodium*. After erythrocyte rupture, in the bloodstream, the parasite induces a specific immune response (by antigens exposure) and stimulates the release of factors, which might play an important function, for example in the activation of the host's monocytes, neutrophils, T cells and NK cells.

The antigen exposition based on the surface of the infected erythrocyte (*PfEMP1*), on the surface of the merozoite and on the external proteins from the apical complex leads to antibody production that could neutralise the parasitic forms and to death of the *Plasmodium* by macrophages. Then, these white blood cells can control the infection by phagocytosis (antibody-dependent and independent) and by secretion of factors that are,

directly or indirectly, toxic to the parasite (*e.g.* interleukin 1, tumor necrosis factor or TNF $\alpha$ , reactive nitrogen and oxygen radicals).

Interferon  $\gamma$  is a macrophage-activating factor involved in the innate immune response to malaria. It is mainly produced by CD8<sup>+</sup> and CD4<sup>+</sup> T lymphocytes, and by NK cells, in a specific and non-specific immune response, respectively. Some studies demonstrated that it could be associated with protection against malaria reinfection in Africa. This cytokine may also help to induce IgG (Immunoglobulin G) and assist in antibody-dependent cellular inhibitory mechanisms, as well as to induce releasing of the factors by the macrophages activation.

Haemozoin is an obstacle for the immune system because it affects the antigen processing and its accumulation inside macrophages interferes in their activation and function.

The inflammatory response, induced by the released cytokines, to remove parasites, leads to considerable tissue damage and production of inflammatory cytokines, which can cause systemic effects.<sup>19</sup>

There are also aspects in the host that inhibit or decrease the erythrocyte cycle, mainly by inherited disorders such as sickle-cell disease, thalassemia, absence of the Duffy antigen and glucose-6-phosphate dehydrogenase deficiency. In areas with higher transmission rate, babies can be protected from severe malaria by maternal antibodies.<sup>20</sup>

### **1.1.7. Symptomatology**

Infection with malaria parasites may result in a wide variety and variability of symptoms, ranging from absent, very mild symptoms, severe disease and even death, depending of the *Plasmodium* species and the host's immunity response. Then, malaria disease can be categorized as uncomplicated or severe (complicated).

The liver stage is asymptomatic (non-pathogenic) and it is related with an incubation period from 7 to 30 days, depending on the *Plasmodium* species (shorter periods for *P. falciparum* and longer for *P. malariae*). Furthermore, antimalarial drugs taken for prophylaxis by travellers can delay the appearance of malaria symptoms by weeks or months. These long delays between exposure and symptoms can result in misdiagnosis or delayed diagnosis, especially in countries where malaria is uncommon.<sup>4,12</sup>

This stage is followed by the erythrocytic cycle that produces the clinical symptoms of malaria (pathogenic stage). The regular, intermittent paroxysms of fever

caused by malaria infections were first clearly described by Hippocrates. However, other symptoms are associated to malaria disease, especially with the erythrocytic cycle and the release of parasites and other substances to the bloodstream.<sup>11</sup>

The periodic release of merozoites, haemozoin and other toxic factors from red blood cells to human bloodstream (stimulating the production of cytokines, *e.g.* TNF) is responsible for the characteristic periodicity of the fever (the temperature may rise above 41 °C) in malaria. This process occurs in cycle, after 48 (*P. falciparum*, *P. vivax* or *P. ovale*) or 72-hours (*P. malariae*). In general, this paroxysm begins suddenly and is characterized by 10-15 minutes of shaking chills, followed by high fever from 2 to 6 hours or longer. The temperature returns to normal and the patient begins sweating profusely.

More commonly, the patient presents a combination with other symptoms, such as: headaches; nausea, vomit and/or diarrhoea; body aches (back and joint aches) and myalgia; fatigue; cough; and general malaise. These symptoms can be easily confused with influenza, especially in countries where malaria is not frequent. Populations from areas where malaria is frequent, often recognize the symptoms as malaria and treat themselves before the diagnostic confirmation.<sup>4,14</sup>

Usually, other symptoms like anemia, jaundice, splenomegaly and hepatomegaly also arise, which may be exacerbated in *P. falciparum* infections.

Severe or complicated malaria is almost exclusively caused by *P. falciparum* (occasionally by *P. vivax*), it is associated with higher parasite burdens and with the presence of parasite protein PfEMP1 in infected red blood cells.<sup>12</sup>

The manifestations of severe malaria include:

- Severe anemia: the rupture of the infected red blood cells and the destruction of both infected and uninfected erythrocytes by the organism provides the progression to normochromic normocytic anemia;<sup>11</sup>
- Splenomegaly and hepatomegaly: host responses to red-cell remnants and other parasitic debris lead to more erythrocyte lysis and erythrocyte's clearance by the spleen, causing enlargement of the spleen and liver;<sup>14</sup>
- Jaundice: the increased rate of hemolysis from the rupture of the red blood cells and the breakdown of the haem of the haemoglobin, lead to an increase of unconjugated bilirubin in the blood and its consequent deposition into various tissues;

- Haemoglobinuria: uncommonly, massive intravascular hemolysis may lead to “blackwater fever” with the passage of dark urine (presence of haemoglobin in the urine);
- Thrombocytopenia: and other abnormalities in blood coagulation are common and result from the increased splenic clearance;
- Bone marrow suppression: contributes to anemia and may take weeks to recover after infection;
- Metabolic disorders: metabolic acidosis can be evidenced; hypoglycemia arises from the increased demand for glucose due to the metabolic demands of the illness and glucose consumption by the parasites; hepatic glycogen stores are rapidly depleted and gluconeogenesis fails;<sup>11</sup>
- Tissue obstruction, organ failure, coma and death: infected erythrocytes, by PfEMP1, adhere to the vascular endothelium of blood vessel resulting in a microvascular obstruction and subsequent tissue hypoperfusion (hypoxia) of vital organs. It is the main factor leading to organ failure, such as, pulmonary or renal failure. When this sequestration occurs in the brain, cerebral malaria ensues, usually associated with neuronal degeneration, meninges inflammation, coma and death.<sup>12</sup>

In pregnancy, the adherence of a large number of infected erythrocytes within the placenta in combination with maternal anemia result in placental insufficiency and intrauterine growth retardation, leading to stillbirth, low birth weight infants or perinatal mortality.<sup>11,12</sup>

On rare occasions, *P. vivax* can cause rupture of the spleen and chronic *P. malariae* infection can be associated with nephrotic syndrome (kidney shows histological hypertrophy), caused by the deposition of immune complexes.<sup>4</sup>

In *P. vivax* and *P. ovale* infections, the development of dormant parasitic forms (hypnozoites) allows the parasite to remain quiescent in the liver and then a new wave of merozoites can emerge from the hepatocytes, causing several additional attacks (relapses) after months or years.

All *Plasmodium* species can induce a recurrence of symptoms of malaria in cases where the blood stages of malaria are maintained at very low levels after inadequate drug treatment or when parasites become drug resistant. Mixed infections (*P. falciparum* with one other species) are possible and the successful treatment of one species may be followed by symptoms due to the second species.<sup>12</sup>

### **1.1.8. Diagnosis**

When any person who lives, has lived or has passed through a malaria-endemic area presents febrile illness, malaria should be assumed until proven otherwise. Specially in travellers, an inadequate malaria prophylaxis may prolong the incubation time of infection (delay in the first symptoms).<sup>11</sup>

A rapid and accurate diagnostic is crucial to the appropriate treatment and to the prevention of further spread of the infection in the world. Malaria suspicion is based on the patient's travel history, symptoms and physical findings at examination.<sup>4</sup>

In malaria suspicion, World Health Organization (WHO) recommends the diagnosis by microscopy and/or by rapid diagnosis test (RDT) to demonstrate the presence of malaria parasites, their components or metabolic products. The African region has seen the largest increase in the proportion of suspected malaria cases receiving a malaria diagnostic test (from 47% when WHO's recommendation was introduced in 2010 to 62% in 2013).<sup>1</sup>

Microscopy is the standard malaria diagnosis test. *Plasmodium* sp. can be identified by microscope examination of a drop of the patient's blood as a stained blood smear. The detection limit for malaria infection by examination is a parasitaemia of around 0.001% (approximately 50 parasites per  $\mu$ l blood).

More parasites may be visible when blood is collected between paroxysms. The most common stain is Giemsa and it gives the parasite a distinctive appearance from the blood cells. Thin films allow calculation of the percentage of red blood cells containing parasites and the differentiation of *Plasmodium* sp.. The ring form, trophozoite, schizont and gametocyte stages may all be distinguished by microscopy, depending on the parasite species. By microscopy, ring forms of *P. falciparum* can be seen in peripheral blood, while trophozoites and schizonts are rarely identified due to the sequestration of these parasitic forms in the microcirculation (estimation of total parasite burden is unreliable). Sequestration does not occur in *P. vivax*, *P. ovale* and *P. malariae*, then all parasitic forms are seen in the peripheral blood smears.<sup>11</sup>

Microscopy provides good sensitivity and specificity, but results depend on the handler and technical skills (quality of the reagents and microscope) that may be problematic especially in poor countries and/or where the disease is not endemic.<sup>12</sup>

Consequently, different nonmicroscopic malaria-diagnostic methods have been developed from 1990, including antigen detection by RDT, molecular diagnostic and serology.



The measurement of circulating specific products derived from malaria parasites by RDT (immunochromatographic test) provides results in 2-15 minutes, decreasing the amount of time to determine if a patient is or is not infected with *Plasmodium sp.*. It is recommended that RDT are followed-up by microscopy to confirm the result and, if positive, to define which strain is responsible for the infection and to quantify the proportion of erythrocytes infected. This methodology may not detect early infections with low parasitaemia.<sup>4,14</sup>

The antigens or metabolic products targeted with RDT include *P. falciparum* histidine-rich protein 2 (HRP-2), *Plasmodium* aldolase and *Plasmodium* lactate dehydrogenase (PLDH). HRP-2 is produced only by *P. falciparum*, plays a role in haemozoin formation and is released from erythrocytes at schizont rupture. It may persist for up to 4 weeks in the bloodstream after the resolution of an infection (not useful to monitor the treatment's response neither to diagnostic re-infection). *Plasmodium sp.* use large amounts of glucose (by glycolysis) and the species of this parasite produce different isomers of PLDH (involved in the conversion of pyruvate to lactate) at high levels during the asexual erythrocytic cycle. This metabolite is thus useful for treatment's monitoring because its levels may be correlated with the microscopic parasitaemia. *Plasmodium* aldolase intervenes in the glycolytic pathway of all *Plasmodium* species and its detection may be combined with the HRP-2 detection.

Molecular diagnostic tests (nucleic acid-based tests) using polymerase chain reaction (PCR) may be significantly more sensitive than microscopy for the diagnosis of malaria infection and may be used for identification of *Plasmodium* species. However these tests are not widely available, because they are expensive and require technical expertise.<sup>11</sup>

Serology detects antibodies against malaria parasites (using indirect immunofluorescence – IFA – or enzyme-linked immunosorbent assay – ELISA). However, because of the time required for development of antibodies and also their persistence in the blood, this methodology may not be useful to diagnose malaria but rather to measure past exposure.

To complement the diagnostics of infection, drug resistance tests that must be performed, including *in vitro* tests and/or molecular characterization, to assess the susceptibility of parasites to antimalarial compounds.<sup>4</sup>

### **1.1.9. Preventing and control of malaria**

Prevention of malaria involves knowledge about the transmission risk, avoiding mosquito bites and undertaking chemoprophylaxis when appropriate. The risk of acquiring malaria varies according to the geographic area (*e.g.* Asia or Africa; urban or rural area), type of accommodation (*e.g.* air conditioned may be protective; camping is a risk), duration of stay, season (transmission may decrease during the colder or drier months) and altitude (malaria transmission is rare above 2000 meters).

Besides the localization (often uncontrollable), any measures that reduce exposure to female *Anopheles* mosquito and avoid mosquito bites can reduce the risk of infection. Insecticide-impregnated bed nets (with pyrethroids), insect repellents containing DEET (*N,N*-diethyl-*meta*-toluamide), flying insect spray (such as dichloro-diphenyl-trichloroethane – DDT) and appropriate clothing (long-sleeved shirts, long pants, boots and hat) may minimize transmission.<sup>4</sup>

The use of bed nets impregnated with, for example, permethrin, represents an effective measure and it is safe for children and pregnant women. However, most of them require repeated re-impregnation to remain effective. Despite their benefits, bed nets are associated to cost and distribution barriers and there is evidence of development of resistance to pyrethroids by parasites in some areas.

The use of repellents with DEET should be localized and minimized (only to exposed skin or clothing from dusk to dawn; the malaria vector is most active in twilight periods), especially in pregnant women. Although with side-effects on pregnancy and lactation, DDT is very effective as insecticide for female *Anopheles* mosquitoes if used indoors, but its use in excess (especially in the beginning; indoors and outdoors) has facilitated the development of resistance by mosquitoes.<sup>11,12</sup>

Other biological measures have been explored to control the mosquito population, including the drainage of breeding sites, the use of predators for insects (*e.g.* snails or voracious fish to control mosquitoes larvae), insect traps using pheromones and also the use of genetically modified mosquitoes, unable to be infected with *Plasmodium*.<sup>11</sup>

Chemoprophylaxis of malaria is not truly a way to prevent infection because none of the drugs kill sporozoites (parasitic forms inoculated from the mosquitoes). However, it represents an effective strategy for prevention of the development of symptomatic malaria, since all effective chemoprophylactic agents kill erythrocytic parasites before they grow sufficiently in number to cause clinical disease. Considering the growing emergence of strains of *Plasmodium* resistant to conventional drugs and the evidence for toxicity of

some therapeutic regimens, the recommendations for the use of malaria prophylaxis have been made more rigorous and should be reserved for those at high risk. Advice on prophylaxis differs around the world, but WHO generally recommends that it should start about 1 week (or longer) before exposure or, if this is not possible, at the earliest up to 1 or 2 days before exposure to ensure that the patient tolerates the drug. Also, it should continue throughout exposure and for, at least, 4 weeks after exposure (atovaquone-proguanil, *Malarone*<sup>®</sup>, may be stopped one week after exposure). Based on the risk of infection and the susceptibility of *Plasmodium* strains, various prophylactic regimens may be adopted. Chloroquine can be taken in areas where *P. falciparum* is absent or still sensitive to this drug, and concomitantly with proguanil in areas with a risk of *P. vivax* and *P. falciparum* with information/risk of emerging resistance. *Malarone*<sup>®</sup>, mefloquine or doxycycline are recommended where there is a high risk of *P. falciparum* multidrug resistance.

Considering the side-effects of the drugs for prophylaxis and the consequences of this parasitic disease, WHO also advises pregnant women, children and elderly to avoid travelling to areas where *P. falciparum* malaria is endemic. If it cannot be deferred, the use of an effective, safe and specific chemoprophylaxis regimen must be adopted.<sup>21,22</sup>

Chemoprophylaxis of malaria is becoming increasingly problematic and the development of effective antiplasmodial vaccines remains a priority. Developed vaccines may be categorized into three main groups: against sporozoite antigens; directed to merozoite antigens; and targeting gametocyte and ookinete surface proteins.<sup>11,14</sup>

Vaccines targeting sporozoites and liver stages (pre-erythrocytic forms) could prevent infection blocking the invasion of liver cells and/or destroying infected liver cells, preventing the release of parasites into the bloodstream. When the target for the vaccines are asexual erythrocytic stages (merozoite forms), a reduction of the blood-parasite density should be achieved and, consequently, a decrease in the severity and duration of the disease. Transmission-blocking vaccines consist in inoculation of antibodies in the human organism that act against the gamete and ookinete stage of the parasite, in the mosquito. The antibodies are to be taken by the mosquito during its blood meal and will block further parasite development in the mosquito, reducing the infectivity. A fourth vaccine group, acting against the toxins produced by the parasite could be considered. The best approach to effective vaccination against malaria is the administration of a multi-antigen and multistage combination vaccine.<sup>21</sup>

Malaria vaccine trials have shown promising results against *P. falciparum* and *P. vivax*. However the technical and financial problems associated to production, distribution, storage and administration will be a great and costly barrier.

None of the prevention measures are 100% effective, so a premature diagnostic and a quick treatment are essential in the control of the disease. Then, if symptoms of malaria occur, the patient should be able to identify them and seek immediate medical attention. Some countries where the risk of malaria is high may sell counterfeit drugs that may not be effective. WHO recommends that people travelling for these countries should consider carrying with them a full treatment course of malaria medicines for emergency self-treatment.<sup>4,21</sup>

## **1.2. Chemotherapy**

During the last 2 decades, the implementation of effective control measures led to the eradication of malaria from some of the endemic countries. However, following the rapid and recent emergence of the drug-resistance by *Plasmodium* and insecticide-resistance by *Anopheles*, the disease has been reintroduced into controlled areas.<sup>14</sup>

The fight to discover more effective chemotherapeutic agents led to promising leads, but their usefulness is sometimes limited by high cost and toxicity. The existence of different species of *Plasmodium* (some chemotherapeutic agents are not effective against all of strains) and various stages of the malaria life cycle complicates matters, further worsened by the fast development of drug resistance (most notably by *P. falciparum*). Furthermore, these potential drugs should act selectively in the parasite and not in the host, so a rational approach to antimalarial chemotherapy requires comparative biochemical and physiologic information of host and parasite. Then, three major types of potential drug targets can be considered: unique essential enzymes found only in the parasite; similar enzymes found in parasite and host but just indispensable for the first one; and common biochemical functions found in parasite and host but with different pharmacologic properties.<sup>23</sup>

The treatment of malaria follows the strategies of a clinical cure and a radical cure. The first one aims to relieve the symptoms, but it does not necessarily mean that all the parasites are eradicated from the body. An elimination of all parasite forms from the body, including secondary tissue schizonts, is termed as radical cure. Patient variables, such as age, weight and sex (*e.g.* pregnancy status), may limit the available options for malaria cure.<sup>4,14</sup>

There chemotherapy agents against *Plasmodium* (available drugs as well those under development) may be classified according to the pharmacophore structure and can be, mainly, grouped in: quinolines, peroxides, tetracyclines and lincosamides, biguanides and sulphonamides, dipeptides, naphthoquinones, pyridones, acridones, acridinediones and quinolones.

In the context of the life cycle, three classes of antimalarial drugs are considered:

- blood schizonticides – directed against asexual erythrocytic forms, treating or preventing clinically symptomatic malaria (clinical cure);

- tissue schizonticides - eliminate developing or dormant liver forms, preventing invasion of the blood cells, or useful as anti-relapse drugs to produce radical cures of *P. vivax* and *P. ovale*;
- gametocidals - kill sexual stages, preventing transmission to the mosquito vector.

Hypnozoite is not eradicated by most agents and no one available drug can eliminate both hepatic and erythrocytic stages that could coexist. None of the agents kills sporozoites (parasitic form inoculated from the mosquito).<sup>21-23</sup>

*Plasmodium* offers a variety of possible drug targets associated with its various organelles (cytosol, apicoplast, mitochondria, parasite plasma membrane and lysosomal food vacuole), enabling the development of antimalarials directed to different targets and with different mechanisms of action (Figure 1.4). Therefore antimalarial agents can be divided into: haemozoin formation inhibitors; folate antagonists (nucleic acid biosynthesis inhibitors); protein synthesis inhibitors; precursors of free radicals (oxidative and alkylating activity); cysteine protease inhibitors; and mitochondrial electron transport chain inhibitors.

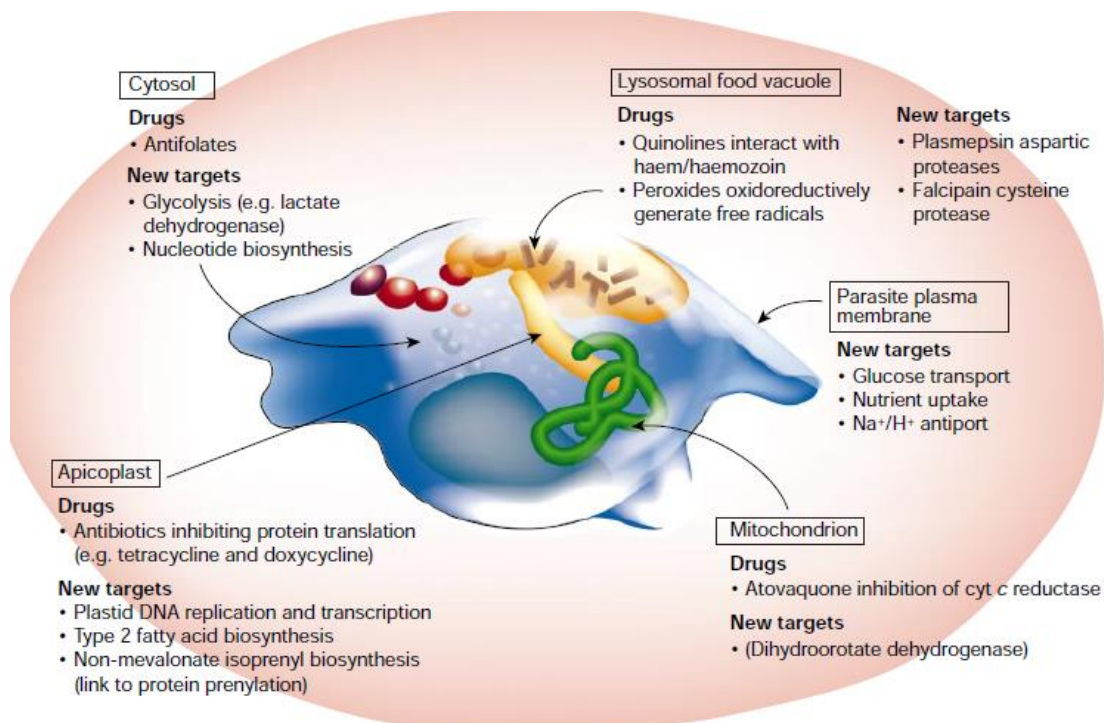


**Figure 1.4** - Diagram of a *Plasmodium falciparum* trophozoite residing in an erythrocyte, highlighting the targets of current antimalarials and of new targets that are under investigation.<sup>24</sup>

### 1.2.1. Inhibitors of haemozoin formation (quinolines)

In acidic/food vacuoles, the trophozoite parasitic forms break down haemoglobin for protein synthesis and energy. From this proteolysis haem is released and it can be toxic to the parasite via oxidative damage to membranes. Then, the parasite converts haem into dimers which subsequently polymerise to form haemozoin, a polymer non-toxic for the parasite. There are evidences that quinoline-like compounds (*Cinchona* alkaloids, their derivatives and synthetics analogues, described on this section) interfere with haem detoxification by binding to the porphyrin ring system of haem or by raising intravesicular pH, inhibiting haem polymerization. These compounds accumulate in high concentrations inside the parasite vacuole because the nitrogens atoms of the side chains of these drugs are protonated preventing them from passing back out through the vacuole membrane.<sup>14,22</sup>

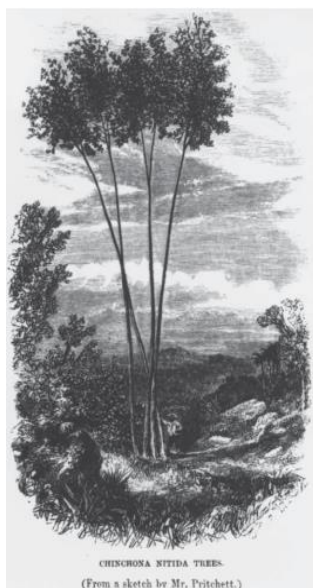


**Figure 1.5** - Sketch of Cinchona tree (by Mr. Pritchett).<sup>25</sup>

In the early 17<sup>th</sup> century *Cinchona* (Figure 1.5) was introduced into Europe, as a treatment for malaria by Jesuit priests returning from Peru. The main medicine responsible for this antimalarial activity is known as **quinine** (Figure 1.6) occurring naturally in the bark of *Cinchona* trees (**quinidine**, Figure 1.6, is also obtained from this natural source), originally found in the high hills of South America. Initially its therapeutic results were inconsistent due to the difficulty to distinguish *Cinchona* from other trees and because of the variety in quinine content in the different *Cinchona* species. Its popularity was such that in 18<sup>th</sup> century several species of *Cinchona* trees were becoming extinct.

In the early 19<sup>th</sup> century, quinine was isolated as the active drug and replaced the crude bark in the malaria treatment. Nowadays, quinine and quinidine remain as alternative antimalarials in infections resistant to others drugs (*e.g.* chloroquine), although several side effects are known and related with their use. Due to its toxicity and short  $t_{1/2}$ , quinine is not used for prophylaxis. This drug acts against asexual erythrocytic forms, is gametocidal for *P. vivax* and *P. malariae* and it has little effect on hepatic forms. Quinidine is more potent but more cardiotoxic than quinine.<sup>22,25</sup>

The synthesis of quinine failed until 1944 but, from the efforts towards its investigation, by the end of the 19<sup>th</sup> century **methylene blue** (Figure 1.6) was synthesized

and used in humans, since it stained malaria parasites and was found to be toxic to *Plasmodium spp.* (inhibits glutathione reductase disturbing the redox homeostasis of the parasite).

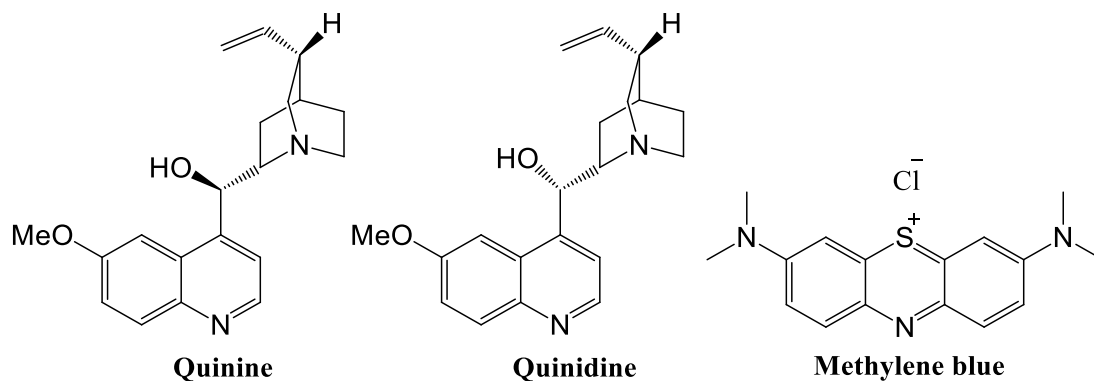


**Figure 1.6** – Structural representation of quinine, quinidine and methylene blue.

**Pamaquine** (plasmoquine), the first 8-aminoquinoline and the first compound useful to prevent relapses in *P. vivax*, was developed in 1925 and, in 1932, **mepacrine** (an acridine) showed be effective against *P. falciparum* (Figure 1.7). During World War II, these two compounds were widely used.<sup>25</sup>

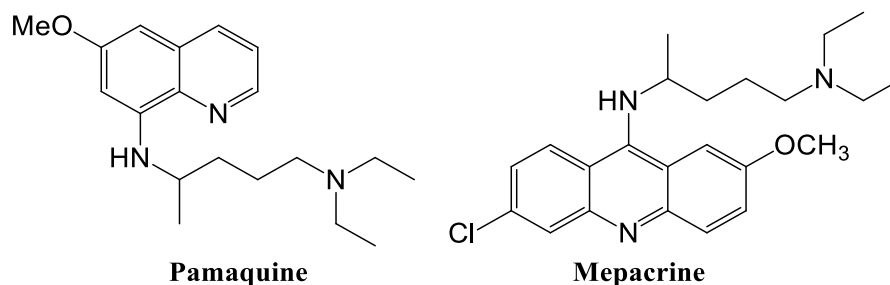


**Figure 1.7** – Structural representation of pamaquine and mepacrine.

Considering the high toxicity of quinine and the development of resistance by the parasite towards this drug, research to find a substitute for this natural compound became a priority. In 1934, the first synthesized 4-aminoquinoline (**chloroquine**; Figure 1.8) demonstrated to be highly effective against parasites, well-tolerated by human (less toxic and more effective than quinine) and relatively cheap. **Hydroxychloroquine** (Figure 1.8) is essentially equivalent to chloroquine against *P. falciparum*. In the liver, chloroquine is bio transformed in two active metabolites and, at the same time, inhibits CYP2D6, interacting with a variety of drugs.<sup>22,25</sup>



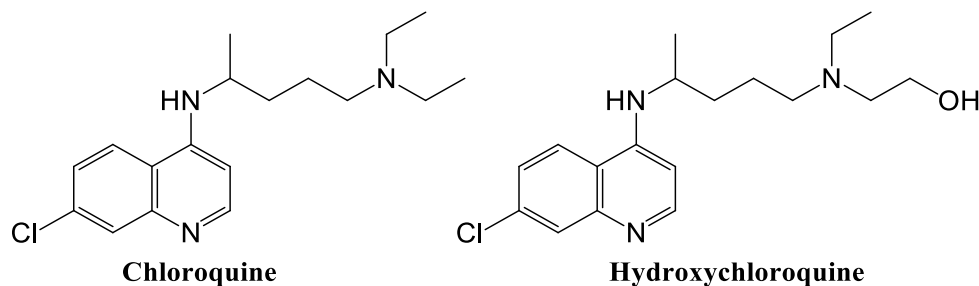


**Figure 1.8** – Structural representation of chloroquine and hydroxychloroquine.

Chloroquine provides a clinical cure but it does not treat latent hypnozoites from *P. vivax* and *P. ovale*, which may reactivate after months or years to cause recurrent clinical episodes of malaria. Its uncontrolled use led to the development of chloroquine-resistant strains of *P. falciparum* (first cases detected in 1950), which are currently common in all endemic areas around the world. Despite those limitations, chloroquine is still used for prophylaxis and treatment in some African regions where *Plasmodium* remains sensitive to this drug.<sup>11,14,22,25</sup>

Resistance of erythrocytic asexual forms of *P. falciparum* to antimalarial quinolines, especially chloroquine, has been ascribed to multiple mutations. Genetic alterations in the gene encoding a chloroquine resistance transporter (*PfCRT*), in multidrug resistance protein 1 (*PfMDR1* or *P-glycoprotein*) and/or in other transporters, may induce a reduction in drug levels within the parasite food vacuole.<sup>11,22</sup>

For example, in the presence of a mutant form for *PfCRT*, protonated chloroquine can move rapidly out of the food vacuole, reducing the concentration of this drug, while in the “wild-type” there are three basic residues that would repulse this passage, keeping the drug inside of the vacuole.<sup>26</sup>

The efforts to the discovery of new antimalarial drugs, effective against chloroquine-resistance strains, resulted in the synthesis of various antimalarial compounds, represented in Figure 1.9: **mefloquine** (4-methanolquinoline used for prophylaxis and chemotherapy of infections due to drug-resistant *P. falciparum* and *P. vivax*); **halofantrine**, **pyronaridine** and **lumefantrine** (aryl amino alcohols); **piperaquine** (a bisquinoline used extensively in China and Indochina for prophylaxis and treatment); and more effective versions of 8-aminoquinolines (*e.g.* **primaquine** and **tafenoquine**) and 4-aminoquinolines (**amodiaquine**, **isoquine**). However, some of this new drugs have limitations, mainly due to side effects and cost: hepatotoxicity by amodiaquine; seizures, depressions, hallucinations and anxiety by mefloquine; cardiotoxicity by halofantrine; and haemolytic anemia in patients with glucose-6-

phosphate dehydrogenase (G6PD) deficiency by primaquine. Furthermore, in some areas where malaria is endemic, development of resistance towards these drugs has been reported.<sup>14,22,25</sup>

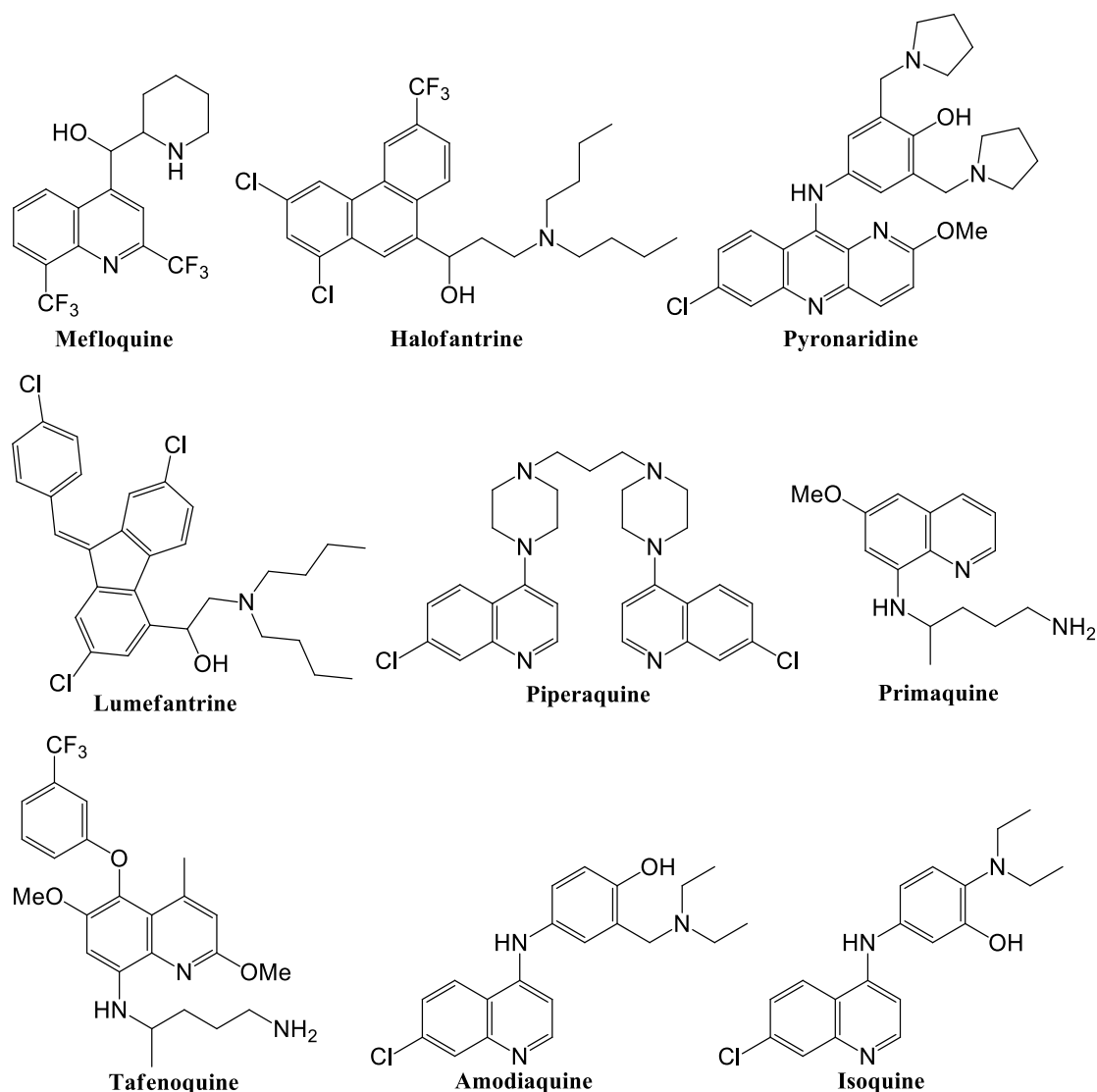


**Figure 1.9** – Structural representation of the antimalarial drugs with historical and/or current importance.

Chloroquine-resistant alleles of the CRT gene may confer increased sensitivity to mefloquine and the amplification of the *PfMDR1* gene is associated with resistance to mefloquine and quinine. Mefloquine is a highly effective blood schizonticide but has no activity against early hepatic stages and mature gametocytes of *P. falciparum* or latent tissue forms of *P. vivax*.<sup>22</sup>

8-aminoquinolines (pamaquine, tafenoquine and primaquine) are also effective as gametocidal agents and acts on tissue stages in the liver. Since primaquine produces a radical cure for *P. vivax* and *P. ovale*, it is currently used as the second course of treatment

and for the terminal prophylaxis (initiated before or immediately after leaving an endemic area). The mechanism of antimalarial action of the 8-aminoquinolines is not very well defined, but some studies demonstrate that primaquine may be converted to electrophiles that act as oxidation-reduction mediators which might be toxic.<sup>11,14,22</sup>

Lumefantrine is administered only in combination with an artemisinin derivative (artemether) for the treatment of acute uncomplicated malaria caused by *P. falciparum* (including for chloroquine-resistant strains). It has a relatively slow onset of action and, although its mode of efficacy is not fully understood, some studies suggest that this drug inhibits haemozoin formation and may also interfere with the nucleic acid and protein synthesis.<sup>21,27</sup>

### 1.2.2. Folate antagonists

Intracellular protozoa of the Phylum Apicomplexa such as *Plasmodium* must synthesize their own folates in order to survive (Figure 1.10). Folate derivatives are important cellular cofactors involved in the biosynthesis of methionine, purines and pyrimidines, which are essential for deoxyribose nucleic acid (DNA) generation and protein synthesis.<sup>23,28</sup>

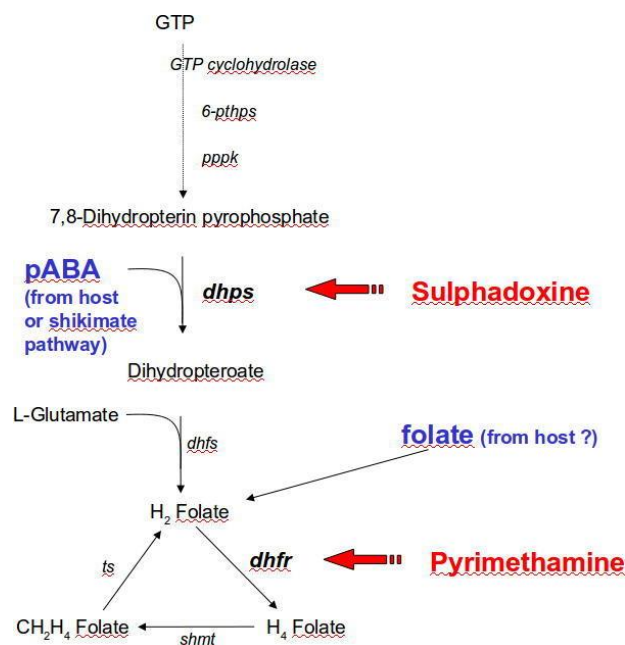


**Figure 1.10** - Folate pathway in *Plasmodium* parasites, showing the target enzyme for two commonly used folate antagonists.<sup>29</sup>

*Para*-amino benzoic acid (pABA) is a substrate for dihydropteroate synthase (DHPS), where it reacts with 7,8-dihydropterin pyrophosphate to give 7,8-dihydropteroate (Figure 1.10). Sulphonamides (*e.g.* **sulfadoxine**; Figure 1.11) act as

competitive inhibitors of pABA. Dihydrofolate reductase (DHFR), another enzyme in the folate synthetic pathway, is responsible for the conversion of dihydrofolate into tetrahydrofolate (folic acid derivatives) and may be inhibited by biguanides (including **proguanil**; Figure 1.11) or by **pyrimethamine** (Figure 1.11; purine analogue). Proguanil was developed during World War II and served as a prototype for the development of pyrimethamine in 1950.<sup>23,25,29</sup>

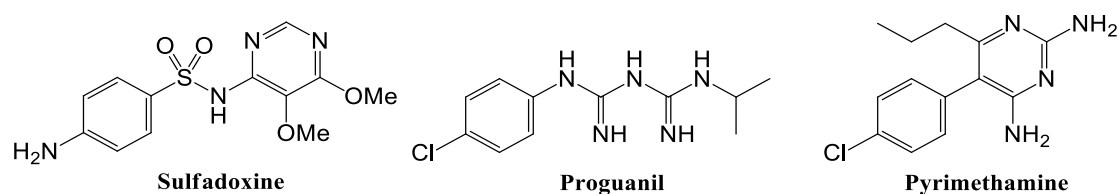


**Figure 1.11** – Structural representation of the established folate antagonists.

Reports of resistance to these drugs have increased and are largely attributable to mutations in the sequences of the genes from *P. falciparum* dihydropteroate synthase and *P. falciparum* dihydrofolate reductase (*PfDHPS* and *PfDHFR*), rendering those enzymes less susceptible to the folate inhibitors. At the same time, pyrimethamine and sulfadoxine act more slowly than quinolines as blood schizonticides and their prolonged clearance encourages the selection of resistant parasites.

Proguanil is well tolerated when administered orally but has little antimalarial activity until oxidized in the body by CYP2C isoforms to the active metabolite (cycloguanil). This active metabolite exerts activity against both the primary liver stages and the asexual red cell stages. Pyrimethamine demonstrates a higher antimalarial potency than cycloguanil but its efficacy against hepatic forms is lower. At therapeutic doses, both drugs fail to eradicate the latent tissue forms of *P. vivax* or gametocytes of any species.<sup>22,23</sup>

The use of proguanil is limited by the rapid development of resistance and by the too slow schizontocidal activity on erythrocytic forms. As such, this prodrug is administered in combination with atovaquone or chloroquine, for the treatment or prophylaxis of malaria.<sup>21</sup>

Sulfadoxine and pyrimethamine, used in a synergistic combination (to inhibit two steps in folate synthesis pathway), were introduced in the mid-1970s, and this strategy has been effective in controlling malaria, especially some strains of chloroquine-resistant *P. falciparum*. Pyrimethamine inhibits *PfDHFR* at concentrations far lower than the required to inhibit the mammalian enzymes, so it causes little toxicity. However, the drug combination sulfadoxine-pyrimethamine is not recommended for prophylaxis due to

toxicity of the sulphonamide (including Stevens-Johnson's syndrome, hepatotoxicity and myelosuppression).<sup>21–23</sup>

### 1.2.3. Protein synthesis inhibitors

Some antibiotics, such as tetracyclines and lincosamides, demonstrate antimalarial activity, possibly due to specific inhibition of the parasite's plastid-like organelle, the apicoplast, where protein synthesis occurs. From the tetracycline family, **tetracycline** and **doxycycline** (Figure 1.12) are the most frequently used antibiotics in antimalarial therapy, but their relative slowness of action as blood schizonticides makes them ineffective as single agents. However, they are successfully applied in combination regimens, with quinine or artesunate. These two tetracyclenic antibiotics have marked activity against primary tissue schizonts of chloroquine-resistant *P. falciparum*. **Clindamycin** (lincosamide; Figure 1.12) in combination with quinine is effective to treat patients with *falciparum* malaria who could not take doxycycline. Doxycycline may be used by travellers for short-term prophylaxis of malaria by multidrug-resistance species.<sup>22</sup>

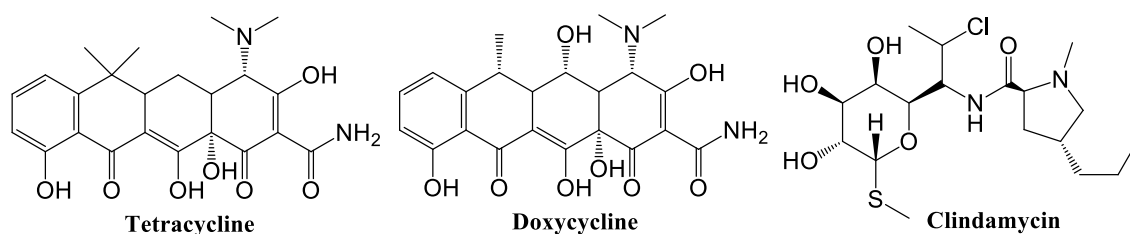


**Figure 1.12** – Structural representation of the antibiotics with antimalarial activity.

### 1.2.4. Precursors of free radicals

The Qinghao plant (*Artemisia annua*) was described for its anti-fever properties, in a Chinese medical treatise, during the second century BC. However, the isolation of its active ingredient (**artemisinin**; Figure 1.13) was reported only in 1971, and even raised some scepticism. After structure elucidation of this active pharmaceutical ingredient (API), many studies ensued to elucidate the pharmacophore, mode of action and to evaluate pharmacologic properties, for example. To improve the poor bioavailability of this sesquiterpene containing a 1,2,4-trioxolane, some semisynthetic derivatives, known as artemisinins (**artenimol** or **dihydroartemisinin**, **artemether**, **arteether**, **artesunate** and **artelinic acid**; Figure 1.13) have been developed from the manipulation of the lactone function. It was found that these derivatives are metabolized to dihydroartemisinin, which appears to be the main bioactive form of the artemisinin-based

drugs. The artemisinins are very potent and effective antimalarial drugs, widely used in our days, especially in combination regimens with other antimalarials.<sup>4</sup>

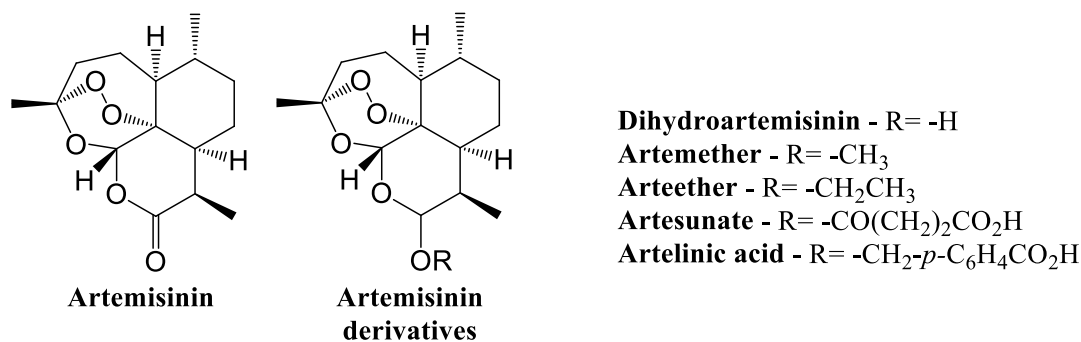


**Figure 1.13** – Structural representation of artemisinin and its derivatives (artemisinins).

Several studies have confirmed that the mechanism of action of these artemisinins involves the production of free radicals, which are toxic to the parasites. So, an endoperoxide moiety is required for antimalarial activity. It has been postulated that the endoperoxide bridge is cleaved within the parasite (through a process catalysed by the haem iron), forming oxygen-centered radicals that, after rearrangement, produce carbon-centered radicals that alkylate and damage macromolecules in the parasite. Then, these drugs are active especially for the asexual erythrocytic stages of *P. vivax* and *P. falciparum*, and could evidence some gametocytocidal activity, but do not affect liver stages.

Artemisinins are associated with a high level of parasite recrudescence when used alone and should not be used as prophylaxis due their rapid metabolism (short half-life). They are not cross-resistant with other drugs and, indeed, some studies have shown an increase in sensitivity to the artemisinins among chloroquine-resistant parasites. Then, artemisinin and its derivatives are being used widely in combination with other agents with different mode of action (artemisinin combination therapy – ACT), maximizing treatment efficiency and reducing the emergence of further drug resistance. However, despite these efforts resistance is still being seen to emerge in cases of *P. falciparum* infection.<sup>11,22</sup>

The artemisinins enjoy a deserved reputation of safety. However, reports of mild gastrointestinal disturbance, haemolytic anaemia and bradycardia have emerged. Barriers to effective ACT programs include the relatively high cost, the difficulty in obtain large quantities of artemisinin and the counterfeit drugs. Combination treatments of artesunate with mefloquine, amodiaquine or pyrimethamine-sulfadoxine, and artemether with lumefantrine are examples of ACT regimens.<sup>11,21</sup>

Besides the antimalarial activity, artemisinin and its derivatives exhibit antiparasitic activity against other protozoa, including *Leishmania major*, *Leishmania infantum*<sup>30</sup> and *Toxoplasma gondii*.<sup>22</sup>

In addition to the artemisinin-derivatives described above, numerous semisynthetic derivatives have been studied for their antiparasitic properties, such as fluorinated dihydroartemisinin derivatives, fluoroaryl artemisinins, hybridized artemisinin derivatives and dimeric artemisinins.<sup>31</sup>

The short supply of natural artemisinin and its difficult and costly total synthesis still make it unaffordable to most. So, the use of a microbial source (like engineered yeast) to obtain artemisinin or derivative has been investigated.<sup>32</sup>

Another approach is based in the synthesis of fully synthetic endoperoxides (especially 1,2,4-trioxolanes and 1,2,4,5-tetraoxanes)<sup>33</sup> without a artemisinin core. Among these, trioxolanes **OZ277** (or **arterolane**) and **OZ439** and tetraoxane **RKA182** (Figure 1.14) attained clinical trials. **OZ277** shows potent antimalarial activity and, besides its clinical trials disappointing results (unstable in the plasma of malaria patients), the investigation of this drug in combination regimens continues in development. **OZ439** is now under a clinical development program to investigate its efficacy when administered alone or when co-administered (*e.g.* with piperazine phosphate) to adults and children with uncomplicated *P. falciparum* malaria.<sup>34–37</sup>

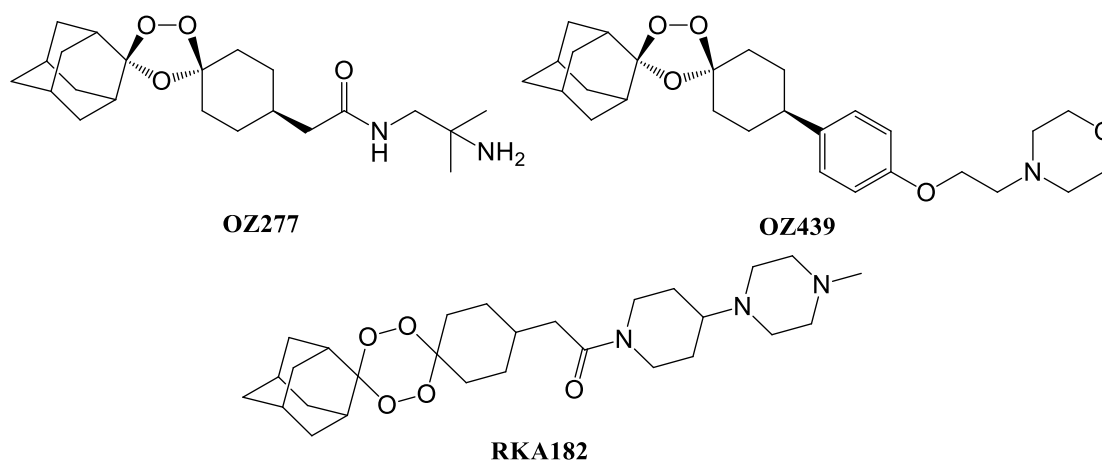


**Figure 1.14** – Structural representation of **OZ277** and **OZ439** (1,2,4-trioxolanes) and **RKA182** (1,2,4,5-tetraoxane).

Studies about endoperoxide stability have shown that 1,2,4,5-tetraoxanes have significantly higher stability than their 1,2,4-trioxolane counterparts. **RKA182** demonstrated superior properties to the semisynthetic artemisinins: better antimalarial

activity, stability, ADME (absorption, distribution, metabolism and excretion) properties and lower toxicity.

### **1.2.5. Other approaches and emerging chemotherapeutic tools against malaria**

The development of resistance to available drugs by *Plasmodium* parasites continues growing, increasing the difficulty to control malaria. Many new approaches to antimalarial drug discovery are under development or in study, considering new scaffolds and new therapeutic targets.

#### **A. Protease inhibitors**

Proteases are required for the parasite survival, intervening in crucial processes such as the erythrocyte invasion (*PfSUB1* and *PfSUB2*),<sup>16</sup> the haemoglobin degradation and the erythrocyte rupture (cysteine proteases)<sup>38</sup>. These proteases are potential chemotherapeutic targets.

The haemoglobin degradation has been explored in antimalarial drug design programmes, and most studies are directed to find inhibitors of the proteases acting in this pathway, with the aim of blocking the production of free amino acids by the parasites, for feeding purposes. Aspartic proteases *plasmepsin* I, II and IV (involved in initial cleavage of haemoglobin),<sup>39</sup> cysteine protease *falcipain-2* (involved in cleaving relatively large globin fragments)<sup>38</sup> and metalloprotease *falcilysin* and histoaspartic protease (involved in cleavage of smaller peptides) are some of the proteases involved in the parasite's feeding and, as such, suitable targets for antimalarial drug design.<sup>40</sup>

#### **B. Utilization of parasite-induced transport systems**

The cell membranes of the host (including of erythrocytes) contain many transporters responsible for the movement of molecules between the plasma and the cell cytosol. However, upon a malarial infection new permeation pathways are induced and have demonstrated functional characteristics that are quite different from those of the host transporters. Thus, one potential approach to fight malaria may consist in the administration of a parasitocidal agent that is not taken by host cells but is transported by the new permeation pathways, allowing its accumulation inside the infected erythrocyte and subsequent destruction of the parasite.<sup>41</sup>



### **C. Inhibitors of phospholipid and fatty acid synthesis**

In the erythrocytic phase, *Plasmodium* needs to synthesize its own components of parasite membranes, predominantly phospholipids. So, inhibition of the synthesis and/or transport of some precursors required for the synthesis of phospholipids, has shown to be a promising strategy for drug design.<sup>42</sup>

Fatty acids play an important role to provide precursors of biological membranes and represent an important form of metabolic energy. The human host synthesizes fatty acids using a type I fatty acid synthase (FAS-I). However, and differently, *Plasmodium* parasites use a type II system (FAS-II). Since the human host and the parasite synthesize fatty acids via different pathways, this could be an important intervention focus for the development of new antimalarials.<sup>43</sup>

### **D. Inhibitors of protein farnesylation**

Protein prenylation or lipidation are processes of post-translational modification of proteins by the addition of hydrophobic moieties of 15 carbons (farnesyl group) or 20 carbons (geranylgeranyl group). These groups facilitate attachment to membranes, as well as protein interactions. Protein farnesyl transferase (PFT) is one of the enzymes responsible for the protein prenylation and occurs in eukaryotic cells but also in a wide variety of pathogenic protozoa, including *P. falciparum*. Some studies have shown that PFT inhibitors are more toxic to cancer cells and parasites than to normal mammalian cells.<sup>44</sup>

### **E. Inhibitors of heat-shock proteins**

Heat-shock proteins (HSP) have an important role in stress tolerance and in the folding, activation and assembly of many proteins, such as steroid hormones, protein kinases and molecules regulating the cell cycle. During host invasion, establishment and development, parasites are exposed to environmental stress and the parasitic heat-shock protein (expressed during the erythrocytic stages) has an important role in the parasite survival. HSP inhibition may affect the parasite's progression from ring to trophozoite.<sup>45</sup> Furthermore, human host humoral response against parasite's HSP has been observed, placing this protein as an important antigen target for the development of vaccines.<sup>46</sup>

### **F. Protein kinase inhibitors**

Protein kinases are key regulators of cell cycle control. One family of kinases, the cyclin-dependent protein kinases (CDK), regulates directly the timely progression

through the cell cycle. Some CDK inhibitors effectively inhibit *PfPK5* (*P. falciparum* protein kinase 5) and/or *PfMRK* (*P. falciparum* MO15-related protein kinase), two plasmodial CDK that are structurally different from the host's CDK.<sup>47</sup>

### G. Inhibitors of glycolysis

*Plasmodium* parasites do not have a functional Krebs cycle and hence rely extensively on ATP (adenosine triphosphate) generation via the anaerobic fermentation of glucose. Lactate dehydrogenase (LDH), the last enzyme in the glycolytic pathway, converts pyruvate to lactate with simultaneously conversion of NADH to NAD<sup>+</sup> (nicotinamide adenine dinucleotide). Thus, inhibition of LDH is expected to stop production of ATP, with subsequent *Plasmodium* cell death.

Structural and kinetical discrepancies between these malarial enzymes (*PLDH*) and the three human counterparts (*HsLDH*) suggest that specific and potent malarial inhibitors can be designed or identified.<sup>48</sup>

### H. Inhibitors of the shikimate pathway

The shikimate pathway, known to exist in *P. falciparum* but not in mammals, leads to the biosynthesis of aromatic aminoacids. The inhibition of 5'-enolpyruvylshikimate 3-phosphate synthase by **glyphosate** (Figure 1.15) was found to inhibit the growth of *P. falciparum*. However, it is not clear if biosynthesis of aromatic aminoacids plays an essential role in this parasite and if this compound inhibits growth of the parasite by inhibition of this enzyme of the shikimate pathway.<sup>23</sup>

### I. Inhibitors of isoprenoid biosynthesis

A mevalonate-independent isoprenoid biosynthetic pathway was identified in *P. falciparum* and *T. gondii*, but not in humans. Inhibiting 1-deoxy-D-xylulose-5-phosphate isomerase by **fosmidomycin** (Figure 1.15), leads to an *in vitro* inhibition of the growth of *P. falciparum*. However, it has not been demonstrated that this pathway plays an indispensable role in this parasitic organism, neither that the inhibition of the parasites is due to inhibition of this particular enzyme.<sup>23</sup>

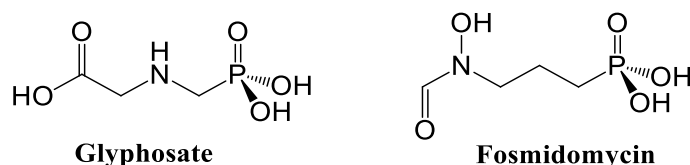


**Figure 1.15** – Structural representation of glyphosate and fosmidomycin.

### **1.3.Mitochondria – an essential organelle**

Mitochondria as an organelle emerged from a symbiotic arrangement is also characterized by loss and transfer of some genes from the mitochondria to the host genome.<sup>49–51</sup>

The phylum Apicomplexa contains the smallest mitochondrial genome known and, despite the relatively low activity of the mitochondrial electron transport chain (mtETC), mitochondria plays a critical and essential role in the life cycle of the parasite as the primary source of the proton electrochemical gradient. The blood-stage of *P. falciparum* maintains an active mitochondrial electron transport chain to serve the regeneration of ubiquinone (CoQ).<sup>50,52</sup> The molecular and functional differences between the human's mitochondria and the parasite's mitochondria highlight this organelle as a target for medicinal chemistry.<sup>53–55</sup>

#### **1.3.1. The mitochondrial electron transport chain of *P. falciparum***

Conventionally, the mitochondria is viewed as the source of cellular energy in the form of ATP, but previous studies have demonstrated that glycolysis is the main source of ATP in the intraerythrocytic stage of *Plasmodium*, with little or no contribution from oxidative phosphorylation driven by the TCA (tricarboxylic acid) cycle and from respiratory chain.<sup>53,56</sup>

However, mtETC continues to be the main generator of the proton electrochemical gradient which, while not appearing to power the mitochondrial ATP synthesis in blood stages of *Plasmodium*, is required to transport metabolites and proteins in and out of the mitochondria to fuel carbon metabolism in this organelle (*Plasmodium* parasites do not have a functional Krebs cycle).<sup>57,58</sup>

Instead of the canonical multimeric complex I (NADH: dehydrogenase), found in mammalian mitochondria, the intraerythrocytic malaria parasites encode four dehydrogenases or oxidoreductases belonging to the mtETC (Figure 1.16): type II NADH ubiquinone oxidoreductase (*PfNDH2*), dihydroorotate dehydrogenase (*PfDHODH*), glycerol 3-phosphate dehydrogenase (GPDH) and malate quinone oxidoreductase (MQO). Some of these dehydrogenases act concomitantly with succinate ubiquinone oxidoreductase (Complex II or SDH) to reduce CoQ (ubiquinone) to ubiquinol (dihydrubiquinone or CoQH<sub>2</sub>), providing electrons to the other complexes involved in the mtETC: ubiquinol cytochrome *c* oxidoreductase (Complex III or cytochrome *bc*<sub>1</sub>),

cytochrome *c* oxidase (Complex IV) and ATP synthase (Complex V). Complex III is responsible for the reoxidation of CoQH<sub>2</sub> to CoQ.<sup>53</sup>

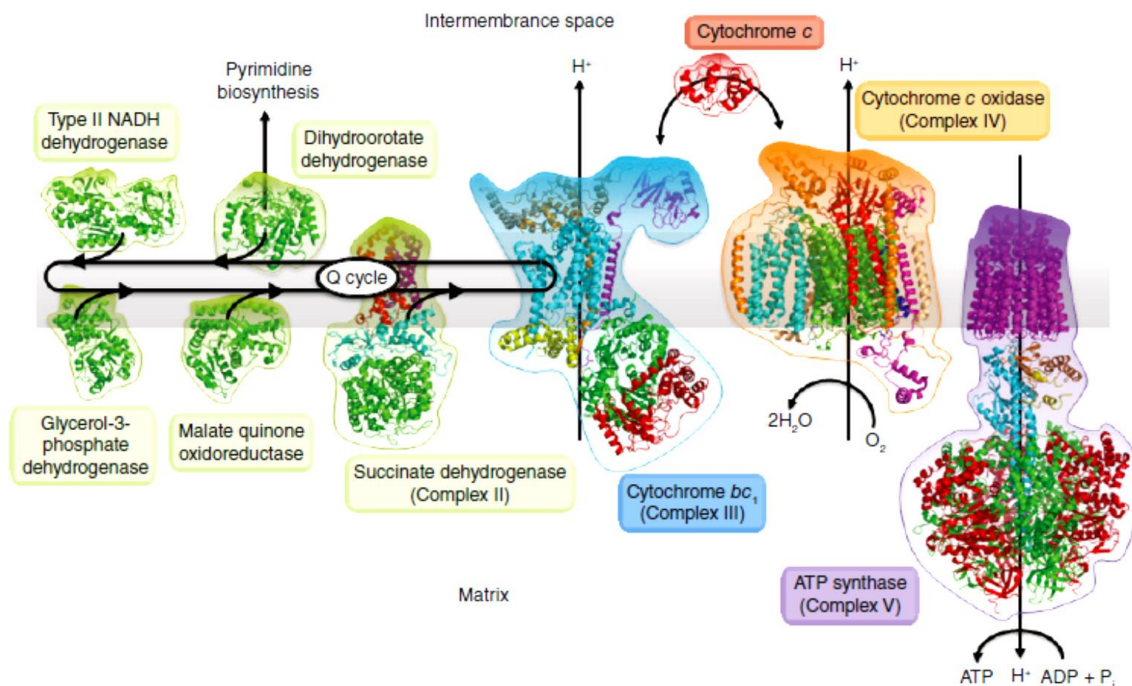


**Figure 1.16** – Representative diagram of *Plasmodium* mitochondrial electron transport chain.<sup>55</sup>

*Pf*N<sub>DH2</sub> catalyses the oxidation of NADH with concomitant reduction of CoQ to CoQH<sub>2</sub>. While this mitochondrial enzyme is not involved in the vectorial transfer of protons across membranes, due to the absence of transmembrane domains, its activity may indirectly contribute to the formation of an electrochemical transmembrane potential. Similar type II NADH dehydrogenases may be found in other organisms, including plants, fungi and bacteria, such as *Mycobacterium tuberculosis*.<sup>55,59–61</sup>

*Pf*DHODH is involved in pyrimidine biosynthesis, essential for the formation of DNA, RNA (ribonucleic acid), glycoproteins and phospholipids, therefore crucial for the parasite survival. It is responsible for the conversion of dihydroorotate to orotate, where CoQ is the co-substrate electron acceptor being reduced to CoQH<sub>2</sub>.<sup>50,55,57</sup>

Mitochondrial GPDH plays a very important role in the bioenergetic metabolism, interfering with glycolysis, oxidative phosphorylation and fatty acid metabolism. This isoform catalyses the oxidation of glycerol-3-phosphate to dihydroxyacetone phosphate, with concurrent reduction of flavin adenine dinucleotide (FAD) to FADH<sub>2</sub> and, via another independent protein domain, transference of electrons to CoQ, giving CoQH<sub>2</sub> and FAD regeneration.<sup>62,63</sup>

MQO exists in multiple forms that differ in cofactor specificity and subcellular localization. Mitochondrial MQO catalyses the conversion of malate to oxaloacetate (for the biosynthesis of citrate) and the generation of NADH to feed the respiratory chain.<sup>58</sup>

The *Plasmodium* Complex II is composed by four subunits, where a flavoprotein (Fp) and iron-sulphur (FeSp) subunits form a catalytic portion. The Fp subunit converts succinate to fumarate with oxidation of FADH<sub>2</sub> to FAD. The FeSp subunit contains three iron-sulphur clusters [2Fe-2S], [4Fe-4S], and [3Fe-4S], and provides the reduction of CoQ to CoQH<sub>2</sub> using the electrons derived from the succinate oxidation via FAD.<sup>56</sup>

With the reoxidation of CoQH<sub>2</sub> to CoQ in Complex III, cytochrome *c* acts as electron carrier to Complex IV transferring the electrons to one oxygen molecule to get two molecules of water. In addition, protons are translocated across the membrane to the intermembrane space, helping to establish a transmembrane difference of the proton electrochemical potential that can be used by ATP synthase (Complex V) to synthesize ATP from ADP (adenosine diphosphate).<sup>53,55</sup>

### **1.3.2. Cytochrome *bc*<sub>1</sub> protein complex (Complex III)**

The cytochrome *bc*<sub>1</sub> is a protein complex that should not be referred to as an enzyme. This homodimeric system is member of the larger family of *bc*-type complexes that spans the inner mitochondrial membrane. Each functional unit of the homodimeric complex is composed by ten polypeptide chains embedded with some haem units. The catalytic core contains three electron transfer subunits: cytochrome *b*; cytochrome *c*<sub>1</sub>; and an iron-sulphur protein known as the Rieske protein (ISP) – see Figure 1.17.<sup>64,65</sup> The other seven subunits are not well understood, presuming that they are involved in the complex anchoring at the mitochondrial membrane.<sup>66</sup>

Cytochrome *b* is a transmembrane protein in which two *b*-haem groups (low potential *b*<sub>L</sub> and high potential *b*<sub>H</sub>) form an electrical circuit across the subunit from the Q<sub>o</sub> site (or *P*), on the outer electropositive portion, to the Q<sub>i</sub> site (or *N*), on the inner electronegative portion. The ISP is anchored to the complex by a hydrophobic helix, at the N-terminal, and the C-terminal domain, that contains a [2Fe-2S] cluster, is located near the electropositive surface of the membrane. Cytochrome *c*<sub>1</sub> is held to the complex by a hydrophobic helix at the C-terminal and the domain of the protein, that contains the haem, is accessible at the electropositive surface of the membrane, where it reacts with cytochrome *c*.<sup>64</sup>

### 1.3.2.1. Protonmotive Q-cycle

The cytochrome  $bc_1$  complex transfers electrons from **ubiquinol** ( $\text{CoQH}_2$ ) to cytochrome  $c$ , regenerating **ubiquinone** ( $\text{CoQ}$ ) and translocating protons across the membrane (from the matrix of mitochondria to the intermembrane space). This process, described by Mitchell's Q-cycle hypothesis (Figure 1.17 and Figure 1.18), is designated protonmotive Q-cycle and maintains a membrane potential across the mitochondrial membrane, essential for some biological processes (pyrimidine and ATP synthesis).<sup>67-69</sup>

In each complete cycle, two molecules of  $\text{CoQH}_2$  are oxidised to  $\text{CoQ}$  at  $Q_o$  and four protons ( $\text{H}^+$ ) are translocated to the intermembrane space. At the same time, four electrons ( $e^-$ ) are released and, while two of them reduce one molecule of  $\text{CoQ}$  to  $\text{CoQH}_2$  (at  $Q_i$ ), the other two move to the  $[2\text{Fe}-2\text{S}]$  cluster of the ISP. Upon reduction of ISP its cytoplasmic region changes, favouring the transfer of these two electrons to the haem group bound in cytochrome  $c_1$ , which is then reoxidised by cytochrome  $c$ , that acts as electron carrier to Complex IV.<sup>68-71</sup>

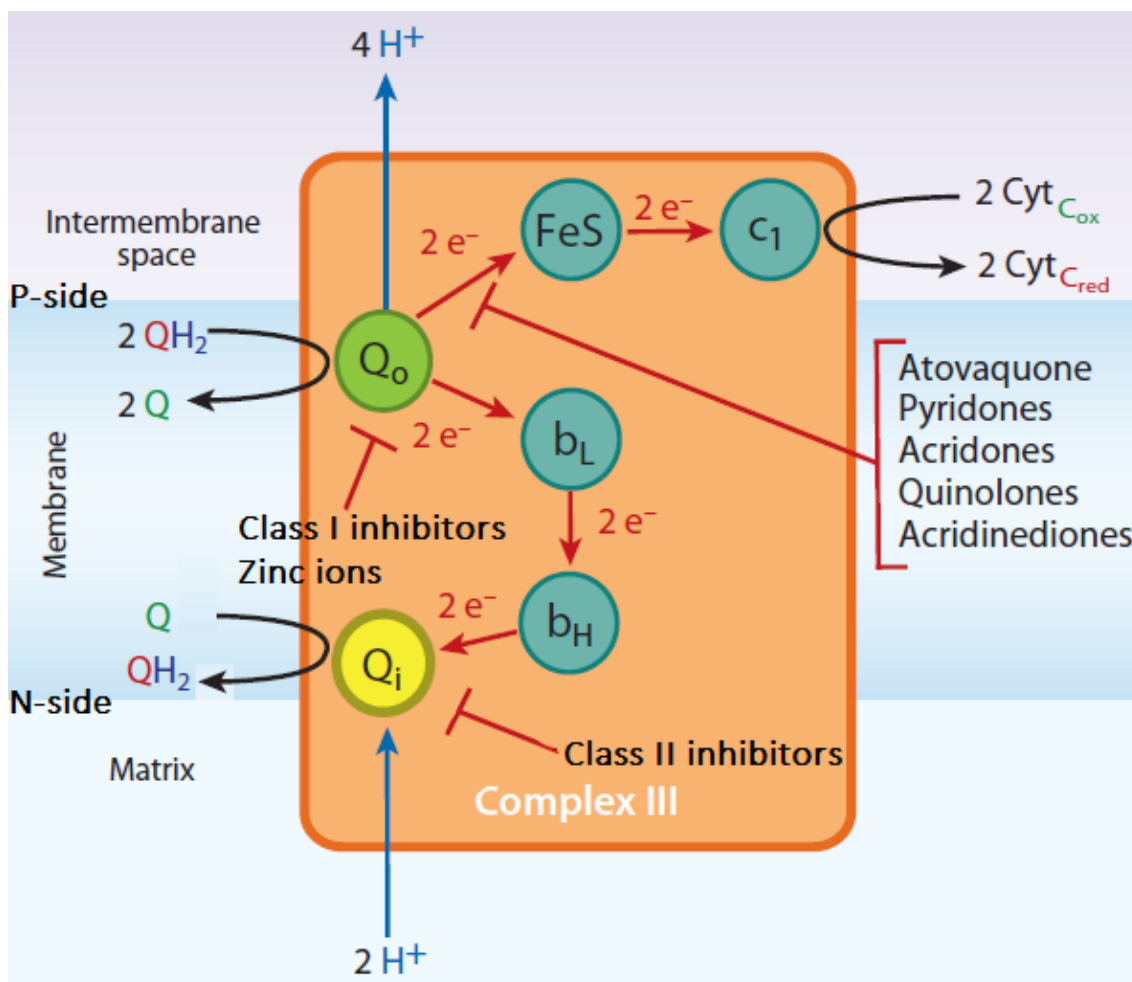


**Figure 1.17** – Representative diagram of the reactions held in complex III (Protonmotive Q-cycle), targeted by some drugs or drug candidates. Adapted from Vaidya *et al.*<sup>53</sup>

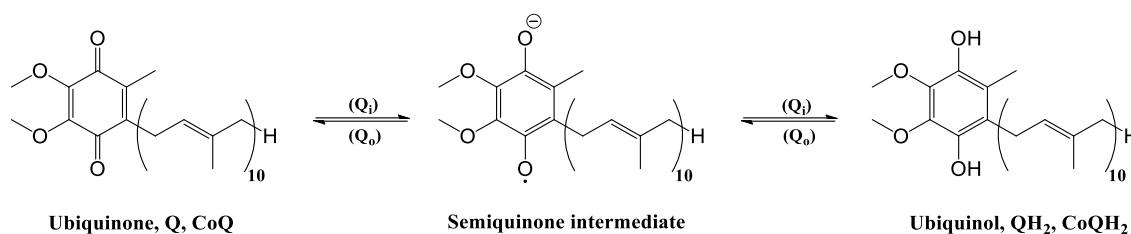


**Figure 1.18** – Representation of structural changes from ubiquinone to ubiquinol (at Q<sub>i</sub> site) and from ubiquinol to ubiquinone (at Q<sub>o</sub> site).

### 1.3.3. Inhibition of the cytochrome *bc*<sub>1</sub>

Malaria parasites have retained the ability to generate a large electrochemical potential across their mitochondrial membrane. mtETC is critical for parasite survival and, as the inhibition of respiratory enzymes has severe consequences, drugs targeting these enzymes could be efficient tools for pathogen control. While complexes I and III are the main targets of mtETC in study for development of new antimalarial, the *P. falciparum* *bc*<sub>1</sub> complex is the only component with an inhibitor clinically used as antimalarial drug (atovaquone).<sup>55,60,72</sup>

Cytochrome *bc*<sub>1</sub> inhibitors block the catalytic activity of the Complex III and, consequently, the respiratory chain is implicated. However, as the structure of cytochrome *bc*<sub>1</sub>, especially its catalytic core, is highly conserved between species, these inhibitors could evidence high toxicity to mammals and other non-pathogenic organisms. Despite this, some light unusual structural features in *P. falciparum* cytochrome *b* may be used to facilitate the design of inhibitors with some selectivity (decreased toxicity). In addition, the target (cytochrome *b*) is encoded by a mitochondrial gene that appears to accumulate mutations at a higher frequency than nuclear genes and resistance mutations are thus a possibility. From this viewpoint, the Q<sub>i</sub> site is a more desirable target than Q<sub>o</sub> because the first one reflects less point mutation issues.<sup>72–74</sup>

Considering that the protonmotive Q-cycle (in cytochrome *bc*<sub>1</sub> complex) requires two reaction sites (Q<sub>i</sub> or *N*; and Q<sub>o</sub> or *P*), the cytochrome *bc*<sub>1</sub> complex inhibitors can be grouped in two categories, based on their binding site.<sup>67,69,75</sup>

Class I inhibitors inhibit electron bifurcation at the Q<sub>o</sub> site and, historically, can be further subdivided into three or two subclasses, based on their chemical characteristics or on their structural effects on the protein target, respectively. **Myxothiazol (Ia)**, **stigmatellin (Ib)** and 2-hydroxy quinone (Ic) analogues (such as **5-n-undecyl-6-hydroxy-4,7-dioxobenzothiazole - UHDBT**) are some examples of compounds that bind at the Q<sub>o</sub> site (Figure 1.19).<sup>67,76</sup>

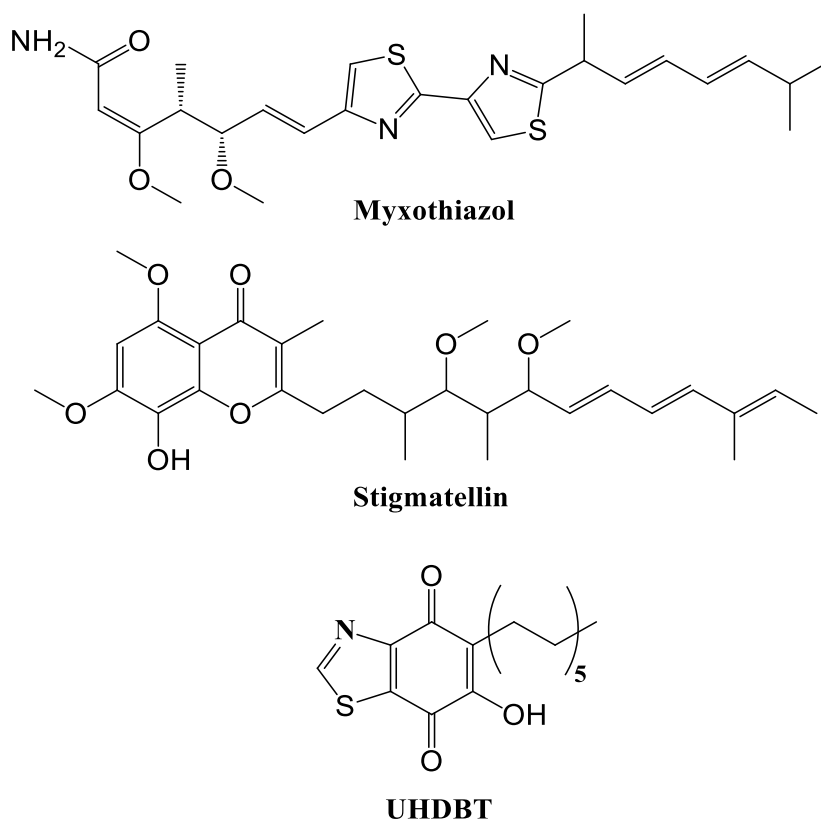


**Figure 1.19** – Structural representation of myxothiazol, stigmatellin and UHDBT.

Class Ia inhibitors (*e.g.* myxothiazol) bind at the  $Q_o$  site, leaving the ISP mobile, while Ib and Ic inhibitors, when bound at the  $Q_o$  site, fix the ISP region in a set position (temporary locking).<sup>76</sup>

In addition to these three subclasses of organic compounds, zinc ions bind at the  $Q_o$  site and prevent the release of protons formed during the ubiquinol oxidation, inhibiting reversibly the  $bc_1$  complex. However,  $Zn^{2+}$  is not competitive to the binding of other  $Q_o$  site inhibitors.<sup>75</sup>

Class II inhibitors target the  $Q_i$  site and are represented by **antimycin A** (Figure 1.20), a natural fungicide produced by *Streptomyces sp.*. Although less susceptible to development of resistance,  $Q_i$  is situated on the inner face of the inner mitochondrial membrane, making it relatively inaccessible.<sup>67,75</sup>

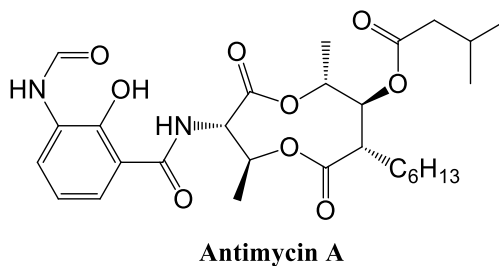


**Figure 1.20** – Structural representation of antimycin A.



#### 1.3.4. Atovaquone

**Atovaquone** is a 2-hydroxynaphthoquinone, an analogue of ubiquinone, and acts as a competitive inhibitor of the cytochrome *bc*<sub>1</sub> protein complex (binding specifically to Q<sub>o</sub> site – class Ib inhibitor) in the parasite mitochondria, disrupting the membrane potential that provides energy for mitochondrial function and is essential for pyrimidine synthesis. Besides, some recent studies have suggested that the inhibition of purine biosynthesis may be a further cellular consequence of mitochondrial inhibition by atovaquone.<sup>59,77,78</sup>

The beginning of the atovaquone development goes back more than 50 years, when World War II caused substantial shortages in the supply of quinine. Thousands of compounds were then investigated and some members of the hydroxynaphthoquinone chemotype showed greater antiplasmodial activity than quinine. However, these compounds revealed low or null activity in clinical trials, due to poor absorption and rapid metabolism. Only in 1991, the chemical synthesis of atovaquone, a compound with good antimalarial activity, metabolic stability and inertness to human liver microsomes, was disclosed.<sup>79–81</sup>

Atovaquone is active against blood-stage parasites but its effect is relatively slower than that showed by other antimalarials, such as artemisinin and chloroquine, because atovaquone acts only on late trophozoites and not on the earlier stages (“ring forms”). It is also active against liver stages of *P. falciparum* (important utility in prophylaxis), but not against *P. vivax* hypnozoites. In addition to the activity against *Plasmodium*, atovaquone shows activity against some opportunistic pathogens, *e.g.* *Pneumocystis jiroveci* and *Toxoplasma gondii*.<sup>22,23,80,82</sup>

Atovaquone is effective at concentrations far lower than those at which the mammalian system is affected. *In vitro*, atovaquone IC<sub>50</sub> (half maximal inhibitory concentration) is very low, ranging from 1 to 3.5 nM. Although the high levels of plasma protein binding (99.5%), atovaquone plasma concentrations (around 1–10 mM) are sufficient to produce total suppression of malaria.<sup>83</sup>

This class Ib inhibitor is generally well tolerated and just causes few and mild side effects, such as rash, fever, vomiting, diarrhoea, abdominal pain and headache. Overdoses (as large as 31500 mg) have been reported to cause little or no symptomatology. The main problem about toxicity in the development of antimalarials targeting the mitochondria of the parasite is the possibility of host mitochondrial toxicity, since some animal models manifest cardiotoxicity.<sup>80,84,85</sup>

Atovaquone has been successful clinically, especially if administered in combination with proguanil (a dihydrofolate reductase inhibitor) – **Malarone**<sup>®</sup> (Figure 1.21). Malarone<sup>®</sup> combination was released in 2000 by GlaxoSmithKline and has been used for treatment and prevention of chloroquine-resistant infections, especially in Southeast Asia, where highly drug-resistant strains of *P. falciparum* prevail. It has also been used to slow development of resistance, since *P. falciparum* readily develops clinical resistance to monotherapy with either proguanil or atovaquone.<sup>22,55,59</sup>

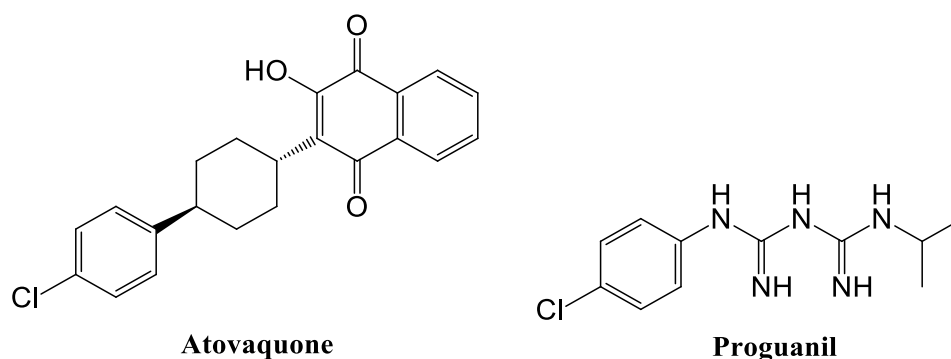


**Figure 1.21** – Structural representation of the active compounds of the Malarone<sup>®</sup> (atovaquone and proguanil).

One reason for the preference of combinations with atovaquone, as Malarone<sup>®</sup>, in detriment of monotherapy, is the synergism that the proguanil exerts. Proguanil as monotherapy has no effect on mitochondrial membrane potential, but significantly enhances the ability of atovaquone to collapse mtETC. Even in the presence of documented proguanil resistance or in patients who are deficient in cytochrome P450 enzymes, required for the conversion of proguanil to cycloguanil, this synergetic activity emerges.<sup>86</sup>

Despite well tolerated, the cost of Malarone<sup>®</sup> limits or even precludes its widespread use in resource-poor settings and disease-endemic areas, where it is most needed. The need of addition of proguanil in therapeutic doses and the obligation to keep the central cyclohexane ring of atovaquone in *trans* configuration have increased the complexity and the cost of this preparation.<sup>22</sup>

#### **1.3.4.1. Atovaquone binding at Q<sub>o</sub>**

Some studies have been carried out to define the exact binding position of atovaquone at Q<sub>o</sub> of *P. falciparum*. The plasmodial cytochrome *bc*<sub>1</sub> has not been successfully isolated and crystallized, so the studies have analysed the interactions between atovaquone and *bc*<sub>1</sub> complex homologs in bacterial and yeast based systems.

Trumpower *et al.* used the crystal structure coordinates of stigmatellin-bound *Saccharomyces cerevisiae* yeast  $bc_1$  as reference to model the interactions of atovaquone with the  $Q_o$  pocket (Figure 1.22). *S. cerevisiae* yeast  $bc_1$  has a high sequence identity with *Plasmodium*  $bc_1$  complex, can be easily purified and its crystal structure is available.<sup>87-90</sup>

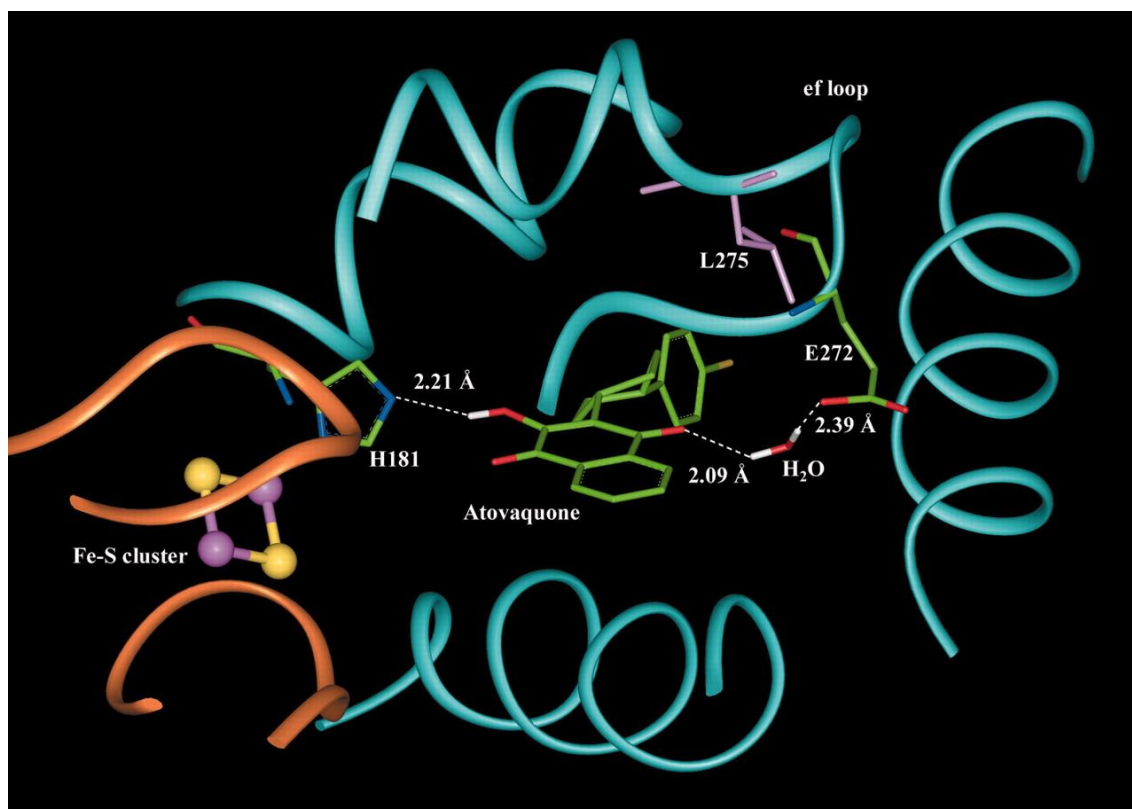


**Figure 1.22** - Trumpower *et al.* study: *in silico* docking results for atovaquone binding in the ubiquinol oxidation pocket at center P of the yeast  $bc_1$  complex. (cyan) cytochrome  $b$ ; (orange) portion of the Rieske ISP; (yellow and purple atoms) iron-sulfur cluster [2Fe-2S]; (green) atovaquone (oxygen atoms are red and chlorine atom is yellow); key amino acids His181, Glu272 and Leu275 are shown and highlighted.<sup>87-90</sup>

As observed for stigmatellin (Ib inhibitor) and UHDBT (Ic inhibitor), the results obtained by Trumpower *et al.* indicate that atovaquone binds to the  $Q_o$  pocket when the water-soluble mobile region of the ISP is proximal to cytochrome  $b$ , allowing the direct interaction of atovaquone with both protein chains. Through docking studies, Trumpower *et al.* found that the hydroxyl group on the naphthoquinone ring of atovaquone forms a hydrogen bond with the His181 of ISP. A second hydrogen bond, water mediated, is formed between the Glu272 of cytochrome  $b$  and the quinone carbonyl of the naphthoquinone ring.<sup>87,89,90</sup>

The same research group proposed to explain the difference in efficacy of inhibition of the yeast and the bovine (mammalian)  $bc_1$  complexes by atovaquone

(atovaquone is about eight times more potent against yeast  $bc_1$  complex than against the bovine enzyme). To be clinically used, atovaquone must exhibit selective inhibition of the targeted pathogen compared with the mammalian host. The bovine  $bc_1$  protein is 80% identical to the human protein and, for example, the *ef* loop of cytochrome *b* is a conserved domain containing residues in close contact to the atovaquone-binding pocket. However, in the mammalian sequence (both in bovine and human proteins), the Leu275 found in yeast is replaced by phenylalanine. Computational modelling for this change results in steric constraint to atovaquone binding, with a predicted decrease in the affinity of the inhibitor to the binding pocket.<sup>90</sup>

#### **1.3.4.2. Atovaquone and selection for resistance**

From the last four decades, *P. falciparum* has developed resistance to almost every available antimalarial drug. Selection for resistance by the parasite is a major obstacle in the control of the malaria. Thus, besides the study of new and more cost-effective inhibitors, other strategies are urgently needed to control the development of resistance and, ideally, to reverse existing resistance.

The most common measures to circumvent or delay selection for resistance are the use of combinations of synergetic antimalarials (*e. g.* Malarone<sup>®</sup>) and the immediate interruption of a particular drug when a certain level of treatment failure is observed. The removal of the selection pressure exerted by the drug in question may enable a susceptible parasites population to reestablish itself and gradually replace the resistant counterpart. In many organisms, mutations that confer resistance to drugs clearly provide the organism with a survival advantage in the presence or absence of drug. However, in other organisms, mutations that confer resistance can be a disadvantage for the survival of the population in the absence of drug pressure. In the case of *Plasmodium*, the relative fitness of the resistant strains in the absence of drug pressure is unclear.<sup>91</sup>

*Plasmodium* resistance to atovaquone may be attributable to single point mutations in plasmodial cytochrome *b* that arise from increased oxidative damage to mitochondrial DNA generated by the action of the drug, reducing the binding affinity for the atovaquone to the  $Q_o$  site. Besides that reason, the mitochondrial genome has, by nature, a high frequency of mutations. Several authors claim that these mutations can confer up to a 760-fold drop in potency, rendering the drug ineffective at safe therapeutic

doses. Several of these mutations cause alterations in the amino acids forming the hydrophobic channel of Q<sub>o</sub> rather than alterations in the structure of Q<sub>o</sub> itself, because an alteration of the catalytic site could render the protein complex inactive.<sup>23,92-95</sup>

Over one-third of the patients treated with atovaquone as monotherapy are expected to evidence post-treatment recrudescence – one of the many reasons to use atovaquone in combination with proguanil. While parasites resistant to proguanil are affected by Malarone<sup>®</sup>, parasites resistant to atovaquone are not inhibited by this one. The first cases of Malarone<sup>®</sup> resistance were observed in Africa and were linked to the single amino acid mutation at codon 268, resulting in a change from tyrosine to serine (Tyr268Ser) or asparagine (Tyr268Asn) in the cytochrome *b* structure. This residue is involved in a hydrophobic interaction with the ubiquinol, so the mutation is likely to result in a significant respiratory penalty for the parasite. Similar mutations in other codons associated with atovaquone resistance have been identified, in clinical isolates and in experimental rodent malaria models.<sup>72,87,96,97</sup>

### **1.3.5. Other antimalarial compounds targeting cytochrome *bc*<sub>1</sub> protein complex**

Considering the growing emergence of resistance, development of new and effective antiplasmodial drugs is a priority. From the validation of mtETC as an important target and the knowledge regarding atovaquone interactions with the cytochrome *bc*<sub>1</sub> complex, new inhibitors for use against *P. falciparum* have been studied. The mtETC is an attractive target owing to the multistage activity of its inhibitors. However there are barriers to development of novel inhibitors, such as poor solubility and the possibility of cardiotoxicity.

Furthermore, since some mutations associated to atovaquone resistance tend to confer cross resistance to other Q<sub>o</sub> inhibitors, the new and more cost-effective inhibitors of the *bc*<sub>1</sub> complex must overcome the resistance mechanisms. So far, the more established compounds for the study of antimalarial *bc*<sub>1</sub> inhibition are, essentially, based on aromatic ring systems and are classified into five classes, according with their core chemical structure.<sup>55</sup> Studies about these classes have been reviewed by various authors, highlighting the works of Trumpower *et al.*,<sup>87</sup> P. O'Neill *et al.*,<sup>73</sup> G. Biagini *et al.*,<sup>55</sup> Beteck *et al.*<sup>98</sup> and P. Gomes *et al.*<sup>99</sup>.

### 1.3.5.1. Atovaquone analogues (1,4-naphthoquinones)

As discussed before, a sudden shortage of quinine (in 1950's) boosted the investigation of thousands compounds, a large number of which being hydroxynaphthoquinone-type structures. From this huge effort resulted atovaquone, a hydroxynaphthoquinone with excellent antimalarial activity but with poor pharmaceutical properties, such as low bioavailability and high plasma protein binding. As such, several atovaquone analogues (1,4-naphthoquinones) have been investigated to improve atovaquone's profile (Figure 1.23).<sup>55,73</sup>

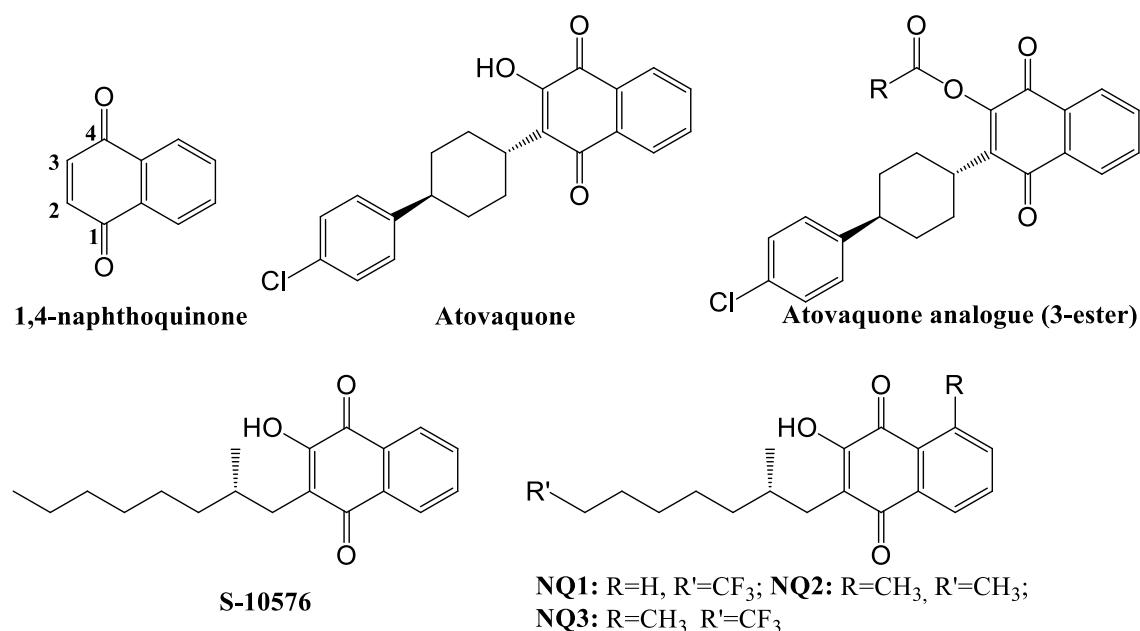


**Figure 1.23** – Representation of the core structure of 1,4-naphthoquinone class; structures of naphthoquinones studied as antimalarials.

El Hage *et al.* designed a library of compounds replacing the 3-hydroxyl functional group of atovaquone by more lipophilic ester and ether groups. Most of them showed potent activities with IC<sub>50</sub> values in the range of 1.25–5 nM, however these modifications did not lead to an improvement in the atovaquone's profile.<sup>100</sup>

In another strategy, Trumpower's group developed a series of atovaquone analogues based on a potent hydroxynaphthoquinone *Plasmodium bc*<sub>1</sub> inhibitor (**S-10576**) that had proved to be inactive in humans due to rapid metabolic degradation. Incorporation of a trifluoromethyl group into branched and straight chain alkyl groups and/or a methyl group on the aromatic ring led to the synthesis of **NQ1-NQ3**. This methyl group has been associated to van der Waals interactions with the Rieske ISP. While overcoming the metabolic instability, these compounds demonstrated reduced species

selectivity and reduced potency. 1,4-naphthoquinone-based compounds have potential as *bc*<sub>1</sub> inhibitors but their drug-like profile needs to be improved.<sup>101</sup>

### 1.3.5.2. 4(1H)-pyridones

Pyridones have been known as potent antimalarials since 1960's, when **clopidol** (Figure 1.24) was found to exhibit activity against chloroquine resistant strains of *P. falciparum*. Actually, clopidol is also known to potentiate the action of hydroxynaphthoquinones and sustains activity against atovaquone-resistance strains. The overcome of the atovaquone resistance may suggest that pyridone derivatives could bind at a different site (not just at the Q<sub>o</sub> pocket).<sup>55,73,85</sup>

Considering the chemical structure of clopidol, various pyridone-based compounds have been synthesized and studied as potential antimalarials (Figure 1.24).

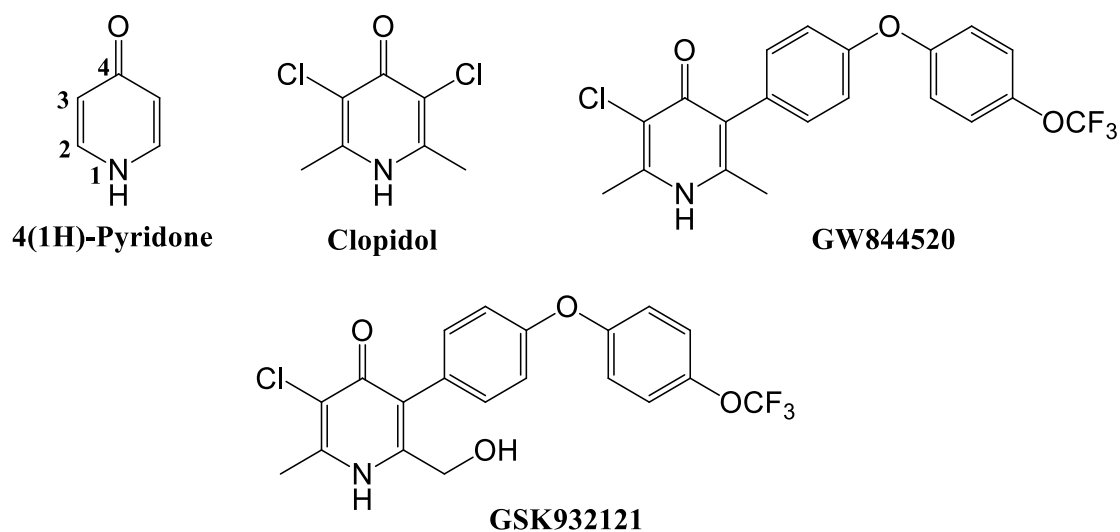


**Figure 1.24** – Structural representation of clopidol and other pyridone-based compounds with antimalarial properties.

In 2006, GlaxoSmithKline (GSK) in collaboration with Yeates *et al.*, reported the preclinical evaluation of new 4(1H)-pyridones targeting the *bc*<sub>1</sub> complex of *P. falciparum*, highlighting that halogenation at the C-3 position (Figure 1.24) leads to a 10-fold increase in activity *in vitro*, while the introduction of a phenoxyaryl side chain at C-5 also gave an increased activity.

The most promising candidate, **GW844520** (Figure 1.24), exhibited impressive antimalarial potency (IC<sub>50</sub> of 2 nM) and activity against atovaquone resistant strains. Further development, to solve the solubility issues often encountered with these compounds, by introduction of a hydroxyl group originated the synthesis of **GSK932121** (Figure 1.24), also potent against resistant strains. Unfortunately, these pyridones have

been suspended at clinical trials due to toxicity issues (unexpected cardiotoxicity) that have yet to be resolved.<sup>85,102,103</sup>

### 1.3.5.3. Acridinediones and acridones

Acridinediones (Figure 1.25) and acridones (Figure 1.26) are tricyclic compounds incorporating the 4-oxo-1,4-dihydroquinoline skeleton, being structurally related to quinolones.

The antimalarial activity of selected acridinediones is known since 1947 and the interest in this class grew when **floxacrine** (Figure 1.25) revealed prophylactic properties (in 1970's), although this drug had limited solubility, unacceptable side-effects (it was temporarily abandoned) and eventually became useless due to rapid development of resistance.<sup>98,104</sup>

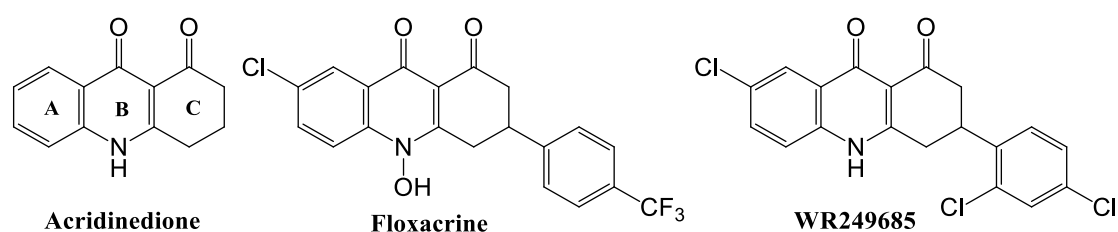


**Figure 1.25** – Structural representation of the acridinedione ring system, of floxacrine and of WR249685.

Floxacrine (Figure 1.25) was initially shown to bind to haem, preventing the crystallization of haemozoin, but a second mode of action has been considered recently. **WR249685** (Figure 1.25) showed a higher *in vitro* antimalarial activity than floxacrine (IC<sub>50</sub> around 15 nM for **WR249685** vs 140 nM for floxacrine) and was found to inhibit the *Plasmodium bc*<sub>1</sub> complex. This compound revealed a significant selectivity, with a ratio of inhibition towards *P. falciparum bc*<sub>1</sub> protein of 4600, compared to the mammalian protein, while floxacrine failed to selectively inhibit the *P. falciparum bc*<sub>1</sub> protein complex.<sup>105</sup>

Acridones were initially isolated as intermediates in the synthesis of haem-complexing compounds and have also been found to possess a dual mechanism of action, like some acridinediones: some acridone analogues expressed moderate to significant cross resistance with the atovaquone-resistant TM90 strain (mechanism of action may be similar to atovaquone). It is possible that the acridones exhibiting no cross resistance have overcome the resistance mechanism or they are predominantly haem binders.<sup>55,73</sup>

Acridones are fully aromatic, so the issue of chiral isomers that can arise from the substitution of the alkyl C-ring of acridinediones is avoided. A variety of highly potent



acridone compounds was synthesized, from which some acridone 3-ethers steamed as very promising scaffolds.<sup>106,107</sup>

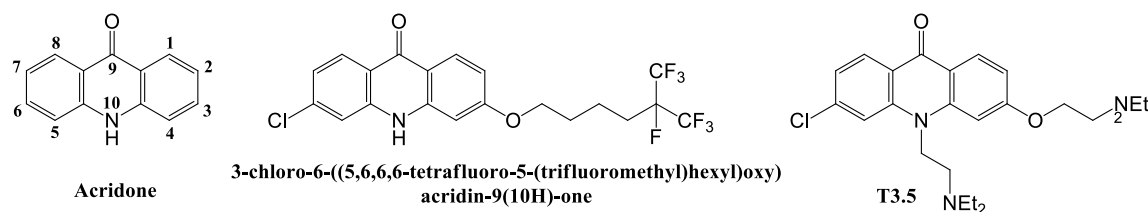


**Figure 1.26** – Structural representation of the acridone ring system and of antimalarially active 3-ether derivatives.

After synthesis and optimization, a compound with an *in vitro* activity of around 1 pM against *P. falciparum* (D6 and Dd2 strains) was selected for development. Considering its  $IC_{50}$ , this compound, **3-chloro-6-((5,6,6,6-tetrafluoro-5-(trifluoromethyl)hexyl)oxy)acridin-9(10H)-one** (Figure 1.26), appears to be the most effective antimalarial ever synthesized and tested in laboratory, although its mode of action is still unknown. It bears a flexible alkoxy side chain at C-3, which resembles the isoprenyl side chain of ubiquinones, terminating with two trifluoromethyl units. This flexibility, currently used at the side-chains, may lead to problems of selectivity. However, in this case, no toxicity problems were reported following *in vivo* tests.<sup>98,106,107</sup>

More recent studies with this class resulted in the synthesis of **T3.5** (Figure 1.26), an acridone derivative that incorporates a N-10 moiety that confers, additionally, a chemosensitization function (capacity to reverse *Plasmodium* resistance to classical antimalarial drugs, such as chloroquine).<sup>108</sup>

#### 1.3.5.4. Quinolones

The scientific community dedicated to malaria chemotherapy has placed a number of antimalarially active quinolones at various stages of pre-clinical development. These compounds contain the 4-oxo-1,4-dihydroquinoline (4(1H)-quinolone or 4-oxoquinoline) scaffold (Figure 1.27) and were shown to bind to the  $Q_o$  site of the cytochrome  $bc_1$  complex in 2008.<sup>55</sup>

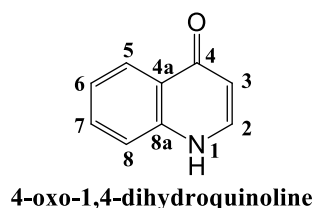


**Figure 1.27** – Structural representation of the quinolone scaffold.

This thesis is based on a PhD project that aims to explore the quinolone chemotype in view of the design and synthesis of quinolone-based antimalarial drugs. The rationale behind the use of these class is based on recent studies showing that selected quinolones are relatively potent against the blood, liver and transmission stages of malaria parasite, thus validating the selection on this chemotype in strategies for the development of drugs to eradicate malaria. However, additional studies are required in order to circumvent difficulties associated with quinolone compounds, including poor aqueous solubility and metabolic instability. Along this thesis, several aspects related to quinolones will be addressed.

## 1.4. Quinolones in medicinal chemistry

The versatility of the quinolone chemotype has attracted intense research for several decades among medicinal chemists, and the interest in this class of compounds does not appear to fade. Many quinoline derivatives are known for their pharmacological properties targeting a variety of diseases, *e.g.* bacterial infections,<sup>109,110</sup> cancer,<sup>111</sup> hepatitis,<sup>112,113</sup> HIV,<sup>114</sup> herpes,<sup>115</sup> fungal infections, immunodepression,<sup>116</sup> tuberculosis<sup>117</sup> or malaria.<sup>82,118–120</sup>

Chemically, the quinolones are a group of chemical analogues derived from a bicyclic aromatic fused six-membered heterocyclic nucleus containing one to four nitrogen atoms. Some classic examples are represented in Figure 1.28.<sup>121</sup>

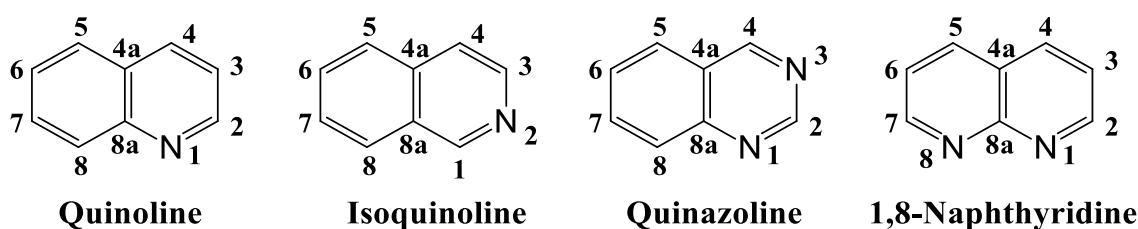


**Figure 1.28** – Structural representation of classic examples of the quinolone group.

### 1.4.1. From antibacterial to antimalarial agents

The use of quinolones as antibacterial agents (a well-established class of antibiotics) began in 1963, with the discovery of **nalidixic acid** (Figure 1.29), a 1,8-naphthyridone 3-acid, during the synthesis of the antimalarial agent, chloroquine. Nalidixic acid is an example of a *first-generation quinolone*, which common structural features are the ethyl group at N-1 position and the good Gram-negative activity. However, nalidixic acid never became a useful agent to treat systemic infections due to its narrow spectrum of action, poor tissue penetrability, rapid emergence of bacterial resistance and frequent adverse effects in the central nervous system.<sup>110,121,122</sup> However, this 1,8-naphthyridone provided the chemical foundations upon which modifications to improve the pharmacologic profile and limit adverse effects were built. More than 10 000 analogues of nalidixic acid were studied and/or synthesized and, after 20 years, only one analogue was approved for clinical use, the first fluoroquinolone antibiotic.<sup>121</sup>

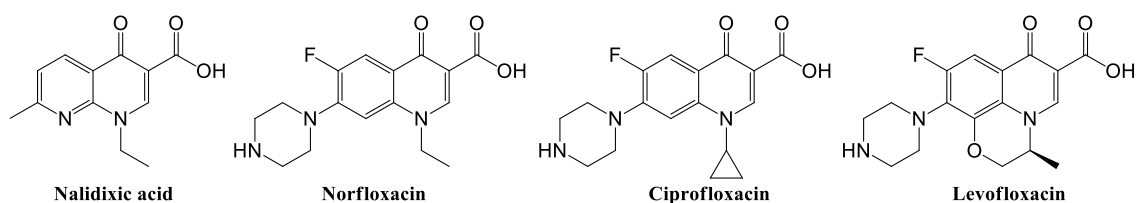


**Figure 1.29** – Structural representation of quinolones used as antibacterial agents.

Fluoroquinolones (Figure 1.29) are 4-oxo-quinolines (usually just named as quinolones) bearing a fluorine atom at C-6 that increases the activity of the compound against both Gram-negative and Gram-positive organisms and expands the spectrum of action. This atom is also responsible for improving the penetration of quinolones into bacterial cells. **Norfloxacin** and **ciprofloxacin** (*second-generation quinolones*) and **levofloxacin** (*third-generation quinolones*) are examples of fluoroquinolone antibiotics with a piperazine ring at position 7, a structural feature that appears to be essential for enhancing potency, spectrum of action and pharmacokinetic profile. However, the comparatively lower potency against some Gram-positive bacteria, particularly *S. aureus* and *Streptococcus pneumoniae*, the rapid development of quinolone-resistance by *Plasmodium* parasites and the remaining adverse effects have prompted further research towards a more general utility of fluoroquinolones.<sup>109,110</sup>

There are other aspects in the structure of fluoroquinolones that have direct impact on antibacterial activity: the 3-carboxylate and 4-carbonyl groups were found to mediate the binding to DNA gyrase and the transport across the bacterial membrane; and alterations at N-1, C-5 as well as at position 7 and 8 of the quinolone core were found to affect the potency, spectrum of activity, pharmacokinetics and safety profile.<sup>121</sup>

Norfloxacin, the first fluoroquinolone (approved in 1986), has poor tissue distribution, which limited its applications to the treatment of urinary tract infections. Over the following decades, several compounds have derived from this quinolone lead and, for example, modification of the substituent at N-1 to a cyclopropyl group led to ciprofloxacin (approved in 1987), an antibiotic with a better clinical success. Ciprofloxacin presents an excellent systemic activity upon oral administration and is one of the most frequently prescribed antibiotics.<sup>109</sup>

Levofloxacin, a *third-generation quinolone*, was approved in 1996. It is the levo isomer of the racemate ofloxacin (another quinolone antimicrobial agent). This generation exhibits more structural diversity (*e.g.* heteroaromatic ring between N-1

and C-8 for levofloxacin; and methylation of the piperazine ring at position 7 for other analogues not presented in this work) that results in novelties regarding biological properties. The *third-generation quinolones* preserve excellent potency against Gram-negative bacteria while showing an increased activity towards Gram-positive bacteria, compared to ciprofloxacin.<sup>109,110</sup>

The pharmacologic properties of fluoroquinolones justify their extensive use as second line therapeutics, not only in urinary tract infections but also for the treatment of certain sexually transmitted diseases, prostatitis, gastrointestinal infections, nosocomial acquired pulmonary infections, pseudomonas infections and osteomyelitis.<sup>109</sup>

Other structural modifications may bring further improvements in the usefulness of fluoroquinolones for treatment of mycobacterial infections. The structural relationship of the quinolone core with some antimalarial drugs (for example atovaquone) can open new perspectives for the malaria treatment. Quite interesting is the fact, that during 1980s and 1990s, fluoroquinolones antibiotics, such as ciprofloxacin, were shown to have antimalarial properties, and the possibility of replacing the failing aminoquinolines by fluoroquinolones was considered, despite the lower potency of fluoroquinolones. However, the advent of more promising antimalarial drugs, like artemisinin, devalued the use of fluoroquinolones in malaria.<sup>123–125</sup>

#### **1.4.2. State of the art: endochin and endochin like quinolones (ELQ)**

The activity of quinolones against malaria was established in the 1940s with the synthesis of **endochin** (Figure 1.30).<sup>98</sup> The antimalarial activity of endochin has been known since 1948, after disclosure by Bayer of evidence for its synthesis and activity against avian malaria, both as a prophylactic as a therapeutic agent. Further research with this compound established that it was active against the liver and blood stages of parasites. However, it was demonstrated that endochin is ineffective in mammal models due to its rapid metabolism to inactive metabolites by cytochrome P450 enzymes.<sup>106,126,127</sup> Besides that, the quinolone core continued to be considered as model for potential antimalarial compounds.

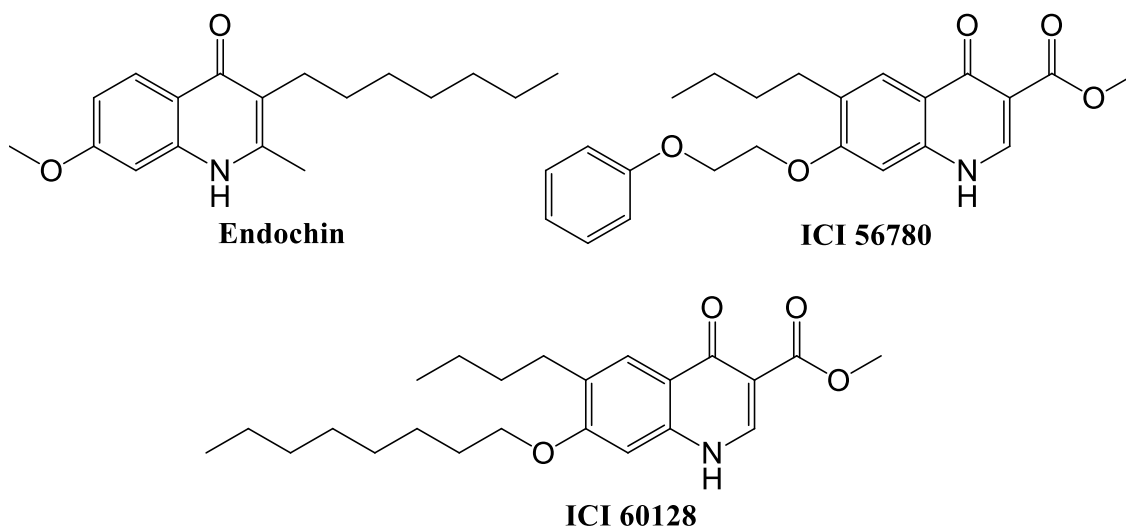


**Figure 1.30** - Structural representation of endochin, by Bayer, and quinolone 3-esters, by Ryley.

Ryley *et al.*, during their research for anticoccidial drugs, noted that a number of the quinolone 3-esters developed (*e.g.* **ICI 56780** and **ICI 60128**; Figure 1.30) were active against malaria (in rodent and monkey models), both as prophylaxis and treatment. These compounds appeared to be effective against all stages of the parasite (with a potency of up to 50 times that of chloroquine) and also against chloroquine resistant strains but there were problems related to fast resistance development in rodent models.<sup>128</sup>

Recent advances suggest that previously abandoned lead molecules may be reexamined to generate more robust and potent analogues. A good example is the development of new endochin analogues (or endochin like quinolones – ELQ) with improved therapeutic properties compared to the parent compound. For example, in 2008, Riscoe and Winter found that by extending the 3-heptyl chain of endochin to an undecyl (11C) chain, and terminating with a trifluoromethyl moiety (synthesis of **ELQ-103**, Figure 1.31), the activity against *P. falciparum* chloroquine resistant parasite strains was doubled *in vitro* ( $IC_{50}$  1.4nM vs 2.8nM). Additionally, the cross-resistance for atovaquone resistant parasite strains was significantly diminished ( $IC_{50}$  4.7nM vs 17.4nM for endochin). However, the solubility and *in vivo* activity of this compound was still very poor.<sup>106</sup>

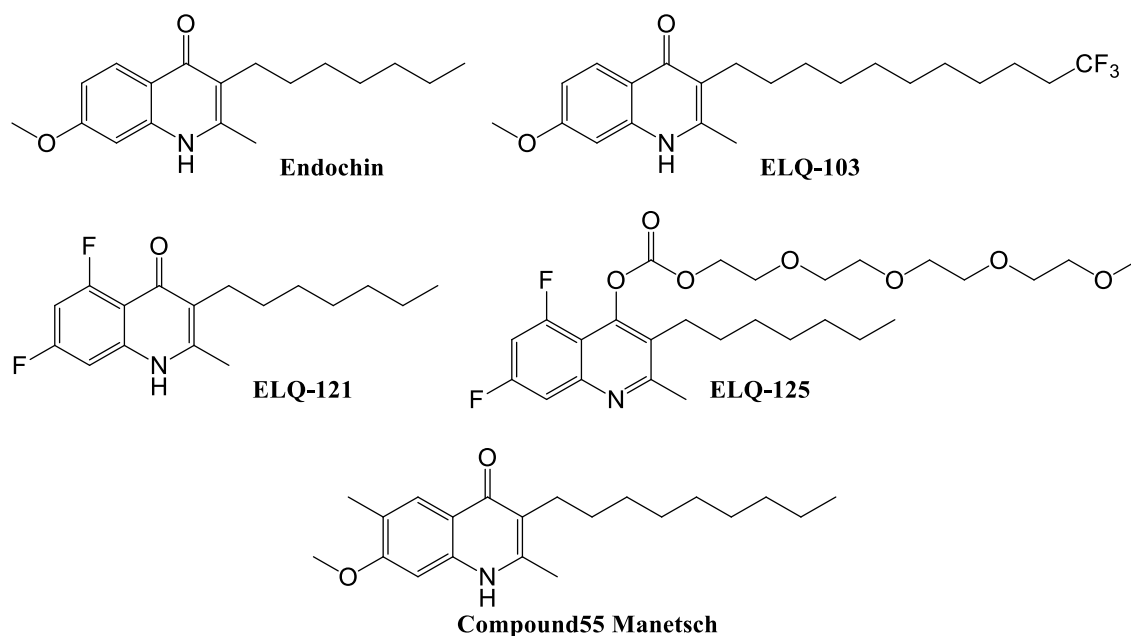


**Figure 1.31** – Structural representation of endochin and of ELQs, studied by Riscoe *et al.* and Manetsch *et al.*.

In 2011, the same research group, in an effort to increase solubility and reduce metabolic instability, optimized the structure of ELQ-103 by changing the substitution pattern of the quinolone ring. From a library with several ELQs, **ELQ-121** (Figure 1.31) was established as a new lead, exhibiting a potency 10-fold higher than ELQ-103 and enhanced metabolic stability. However, ELQ-121 exhibited increased cross-resistance with atovaquone when compared to ELQ-103. The problem of solubility was not circumvented by this drug, but its prodrug (with a poly(ethylene) glycol group linked to the oxygen of the quinolone core) **ELQ-125** (Figure 1.31) demonstrated a better solubility profile.<sup>129</sup>

Manetsch *et al.* designed and synthesized several endochin-type quinolones to better understand the structure-activity relationship (SAR) profiles against *P. falciparum*. Some important aspects about SAR were established: the carbonyl at position 4 and the lack of substitution at N-1 are key factors; a halogen substituent (chlorine) at C-6 and/or a methoxy group at position 7 enhance activity and reduce cross-resistance; shortening the 3-alkyl chain length increases the solubility but results in a dramatic reduction in parasite selectivity (alkyl chain with at least 7 carbons at C-3 is preferred); and 3-aryl substituted analogues exhibit a drop in potency, but less severe, while both solubility and metabolic stability are much improved. The most potent analogue from the library studied by Manetsch *et al.* is represented in Figure 1.31 – **Compound55 Manetsch**.<sup>130</sup>

More recently, Manetsch and Riscoe studied analogues containing a diarylether substituent at C-3 and, from them, the *P. falciparum*  $bc_1$  complex inhibitor **ELQ-300** (Figure 1.32), was selected as a preclinical candidate ( $IC_{50}$  around 1.8nM against chloroquine resistant strains). Considering the side chain of the previously described pyridone (**GW844520**) and the endochin structure, **ELQ-271** (Figure 1.32) was synthesized and, by introduction of a methoxy substituent at C-7 and a chlorine substituent at C-6, originated ELQ-300. In preclinical studies with mice, ELQ-300 was found to be highly active against *P. falciparum* and *P. vivax* at all life cycle stages that play a role in the transmission of malaria, and to have good oral bioavailability. ELQ-300 was also shown to have no effect on intracellular ATP levels in two different mammalian cell lines (no toxicity) and no cross-resistance with atovaquone was observed.

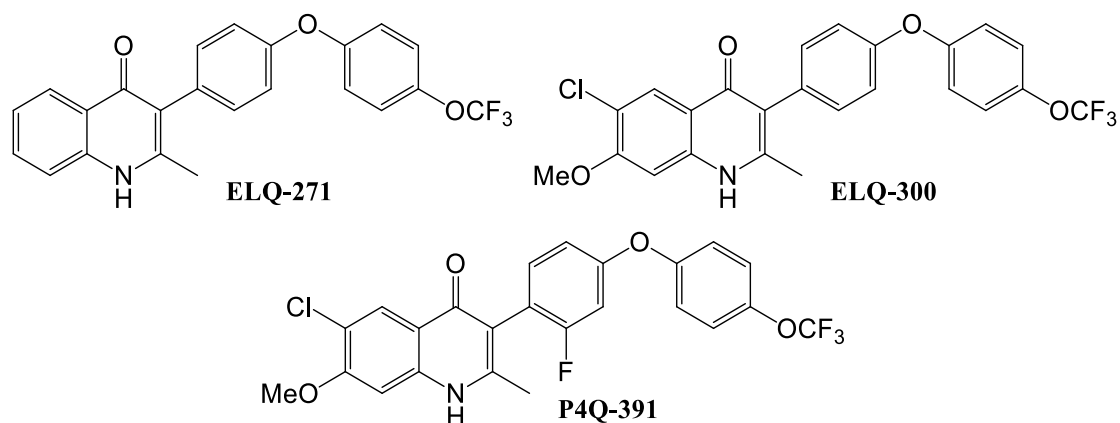


**Figure 1.32** – Structural representation of ELQ-300 (a preclinical candidate), its precursor ELQ-271 and the analogue P4Q-391.

Compound **P4Q-391** (Figure 1.32), containing a fluorine substituent in the diaryl ether side chain, has also demonstrated a promising profile ( $IC_{50}$  of around 7.6nM against chloroquine resistant strains). However ELQ-300 was shown to be more potent and selective.<sup>131</sup>

In parallel, Da Cruz *et al.* and Cowley *et al.* have investigated 3-ester substituted quinolones as *P. falciparum*  $bc_1$  complex inhibitors. From the libraries investigated, Da Cruz *et al.* have selected **decoquinate** (Figure 1.33) as the most potent compound against the liver stages ( $IC_{50}$  around 2.6nM)<sup>132</sup>, while Cowley *et al.*, have demonstrated by SAR studies that **RCQ** (Figure 1.33) is a highly potent antimalarial, exhibiting an  $IC_{50}$  value of 0.46nM.<sup>120</sup>



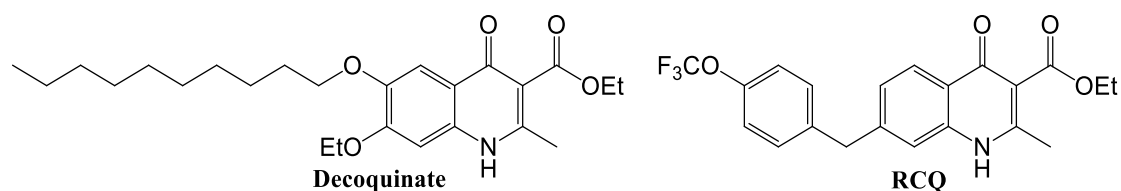


**Figure 1.33** – Structural representation of decoquinate and RCQ, proposed by Da Cruz et al. and Cowley et al., respectively.

Some quinolones derivatives are also known as potential inhibitors of *Pf*NDH2 in the respiratory chain of *P. falciparum*. **Hydroxy-2-dodecyl-4-(1H)-quinolone (HDQ)**, represented in Figure 1.34, exhibits inhibitory activity both towards *Pf*NDH2 and the *bc*<sub>1</sub> complex and, as such, was used as a starting point for drug discovery, leading to libraries with several new quinolone analogues with promising antimalarial activities. This multi-target inhibition confers a benefit over the single-target inhibition, due to delay in selection for drug resistance.<sup>82</sup>

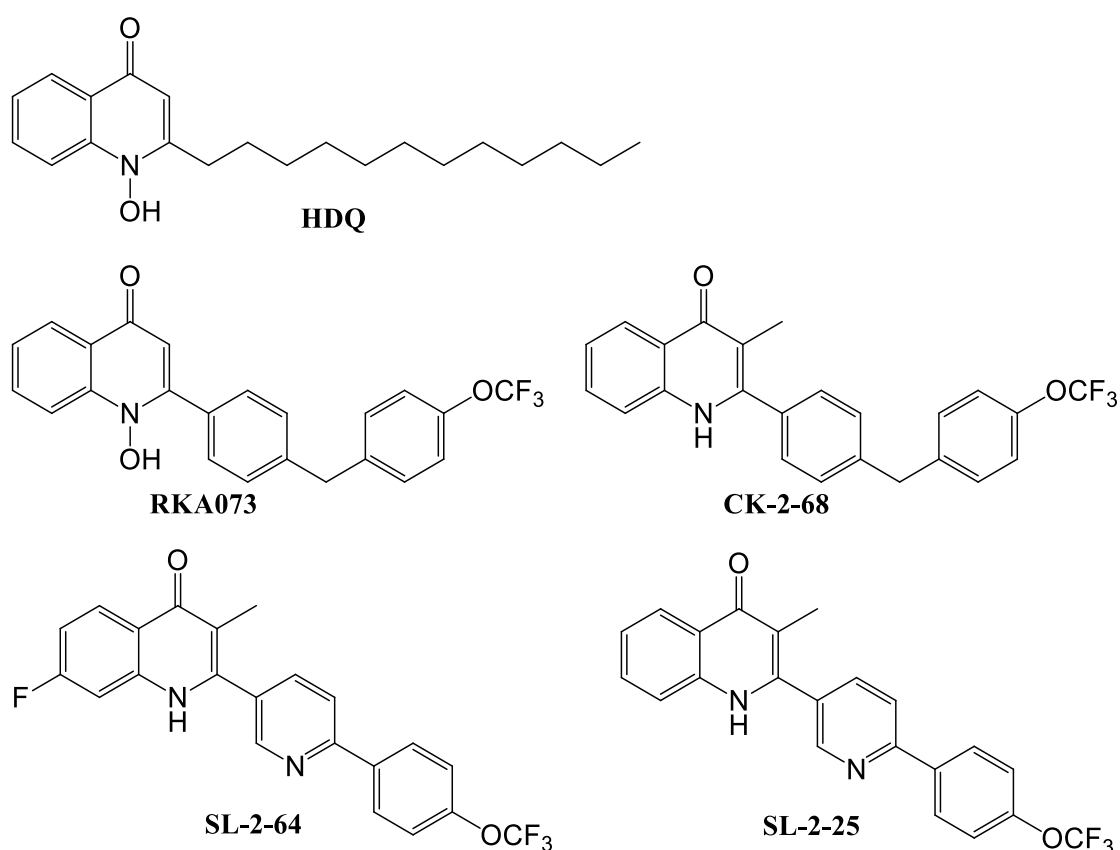


**Figure 1.34** – Structural representation of HDQ and of some quinolones substituted at positions 2 and/or 3 (studied by Pidathala *et al.* and Leung *et al.*).

The metabolic liabilities evidenced by HDQ led to additional structural alterations. Pidathala *et al.* changed the HDQ-side chain at position 2, to a biaryl or phenoxy biaryl (*e.g.* **RKA073**, Figure 1.34). After conversion of N-OH to N-H and

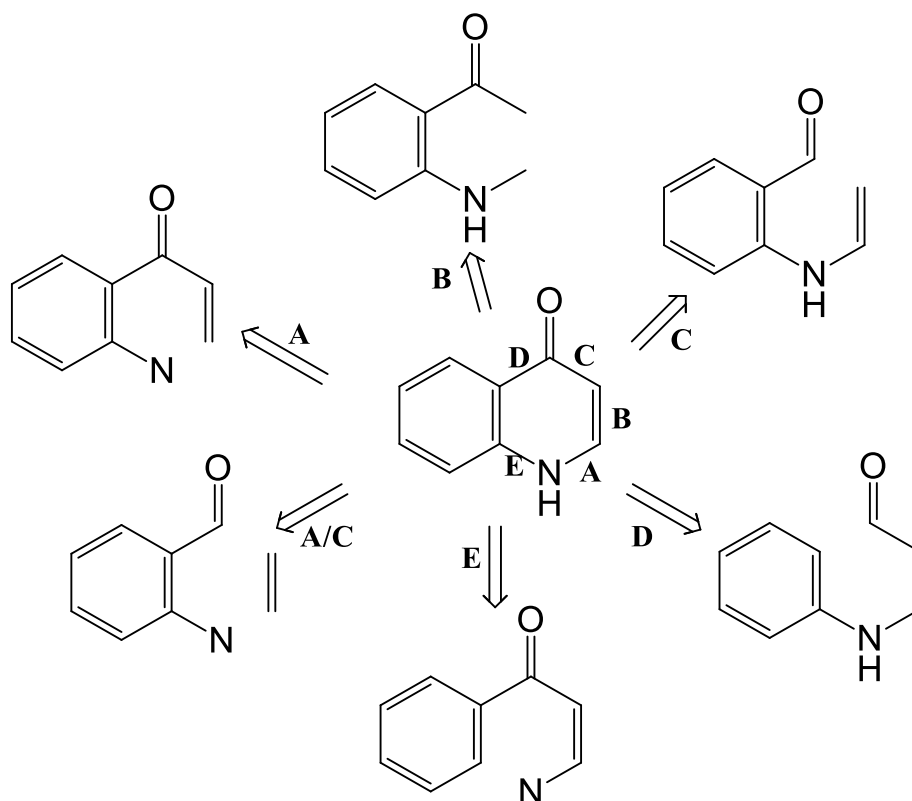
introduction of 7-Cl and 3-methyl substituents, **CK-2-68** (Figure 1.34) was selected as a lead for further development, showing an activity *in vivo* of 31nM against *P. falciparum*, compared with 263nM for RKA073.<sup>118</sup> Leung *et al.* introduced a heterocyclic substituent (pyridine group) into the quinolone side chain to improve solubility, leading to the analogs **SL-2-64** and **SL-2-25** (Figure 1.34) that evidenced IC50 values of 75nM and 54nM, respectively, against whole-cell *P. falciparum*.<sup>119</sup> It was observed that, when moving from 2-aryl to 3-aryl substituted analogues, there is a loss in *Pf*NDH2 activity.<sup>118,119</sup>

### 1.4.3. Synthetic routes to the 4-oxo-quinoline core

Given the interest of quinolones in major areas, including medicinal chemistry, the availability of mild, high yielding, selective and versatile synthetic routes to this class is a matter of utmost relevance.

Skraup reported on the first formal synthesis of the quinoline core (part of the structure of quinine), over a century ago.<sup>133</sup> Later, several variations to the original Skraup synthesis and new methods have been reported to afford quinoline derivatives, such as the Combes reaction,<sup>134</sup> the Friedländer synthesis,<sup>135</sup> the Doebner-von Miller synthesis,<sup>136</sup> the Pfitzinger-Borsche reaction<sup>137</sup> and the Povarov reaction.<sup>138</sup>

In parallel, many different synthetic approaches have been developed for 4-oxo-quinoline synthesis, from a variety of starting points. These can be classified according to the bond or bonds that complete the ring-closure and the method used to increase the carbon chain length. A retrosynthetic diagram showing the possibilities for construction of the quinolone ring is represented in Scheme 1.1 and some of the available methodologies are described in following subtopics.

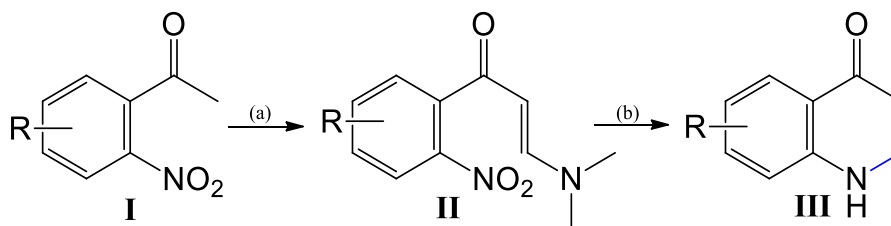


**Scheme 1.1** – Approaches to the preparation of the 4-oxo-quinoline scaffold.

#### 1.4.3.1. Cyclisation of *ortho*-COR-substituted aromatic amines

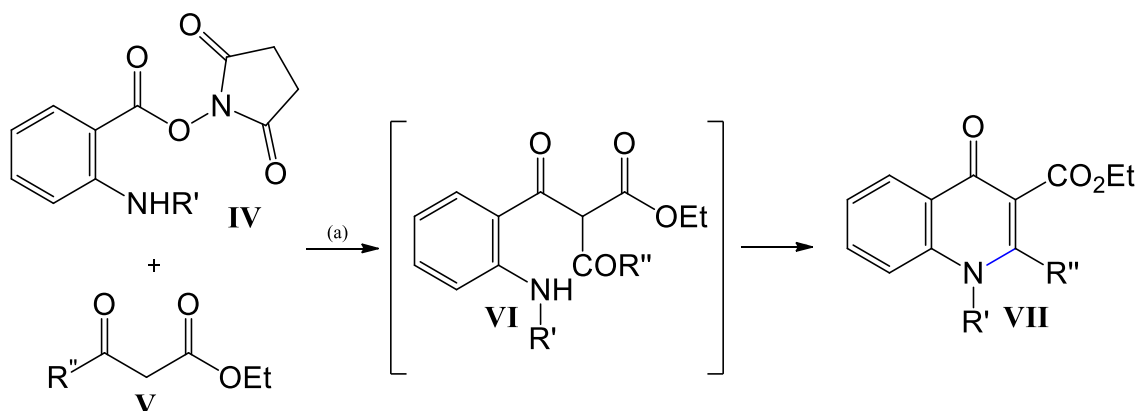
For ring closure to form quinolones through formation of A (Scheme 1.2 and Scheme 1.3) to afford 4-oxo-quinolines, two methods of cyclisation of *ortho*-COR-substituted aromatic amines were proposed, by Koskinen<sup>139</sup> and Igglessi-Markopoulou<sup>140</sup> groups.

Following Koskinen procedure (Scheme 1.2) it is possible to synthesize 2,3-unsubstituted 4-oxo-quinolines (**III**) from an enamine (**II**) under reducing conditions, in cyclohexene, using 10% Pd on charcoal as catalyst. Enamine **II** may be synthesized by condensation of *o*-nitroacetophenone (**I**) with N,N-dimethylformamide dimethylacetal ((CH<sub>3</sub>)<sub>2</sub>NCH(OCH<sub>3</sub>)<sub>2</sub>) in N,N-dimethylformamide (DMF).<sup>139</sup>



**Scheme 1.2** – Schematic representation of the synthetic approach to 2,3-unsubstituted 4-oxo-quinolines, proposed by Koskinen. Conditions: (a) (CH<sub>3</sub>)<sub>2</sub>NCH(OCH<sub>3</sub>)<sub>2</sub>, DMF, 100 °C, 90 minutes; (b) 10% Pd, cyclohexene, ethanol, reflux, 60 minutes.<sup>139</sup>

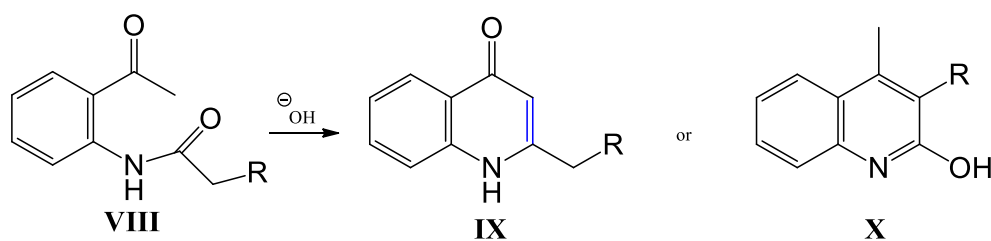
Igglessi-Markopoulou *et al.* (Scheme 1.3) described a methodology for the synthesis of 3-ethoxycarbonyl 4-oxo-quinolines (**VII**). This methodology involves acylation of  $\beta$ -keto esters (**V**) with N-hydroxysuccinimide esters of anthranilic acids (**IV**). The conjugates formed (**VI**) progress spontaneously to the corresponding quinolone 3-esters, through cyclisation.<sup>140</sup>



**Scheme 1.3** – Schematic representation of the synthetic approach to 3-ethoxycarbonyl 4-oxo-quinolines, proposed by Igglessi-Markopoulou group. Conditions: (a) NaH, benzene, 3-5 days, room temperature (rt).<sup>140</sup>

#### 1.4.3.2. Camps cyclisation

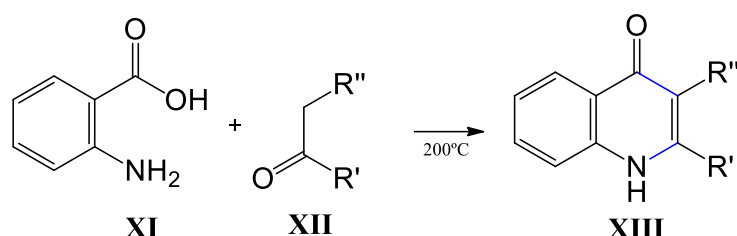
The Camps cyclisation is a base catalysed ring closure methodology to form quinolones, through formation of bond *B* (Scheme 1.4). This methodology provides an access to 2-substituted 4-oxo-quinolines (**IX**). However, depending of the conditions and starting material, the same methodology can also be used to prepare 2-hydroxy-quinolines (**X**).<sup>141</sup>



**Scheme 1.4** – Schematic representation of the Camps cyclisation methodology.<sup>141</sup>

#### 1.4.3.3. Niementowski quinoline synthesis

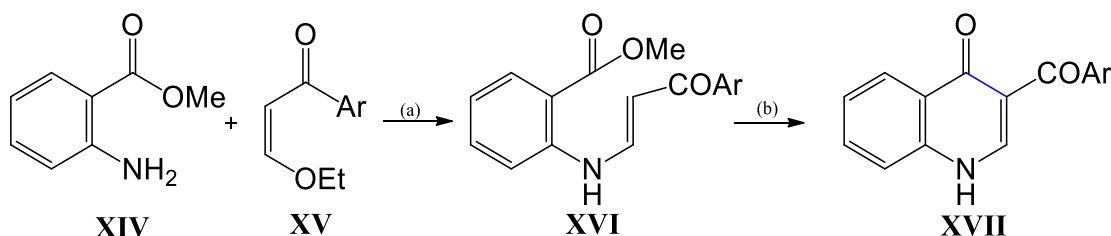
The Niementowski methodology for quinoline synthesis consists in the condensation of anthranilic acids (**XI**) with ketones (**XII**) or aldehydes, at 200 °C, to form 2,3-substituted 4-oxo-quinolines (**XIII**) or 3-substituted 4-oxo-quinolines, respectively.<sup>142</sup> It is a cyclisation reaction leading to a bicyclic core through the formation of bonds *A* and *C* (Scheme 1.5).



**Scheme 1.5** – Schematic representation of the Niementowski methodology for quinoline synthesis.<sup>142</sup>

#### 1.4.3.4. Cyclisation from a Michael-type addition product

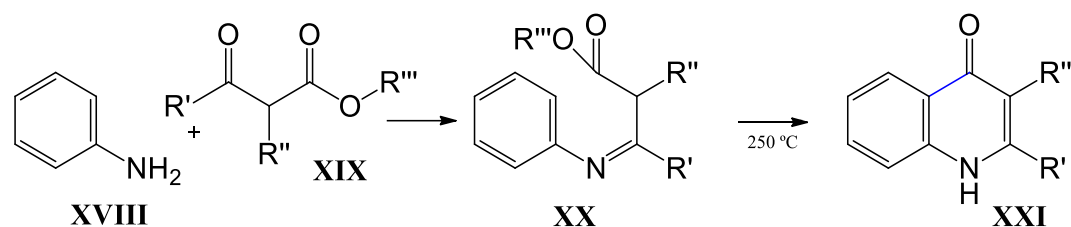
The preparation of 3-aryl 4-oxo-quinoline derivatives (**XVII**) through formation of bond *C* (Scheme 1.6) may be carried out, for example, by a Michael-type addition of methyl anthranilate (**XIV**) to  $\beta$ -ketonic enol ethers (**XV**). From this conjugate addition results a Michael adduct (**XVI**) that, through based promoted cyclisation originates the 4-oxo-quinoline derivatives **XVII**. The ring closure is facilitated by heating at reflux in diphenyl ether, in the presence of sodium methoxide.<sup>143</sup>



**Scheme 1.6** – Schematic representation of the synthetic approach to 3-aryl 4-oxo-quinolines, proposed by Hénichart group. Conditions: (a) THF (tetrahydrofuran),  $\text{ZnCl}_2$ , rt, 24 hours. (b)  $\text{MeONa}$ ,  $\text{Ph}_2\text{O}$ , reflux ( $240^\circ\text{C}$ ), 4 hours.<sup>143</sup>

#### 1.4.3.5. Conrad-Limpach synthesis

The Conrad-Limpach methodology can be used for the construction of 4-oxo-quinoline derivatives (**XXI**) from the condensation of anilines (**XVIII**) with  $\beta$ -keto esters (**XIX**). The reaction affords an imine (**XX**) as intermediate, which must be heated at  $250^\circ\text{C}$  for the ring closure to occur by the formation of the bond *D* (Scheme 1.7). This methodology can produce quinolones with various substitution patterns, defined by the nature and pattern of substitution present at starting compounds, the aniline and the  $\beta$ -keto esters.<sup>144</sup>

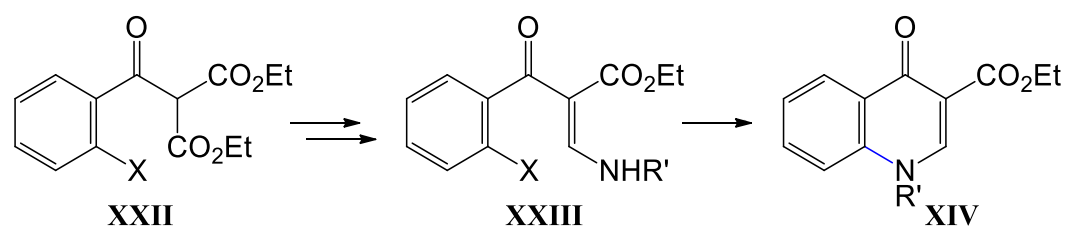


**Scheme 1.7** – Schematic representation of the Conrad-Limpach strategy for quinolone synthesis.<sup>144</sup>

The group of reactions based on closure of bond *D* includes some of the most numerous methods used for the synthesis of 4-oxo-quinolines. The Gould-Jacobs reaction is one adaptation of the Conrad-Limpach synthesis and was chosen as synthetic methodology during the development of our research. As such, the Gould-Jacobs reaction will be discussed in deeper detail in the next section.

#### 1.4.3.6. Cyclisation by formation of bond *E* (multistage reactions)

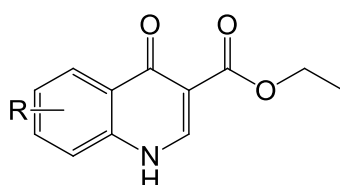
Various substituted 4-oxo-quinolines can be obtained by the formation of bond *E* (Scheme 1.8) and some examples have been reviewed. Scheme 1.8 presents an example of application of a methodology that includes multistage reactions with successive transformations, in which amino vinyl phenyl ketones (XXIII) are formed (for example by hydrolysis, decarboxylation and transamination reactions from XXII). The ring closure at the last stage involves the halogen atom (X) at the *ortho* position of the aryl substituent in XXIII. The cyclisation step to the formation of 4-oxo-quinolines (XXIV) can be achieved in the presence of various reagents.<sup>145</sup>



**Scheme 1.8** – Schematic representation of the synthetic approach to quinolones involving cyclisation by formation of bond *E*, including multistage reactions.<sup>145</sup>

## 1.5. PhD project's presentation

The discovery of the antimalarially active quinolones ICI 56780 and ICI 60128 (Figure 1.30) followed by more recent research on compounds with antimalarial properties based on the quinolone 3-carboxyl core structure (decoquinate and RCQ; Figure 1.33), led us to further investigate the potential of quinolone 3-esters as antimalarials. Besides the inhibitory capacity showed, the compounds mentioned above also present pharmacological liabilities, such as the relatively fast development of resistance, cross-resistance, poor solubility and metabolic instability. As such, a deeper investigation of the structure and properties of this class was considered relevant for the design and preparation of quinolone 3-esters, aiming at the development of new, safe and effective antiplasmodial drugs targeting the *bc<sub>1</sub>* protein complex of *P. falciparum*. We proposed the design, synthesis and structural study of a library of new 4-oxo-quinoline 3-esters bearing different functional groups at positions 6 and/or 7 of the quinolone structure. The structure of the quinolone template proposed (Figure 1.35) includes the key groups required for a *bc<sub>1</sub>* inhibitor (N-H and 4-carbonyl of the quinolone core), in accordance with data from docking studies.<sup>120</sup>



**4-Oxo-quinoline template**

**Figure 1.35** – General structure for 4-oxo-quinoline 3-esters investigated.

The synthetic methodologies and reaction conditions used were optimized and some compounds prepared have been tested for activity *in vitro* against *P. falciparum*. A detailed structural investigation was undertaken on selected compounds. This information is relevant for a better understanding and prediction of chemical reactivity and activity. For the investigation of monomeric structure, contemporary DFT (density functional theory) methods (for theoretical analysis) and matrix isolation techniques coupled to FTIR (Fourier-transform infrared) spectroscopy (for experimental analysis) were used. For the investigation of solid-state structure, X-ray crystallography and spectroscopic techniques were used. Docking studies were also conducted to improve the knowledge regarding drug-target interaction for this class. Additionally, selected quinolones prepared in this project were tested for activity against *Mycobacterium tuberculosis*.

The PhD project in which this thesis is based can be divided in four parts:

- A - Synthesis of quinolone 3-esters with potential activity against *P. falciparum*;
- B – Structural investigation of selected quinolone 3-esters;
- C – Docking studies, CLogP calculations and evaluation of antimalarial activity;
- D - Synthesis of selected quinolone derivatives and evaluation of activity against *M. tuberculosis*.

Along the thesis, a similar distribution of topics will be adopted.

This project benefited from established collaborations between CCMar, Universidade do Algarve (Portugal), and other national and international institutions: CQC, Departamento de Química, Universidade de Coimbra (Portugal); CFisUC, Departamento de Física, Universidade de Coimbra (Portugal); Department of Chemistry, University of Liverpool (United Kingdom); Liverpool School of Tropical Medicine, University of Liverpool (United Kingdom); and CMDT and Instituto de Higiene e Medicina Tropical, Universidade Nova de Lisboa (Portugal).



---

# ***CHAPTER TWO***

---

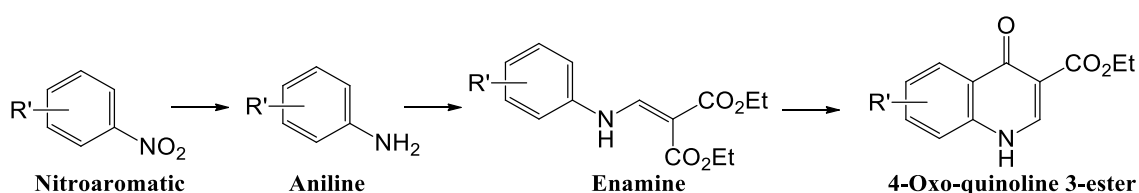
## **RESULTS AND DISCUSSION**

**Synthesis of quinolone 3-esters with  
potential activity against *P. falciparum***



## 2.1. General synthetic approach

In this chapter the synthesis of 4-oxo-quinoline 3-esters substituted at position 7 and/or 6 is described and discussed. The general synthetic approach to these compounds is presented in Scheme 2.1. Three main steps are highlighted in the synthetic strategy proposed: (i) reduction of nitro aromatic compounds, *meta* and/or *ortho* substituted, to the corresponding anilines; (ii) coupling of the aniline with diethyl (ethoxymethylene)malonate (DEEMM) to afford the enamine derivative ( $\alpha,\beta$ -unsaturated ester); (iii) thermally driven intramolecular cyclisation (Gould-Jacobs methodology) to prepare the final 4-oxo-quinoline 3-esters. The reactions involved in each step are described in detail in sections 2.1.1 and 2.1.2.

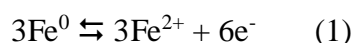


**Scheme 2.1** - Schematic representation of the general synthetic approach to prepare 4-oxo-quinoline 3-esters derivatives.

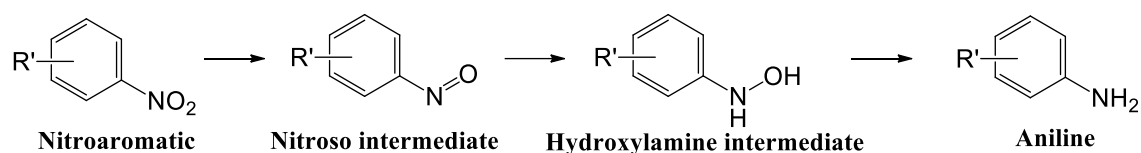
### 2.1.1. Reduction of nitro aromatic compounds to aniline derivatives

The reduction of nitro compounds in the presence of zero-valent metals (*e.g.* Fe, Zn or Sn) is well documented and has been widely used in the synthesis of amines. Iron was one of the first metals employed for the reduction of organic compounds, around 150 years ago, but the detailed molecular mechanism for the reduction is still not well understood.<sup>146–148</sup>

In general, Fe-catalysed reductions are carried out in aqueous media. However, it is common to add methanol or ethanol to increase the solubility of the organic compounds in the medium. It is proposed that, initially, in aqueous system, the zero-valent iron metal ( $\text{Fe}^0$ ) is oxidized to ferrous iron ( $\text{Fe}^{2+}$ ), acting as electron donor, as described by equation (1). Ammonium chloride acts as proton donor, assisting in the conversion of the nitro to the amino group.



The nitro group is then converted to aniline via intermediate species with various degrees of reduction, such as nitroso- and hydroxylamine compounds, in a process that consists of a series of two-electron additions (Scheme 2.2). Products resulting from coupling of reduction intermediates may also be formed, compromising the yield of the product required.<sup>147,148</sup>



**Scheme 2.2** – Schematic representation of reduction pathway for conversion of nitro arenes to the corresponding anilines, via nitroso and hydroxylamine intermediates.<sup>147,148</sup>

Formally, the overall nitro-to-amino reduction is a six-electron-transfer reduction, classically described by equation (2):

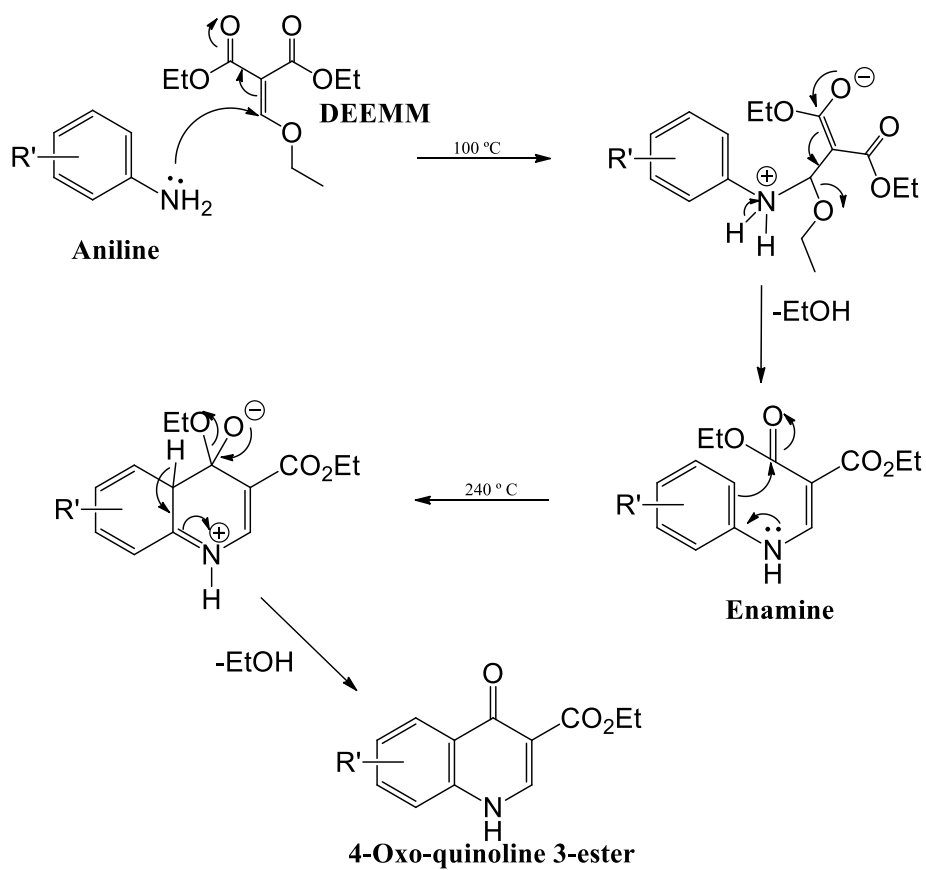


In the general synthetic strategy to quinolone 3-esters (Scheme 2.1) this step can be skipped if the desired aniline is commercially available.

### 2.1.2. Coupling of the aniline derivative with DEEMM and Gould-Jacobs cyclisation

The enamine derivative required for cyclisation to the quinolone is prepared by coupling the aniline with an  $\alpha,\beta$ -unsaturated ester (usually a malonate derivative). Malonic derivatives are very useful reagents in organic synthesis, especially in strategies to afford 5-, 6- or 7-membered rings, enabling the preparation of a variety of “malonyl heterocycles”. In this work we chose diethyl (ethoxymethylene)malonate (DEEMM) as the malonate derivative for the synthesis of 4-oxo-quinoline compounds bearing an ethyl ester group at position 3.<sup>149,150</sup> From the solvent free reaction of an aniline derivative with DEEMM, at 100 °C, an enamine ester is synthesized (Scheme 2.3). This intermediate step allows incorporation of functionalities, such as esters and nitriles, at position 3 of the 4-oxo-quinoline compound.

The enamine ester is then converted to quinolone using the Gould-Jacobs reaction. This methodology was published in 1939 and consists in an adaptation of the Conrad-Limpach synthesis. The mechanism proposed for the Gould-Jacob reaction is represented in Scheme 2.3. In this cyclisation, conducted at 240-250 °C, the aromatic ring acts as nucleophile, attacking the carbon of the ester carbonyl group and leading to a thermally driven intramolecular cyclisation.<sup>149</sup>



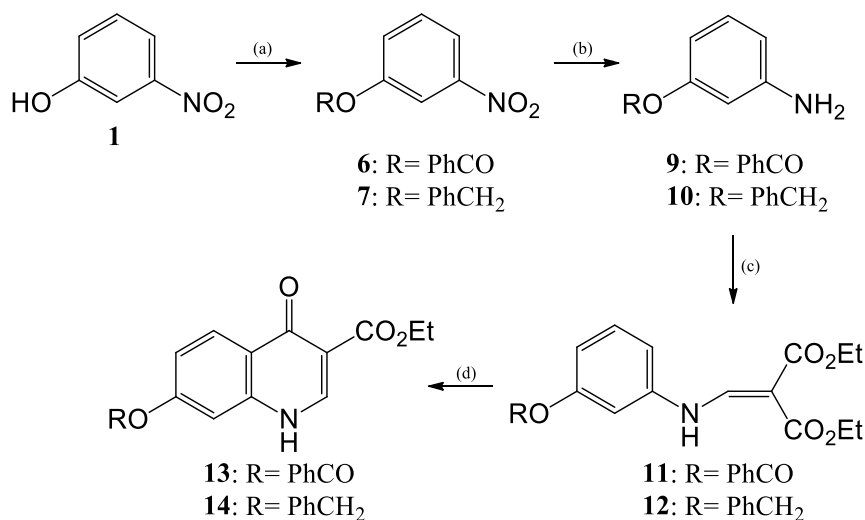
**Scheme 2.3** – Schematic representation of the mechanism proposed for the Gould-Jacobs synthesis of 4-oxo-quinoline 3-esters.<sup>149</sup>

## 2.2. Exploring position 7 – modifying O-link

Following the work of O'Neil's group, and establishing the ethyl ester group as standard in the position 3, the preparation of a library of compounds with chemical diversity at position 7 was envisaged. The compounds prepared and synthetic methods followed are described below.

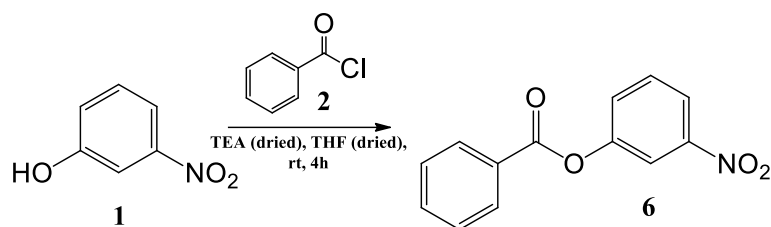
### 2.2.1. Preparation of 4-oxo-quinolines with ester or ether linkage at position 7

These compounds were prepared from 3-nitrophenol (**1**), by modification of the hydroxyl group. The synthetic approach is presented in Scheme 2.4. 3-nitrophenol (**1**) was used, instead of an aniline derivative, to avoid a side reaction resulting from the nucleophilic attack by nitrogen (Ar-NH<sub>2</sub>). Therefore, **1** was used as the starting material. After modification of the hydroxyl groups, the reduction step was conducted, followed by coupling with DEEMM and then by thermal cyclisation in Dowtherm A to afford the required 4-oxo-quinoline 3-ester derivatives (Scheme 2.4).

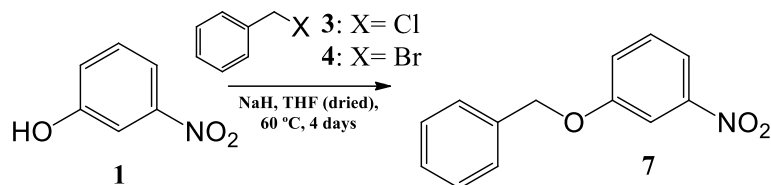


**Scheme 2.4** – General synthetic approach followed to prepare 7-ester and 7-ether substituted 4-oxo-quinoline 3-esters. Conditions: (a) variable and adapted conditions according with the R; (b) NH<sub>4</sub>Cl, Fe, MeOH:H<sub>2</sub>O (1:1), 60 °C, 4 hours; (c) 100 °C, overnight; (d) Dowtherm A, 250 °C, 3 hours.

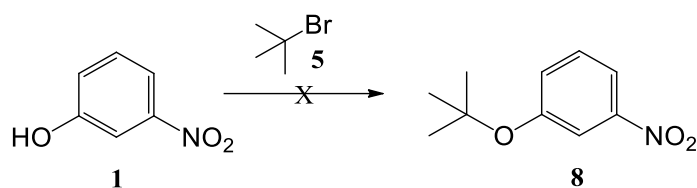
The hydroxyl group was modified introducing directly the intended residue, through reaction with benzoyl chloride **2** or benzyl derivatives **3** (chlorine) / **4** (bromine), to afford a diphenyl ester **6** (Scheme 2.5) or a diphenyl ether **7** (Scheme 2.6), respectively. A similar procedure was used for the synthesis of 1-(*tert*-butoxy)-3-nitrobenzene (**8**) using *tert*-butyl bromide (**5**) as halide derivative (Scheme 2.7), however, the required product was not obtained.



**Scheme 2.5** – Esterification of 3-nitrophenol to afford 3-nitrophenyl benzoate **6**.



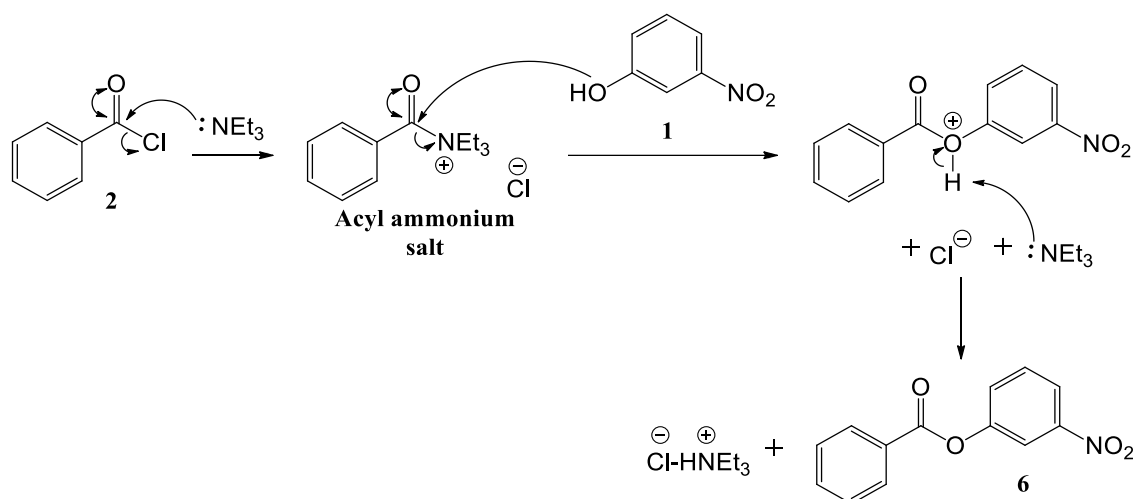
**Scheme 2.6** – Etherification of 3-nitrophenol to afford 3-nitrophenyl benzyl ether **7**.



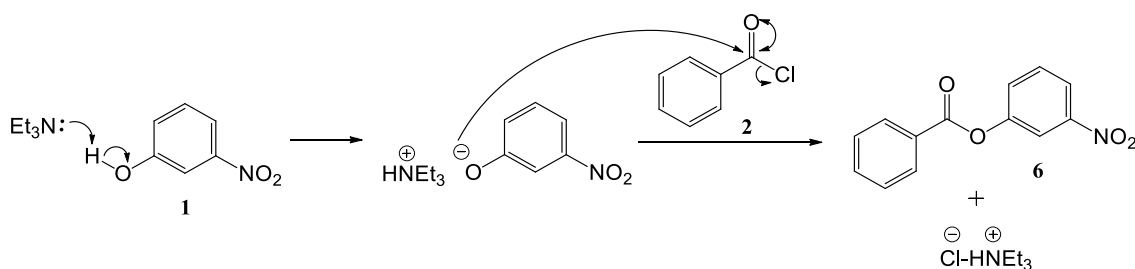
**Scheme 2.7** – Attempted etherification of 3-nitrophenol to afford compound **8**.

3-Nitrophenyl benzoate **6** was obtained as white needles, in good yield (91%), after work-up and crystallization. The procedure for this reaction includes the use of triethylamine as base. Considering the high reactivity of the acyl chlorides (**2**), for example with alcohols (**1**), this reaction is extremely rapid, complicating mechanistic studies. From the literature, two mechanisms, represented in Scheme 2.8 and Scheme 2.9, may be considered.

The mechanism presented in Scheme 2.8 involves attack to the carbonyl bond of **2** by the amine, forming a quaternary acyl ammonium salt after displacement of the chlorine atom. This salt is susceptible to attack by the hydroxyl group of **1**, leading to **6** as the final product. Another mechanistic proposal considers deprotonation of the hydroxyl group of **1** and subsequent attack of the phenoxide to the carbonyl carbon of **2** (Scheme 2.9).<sup>151</sup>



**Scheme 2.8** – Schematic representation of a mechanistic proposal for the triethylamine-catalysed esterification to afford 3-nitrophenyl benzoate **6**.<sup>151</sup>



**Scheme 2.9** – Representation of an alternative mechanistic proposal for the TEA-catalysed esterification to afford compound 3-nitrophenyl benzoate **6**.<sup>151</sup>

As shown in Scheme 2.8 and Scheme 2.9, triethylamine hydrochloride (triethylammonium chloride) is a secondary product from the amine-catalysed esterification described. Clearance of the triethylamine (TEA) in excess, after reaction, can be improved with the acidification with HCl that leads to formation of more triethylammonium chloride salt, which is easily removed because of the higher affinity for the aqueous layer (during extraction).

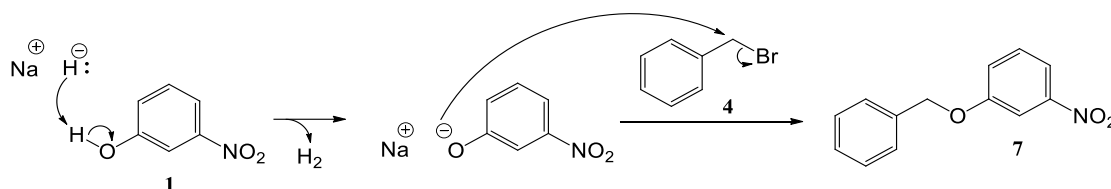
A similar procedure was carried out to afford 1-benzyloxy-3-nitrophenyl **7** from benzyl chloride **3**, but as the yield was poor, an alternative procedure was implemented: NaH for prior deprotonation of the phenol. Benzyl chloride **3** bears a carbon-halogen bond conferring electrophilicity to this carbon (-CH<sub>2</sub>-), but not as great as for the carbonyl carbon of benzoyl chloride (**2**) and, therefore, a stronger base is required for the formation of **7** from **3**.

However, the product **7** was recovered with a low yield (34%) after purification by column chromatography, so the synthesis was repeated, but replacing benzyl chloride **3** by benzyl bromide **4**. Besides less electronegative, bromide is a better leaving group than chlorine because it is bigger, better stabilizes the charge and the C-Br bond is weaker



than the C-Cl bond. It was possible to improve the yield to 87%, using benzyl bromide. The product was recovered, after crystallization, as light yellow crystals.

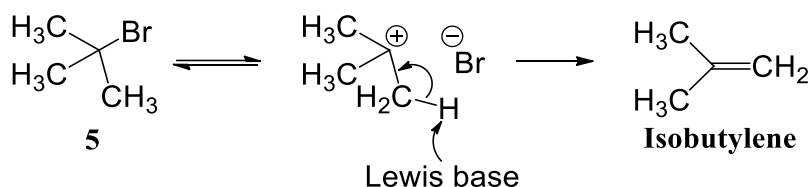
The reaction between 3-nitrophenol (**1**) and **4**, to form ether **7**, using NaH as base, is described as Williamson's synthesis and is represented in Scheme 2.10.<sup>152</sup> This synthesis consists in two steps, with initial deprotonation of the alcohol **1** by NaH followed by nucleophilic attack on benzyl bromide **4** to afford 1-benzyloxy-3-nitrophenyl (**7**).



**Scheme 2.10** – Schematic representation of the mechanism proposed for the synthesis of compound **7**.<sup>152</sup>

The procedure used for the synthesis of **7** was also applied for the synthesis of 1-(*tert*-butoxy)-3-nitrobenzene (**8**) using *tert*-butyl bromide (**5**) as halide derivative (Scheme 2.7).

However, the required product was not obtained, even when reaction conditions, such as, base, solvent, temperature, time of reaction and halide derivative (*tert*-butyl chloride was also considered) were changed. In some cases 3-nitrophenol (**1**) was recovered and, although the product required was not isolated, it is possible that the failure is due to the fact that any hydrogen positioned on any carbon adjacent to the carbon center bearing the leaving group on **5** can participate in an elimination reaction, whereby the carbon rehybridizes from sp<sup>3</sup> to sp<sup>2</sup> and an alkene (isobutylene) is obtained from *tert*-butyl bromide (see Scheme 2.11). Alcohol **1** (or its alkoxide, if proton is removed by NaH) could be the Lewis base responsible for the displacement of the proton involved in the elimination step.<sup>153</sup>

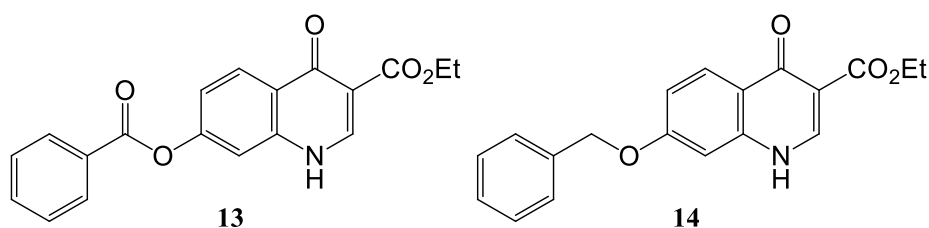


**Scheme 2.11** – Schematic representation of the mechanism of elimination proposed as one possible reason for the failure of the synthesis of compound **8**.<sup>153</sup>

Once synthesized, nitro arenes **6** and **7** (nitro arenes) were reduced to the corresponding anilines (**9** and **10**), considering the reduction pathway represented in Scheme 2.2, with good yields (97% and 99%, respectively). Compounds **9** and **10** were

then reacted with DEEMM (Scheme 2.3) to afford the enamine derivatives (**11** and **12**), in yields of 35% and 99%, respectively. The lower yield for the coupling reaction, in the case of compound **11**, can be explained by the fact that the reaction was not completed (monitoring by TLC – thin layer chromatography) and not all the product was isolated in a pure form from the column chromatography.

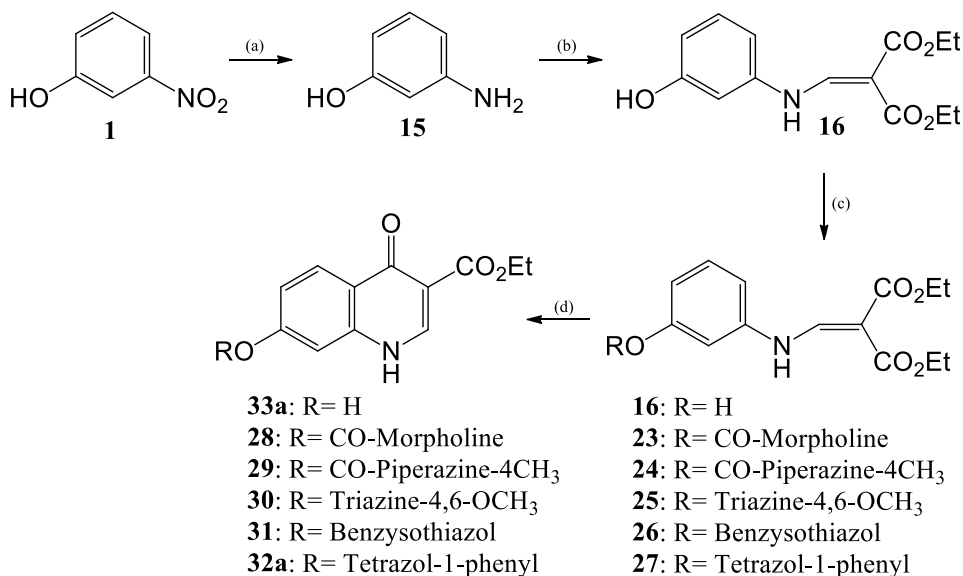
Enamines **11** and **12** were heated at 250 °C in order to perform the cyclisation to afford 4-oxo-quinoline 3-esters **13** and **14** (Scheme 2.4). The 4-oxo-quinoline 3-ester with a benzyloxy substituent at position 7 (**14**) was synthesized, although with low yield (17%) and with some problems of solubility.



The quinolone derivative **13** (with a benzoyloxy at position 7) also presents problems of solubility and thus the characterization results were not easy to interpret. Analysis by mass spectrometry indicated that the desired product had been synthesized (peak of  $m/z$  360 for the adduct  $[M + Na]^+$ ) but the powder obtained was not pure and other peaks, with higher mass, were observed in the spectrum (see Appendix 2 - Figure S1). The NMR (nuclear magnetic resonance) data reinforce the idea that the product **13** has been synthesized:  $^1H$  NMR signals around 4.2 and 1.3 ppm, corresponding to resonances of the ester hydrogens, are present (see Appendix 2 - Figure S2); the  $^{13}C$  NMR signals at 14.8 and 60.1 ppm demonstrate the presence of an ester group and those at 129-130 ppm indicate the presence of a benzoyl substituent (see Appendix 2 - Figure S3). There is no evidence for the presence of the starting material **11** from MS (mass spectrometry) or  $^{13}C$  NMR analysis (since an expected peak around 94 ppm for the  $C(CO_2Et)_2$  is not present, for example; see Appendix 2 - Figure S2 and Figure S3). Elemental analysis indicates that the product isolated is not pure. However, it was not possible to purify the compound due to very low solubility and because the  $R_f$  (retention factor) of the impurities were essentially close to that of the product, rendering the purification of the product impractical.

### 2.2.2. Preparation of 4-oxo-quinolines with an heterocyclic group as substituent in position 7

Continuing the work leading to the preparation of a library of quinolone 3-esters with chemical diversity in position 7 of the quinolone core structure, further modifications of the 7-hydroxyl group were envisaged, with the aim of introducing heterocyclic groups in the same position. Considering that some substituents could be susceptible to the conditions used in the reduction step, an adapted strategy was considered (Scheme 2.12).

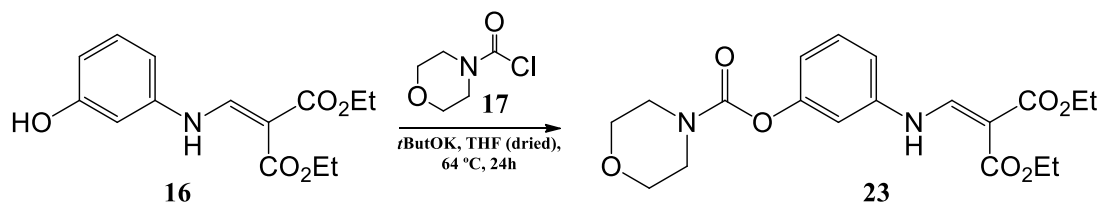


**Scheme 2.12** – Schematic representation of the general synthetic approach followed to prepare 4-oxo-quinolone 3-esters with 7-substituents susceptible to the reduction conditions. Conditions: (a) NH<sub>4</sub>Cl, Fe, MeOH:H<sub>2</sub>O (1:1), 60 °C, 4 hours; (b) 100 °C, overnight; (c) variable and adapted conditions according with the R; (d) Dowtherm A, 250 °C, 3 hours.

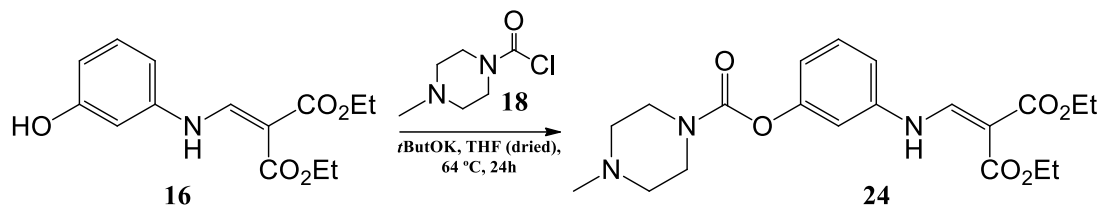
3-Nitrophenol (**1**) was used as starting material and reduced to 3-aminophenol (**15**). Then, to avoid a side reaction between the nitrogen (Ar-NH<sub>2</sub>) and the electrophilic carbon of the compound to be used in the modification of the hydroxyl group, the coupling reaction with DEEMM preceded the esterification/etherification reaction (linkage of the heterocycle at position 7, mediated by the hydroxyl group). Finally, thermal cyclisation in Dowtherm A was carried out to afford 4-oxo-quinolone 3-ester derivatives (Scheme 2.12). The fact that the reduction and coupling reactions are common steps in the strategies to the six target compounds is an advantage to this strategy.

3-Nitrophenol (**1**) was reduced to 3-aminophenol (**15**) and then coupled with DEEMM to afford diethyl 2-(((3-hydroxyphenyl)amino)methylene)malonate (**16**). These reactions were optimized and generally gave yields greater than 90%, after purification. **16** is a common intermediate for the synthesis of a library of target compounds bearing

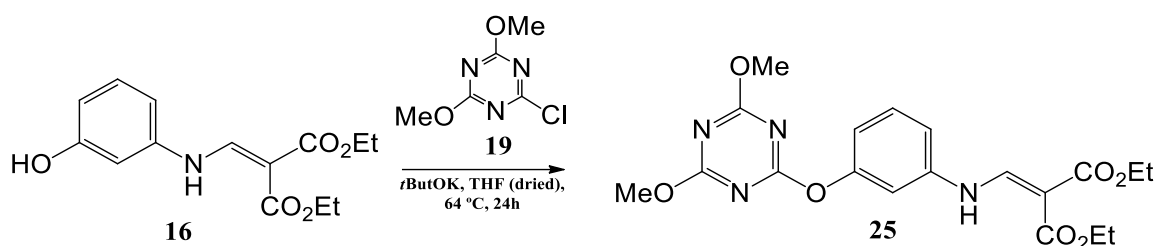
various substituents at position 7, introduced by modification of the hydroxyl group (Scheme 2.13 to Scheme 2.17).



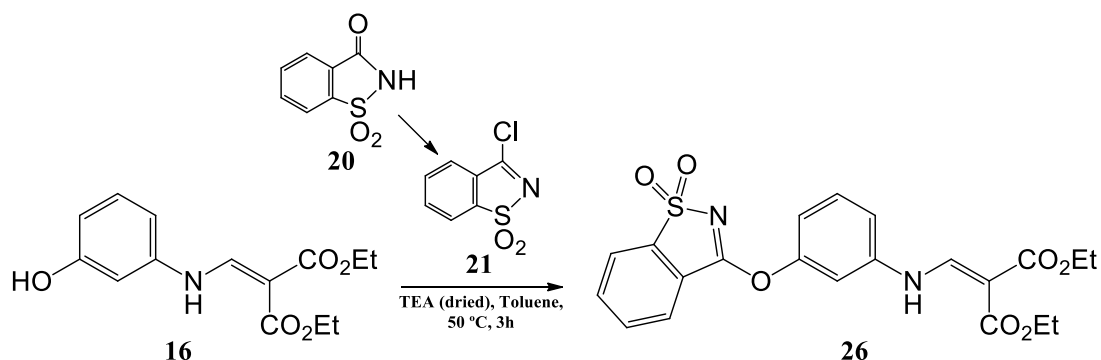
**Scheme 2.13** – Derivatization of the hydroxyl group in **16** to afford compound **23**.



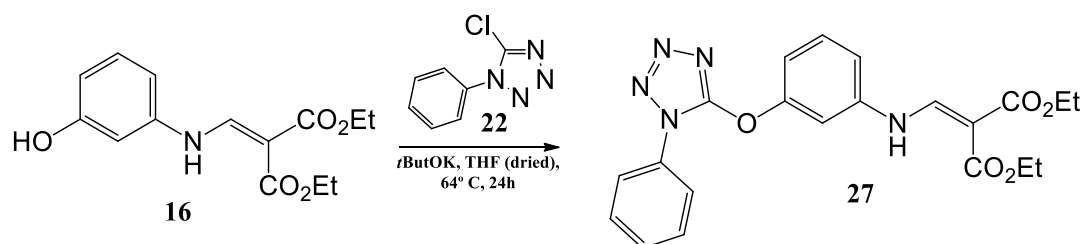
**Scheme 2.14** – Derivatization of the hydroxyl group in **16** to afford compound **24**.



**Scheme 2.15** – Derivatization of the hydroxyl group in **16** to afford compound **25**.

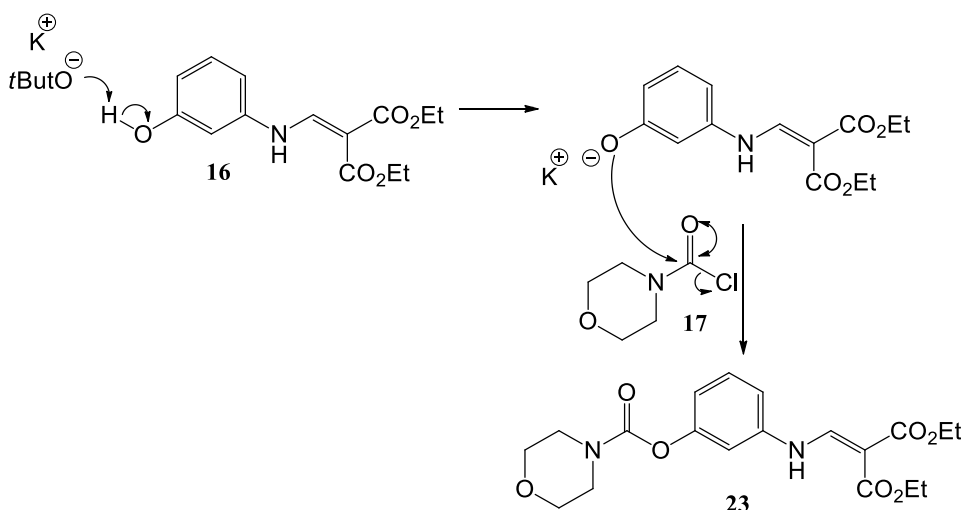


**Scheme 2.16** – Derivatization of the hydroxyl group in **16** to afford compound **26**.



**Scheme 2.17** – Derivatization of the hydroxyl group in **16** to afford compound **27**.

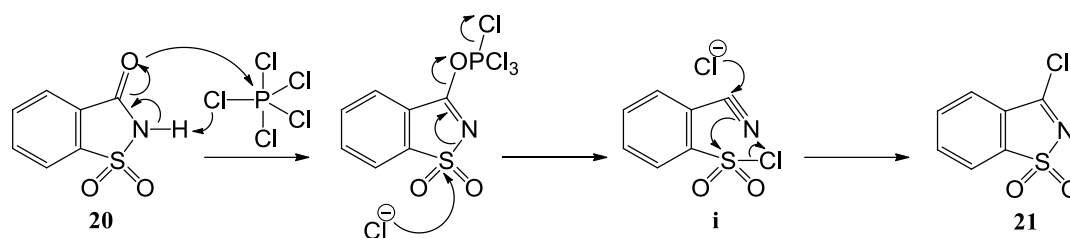
The reactions conducted to prepare compounds **23**, **24**, **25** and **27** were carried out using potassium *tert*-butoxide in dry THF (tetrahydrofuran), adapting the methodology of etherification or esterification known as Williamson synthesis. Firstly there is formation of alkoxide from **16**, which is able to attack the electrophilic carbon linked to the halide atom present in **17** (exemplified in Scheme 2.18), **18**, **19** and **22**. *Tert*-butoxide anion (*t*-ButO<sup>-</sup>) is a strong base that can remove the hydrogen from the hydroxyl group and is also very hindered, avoiding its attack to the halide-carbon (side-reaction). ButO<sup>-</sup> is also a strong base and may lead to elimination products, especially when primary alkyl halides are used, which is not the case of our substrates.<sup>152,153</sup>



**Scheme 2.18** – Schematic representation of the mechanism proposed for the *t*-ButOK-catalysed esterification to afford compound **23**.<sup>151</sup>

Among the four reactions carried out using this methodology, only one led to a low yield of product (16% for the synthesis of **25**) while the synthesis of **23**, **24** and **27** were conducted with moderate to good yields.

To afford compound **26** a different methodology was carried out, adopting a similar procedure to that followed for the synthesis of **6**, *i.e.* TEA-catalysed etherification but, in this case, using toluene as solvent. Before the coupling to get **26**, it was required to synthesize 3-chloro-1,2-benzisothiazole 1,1-dioxide (pseudo-saccharyl chloride, **21**) from saccharin (**20**), by halogenation using PCl<sub>5</sub> (at 180 °C) (Scheme 2.19). The reaction affords HCl and POCl<sub>3</sub> as side products.



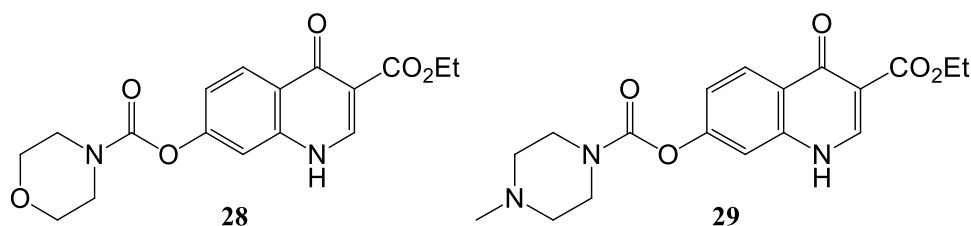
**Scheme 2.19** – Schematic representation of the mechanism proposed for the synthesis of pseudo-saccharyl chloride (**21**).<sup>154</sup>

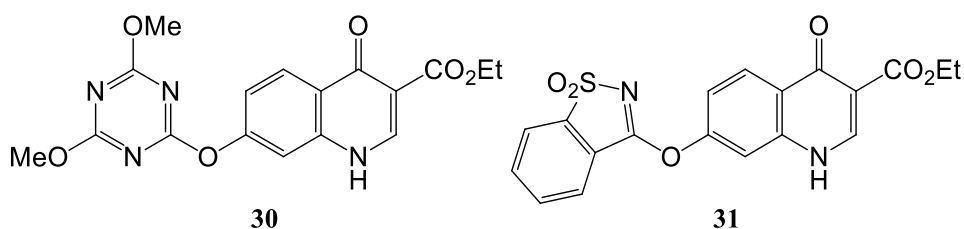
The intermediate compound formed by this halogenation reaction is sulfonyl chloride (**i**, Scheme 2.19) and, once synthesized, the cyclisation to give **21** requires the attack of a chlorine anion on the carbon atom of the cyano group, which has a low nucleophilic susceptibility. Therefore, it is necessary to use higher temperatures (180 °C) and/or longer reaction times (3 hours) to improve the yield for the saccharine chlorination. Furthermore, phosphorus oxychloride and HCl must be distilled before the crystallization step. Some reports described that when recrystallized from toluene, **21** was found to be quite stable over a period of months.<sup>154</sup>

Saccharyl chloride **21** was synthesized, evidencing a melting range compatible to that reported in the literature,<sup>154</sup> however with a poor yield (25%), due to the possibility of the process to stop at intermediate compound **i** or to a possible conversion to the starting material **20** (by hydrolysis of **21** in the presence of water), suggesting some instability for this product.

The instability of **21** is the reason why we used a different methodology for the synthesis of **26** (hydroxyl group modification), to avoid side reactions: TEA is a weaker base than *t*ButOK; toluene is not miscible with water (THF is miscible with water, extremely hygroscopic and upon exposure to air decomposes to form unstable compounds) and the desired product **26** is not soluble in toluene, leading to an easy purification or isolation (occurs precipitation).

Enamines **23**, **24**, **25** and **26** (malonate derivatives substituted with heterocyclic groups) were heated at 250 °C in order to perform the cyclisation step to afford 4-oxo-quinoline 3-ester derivatives **28**, **29**, **30** and **31** (Scheme 2.12).

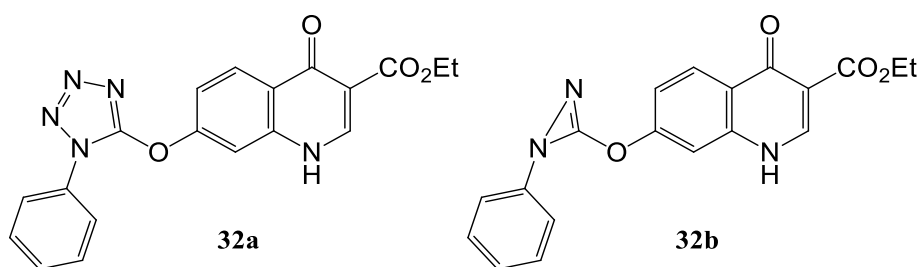




4-Oxo-quinolone 3-ester **31** was recovered with a yield of around 48%. However analysis indicated contamination of the solid with a trace amount of solvent (Dowtherm A). The characteristic  $^1\text{H}$  NMR peaks for Dowtherm A appear typically at 7.65 (d), 7.47 (t), 7.39 (t), 7.14 (t) and 7.02 (d) ppm and are visible in the spectrum of **31** (see Appendix 2 - Figure S4). The solubility problems did not allow to get a  $^{13}\text{C}$  NMR with quality and the presence of Dowtherm A masked the elemental analysis of this quinolone.

From the cyclisation steps to afford quinolones derivatives **28**, **29** and **30** it was not possible to isolate the product: no precipitate appeared after cooling and adding appropriated solvents; the high boiling point for Dowtherm A complicates its extraction or separation from the desired organic products; the insolubility problems also render the purification, for example by column chromatography, difficult or impossible.

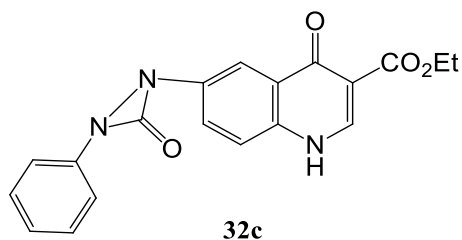
In an attempt to synthesize **32a** by the Gould-Jacobs methodology, from enamine **27**, an unwanted diazirine (**32b**) was obtained as product. The synthesis of **32b** is easily explained, considering the high temperatures required for intramolecular cyclisation of **27** that lead to problems adjacent to this methodology such as the susceptibility to degradation of the tetrazole residue, releasing  $\text{N}_2$ .



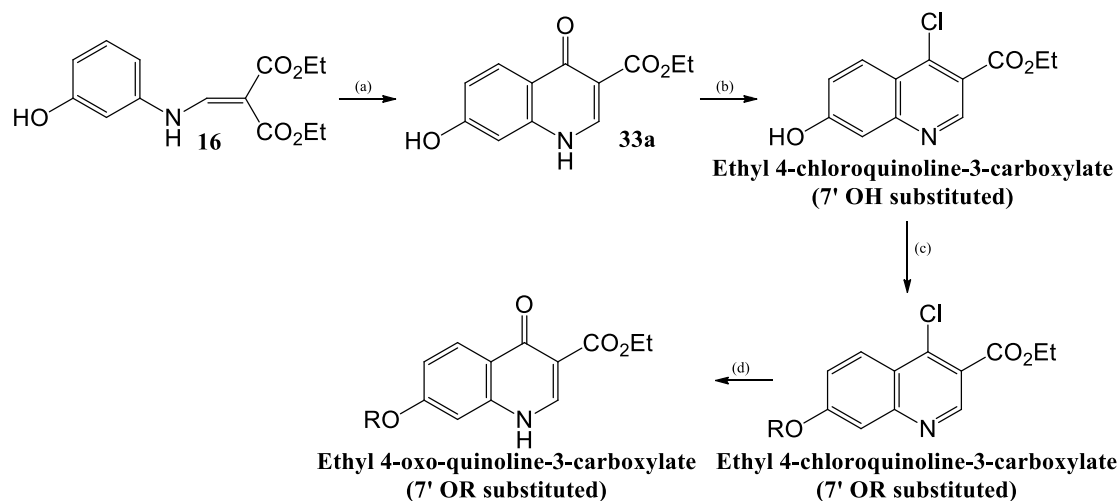
By NMR it is not easy to find spectral differences that can prove the presence of **32b** and/or the absence of **32a**, thus, the characterization method used to distinguish **32a** (377.35 g/mol) from **32b** (349.34 g/mol) was mass spectrometry. Initially, by EI, a peak around 349 was observed (see Appendix 2 - Figure S5). To exclude the hypothesis that this peak could be due to a mass spectrometric fragment from the ionisation of **32a**, other MS analysis, with different ionisation methods, were carried out, all of them demonstrating the presence of **32b** and the absence of **32a**.

At the same time, the presence of a diazirone residue at position 7 (compound **32c**) instead of a diazirine, was considered. However, the chemical shifts observed by  $^1\text{H}$  NMR

and, especially, by  $^{13}\text{C}$  NMR (see Appendix 2 - Figure S6), are compatible with **32b** and not with **32c**.



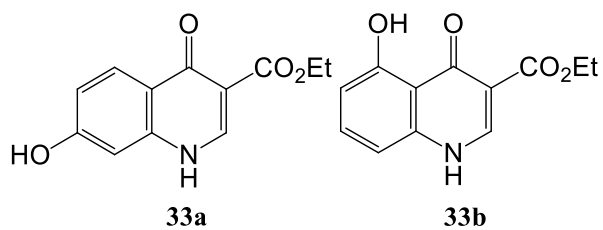
To overcome the possibility of thermolysis of fragile residues, for example the tetrazole ring (in **27** and **32a**), during the cyclisation step using Gould-Jacobs methodology (250 °C, 3 hours), a new synthetic approach was considered, based in direct cyclisation of **16** followed by synthesis of 4-chloroquinoline intermediate, modification of the hydroxyl residue and conversion to the corresponding 4-oxo-quinoline (Scheme 2.20). Thus, only the hydroxyl group of compound **16** would be subject to high temperatures, protecting the more susceptible residue from extreme conditions.



**Scheme 2.20** – Representation of the general synthetic approach followed to afford 7-substituted 4-oxo-quinoline 3-esters, using ethyl 4-chloroquinoline as intermediate compound. Conditions: (a) Dowtherm A, 250 °C, 3 hours; (b)  $\text{POCl}_3$ , 97 °C, overnight; (c) variable and adapted conditions according to the nature of R; (d) DMF (*N,N*-dimethylformamide),  $\text{HCO}_2\text{H}/\text{EtOH}$  (80/20), 145 °C, 18 hours.

The problems encountered with this approach were ascribed to the presence of a mixture of structural isomers. Considering that cyclisation involves an aromatic substitution at the adjacent carbon to the NH group of the enamine, when both carbons are unsubstituted (as in compound **16**) two substitution patterns are possible, leading to final quinolones with substituents in different positions (hydroxyl group at position 7 for **33a**; or at position 5 for **33b**).

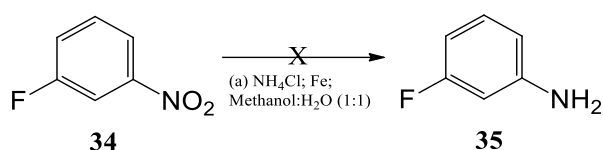




It was not possible to separate the isomers, so the synthetic strategy (Scheme 2.20) for the synthesis of ethyl 4-oxo-quinoline 3-ester derivatives with an ether or ester at position 7, using the 4-chloroquinoline as intermediate compound, was not successful.

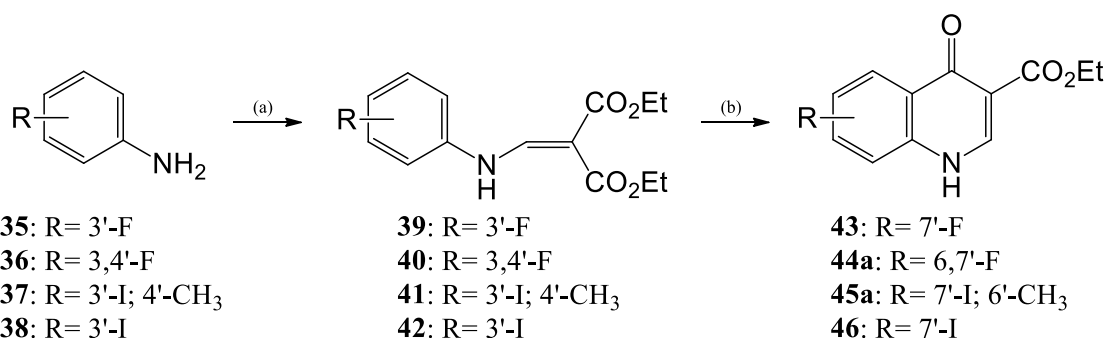
### 2.3. Exploring position 7 – from nucleophilic aromatic substitution

Nucleophilic aromatic substitution normally consists of substitution of halogen, linked to an aromatic ring carbon, by a nucleophile group. Aiming to incorporate tetrazolyl and morpholinyl groups at position 7 of 4-oxo-quinoline 3-esters, a general synthetic approach was considered, involving aniline derivatives with halide atoms as substituents (iodine<sup>155</sup> and fluorine) in *meta* and/or *para* position at the starting material. The synthesis of 3-fluoroaniline **35** was attempted, from the 3-fluoronitrobenzene **34** by reduction using iron and ammonium chloride (Scheme 2.21), but proved unsuccessful (reaction did not progress). As such, considering the commercial availability of **35** and its cost, we used this aniline as starting material and did not invest in the reduction optimization.



**Scheme 2.21** – Attempted reduction of **34** to **35**.

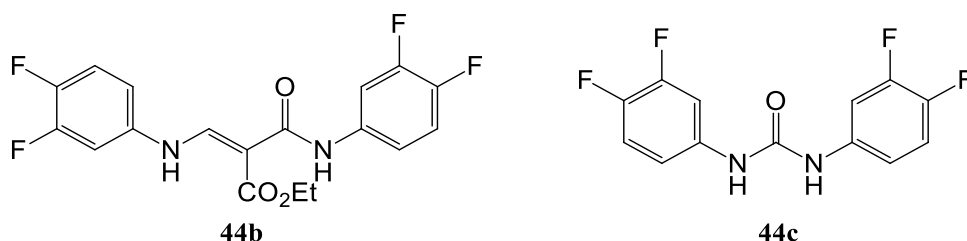
From selected anilines with *m*-fluorine (**35**), *m*- and *p*-fluorine (**36**), *m*-iodine and *p*-methyl (**37**) and *m*-iodine (**38**)<sup>155</sup>, we proceeded to the coupling step with DEEMM to prepare enamine derivatives and, subsequently, to the Gould-Jacobs intramolecular cyclisation to afford corresponding 4-oxo-quinoline 3-esters (Scheme 2.22) bearing halide substituents at positions 6 and/or 7 (**43**, **44a**, **45a** and **46**).



**Scheme 2.22** – General synthetic approach followed to prepare 4-oxo-quinoline 3-esters with halide substituents at positions 6 and/or 7. Conditions: (a) 100 °C, overnight; (b) Dowtherm A, 250 °C, 3 hours.

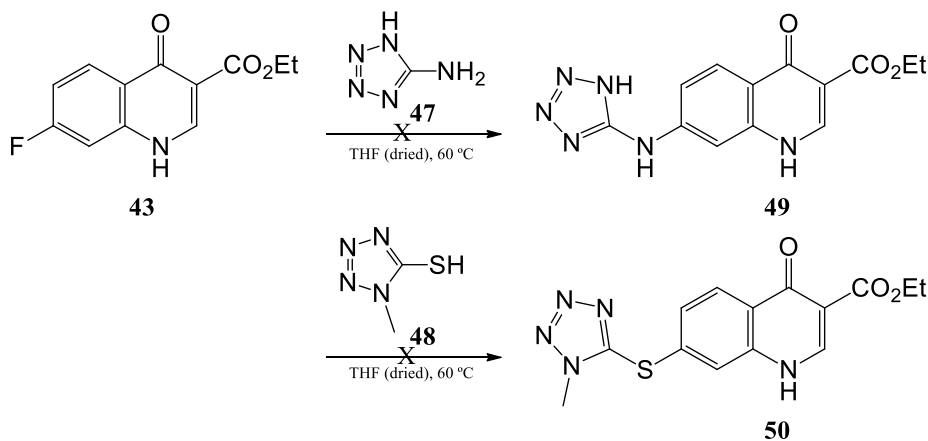
Enamines **39-42**, were synthesized with excellent yields: 90% for **39**; 99% for **40**; 91% for **41**; and 99% for **42**. However, in the cyclisation step to the synthesis of the corresponding quinolones **43**, **44a**, **45a** and **46**, the results are not so good due to the different yields obtained (around 3% for **44a**; 44% for **43** and **46**; 62% for **45a**).

Considering the poor yield of **44a** obtained from the cyclisation reaction of **40** we envisaged to optimize the reaction conditions to improve this yield. Two alterations were implemented separately: a) decrease the temperature to 200 °C (during 24 hours); b) change the concentration of enamine **40** in Dowtherm A. However, these alterations did not lead to successful results, as we could not isolate quinolone **44a**. Instead, two different side products were recovered (**44b** and **44c**).

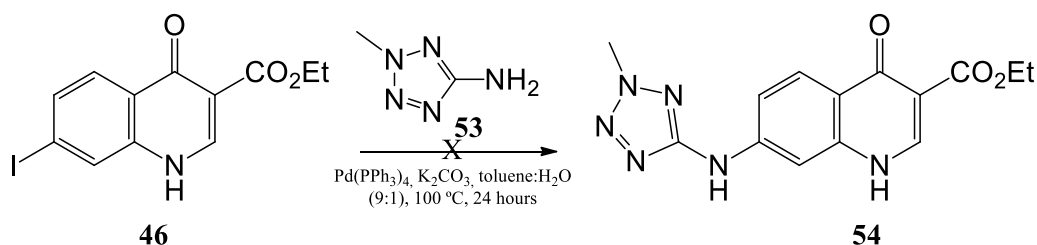


The side products in question were characterized by mass spectrometry, <sup>1</sup>H NMR spectroscopy, elemental analysis and their structure were proved by X-ray crystallography (see Appendix 2 - Figure S7 for **44b** and Figure S8 for **44c**). A possible route to the synthesis of these compounds involves reaction between molecules of enamine **40**, however, studies to mechanism elucidation are required and should be performed.

To introduce chemical diversity at position 7, a strategy approaching nucleophilic aromatic substitution was considered to replace the halogen atoms by tetrazole residues. However, due to the residual amount of **44a**, this strategy was not implemented for this quinolone derivative. Modification of quinolone **43** (Scheme 2.23) was attempted, through reaction with aminotetrazole **47** and mercapto-1-methyl tetrazole **48**, in an attempt to synthesize **49** and **50**, but the poor character of fluorine as leaving group and the poor solubility of **43** compromised the reactions (**43** was recovered from the reaction).

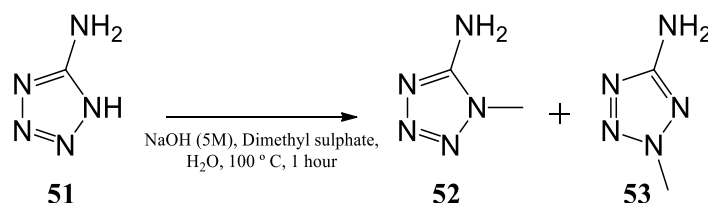


**Scheme 2.23** – General synthetic approach followed to the attempted preparation of 4-oxoquinoline 3-esters linked to tetrazole residues at position 7 (**49** and **50**) from **43**.



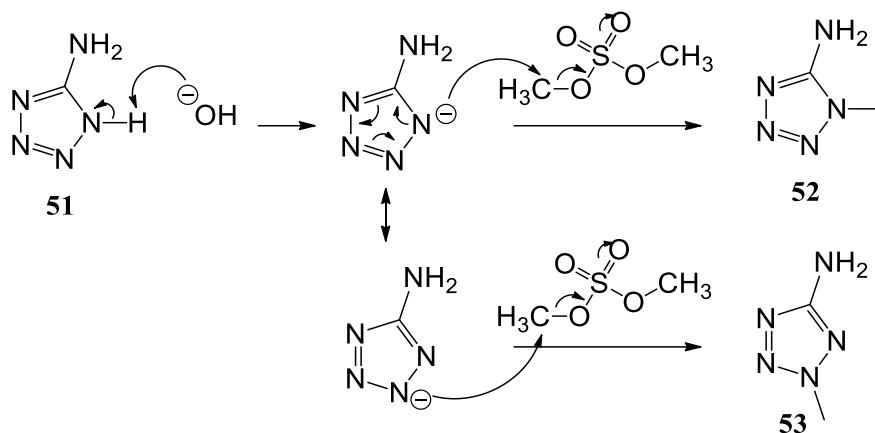
**Scheme 2.24** – General synthetic approach followed for the attempted preparation of 4-oxoquinoline 3-esters linked to a 2-methyl tetrazole residue at position 7 (**54**).

Considering that iodine is a better leaving group than fluorine, quinolone 3-ester **46** was submitted to the above devised strategy (Scheme 2.24), so as to introduce a 2-methyl-aminotetrazole residue (**53**) in position 7. **53** was previously synthesized from **51**, albeit in low yield (1-methyl-aminotetrazole **52** is another product; Scheme 2.25). The two products obtained from methylation of aminotetrazole **51** can be distinguished by mass spectrometry, considering their fragmentation patterns (see Appendix 2 - Figure S9).



**Scheme 2.25** – Representation of the synthetic approach followed for methylation of aminotetrazole **51** to afford **52** and **53**.

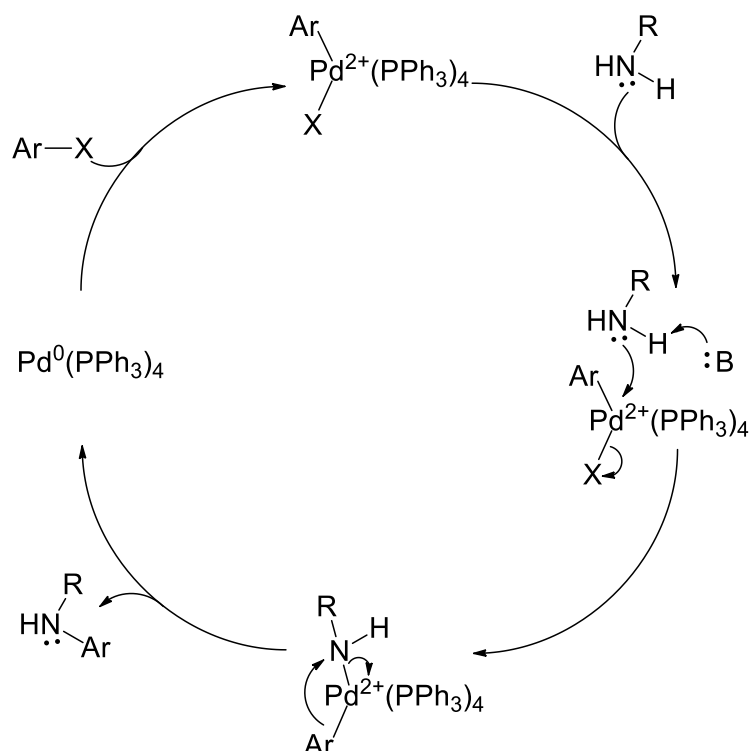
The procedure for the mono-methylation of 5-aminotetrazole in aqueous medium has been optimized<sup>156,157</sup> to give around 51% of **52** and 25% of **53**. In this context we used dimethyl sulfate (DMS) as methylating agent. The mechanism proposed is depicted in Scheme 2.26. DMS (liquid and its vapors) is especially dangerous, as it may cause delayed burns to lungs and tissues, may be fatal if inhaled, is carcinogenic and mutagenic and is environmentally hazardous. So, its use should be prudent and, if possible, it should be replaced by dimethyl carbonate, a safer and environmentally friendly methylating agent. DMS is generally employed for methylation of hydroxyl compounds and for primary and secondary amines. Despite the presence of a primary amine in **51**, some studies have shown that the alkylation of the 5-amino group (to afford mono and dimethylated derivatives) apparently occurs only in a very limited extension. The methylation occurs preferably at position 1, to afford **52**, because the H-N of the tetrazole ring is the most acidic proton. However, 2-methylated isomer **53** can be recovered. **53** is more soluble in organic solvents than **52** so we chose it to incorporate at position 7 of quinolone **46**.



**Scheme 2.26** – Schematic representation of the mechanism proposed for the mono-methylation of **51** to afford 1- and 2-methyl-5-aminotetrazoles **52** and **53**.

Notwithstanding the good solubility in THF demonstrated by **53** and the better profile of iodine as leaving group (comparing to fluorine), the attempt to incorporate the tetrazole residue in position 7 of **46** (Scheme 2.24) to synthesize **54**, following the Buchwald-Hartwig methodology, was not successful.

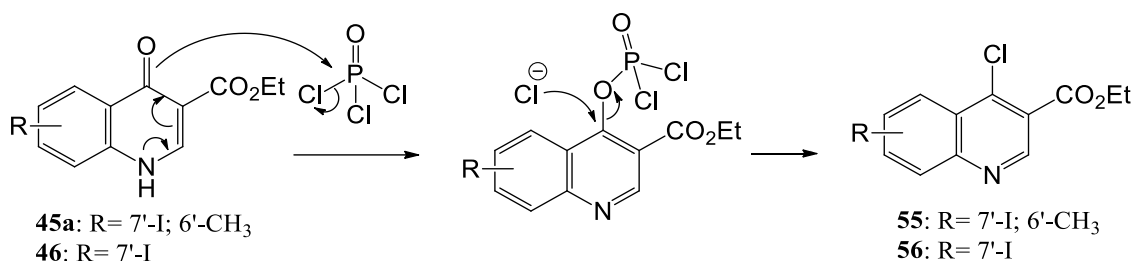
The Buchwald-Hartwig amination is a methodology used to construct carbon-nitrogen bonds based on the cross-coupling reaction of an aryl halide with an amine, using palladium, as a catalyst, and a strong base. However, using as substrate a 4-oxo-quinoline 3-ester, since the ester group was found important for antiplasmodial activity, and should therefore be conserved, it is convenient to use a weaker base (*e.g.* K<sub>2</sub>CO<sub>3</sub>) because the 3-ethyl ester moiety can be affected by a stronger base. The mechanism proposed for this methodology (Scheme 2.27) is firstly based in oxidative addition of the aryl halide to palladium (0), followed by coordination of the amine to palladium. Then, a base removes a proton from the amine, which attacks the palladium, and the halide is removed as a leaving group. Finally, a reductive elimination step leads to the final desired aryl amine, regenerating the catalyst [Pd(0)].<sup>158,159</sup>



**Scheme 2.27** – Schematic representation of the mechanism proposed for the Buchwald-Hartwig coupling.<sup>158,159</sup>

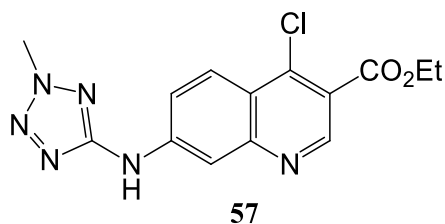
Considering the poor solubility of quinolones (*e.g.* derivative **46**), an alternative methodology, involving the synthesis of a 4-chloroquinoline as intermediate, was proposed (quinolone halogenation by using phosphorus oxychloride). 4-Chloroquinolines are more easily solubilized and isolated and may be subsequently converted into the corresponding quinolones. Then, these intermediates (**55** and **56**, obtained from halogenation of **45** and **46**, respectively; Scheme 2.28) represent versatile building blocks from which several compounds can be synthesized, introducing chemical diversity at position 7 (and position 4), for example by Buchwald-Hartwig amination or by Suzuki coupling reactions.

Inexplicably, it was not possible to synthesize 4-chloroquinoline **55** by chlorination, while the analogue without a methyl group at position 6 (**56**) was synthesized and recovered with very good yield (95%). The detailed structure of **56** was studied experimentally, using X-ray crystallography and matrix isolation techniques coupled to infrared spectroscopy, and also theoretically, using contemporary molecular orbital calculations. Results are described in the next chapter.<sup>155</sup>

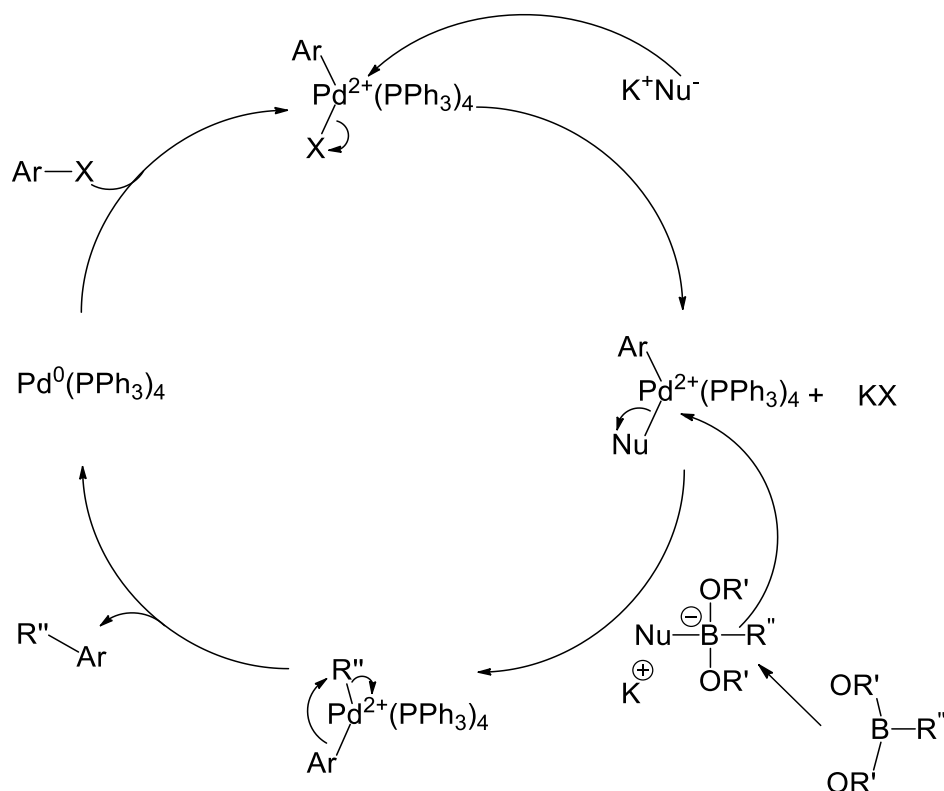


**Scheme 2.28** – Schematic representation of the mechanism proposed for the chlorination of 4-oxo-quinolines at position 4.

Although **56** exhibits a better solubility profile than its 4-oxo precursor, the attempted Buchwald-Hartwig amination reaction between that 4-chloroquinoline and tetrazole derivative **53**, to afford derivative **57**, was not successful, probably because the base used is not strong enough for this methodology.



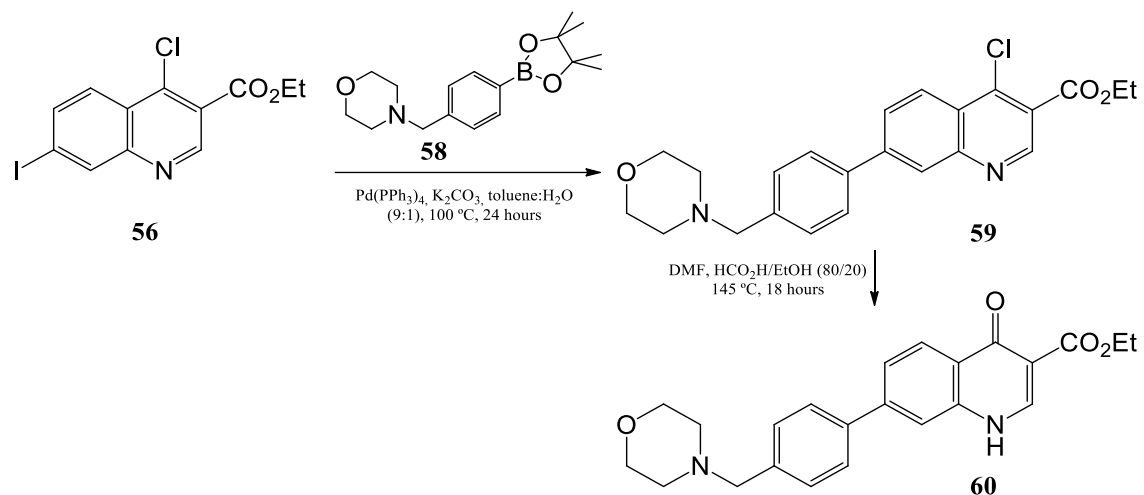
An alternative procedure was applied to introduce variability at position 7 of ethyl 4-chloro-7-iodo-quinoline-3-carboxylate (**57**), based on the Suzuki coupling methodology. This approach involves coupling between an organoborane and an organohalide, catalysed by a palladium [Pd(0)] complex and a base, leading to carbon-carbon single bond formation. The mechanism proposed for the Suzuki coupling (Scheme 2.29) bears similarities with the mechanism proposed for the Buchwald-Hartwig methodology, starting with oxidative addition of the aryl halide to the Pd(0). Thereafter, a molecule of base (K<sub>Nu</sub>) replaces the halide on the palladium complex, and another one forms a borate with a more nucleophilic R'' group. This activation of the boron atom enhances and facilitates transmetalation, where R'' replaces the Nu group on the palladium complex. Reductive elimination ensues, leading to the final coupled product and regenerating the palladium catalyst.<sup>160</sup>



**Scheme 2.29** – Schematic representation of the mechanism proposed for the Suzuki-Miyaura coupling reaction.<sup>160</sup>

In this project we choose to introduce a 4-(4-morpholinomethyl)-phenyl group at position 7, following the Suzuki-Miyaura methodology described above and considering **56** as starting material (Scheme 2.30). The reaction was carried out successfully, affording the 4-chloroquinone derivative with the desired substituent at position 7 (**59**) in a reasonable yield (52%). The presence of a chlorine substituent at position 4 may interfere in this step, since coupling could occur at the carbon 4 (with displacement of a chlorine atom). After the coupling reaction, compound **59** was converted to the corresponding quinolone **60**, the active form that has been shown to act as strong inhibitor of the parasitic  $bc_1$  protein complex. The solubility problems related to compound **60** have complicated its purification and isolation, and this led to the poor yield obtained (13%) for the isolated product.

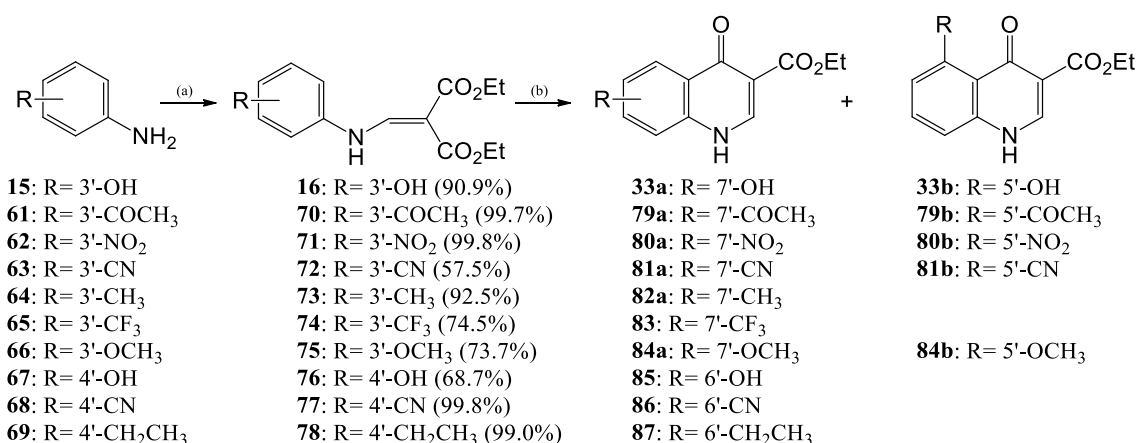




**Scheme 2.30** – Representation of the synthetic approach to 7-(4-(4-morpholinomethyl)-phenyl)-4-oxo-quinoline 3-ester (**60**) from 7-iodo-4-chloroquinoline 3-ester (**56**).

## 2.4. Exploring positions 6 and 7 – the issue of isomeric mixture

Throughout this project, some criticisms were raised regarding the Gould-Jacobs methodology. Considering the mechanism proposed for this cyclisation, one of the criticisms is related with the possibility of formation of structural isomers. In the thermally driven intramolecular cyclisation, the phenyl ring of the malonate derivative (**70** to **78**, for example) acts as nucleophile, attacking the carbon of the ester carbonyl group. Then, this step may result in a cyclisation to both *ortho* carbons adjacent to the NH group of the malonate derivative, and an isomeric mixture can thus be obtained (7- or 5-substituted 4-oxo-quinolines). This problem was evident throughout the research described in this thesis, affecting compounds with various substituent groups (Scheme 2.31, **79a-84a** vs **79b-84b**) although with different impact.



**Scheme 2.31** – Summary of the synthetic approach followed and results obtained for the preparation of a library of 4-oxo-quinoline 3-esters bearing substituents at positions 6 and/or 7; in some examples, a 5-substituted structural isomer was obtained upon Gould-Jacobs cyclisation. Conditions: (a) 100 °C, overnight; (b) Dowtherm A, 250 °C, 3 hours.

As represented in Scheme 2.31, the coupling step gave high yield of the required products, but the results for the following cyclisation steps were generally poor, considering the yields and the ratio of structural isomers (5- vs 7-substituted) obtained. These isomers are not easy to isolate and separate from each other, furthermore they have the same molecular weight and, consequently, the MS and CHN (elemental analysis) data are similar, but by NMR (especially by <sup>1</sup>H NMR) it is possible to differentiate these compounds and estimate the ratio of structural isomers since the chemical shifts and the splitting patterns are distinct. However, in some cases, the poor solubility of quinolones hinders this characterization (NMR spectra with poor resolution).

As reported in a previous section, during the synthesis of 7-hydroxy-4-oxo-quinoline 3-methylester (**33a**) an isomeric mixture was obtained and detected by <sup>1</sup>H

NMR. In the spectrum we observed the presence of two quartets at 4.27-4.17 ppm referring to the  $\text{CH}_2$  and two triplets at 1.31-1.25 ppm corresponding to the  $\text{CH}_3$  of the 3-ethyl ester (instead of one quartet and one triplet, respectively). In the spectrum, 8 aromatic peaks (between 8.6 to 6.6 ppm) are noticed (Figure 2.1), while the quinolone **33a** only has four aromatic hydrogens (one of them at the heterocyclic ring, with a characteristic chemical shift around 8.6 ppm). So, considering the integration value (singlet peak at 8.59 ppm as reference) and the splitting shift, we can associate signals 8.59 (s), 7.56 (t), 7.03 (d) and 6.70 (d) to isomer **33b** and 8.42 (d), 7.97 (d), 6.87 (s) and 6.86 (d) ppm to isomer **33a**. So, there is an isomeric mixture, in a proportion of around 60% for quinolone **33b** (5-substituted) and around 40% for **33a** (7-substituted). Analysis of the  $^{13}\text{C}$  NMR spectrum is in keeping to those results.

The same rationale was applied to the synthesis of 4-oxo-quinolines 3-esters substituted with acetyl, nitro or nitrile, and the  $^1\text{H}$  NMR signals obtained for each case (Figure 2.1) were used to estimate the approximate ratio of structural isomers: 48% of **79a** vs 52% for **79b**; 44% of **80a** vs 56% for **80b**; and 45% of **81a** vs 55% for **81b**.

Noteworthy is the fact that the antiplasmodial activity may differ substantially between 5-substituted and 7-substituted isomers, since the two isomers may bind differently to the enzyme active site.

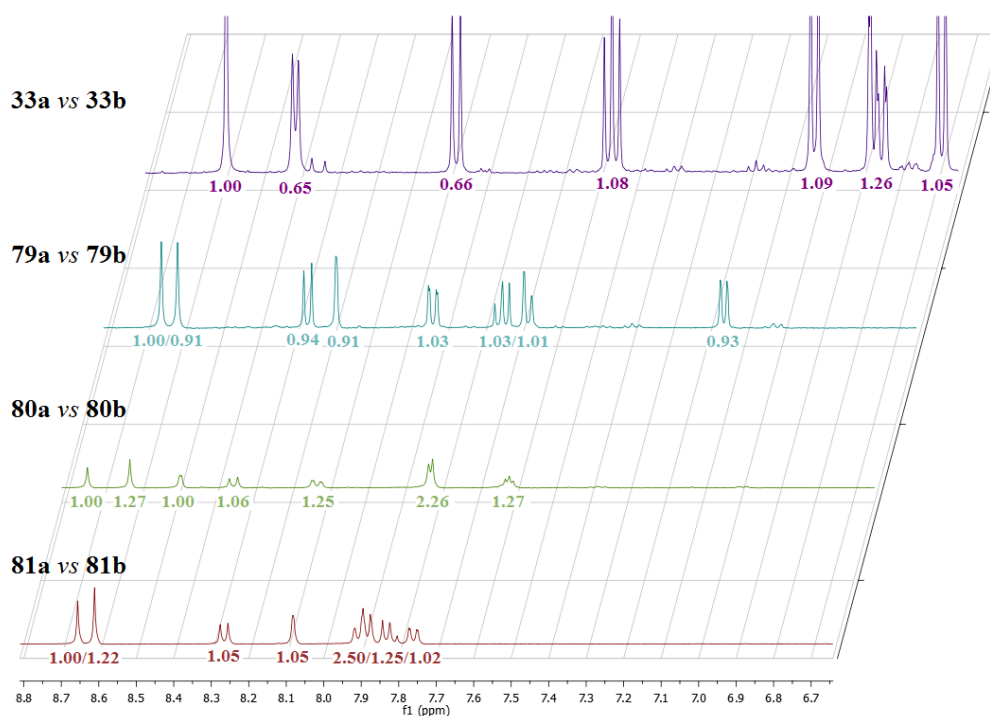
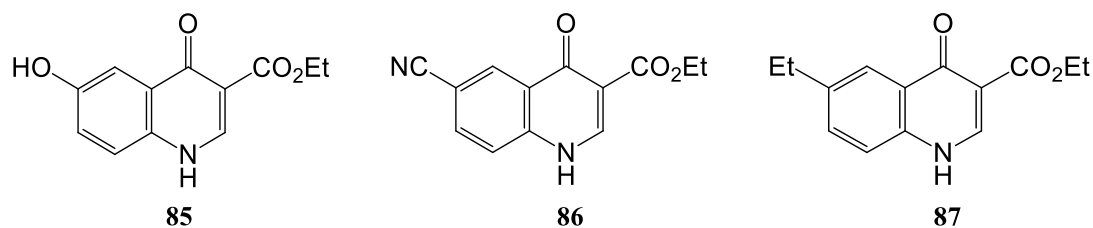


**Figure 2.1** -  $^1\text{H}$  NMR spectra showing the chemical shifts of aromatic protons (8.6-6.7 ppm), for the isomeric mixtures of **33a/33b**, **79a/79b**, **80a/80b** and **81a/81b** in  $\text{D}_6$ -DMSO (dimethyl sulfoxide); integration values are indicated below the corresponding peaks.

Three other 7-substituted-4-oxo-quinoline-3-esters have been synthesized (with methyl, trifluoromethyl and methoxy as substituents) and the results are distinct. Cyclisation by Gould-Jacobs methodology to afford compound **82a** (7-methyl substituted derivative) was achieved with a yield of around 12% (this compound and its derivatives will be studied in detail in the next chapter). Apparently, **83** (ethyl 7-trifluoromethyl-4-oxo-quinoline-3-carboxylate) was synthesized relatively pure, although its poor solubility does not allow us to ensure it with security. Applying the same methodology to obtain a methoxy substituted quinolone (**84a** and **84b**), it was afforded a powder that also demonstrated solubility problems: the  $^1\text{H}$  NMR spectrum did not have good resolution but, by integration, only one ester group appeared to be present; however, in the  $^{13}\text{C}$  NMR spectrum two signals for the  $\text{CH}_3\text{O}$  are observed at 56.0 ppm and 55.9 ppm (see Appendix 2 - Figure S10).

Simultaneously, the cyclisation of enamine malonate derivatives with *para*-substituents (**76-78**) was considered. For these compounds, the issue about structural isomerism does not arise since the intramolecular cyclisation to either of the carbons adjacent to the NH group always gives rise the same substitution pattern (6-substituted quinolone derivative: **85-87**).

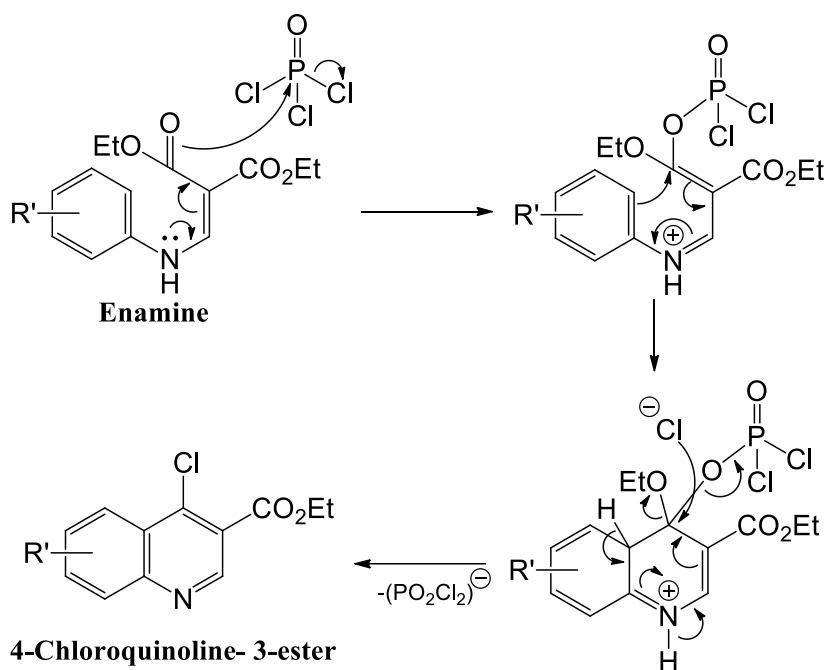


In an attempt to synthesize **85**, only the starting material **76** was recovered. However, 4-oxo-quinoline derivatives **86** and **87** were successfully synthesized with a yield of around 17% and 13%, respectively.

## 2.5. Cyclisation by using phosphorus oxychloride

The thermally driven intramolecular cyclisation previously discussed, known as Gould-Jacobs methodology, presents limitations, mostly related to the high temperature (above 225 °C) required for reaction. Cyclisation was found to be concentration dependent and the product may undergo thermal degradation.<sup>115</sup> At the same time, as has been demonstrated in this project, most quinolones exhibit low solubility, leading to difficulties in extraction and purification and, consequently, poor yields of isolated product. Furthermore, it was demonstrated that this procedure may lead to side products, some of them resulting from structural isomerism.

The liabilities of the Gould-Jacobs cyclisation called for the development of an alternative methodology for cyclisation. An alternative approach was proposed, involving the cyclisation of an enamine and chlorination at position 4, in one pot, mediated by phosphoryl chloride (Scheme 2.32).<sup>161</sup>

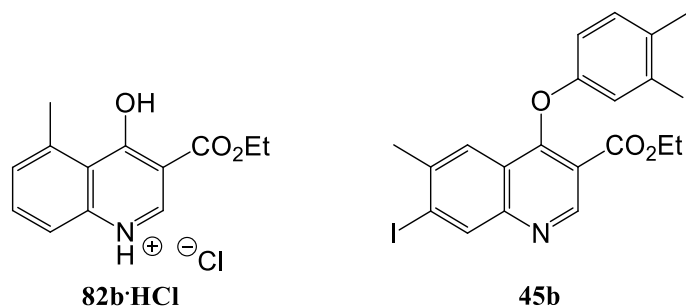


**Scheme 2.32** – Schematic representation of the mechanism proposed for the phosphorus oxychloride mediated cyclisation to afford 4-chloroquinoline-3-esters.<sup>161</sup>

This alternative synthetic approach was applied to several of the enamines mentioned in the previous section, in an attempt to improve results, regarding yields and purity of the products. However, in all of them, the 4-chloroquinoline intermediate was not isolated: either the reaction did not progress or it was not possible to isolate a pure product (as observed for the attempted cyclisation of enamines **13**, **16**, **26**, **70**, **71**, **72** and **74**); or, instead, unexpected products were obtained (as were the case for the attempted

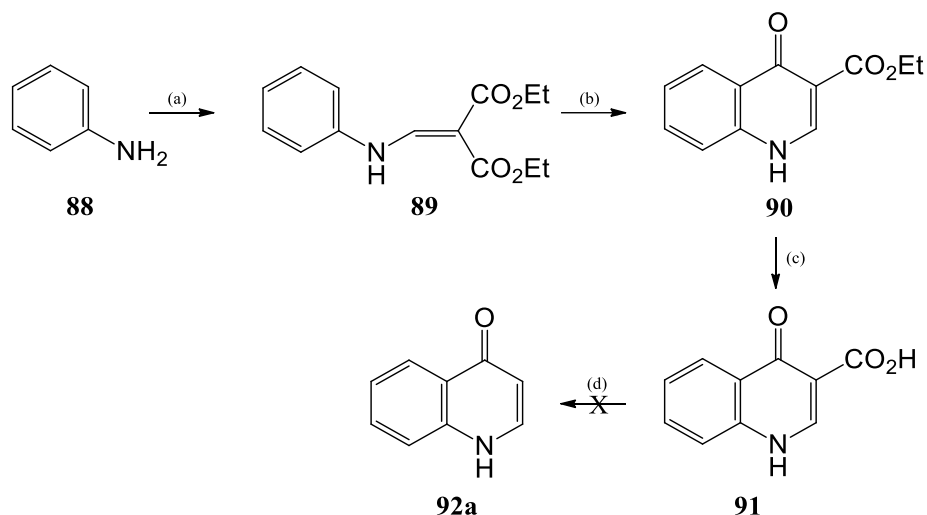
cyclisation of enamines **12**, **39**, **41** and **73**). Interestingly, the cyclisation of enamines **12** and **39** mediated by phosphorus oxychloride was successful, affording products that coincided with the quinolones obtained by using the Gould-Jacobs methodology (**14** and **43**), although in improved yields (40% vs 17% and 49% vs 44%, respectively). Applying the methodology based on phosphorus oxychloride mediated cyclisation to enamine **73** afforded a salt, 4-hydroxy-quinolone **82b·HCl**, while **41** originated a quinolone-4-phenoxyether derivative (**45b**), this implying, once again, that prior synthesis of the corresponding hydroxy-quinolone had occurred.

These results prompted us to undertake a more detailed investigation regarding the structure of the quinolone core, the possibility of tautomerism in quinolone 3-esters and its possible impact on activity.



## 2.6. Synthesis of 4-oxo-quinoline

Considering the data gathered regarding substituted quinolone 3-esters it was decided to investigate further the effect of substituents at positions 6 or 7, regarding consequences on the tautomeric and conformational preferences of the quinolone core and corresponding impact in pharmacodynamic and pharmacokinetic profiles. As such, and in view of a deeper analysis, we deemed important to synthesize the parent unsubstituted 4-oxo-quinoline (**92a**), the 3-ethyl ester derivative (**90**) and the 3-carboxylic acid derivative (**91**). As shown in Scheme 2.33, compounds **90** and **91** are intermediate compounds in the preparation of **92a**.



**Scheme 2.33** – Representation of the synthetic approach followed to the unsubstituted 4-oxo-quinoline (**92a**); Conditions: (a) 100 °C, overnight; (b) Dowtherm A, 250 °C, 3 hours; (c) Methanol, NaOH (10%), 100 °C, overnight; (d) heating at 300 °C, 20 minutes.

The synthetic approach followed was based on the general method adopted along the work (Scheme 2.33), starting with the coupling of the aniline **88** with DEEMM to give enamine **89** in good yield (99%) and following to the cyclisation step by using Dowtherm A to afford ethyl 4-oxo-quinoline-3-carboxylate **90** (31%). The ethyl ester group was then successfully hydrolyzed with a yield of 75%, forming 4-oxo-quinoline 3-carboxylic acid (**91**) that, upon decarboxylation, led to **92a**. The reaction conditions for the last step still need optimization since the melting point of **91** is higher than 250 °C.

## 2.7. Summary, conclusions and future work

This chapter was dedicated to the synthesis of quinolone 3-esters, with general structure represented in Scheme 2.1 (the target template proposed), with potential activity as inhibitors of the *bc<sub>1</sub>* protein complex of *P. falciparum*. A general synthetic approach to the designed scaffolds was devised (Scheme 2.1), generally starting from nitro arenes. Reaction conditions for the reduction of *meta* and/or *ortho* substituted nitro arenes to the corresponding anilines (step 1) and for the coupling of anilines with DEEMM (step 2) to afford enamine derivative ( $\alpha,\beta$ -unsaturated ester) were optimized to give high yield of the desired products. Additional reactions to increase the diversity of the compounds were performed, for example by modification of hydroxyl or halogen groups. Regarding the cyclisation of the enamine derivatives to afford the quinolone scaffolds, most reactions were performed following the thermally driven Gould-Jacobs intramolecular cyclisation methodology. However, this step posed some problems that should not be neglected:

- the cyclisation reaction did not occur for all the enamine derivatives prepared and, when occurring, the yields varied from 3% to 62%;
- the cyclisation reaction proved to be concentration dependent;
- the solubility in quinolone derivatives is poor (it is difficult to isolate and purify the compounds and also to characterize by <sup>13</sup>C NMR and sometimes even difficult to obtain <sup>1</sup>H NMR data with good quality);
- the high boiling point of Dowtherm A renders its total extraction or separation from the desired organic products a difficult task;
- the problems associated to the purification of the products (insolubility problems also render difficult the purification, for example, by column chromatography);
- the high temperatures required for Gould-Jacobs intramolecular cyclisation can lead to degradation of susceptible groups (thermolysis);
- the strategy may lead to mixtures of structural isomers, with different substitution patterns on the carbocyclic ring (cyclisation consists in an aromatic substitution at the adjacent carbon to the NH group of the enamine);
- additionally, there is a possibility of oxo-quinoline/hydroxy-quinoline tautomerism, which may impact in activity and/or mode of action, due to functional group interconversions and resulting alterations in drug-target interactions;
- side products may be obtained from the reaction (*e.g.* amide and urea derivatives).



To overcome some of these problems, for example those related to the poor solubility and the high reaction temperatures, a new synthetic approach was considered, based in the synthesis (in one pot from the corresponding enamine) of 4-chloroquinoline derivatives as intermediate compounds, which are more easily solubilized and isolated and may be, subsequently, converted into the corresponding quinolones. However, for this alternative cyclisation methodology, mediated by POCl<sub>3</sub>, some limitations were also found. In some cases the reaction did not progress or it was not possible to isolate a pure product and, in other situations, unexpected products were obtained.

Thus, and considering all the aspects involved in the synthesis of quinolone derivatives, additional studies to elucidate the structure, the possibility of tautomerism and its impact on biological activity, and deep efforts to develop reliable synthetic routes, are a major priority.

## **2.8. Experimental**

### Solvents, reagents and other consumables used in the preparation and isolation of compounds

Commercially available reagents and solvents were purchased from commercial sources (Sigma-Aldrich, Alfa Aesar, Acros Organics, Merck, Apollo Scientific Ltd, Fluorochem, Fisher Chemical, Panreac, VWR, Fluka, LabChem, Laborspirit) and used as received. When required, solvents were freshly distilled in the laboratory, from appropriate drying agents, before use: THF was distilled from metallic sodium, using benzophenone as indicator, under a constant flow of dry nitrogen. Whenever required, inorganic solids were removed by filtration through a layer of Celite<sup>®</sup> 512 medium sourced from Fluka Analytical.

### Synthesis: monitoring and purification

The reactions were monitored by thin layer chromatography (TLC), using pre-coated plates with silica gel 60 with fluorescent indicator UV<sub>254</sub>. After elution, the plates were visualised using an ultra-violet lamp (254 nm) and developed in anisaldehyde dip: previously prepared from ethanol (280 ml), concentrated sulphuric acid (21 ml), glacial acetic acid (6.25 ml) and *p*-anisaldehyde (1.5ml). Purification by column chromatography was carried out using silica gel 60 (particle size 40-63  $\mu\text{m}$ ) sourced from Merck and using hand bellows or air flow to apply pressure to the column.

### Spectroscopy

NMR spectra for compounds were recorded at 400 and 100 MHz, for <sup>1</sup>H and <sup>13</sup>C, respectively, using spectrometers available at the University of Liverpool (Department of Chemistry) as those that are part of The National NMR Facility, supported by Fundação para a Ciência e Tecnologia (RECI/BBB-BQB/0230/2012), in REQUIMTE, Departamento de Química e Bioquímica, Universidade Nova de Lisboa, Monte da Caparica. Chemical shifts ( $\delta$ ) are described in parts per million (ppm) relative to an internal tetramethylsilane standard (TMS;  $\delta=0.0$  ppm). Appropriate deuterated solvents (D<sub>6</sub>-DMSO; D<sub>1</sub>-chloroform; D<sub>4</sub>-methanol) were supplied by Sigma-Aldrich and were used without additional purification. Splitting patterns are designated as singlet (s), broad singlet (bs), doublet (d), triplet (t), quartet (q), doublet of doublets (dd), doublet of triplets (dt), doublet of quartets (dq) or multiplet (m).

Mass Spectrometry data was acquired at Laboratório de Análises / REQUIMTE, Departamento de Química, Universidade Nova de Lisboa or at the University of Liverpool (Department of Chemistry). For electrospray ionisation (ES) and electron impact ionisation (EI), Micromass LCT (liquid chromatography time of flight) and Micromass GCT (gas chromatography time of flight) mass spectrometers were used respectively. Chemical ionisation (CI) was recorded using an Agilent QTOF (quadrupole time of flight) 7200 spectrometer. MALDI (matrix-assisted laser desorption/ionisation) analyses were performed in a Voyager-DE<sup>TM</sup> PRO Workstation. In the description of mass spectra,  $[M]^+$  refers to the molecular ion,  $[M + H]^+$  to the protonated molecular ion peaks, while  $[M + K]^+$ ,  $[M + Na]^+$  and  $[M + NH_4]^+$  represent the peaks for the compound's molecular ion adducts.

#### Other analysis

Melting ranges were recorded on a Stuart Scientific SMP3 melting point apparatus and are uncorrected.

Elemental analysis (CHN) were performed in the micro analytical laboratory available at the University of Liverpool, Department of Chemistry.

#### **Synthesis; general methods**

##### General method A: reduction of nitro arenes to aniline derivatives

The nitro arene derivative (1 eq.) was dissolved in a mixture of methanol and water (1:1; 40 ml). Ammonium chloride (6.7 eq.) was added, followed by iron powder (4.2 eq.) and the resulting mixture was stirred at 85 °C for 4 hours. The reaction mixture was then cooled and diluted with methanol (around 50 mL) and the inorganic solids were removed by filtering through a layer of Celite<sup>®</sup>. The filtrate was concentrated by evaporation under reduced pressure and the aqueous residue extracted with ethyl acetate (2x30 ml). The combined organic extracts were dried over anhydrous MgSO<sub>4</sub>, filtered, and the filtrate was evaporated to dryness under reduced pressure.

##### General method B: coupling of aniline derivatives with DEEMM to afford enamines

The appropriate aniline derivative (1 eq.) was dissolved in diethyl (ethoxymethylene)malonate (DEEMM; 1 eq.) and the mixture was stirred overnight, under reflux (100 °C).

General method C: Gould-Jacobs cyclisation of enamines to 4-oxo-quinoline 3-esters

The diethyl malonate enamine intermediate was suspended in Dowtherm A<sup>®</sup>, under a nitrogen atmosphere, and the mixture was refluxed at 250 °C for some hours (generally 3 hours) according with the reaction progress monitored by TLC. The reaction mixture was cooled to room temperature and the resulting precipitate (that generally appeared) was filtered, washed with hexane and diethyl ether and dried.

General method D: modification of hydroxyl group from **16**, introducing heterocyclic substituents

Diethyl 2-(((3-hydroxyphenyl)amino)methylene)malonate **16** (1 eq.) and potassium *tert*-butoxide (3 eq.) were dissolved in dried THF (30mL) and stirred at 64 °C for 1 hour. The heterocyclic halide derivative (1.2 eq.) was then added, and the mixture was kept stirring at 64 °C (reflux), under a N<sub>2</sub> atmosphere, for 24 hours.

The mixture was cooled to r.t. and the THF was removed under reduced pressure. The solid residue was washed, dissolved and extracted using ethyl acetate (3 x 20 ml). The organic layers were combined, dried over anhydrous MgSO<sub>4</sub>, filtered and the filtrate was concentrated under reduced pressure.

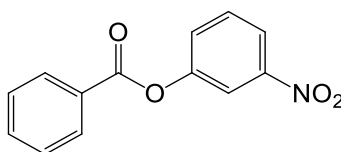
General method E: cyclisation of enamine mediated by phosphorus oxychloride

The diethyl malonate enamine derivative was suspended in phosphorous oxychloride, under a nitrogen atmosphere, and the mixture was refluxed overnight at 95 °C. Evaporation of the phosphoryl byproducts under reduced pressure and heating, followed by co-evaporation with toluene ensued. The final residue was dissolved in isopropanol at 90 °C (around 30 minutes), the solution was cooled to room temperature and the resulting precipitate was filtered and washed with cold isopropanol and light petroleum ether.

**Detailed synthetic procedures**

Synthesis of 7-substituted 4-oxo-quinoline 3-esters involving modification of the hydroxyl group of 3-nitrophenol, to afford diphenyl ester and ether derivatives

*3-Nitrophenyl benzoate (6)*

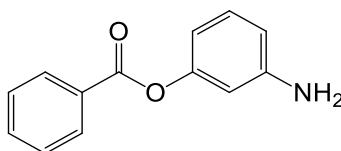


3-Nitrophenol **1** (4.00 g; 28.75 mmol; 1 eq.) was dissolved in dried TEA (2.5 eq.), under a nitrogen atmosphere. Benzoyl chloride **2** (1 eq.) was mixed with dried THF (30 mL) and the mixture was added to the solution of **1** in TEA. The reaction was stirred at room temperature, under nitrogen atmosphere, for 4 hours.

Cold water was added and the mixture was acidified to around pH 3 using hydrochloric acid (37%). The THF was removed under reduced pressure and the aqueous residue was extracted with ethyl acetate (3x20 ml). The organic extracts were combined, dried under anhydrous MgSO<sub>4</sub> filtered and the solvent was removed under reduced pressure. Recrystallization of the solid residue from ethanol (DCM assisted in the dissolution) gave the desired product as white needles (6.33 g; 26.04 mmol; yield 91%).

Melting range: 94-96 °C; <sup>1</sup>H NMR (400 MHz, (CD<sub>3</sub>)<sub>2</sub>SO) δ 8.24-8.14 (m, 4H), 7.83-7.74 (m, 3H), 7.61 (t, 2H); <sup>13</sup>C NMR (101 MHz, (CD<sub>3</sub>)<sub>2</sub>SO) δ 164.64 (C=O), 151.28, 148.73, 134.72, 131.25, 130.37 (2C), 129.50, 129.39 (2C), 128.80, 121.43, 117.94; MS m/z (CI) [M + H]<sup>+</sup> C<sub>13</sub>H<sub>9</sub>NO<sub>4</sub> requires 244.1304, found 244.0604.

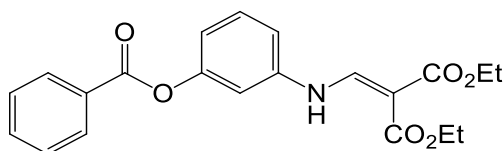
*3-Aminophenyl benzoate (9)*



Synthesised, according to general method A, from 3-nitrophenyl benzoate **6** (4.40 g; 18.1 mmol) to afford a brown oil (3.73g; 17.47 mmol; yield 97%).

<sup>1</sup>H NMR (400 MHz, (CD<sub>3</sub>)<sub>2</sub>SO) δ 8.08 (d, 2H), 7.71 (t, 1H), 7.60-7.56 (t, 2H), 7.07-7.03 (t, 1H), 6.49 (d, 1H), 6.41 (s, 1H), 6.35 (d, 1H); <sup>13</sup>C NMR (101 MHz, CDCl<sub>3</sub>) δ 165.24 (C=O), 151.96, 147.69, 133.51, 130.15 (2C), 129.68, 128.66, 128.54 (2C), 112.74, 111.56, 108.44; MS m/z (MALDI-TOF) [M + H]<sup>+</sup> C<sub>13</sub>H<sub>11</sub>NO<sub>2</sub> requires 214.0868, found 214.0831.

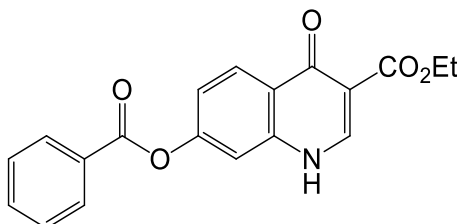
Diethyl 2-(((3-benzoyloxyphenyl)amino)methylene)malonate (**11**)



Synthesised according to the general method B, from 3-aminophenyl benzoate **9** (3.73 g; 17.47 mmol). Isolated as yellow crystals (2.33 g; 6.07 mmol; yield 35%), after purification by column chromatography (eluting with 10% ethyl acetate in 90% hexane).

Melting range: 55-57 °C;  $^1\text{H}$  NMR (400 MHz,  $(\text{CD}_3)_2\text{SO}$ )  $\delta$  10.69 (d, NH), 8.39 (d, CHNH), 8.18 – 8.10 (d, 2H), 7.74 (t, 1H), 7.61 (t, 2H), 7.46 (m, 2H), 7.31 (d, 1H), 7.07 (d, 1H), 4.20-4.11 (m, 2 x OCH<sub>2</sub>CH<sub>3</sub>), 1.23 – 1.14 (m, 2 x OCH<sub>2</sub>CH<sub>3</sub>);  $^{13}\text{C}$  NMR (101 MHz,  $(\text{CD}_3)_2\text{SO}$ )  $\delta$  167.68 (C=O), 165.36 (CO<sub>2</sub>Et), 164.89 (CO<sub>2</sub>Et), 152.09, 151.17 (CHNH), 141.11, 134.51, 130.97, 130.27 (2C), 129.38 (2C), 129.29, 118.33, 115.67, 111.64, 94.49 [C(CO<sub>2</sub>Et)<sub>2</sub>], 60.19 (OCH<sub>2</sub>CH<sub>3</sub>), 59.99 (OCH<sub>2</sub>CH<sub>3</sub>), 14.68 (OCH<sub>2</sub>CH<sub>3</sub>), 14.60 (OCH<sub>2</sub>CH<sub>3</sub>); MS m/z (EI) [M]<sup>+</sup> C<sub>21</sub>H<sub>21</sub>NO<sub>6</sub> requires 383.1369, found 383.1521; CHN for C<sub>21</sub>H<sub>21</sub>NO<sub>6</sub> requires C 65.79%, H 5.52%, N 3.65%, found C 65.83%, H 5.67%, N 3.44%.

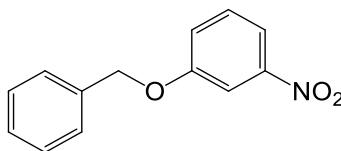
Ethyl 7-benzoyloxy-4-oxo-quinoline-3-carboxylate (**13**)



Synthesised according to the general method C, from enamine **11** (1.05 g; 2.71 mmol) in Dowtherm A (10 ml; 3 hours), to afford a brown powder (0.67 g; crude yield 73%). It was not possible to purify the compound due to insolubility problems and because the  $R_f$  (retention factor) of impurities were essentially close to that of **13**, making efficient purification of the product impractical.

Some characteristic data that prove the presence of **13** in the mixture:  $^1\text{H}$  NMR (400 MHz, DMSO)  $\delta$  4.24 (OCH<sub>2</sub>CH<sub>3</sub>), 1.29 (OCH<sub>2</sub>CH<sub>3</sub>);  $^{13}\text{C}$  NMR (101 MHz,  $(\text{CD}_3)_2\text{SO}$ )  $\delta$  130.49-129.51 (ArCOO), 60.12 (2C, OCH<sub>2</sub>CH<sub>3</sub>), 14.79 (2C, OCH<sub>2</sub>CH<sub>3</sub>); MS m/z (ES) [M + Na]<sup>+</sup> C<sub>19</sub>H<sub>15</sub>NO<sub>5</sub>Na requires 360.0845, found 360.0975.

*1-Benzyloxy-3-nitrobenzene (7)*



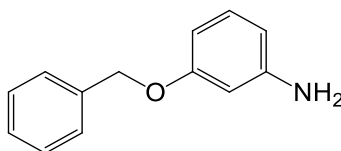
3-Nitrophenol **1** (3.00 g; 21.57 mmol; 1 eq.) and NaH (2 eq.) were mixed in dry THF (30 mL), under a nitrogen atmosphere. The mixture was stirred for 30 minutes at room temperature. Benzyl bromide **4** (1 eq.) was then added and the resulting mixture was kept stirring at 60 °C for 4 days, keeping the anhydrous conditions.

Cold water was added, the mixture was concentrated under reduced pressure (THF was removed) and the aqueous residue was extracted with ethyl acetate (3x20 ml). The organic extracts were dried under anhydrous MgSO<sub>4</sub>, filtered, and the solvent was removed under reduced pressure. Recrystallization of the solid residue from ethanol gave the desired product as yellow crystals (4.29 g; 18.70 mmol; yield 87%).

A similar procedure was applied, to afford the same product, but using benzyl chloride **3** (1 eq.).

Melting range: 59-60 °C; <sup>1</sup>H NMR (400 MHz, (CD<sub>3</sub>)<sub>2</sub>SO) δ 7.80 (d, 2H), 7.57 (t, 1H), 7.48 (m, 3H), 7.40 (t, J = 7.3 Hz, 2H), 7.36 – 7.32 (m, 1H), 5.23 (s, OCH<sub>2</sub>Ar); <sup>13</sup>C NMR (101 MHz, (CD<sub>3</sub>)<sub>2</sub>SO) δ 159.20, 149.09, 136.56, 131.09, 128.90 (2C), 128.48, 128.22 (2C), 122.66, 116.07, 109.39, 70.30 (OCH<sub>2</sub>Ar); MS m/z (CI) [M + H]<sup>+</sup> C<sub>13</sub>H<sub>11</sub>NO<sub>3</sub> requires 230.1504, found 230.0820.

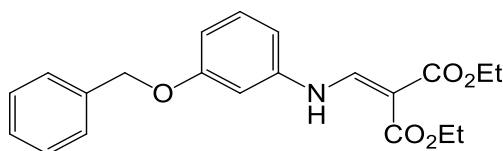
*3-Benzyloxy-aniline (10)*



Synthesised according to the general method A, from 1-benzyloxy-3-nitrobenzene **7** (3.00 g; 13.10 mmol). The product was recovered as a dark oil (2.60 g; 13.05 mmol; yield 99%).

<sup>1</sup>H NMR (400 MHz, (CD<sub>3</sub>)<sub>2</sub>SO) δ 7.41-7.38 (m, 5H), 6.91-6.87 (t, 1H), 6.22 (s, 1H), 6.21-6.15 (d, 2H), 5.05 (s, OCH<sub>2</sub>Ar), 4.98 (s, NH<sub>2</sub>); <sup>13</sup>C NMR (101 MHz, (CD<sub>3</sub>)<sub>2</sub>SO) δ 159.73, 150.36, 137.89, 129.90, 128.73 (2C), 128.00, 127.86 (2C), 107.43, 102.56, 100.67, 69.05 (OCH<sub>2</sub>Ar); MS m/z (CI) [M + H]<sup>+</sup> C<sub>13</sub>H<sub>14</sub>NO requires 200.1075, found 200.1074.

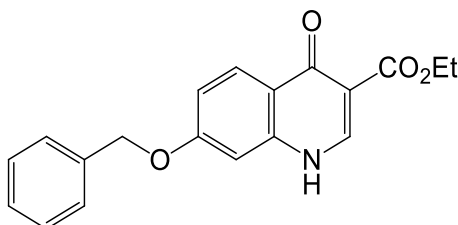
Diethyl 2-(((3-benzyloxyphenyl)amino)methylene)malonate (**12**)



Synthesised according to the general method B, from 3-benzyloxy aniline **10** (1.04 g; 5.24 mmol), to afford a brown solid (1.91 g; 5.16 mmol; yield 99%).

Melting range: 67-68 °C; <sup>1</sup>H NMR (400 MHz, (CD<sub>3</sub>)<sub>2</sub>SO) δ 10.66 (d, NH), 8.40 (d, CHNH), 7.48-7.28 (m, 6H), 7.08 (t, 1H), 6.94 (d, 1H), 6.81 (d, 1H), 5.14 (s, OCH<sub>2</sub>Ar), 4.21 (q, OCH<sub>2</sub>CH<sub>3</sub>), 4.12 (q, OCH<sub>2</sub>CH<sub>3</sub>), 1.28 – 1.23 (m, 2 x OCH<sub>2</sub>CH<sub>3</sub>); <sup>13</sup>C NMR (101 MHz, (CD<sub>3</sub>)<sub>2</sub>SO) δ 167.69 (CO<sub>2</sub>Et), 165.29 (CO<sub>2</sub>Et), 159.79, 151.36 (CHNH), 140.99, 137.21, 130.98, 128.82 (2C), 128.27, 128.12 (2C), 111.60, 110.06, 104.67, 93.68 [C(CO<sub>2</sub>Et)<sub>2</sub>], 69.72 (OCH<sub>2</sub>Ar), 60.06 (OCH<sub>2</sub>CH<sub>3</sub>), 59.87 (OCH<sub>2</sub>CH<sub>3</sub>), 14.61 (OCH<sub>2</sub>CH<sub>3</sub>), 14.54 (OCH<sub>2</sub>CH<sub>3</sub>); MS m/z (ES) [M + Na]<sup>+</sup> C<sub>21</sub>H<sub>23</sub>NO<sub>5</sub>Na requires 392.1474, found 392.1467.

Ethyl 7-benzyloxy-4-oxo-quinoline-3-carboxylate (**14**)



Synthesised according to the general method C, from enamine **12** (1.00 g; 2.71 mmol) in 10 ml of Dowtherm A (3 hours), to afford a brown powder (0.15 g; 0.45 mmol; yield 17%).

Melting range: 269-270 °C; <sup>1</sup>H NMR (400 MHz, (CD<sub>3</sub>)<sub>2</sub>SO) δ 12.08 (s, NH), 8.47 (s, CHNH), 8.05 (d, 1H), 7.49-7.35 (m, 6H), 7.07 (m, 1H), 5.22 (s, OCH<sub>2</sub>Ar), 4.19 (q, OCH<sub>2</sub>CH<sub>3</sub>), 1.26 (t, OCH<sub>2</sub>CH<sub>3</sub>); <sup>13</sup>C NMR data not obtained due to poor solubility in all available deuterated solvents; MS m/z (EI) [M]<sup>+</sup> C<sub>19</sub>H<sub>17</sub>NO<sub>4</sub> requires 323.1158, found 323.1204; CHN for C<sub>19</sub>H<sub>17</sub>NO<sub>4</sub> requires C 70.58%, H 5.30%, N 4.33%, found C 70.34%, H 5.24%, N 4.09%.

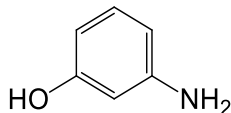
The compound was also synthesized using the general method E. From enamine **12** (0.65 g; 1.76 mmol), in 5 ml of POCl<sub>3</sub>, to afford a beige powder (0.23 g; 0.70 mmol; 40%).



$^1\text{H}$  NMR (400 MHz,  $(\text{CD}_3)_2\text{SO}$ )  $\delta$  12.02 (s,  $\text{NH}$ ), 8.39 (d,  $\text{CHNH}$ ), 7.97 (d, 1H), 7.40 (m, 2H), 7.37 (m, 2H), 7.30 (m, 1H), 7.00 (m, 2H), 5.14 (s,  $\text{OCH}_2\text{Ar}$ ), 4.11 (q,  $\text{OCH}_2\text{CH}_3$ ), 1.19 (t,  $\text{OCH}_2\text{CH}_3$ ).

*Synthesis of 4-oxo-quinolines bearing heterocyclic substituents at position 7, from the common intermediate diethyl 2-(((3-hydroxyphenyl)amino)methylene)malonate (16)*

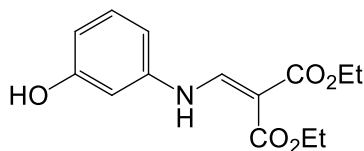
*3-Aminophenol (15)*



Synthesised according to the general method A, from 3-nitrophenol **1** (1.00 g; 7.19 mmol) to afford a brown solid (0.78 g; 7.15 mmol; yield 99%).

Melting range: 110-112 °C;  $^1\text{H}$  NMR (400 MHz,  $\text{CD}_3\text{OD}$ )  $\delta$  6.90-6.86 (t, 1H), 6.22-6.19 (m, 2H), 6.14 (d, 1H);  $^{13}\text{C}$  NMR (101 MHz,  $(\text{CD}_3)_2\text{SO}$ )  $\delta$  158.41 ( $\text{COH}$ ), 150.13 ( $\text{CNH}_2$ ), 129.78, 105.78, 103.66, 101.32; MS  $m/z$  (CI)  $[\text{M} + \text{H}]^+$   $\text{C}_6\text{H}_8\text{NO}$  requires 110.0606, found 110.0600.

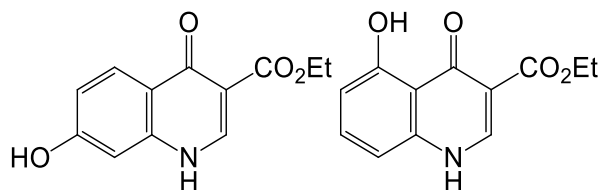
*Diethyl 2-(((3-hydroxyphenyl)amino)methylene)malonate (16)*



Synthesised according to general method B, from 3-aminophenol **15** (2.00 g; 18.33 mmol). Crystallization from ethanol and DCM afforded yellow crystals (4.65 g; 16.66 mmol; yield 91%).

Melting range: 141-142 °C;  $^1\text{H}$  NMR (400 MHz,  $\text{CD}_3\text{OD}$ )  $\delta$  8.53 (s,  $\text{CHNH}$ ), 7.21 (t, 1H), 6.66 (m, 3H), 4.2-4.22 (m, 2 x  $\text{OCH}_2\text{CH}_3$ ), 1.35 (m, 2 x  $\text{OCH}_2\text{CH}_3$ );  $^{13}\text{C}$  NMR (101 MHz,  $(\text{CD}_3)_2\text{SO}$ )  $\delta$  167.69 ( $\text{CO}_2\text{Et}$ ), 165.23 ( $\text{CO}_2\text{Et}$ ), 158.90 ( $\text{COH}$ ), 151.27 ( $\text{CHNH}$ ), 140.81, 130.97, 112.29, 108.59, 104.57, 93.25 [ $\text{C}(\text{CO}_2\text{Et})_2$ ], 60.02 ( $\text{OCH}_2\text{CH}_3$ ), 59.81 ( $\text{OCH}_2\text{CH}_3$ ), 14.63 ( $\text{OCH}_2\text{CH}_3$ ), 14.56 ( $\text{OCH}_2\text{CH}_3$ ); MS  $m/z$  (ES)  $[\text{M} + \text{Na}]^+$   $\text{C}_{14}\text{H}_{17}\text{NO}_5\text{Na}$  requires 302.1004, found 302.0994.

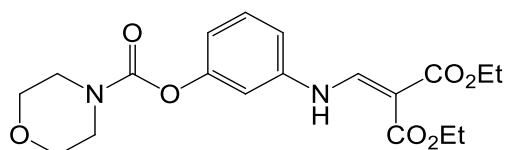
Isomeric mixture: ethyl 7-hydroxy-4-oxo-quinoline-3-carboxylate (**33a**) and ethyl 5-hydroxy-4-oxo-quinoline-3-carboxylate (**33b**)



Obtained following the general method C, from enamine **16** (0.63 g; 2.26 mmol) in 10 ml of Dowtherm A (3 hours). Precipitated as white powder (0.09 g; 0.39 mmol; yield 17%, identified as a mixture of isomers).

$^1\text{H}$  NMR (400 MHz,  $(\text{CD}_3)_2\text{SO}$ )  $\delta$  12.75 (s,  $\text{NH}$ ), 12.00 (s,  $\text{NH}$ ), 8.59 (s,  $\text{CHNH}$ )<sup>33b</sup>, 8.42 (d,  $\text{CHNH}$ )<sup>33a</sup>, 7.97 (d, 1H)<sup>33a</sup>, 7.56 (t, 1H)<sup>33b</sup>, 7.03 (d, 1H)<sup>33b</sup>, 6.87 (m, 2H)<sup>33a</sup>, 6.70 (d, 1H)<sup>33b</sup>, 4.24 (q,  $\text{OCH}_2\text{CH}_3$ ), 4.19 (q,  $\text{OCH}_2\text{CH}_3$ ), 1.30 (t,  $\text{OCH}_2\text{CH}_3$ ), 1.27 (t,  $\text{OCH}_2\text{CH}_3$ );  $^{13}\text{C}$  NMR (101 MHz,  $(\text{CD}_3)_2\text{SO}$ )  $\delta$  180.29, 165.40, 164.29, 162.11, 161.41, 146.36, 144.97, 141.29, 140.35, 135.08, 128.14, 120.86, 119.22, 114.04, 110.49, 109.82, 108.77, 107.99, 102.40, 60.34 ( $\text{OCH}_2\text{CH}_3$ ), 59.87 ( $\text{OCH}_2\text{CH}_3$ ), 14.81 ( $\text{OCH}_2\text{CH}_3$ ), 14.76 ( $\text{OCH}_2\text{CH}_3$ ); MS  $m/z$  (ES)  $[\text{M} + \text{Na}]^+$   $\text{C}_{12}\text{H}_{11}\text{NO}_4\text{Na}$  requires 256.0586, found 256.0581; CHN for  $\text{C}_{12}\text{H}_{11}\text{NO}_4$  requires C 61.80%, H 4.75%, N 6.01%, found C 61.47%, H 4.63%, N 5.82%.

Diethyl 2-(((3-((4-morpholinecarbonyl)oxy)phenyl)amino)methylene)malonate (**23**)

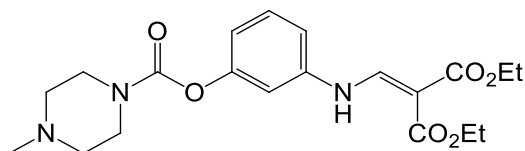


Synthesised following the general method D, from **16** (1.00 g; 3.58 mmol) and 4-morpholine carbonyl chloride **17** (0.49 ml; 4.30 mmol), to afford brown crystals (0.90 g; 2.30 mmol; yield 64%), after crystallization from ethanol and DCM.

$^1\text{H}$  NMR (400 MHz,  $(\text{CD}_3)_2\text{SO}$ )  $\delta$  10.64 (d,  $\text{NH}$ ), 8.36 (d,  $\text{CHNH}$ ), 7.37 (t, 1H), 7.26 (s, 1H), 7.22 (d, 1H), 6.92 (d, 1H), 4.19 (q,  $\text{OCH}_2\text{CH}_3$ ), 4.11 (q,  $\text{OCH}_2\text{CH}_3$ ), 3.64-3.41 (m, 8H), 1.24 (m, 2 x  $\text{OCH}_2\text{CH}_3$ );  $^{13}\text{C}$  NMR (101 MHz,  $(\text{CD}_3)_2\text{SO}$ )  $\delta$  167.60 ( $\text{CO}_2\text{Et}$ ), 165.44 ( $\text{CO}_2\text{Et}$ ), 153.22, 152.57, 151.23, 140.88, 130.72, 118.37, 115.01, 111.70, 94.32 [ $\text{C}(\text{CO}_2\text{Et})_2$ ], 66.23 (2 x  $\text{OCH}_2\text{CH}_2\text{N}$ ), 60.20 ( $\text{OCH}_2\text{CH}_3$ ), 60.02 ( $\text{OCH}_2\text{CH}_3$ ), 45.06 ( $\text{OCH}_2\text{CH}_2\text{N}$ ), 44.30 ( $\text{OCH}_2\text{CH}_2\text{N}$ ), 14.73 ( $\text{OCH}_2\text{CH}_3$ ), 14.64 ( $\text{OCH}_2\text{CH}_3$ ); MS  $m/z$  (ES)  $[\text{M} + \text{Na}]^+$   $\text{C}_{19}\text{H}_{24}\text{N}_2\text{O}_7\text{Na}$  requires 415.1481, found 415.1; CHN for  $\text{C}_{19}\text{H}_{24}\text{N}_2\text{O}_7$  requires C 58.16%, H 6.16%, N 7.14%, found C 58.20%, H 6.90%, N 7.18%.

*Diethyl 2-(((3-((4-methylpiperazine-1-carbonyl)oxy)phenyl)amino)methylene)malonate*

(24)

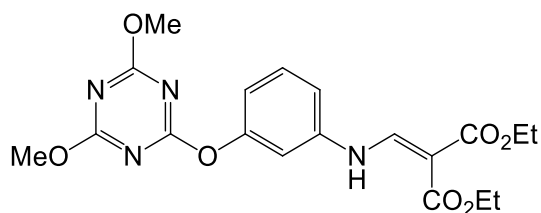


Synthesised following the general method D, from **16** (1.00 g; 3.58 mmol) and 4-methyl-1-piperazine carbonyl chloride **18** (0.70 g; 4.30 mmol). Isolated as an orange oil (0.98 g; 2.41 mmol; yield 67%) after purification by column chromatography (eluting with 5% methanol in 95% DCM).

$^1\text{H}$  NMR (400 MHz,  $(\text{CD}_3)_2\text{SO}$ )  $\delta$  10.64 (d, NH), 8.35 (d, CHNH), 7.36 (t, 1H), 7.24 (s, 1H), 7.21 (d, 1H) 6.95 (d, 1H), 4.20 (q,  $\text{OCH}_2\text{CH}_3$ ), 4.12 (q,  $\text{OCH}_2\text{CH}_3$ ), 3.49 (m, 2 x  $\text{MeNCH}_2\text{CH}_2$ ), 2.35 (m, 2 x  $\text{MeNCH}_2$ ), 2.21 (s,  $\text{H}_3\text{CN}$ ), 1.24 (m, 2 x  $\text{OCH}_2\text{CH}_3$ );  $^{13}\text{C}$  NMR (101 MHz,  $(\text{CD}_3)_2\text{SO}$ )  $\delta$  167.58 ( $\text{CO}_2\text{Et}$ ), 165.43 ( $\text{CO}_2\text{Et}$ ), 153.11, 152.63, 151.23, 140.88, 130.70, 118.37, 114.89, 111.75, 94.34 [ $\text{C}(\text{CO}_2\text{Et})_2$ ], 60.18 ( $\text{OCH}_2\text{CH}_3$ ), 60.01 ( $\text{OCH}_2\text{CH}_3$ ), 54.70 ( $\text{NCH}_2\text{CH}_2\text{N}$ ), 54.55 ( $\text{NCH}_2\text{CH}_2\text{N}$ ), 46.17 ( $\text{H}_3\text{CN}$ ), 44.63 ( $\text{NCH}_2\text{CH}_2\text{N}$ ), 44.61 ( $\text{NCH}_2\text{CH}_2\text{N}$ ), 14.73 ( $\text{OCH}_2\text{CH}_3$ ), 14.65 ( $\text{OCH}_2\text{CH}_3$ ); MS  $m/z$  (EI)  $[\text{M}]^+$   $\text{C}_{20}\text{H}_{27}\text{N}_3\text{O}_6$  requires 405.1900, found 405.2060; CHN for  $\text{C}_{20}\text{H}_{27}\text{N}_3\text{O}_6$  requires C 59.25%, H 6.71%, N 10.36%, found C 59.69%, H 7.18%, N 9.82%.

*Diethyl 2-(((3-((4,6-dimethoxy-1,3,5-triazin-2-yl)oxy)phenyl)amino)methylene)malonate*

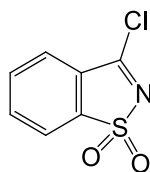
(25)



Synthesised according to the general method D, from **16** (1.00 g; 3.58 mmol) and 2-chloro-4,6-dimethoxy-1,3,5-triazine **19** (0.75 g; 4.30 mmol), to afford a yellow solid (0.24 g; 0.58 mmol; yield 16%) by purification in column chromatography (eluting with DCM).

$^1\text{H}$  NMR and  $^{13}\text{C}$  NMR data not obtained due to insolubility in all available deuterated solvents; MS  $m/z$  (EI)  $[\text{M}]^+$   $\text{C}_{19}\text{H}_{22}\text{N}_4\text{O}_7$  requires 418.1489, found 418.1675.

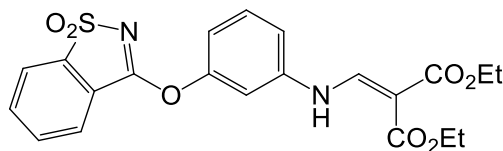
*3-Chloro-1,2-benzisothiazole 1,1-dioxide (pseudo-saccharyl chloride) (21)*



Saccharin **20** (21.00 g; 114.00 mmol) was mixed with phosphorus pentachloride (1.1 eq.) and heated at 180 °C for 3 hours. Phosphorus oxychloride and HCl (side products) and phosphorus pentachloride (in excess) were distilled under vacuum and heating. The residue was cooled to 135 °C, dissolved in toluene (60 ml) and crystallized on cooling to room temperature. The crystals were filtered, washed with cold toluene, dried and recrystallized until the desired pure product was afforded as white crystals (5.93 g; 29.40 mmol; 26% yield).

Melting range: 141-142 °C; <sup>1</sup>H NMR (400 MHz, CDCl<sub>3</sub>) δ 7.95-7.93 (d, 2H), 7.88-7.82 (m, 2H); <sup>13</sup>C NMR (101 MHz, CDCl<sub>3</sub>) δ 166.08 (C-Cl), 140.63 (C-SO<sub>2</sub>), 134.93, 134.41, 129.94, 125.07, 122.49.

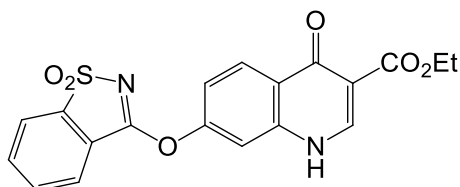
*Diethyl 2-(((3-(((benzysothiazol-3-yl)oxy)phenyl)amino)methylene)malonate (26)*



Diethyl 2-(((3-hydroxyphenyl)amino)methylene)malonate **16** (1.00 g; 3.58 mmol) was dissolved in TEA (2 eq.), under a nitrogen atmosphere. Pseudo saccharin chloride (**21**; 1.3 eq.) was added and the mixture was dissolved in toluene (15 ml), under anhydrous conditions, at 50 °C, for 3 hours. The product appeared as a precipitate, was filtered and washed with cold toluene and recrystallized from ethanol (and DCM) to give white crystals (0.80 g; 1.81 mmol; 51%).

Melting range: 143-144 °C; <sup>1</sup>H NMR (400 MHz, (CD<sub>3</sub>)<sub>2</sub>SO) δ 10.71 (d, NH), 8.37 (d, CHNH), 8.21 (d, 1H), 8.13 (d, 1H), 8.03 – 7.93 (m, 2H), 7.67 (s, 1H), 7.53 (t, 1H), 7.41 (d, 1H), 7.26 (d, 1H), 4.21 (q, OCH<sub>2</sub>CH<sub>3</sub>), 4.11 (q, OCH<sub>2</sub>CH<sub>3</sub>), 1.24 (dt, OCH<sub>2</sub>CH<sub>3</sub>); <sup>13</sup>C NMR data not obtained due to poor solubility in all available deuterated solvents; MS m/z (EI) [M]<sup>+</sup> C<sub>21</sub>H<sub>20</sub>N<sub>2</sub>O<sub>7</sub>S requires 444.0991, found 444.1267.

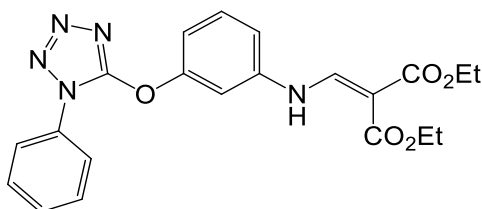
*Ethyl 7-benzysothiazoloxo-4-oxo-quinoline-3-carboxylate (31)*



Synthesised according to the general method C, from enamine **26** (0.50 g; 1.13 mmol) in 10 ml of Dowtherm A (3 hours), to afford a brown powder (0.21 g; 0.54 mmol; yield 48% with Dowtherm A).

Melting range: 265-267 °C; <sup>1</sup>H NMR (400 MHz, (CD<sub>3</sub>)<sub>2</sub>SO) δ 12.51 (s, NH), 8.60 (d, CHNH), 8.29 (d, 1H), 8.23 (d, 1H), 8.16 (d, 1H), 8.00 (m, 2H), 7.80 (s, 1H), 7.55 (d, 1H) and Dowtherm A characteristics peaks; <sup>13</sup>C NMR data not obtained due to poor solubility in all available deuterated solvents; MS m/z (ES) [M + Na]<sup>+</sup> C<sub>19</sub>H<sub>14</sub>N<sub>2</sub>O<sub>6</sub>SNa requires 421.0470, found 421.0466; CHN for C<sub>19</sub>H<sub>14</sub>N<sub>2</sub>O<sub>6</sub>S requires C 57.28%, H 3.54%, N 7.03%, S 8.05% found C 61.50%, H 4.02%, N 5.98%, S 6.34% (presence of Dowtherm A increase the percentage of C and H, decreasing the percentage of N and S).

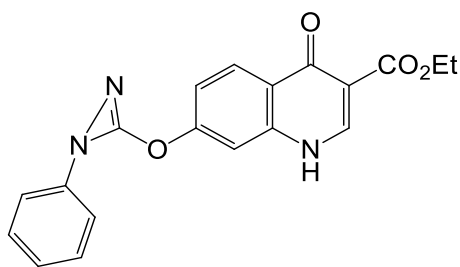
*Diethyl 2-(((3-((1-phenyl-1H-tetrazol-5-yl)oxy)phenyl)amino)methylene)malonate (27)*



Synthesised according to the general method D, from **16** (1.00 g; 3.58 mmol) and 5-chloro-1-phenyl-1H-tetrazole **22** (0.78 g; 4.30 mmol), to afford yellow crystals (1.20 g; 2.84 mmol; yield 79%) from crystallization in ethanol.

Melting range: 117-118 °C; <sup>1</sup>H NMR (400 MHz, (CD<sub>3</sub>)<sub>2</sub>SO) δ 10.72 (d, NH), 8.39 (d, CHNH), 7.87 (d, 2H), 7.74 – 7.65 (m, 3H), 7.62 (d, 1H), 7.51 (t, 1H), 7.37 (d, 1H), 7.29 (d, 1H), 4.22 (q, OCH<sub>2</sub>CH<sub>3</sub>), 4.14 (q, OCH<sub>2</sub>CH<sub>3</sub>), 1.26 (dt, 2 x OCH<sub>2</sub>CH<sub>3</sub>); <sup>13</sup>C NMR (101 MHz, (CD<sub>3</sub>)<sub>2</sub>SO) δ 167.56 (C=O<sub>2</sub>Et), 165.41 (C=O<sub>2</sub>Et), 159.88, 154.73, 150.98, 141.51, 132.98, 131.49, 130.35, 130.31 (2C), 123.69 (2C), 116.12, 116.03, 109.60, 94.89 [C(CO<sub>2</sub>Et)<sub>2</sub>], 60.27 (OCH<sub>2</sub>CH<sub>3</sub>), 60.09 (OCH<sub>2</sub>CH<sub>3</sub>), 14.69 (OCH<sub>2</sub>CH<sub>3</sub>), 14.61 (OCH<sub>2</sub>CH<sub>3</sub>); MS m/z (EI) [M]<sup>+</sup> C<sub>21</sub>H<sub>21</sub>N<sub>5</sub>O<sub>5</sub> requires 423.1543, found 423.1868; CHN for C<sub>21</sub>H<sub>21</sub>N<sub>5</sub>O<sub>5</sub> requires C 59.57%, H 5.00%, N 16.54%, found C 59.32%, H 4.97%, N 16.48%.

Ethyl 7-(1-phenyl-1H-diazirin-3-yl)oxy-4-oxo-quinoline-3-carboxylate (**32b**)

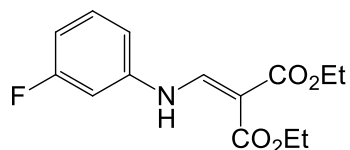


Synthesised according to the general method C, from enamine **27** (0.60 g; 1.42 mmol) in 10 ml of Dowtherm A (3 hours), to afford a yellow powder (0.11 g; 0.31 mmol; yield 22%).

$^1\text{H}$  NMR (400 MHz,  $(\text{CD}_3)_2\text{SO}$ )  $\delta$  10.03 (s, NH), 8.59 (s, 1H), 8.43 (d, 1H), 7.65 (d, 1H), 7.48 – 7.35 (m, 3H), 7.17–7.11 (m, 2H), 6.98 (m, 1H), 4.26 (q,  $\text{OCH}_2\text{CH}_3$ ), 1.29 (t,  $\text{OCH}_2\text{CH}_3$ );  $^{13}\text{C}$  NMR (101 MHz,  $(\text{CD}_3)_2\text{SO}$ )  $\delta$  163.16, 158.52, 156.17, 149.76, 146.59, 141.65, 140.21, 130.80, 130.14, 125.87, 123.09, 118.74, 117.46, 117.07, 115.44, 114.32, 102.36, 60.92 ( $\text{OCH}_2\text{CH}_3$ ), 14.67 ( $\text{OCH}_2\text{CH}_3$ ); MS m/z (EI)  $[\text{M}]^+$   $\text{C}_{19}\text{H}_{15}\text{N}_3\text{O}_4$  requires 349.1063, found 349.1133; MS m/z (MALDI-TOF)  $[\text{M} + \text{H}]^+$   $\text{C}_{19}\text{H}_{16}\text{N}_3\text{O}_4$  requires 350.1141, found 350.0479; MS m/z (ES)  $[\text{M} + \text{Na}]^+$   $\text{C}_{19}\text{H}_{15}\text{N}_3\text{O}_4\text{Na}$  requires 372.0960, found 372.0962.

Synthesis of 7-substituted 4-oxo-quinoline 3-esters from the nucleophilic aromatic substitution of halogen by tetrazolyl and morpholinyl derivatives

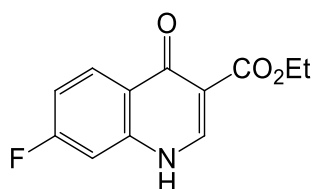
Diethyl 2-((3-fluorophenyl)amino)methylene)malonate (**39**)



Synthesised according to the general method B, from 3-fluoroaniline **35** (3.0 ml; 31.21 mmol). The product was recovered as brown crystals (7.90 g; 28.10 mmol; yield 90%), from crystallization in ethanol.

Melting range: 43–45 °C;  $^1\text{H}$  NMR (400 MHz,  $(\text{CD}_3)_2\text{SO}$ )  $\delta$  10.62 (d, NH), 8.35 (d,  $\text{CHNH}$ ), 7.35 (dd, 2H), 7.18 (d, 1H), 6.95 (s, 1H), 4.15 (m, 2 x  $\text{OCH}_2\text{CH}_3$ ), 1.23 (m, 2 x  $\text{OCH}_2\text{CH}_3$ );  $^{13}\text{C}$  NMR (101 MHz,  $(\text{CD}_3)_2\text{SO}$ )  $\delta$  165.30 ( $\text{CO}_2\text{Et}$ ), 164.49 ( $\text{CO}_2\text{Et}$ ), 162.07 ( $\text{CF}$ ), 151.17 ( $\text{CHNH}$ ), 141.87, 131.78, 113.99, 111.35, 105.31, 94.71 [ $\text{C}(\text{CO}_2\text{Et})_2$ ], 60.25 ( $\text{OCH}_2\text{CH}_3$ ), 60.06 ( $\text{OCH}_2\text{CH}_3$ ), 14.70 ( $\text{OCH}_2\text{CH}_3$ ), 14.67 ( $\text{OCH}_2\text{CH}_3$ ); MS m/z (EI)  $[\text{M}]^+$   $\text{C}_{14}\text{H}_{16}\text{FNO}_4$  requires 281.1063, found 281.1096.

*Ethyl 7-fluoro-4-oxo-quinoline-3-carboxylate (43)*



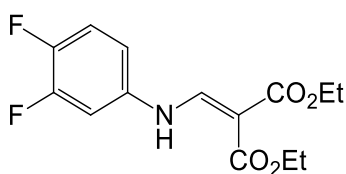
Synthesised according to the general method C, from enamine **39** (1.00 g; 3.56 mmol) in 10 ml of Dowtherm A (3 hours), to afford a white powder (0.37 g; 1.57 mmol; yield 44%).

Melting range: 297-298 °C; <sup>1</sup>H NMR (400 MHz, (CD<sub>3</sub>)<sub>2</sub>SO) δ 12.32 (s, NH), 8.56 (s, CHNH), 8.17 (t, 1H), 7.36 (d, 1H), 7.26 (t, 1H), 4.20 (q, OCH<sub>2</sub>CH<sub>3</sub>), 1.26 (t, OCH<sub>2</sub>CH<sub>3</sub>); <sup>13</sup>C NMR data not obtained due to poor solubility in all available deuterated solvents; MS m/z (EI) [M]<sup>+</sup> C<sub>12</sub>H<sub>10</sub>FNO<sub>3</sub> requires 235.0645, found 235.0652; CHN for C<sub>12</sub>H<sub>10</sub>FNO<sub>3</sub> requires C 61.28%, H 4.28%, N 5.95%, found C 61.12%, H 4.20%, N 5.88%.

The synthesis of this compound was repeated following the general method E, from enamine **39** (4.00 g; 14.22 mmol) in 40 ml of POCl<sub>3</sub>, to afford a beige powder (1.64 g; 6.98 mmol; 49%).

Melting range: 280-282 °C; <sup>1</sup>H NMR (400 MHz, (CD<sub>3</sub>)<sub>2</sub>SO) δ 12.30 (s, NH), 8.57 (s, CHNH), 8.18 (t, 1H), 7.37 (d, 1H), 7.26 (t, 1H), 4.20 (q, OCH<sub>2</sub>CH<sub>3</sub>), 1.26 (t, OCH<sub>2</sub>CH<sub>3</sub>).

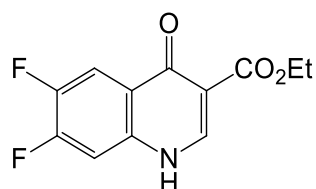
*Diethyl 2-(((3,4-difluorophenyl)amino)methylene)malonate (40)*



Synthesised according to the general method B, from 3,4-difluoroaniline **36** (3.0 ml; 30.25 mmol). The product was recovered as brown crystals (8.99 g; 30.04 mmol; yield 99%), from crystallization in ethanol.

Melting range: 60-62 °C; <sup>1</sup>H NMR (400 MHz, CD<sub>3</sub>OD) δ 8.41 (s, CHNH), 7.27 (m, 2H), 7.07 (s, 1H), 4.23 (dq, 2 x OCH<sub>2</sub>CH<sub>3</sub>), 1.31 (dt, 2 x OCH<sub>2</sub>CH<sub>3</sub>); <sup>13</sup>C NMR (101 MHz, (CD<sub>3</sub>)<sub>2</sub>SO) δ 167.52 (C=O), 165.33 (C=O), 151.71, 151.28, 137.40, 137.34, 118.63, 114.80, 108.04, 94.58 [C(CO<sub>2</sub>Et)<sub>2</sub>], 60.21 (OCH<sub>2</sub>CH<sub>3</sub>), 60.04 (OCH<sub>2</sub>CH<sub>3</sub>), 14.71 (OCH<sub>2</sub>CH<sub>3</sub>), 14.65 (OCH<sub>2</sub>CH<sub>3</sub>); MS m/z (MALDI-TOF) [M + H]<sup>+</sup> C<sub>14</sub>H<sub>16</sub>F<sub>2</sub>NO<sub>4</sub> requires 300.1042, found 300.1100.

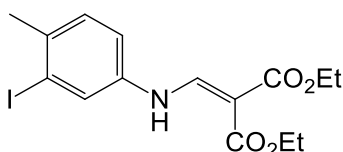
*Ethyl 6,7-difluoro-4-oxo-quinoline-3-carboxylate (44a)*



Synthesised according to the general method C, from enamine **40** (0.50 g; 1.67 mmol) in 10 ml of Dowtherm A (3 hours), to afford a beige powder (12 mg; 0.05 mmol; yield 3%).

Melting point,  $^1\text{H}$  NMR and  $^{13}\text{C}$  NMR data not obtained due to the low quantity obtained and to the insolubility in all available deuterated solvents; MS m/z (CI)  $[\text{M} + \text{H}]^+$   $\text{C}_{12}\text{H}_{10}\text{F}_2\text{NO}_3$  requires 254.0629, found 254.0622.

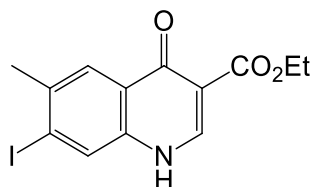
*Diethyl 2-(((3-iodo-4-methylphenyl)amino)methylene)malonate (41)*



Synthesised according to the general method B, from 3-iodo-4-methylaniline **37** (3.00 g; 12.87 mmol). The product was recovered as white crystals (4.74 g; 11.75 mmol; yield 91%), from crystallization in ethanol (and ethyl acetate, to help dissolution).

Melting range: 119-121 °C;  $^1\text{H}$  NMR (400 MHz,  $(\text{CD}_3)_2\text{SO}$ )  $\delta$  10.57 (d, NH), 8.30 (s, CHNH), 7.86 (s, 1H), 7.31 (s, 2H), 4.15 (m, 2 x OCH<sub>2</sub>CH<sub>3</sub>), 2.32 (s, CH<sub>3</sub>), 1.23 (m, 2 x OCH<sub>2</sub>CH<sub>3</sub>);  $^{13}\text{C}$  NMR (101 MHz,  $(\text{CD}_3)_2\text{SO}$ )  $\delta$  167.58 (CO<sub>2</sub>Et), 165.61 (CO<sub>2</sub>Et), 151.41 (CHNH), 138.80, 137.49, 130.88, 127.88, 117.91, 102.01 (CI), 93.99 [C(CO<sub>2</sub>Et)<sub>2</sub>], 60.26 (OCH<sub>2</sub>CH<sub>3</sub>), 60.12 (OCH<sub>2</sub>CH<sub>3</sub>), 27.12 (CH<sub>3</sub>), 14.69 (OCH<sub>2</sub>CH<sub>3</sub>), 14.62 (OCH<sub>2</sub>CH<sub>3</sub>); MS m/z (EI)  $[\text{M}]^+$   $\text{C}_{15}\text{H}_{18}\text{INO}_4$  requires 403.0281, found 403.0353.

*Ethyl 6-methyl-7-iodo-4-oxo-quinoline-3-carboxylate (45a)*

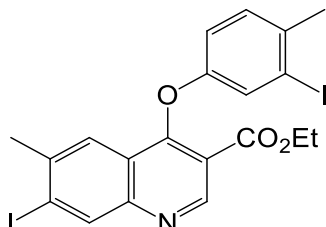


Synthesised according to the general method C, from enamine **41** (1.00 g; 2.48 mmol) in 10 ml of Dowtherm A (3 hours). The product was recovered as a white powder (0.55 g; 1.53 mmol; yield 62%).



Melting range: 316-318 °C; <sup>1</sup>H NMR and <sup>13</sup>C NMR data not obtained due to insolubility in all available deuterated solvents; MS m/z (ES) [M + Na]<sup>+</sup> C<sub>13</sub>H<sub>12</sub>INO<sub>3</sub>Na requires 379.9760, found 379.9755; CHN for C<sub>13</sub>H<sub>12</sub>INO<sub>3</sub> requires C 43.72%, H 3.39%, N 3.92%, found C 43.67%, H 3.30%, N 3.73%.

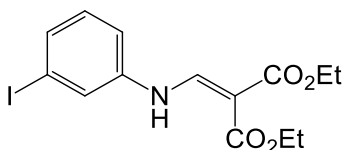
*Ethyl 7-iodo-4-(3-iodo-4-methylphenoxy)-6-methylquinoline-3-carboxylate (45b)*



Synthesised according to the general method E, from enamine **41** (2.00 g; 4.96 mmol) in 15 ml of POCl<sub>3</sub>. The product was recovered as a mixture of yellow powder/crystals (0.35 g; 0.61 mmol; 12%).

Melting range 216-218 °C; <sup>1</sup>H NMR (400 MHz, (CD<sub>3</sub>)<sub>2</sub>SO) δ 8.87 (s, CHN), 8.60 (s, 1H), 8.57 (s, 1H), 7.73 (s, 1H), 7.36 (d, 1H), 7.21 (d, 1H), 3.76 (q, OCH<sub>2</sub>CH<sub>3</sub>), 2.53 (s, CH<sub>3</sub>), 2.37 (s, CH<sub>3</sub>), 1.10 (t, OCH<sub>2</sub>CH<sub>3</sub>); <sup>13</sup>C NMR (101 MHz, (CD<sub>3</sub>)<sub>2</sub>SO) δ 166.95 (CO<sub>2</sub>Et), 164.36 (COAr), 151.31, 146.70, 139.85, 139.20, 138.34, 131.32, 130.04, 128.63, 123.54, 119.30, 109.20, 107.66, 101.07, 61.52 (OCH<sub>2</sub>CH<sub>3</sub>), 27.64 (CH<sub>3</sub>), 26.84 (CH<sub>3</sub>), 13.68 (OCH<sub>2</sub>CH<sub>3</sub>); MS m/z (MALDI-TOF) [M]<sup>+</sup> C<sub>20</sub>H<sub>17</sub>I<sub>2</sub>NO<sub>3</sub> requires 572.9298, found 572.9696.

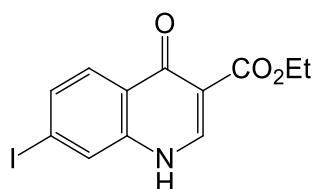
*Diethyl 2-(((3-iodophenyl)amino)methylene)malonate (42)*



Synthesised according to the general method B, from 3-iodoaniline **38** (2.0 ml; 16.63 mmol). The product was recovered as a white solid (6.42 g; 16.50 mmol; yield 99%) from precipitation in hexane, at room temperature.

Melting range: 86-88 °C; <sup>1</sup>H NMR (400 MHz, CDCl<sub>3</sub>) δ 10.97 (d, NH), 8.45 (d, CHNH), 7.51 – 7.46 (m, 2H), 7.11 – 7.08 (m, 2H), 4.28 (dq, 2 x OCH<sub>2</sub>CH<sub>3</sub>), 1.36 (dt, 2 x OCH<sub>2</sub>CH<sub>3</sub>); <sup>13</sup>C NMR (101 MHz, CDCl<sub>3</sub>) δ 168.92 (2 x CO<sub>2</sub>Et), 151.26 (CHNH), 140.44 (CNH), 133.76, 131.22, 125.96, 116.41, 94.97, 94.63, 60.60 (OCH<sub>2</sub>CH<sub>3</sub>), 60.31 (OCH<sub>2</sub>CH<sub>3</sub>), 14.43 (OCH<sub>2</sub>CH<sub>3</sub>), 14.28 (OCH<sub>2</sub>CH<sub>3</sub>); MS m/z (ES) [M + Na]<sup>+</sup> C<sub>14</sub>H<sub>16</sub>INO<sub>4</sub>Na requires 412.0022, found 412.0020.

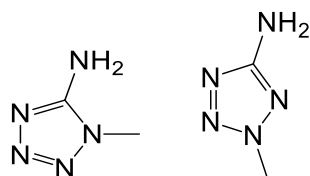
Ethyl 7-iodo-4-oxo-quinoline-3-carboxylate (**46**)



Synthesised according to the general method C, from enamine **42** (10.14 g; 26.06 mmol) in 80 ml of Dowtherm A (3 hours). The product was recovered as a white powder (3.97 g; 11.57 mmol; yield 44%).

Melting range: 306-308 °C; <sup>1</sup>H NMR (400 MHz, (CD<sub>3</sub>)<sub>2</sub>SO) δ 8.56 (s, CHNH), 8.02 (s, 1H), 7.88 (d, 1H), 7.71 (d, 1H), 4.21 (q, OCH<sub>2</sub>CH<sub>3</sub>), 1.27 (t, OCH<sub>2</sub>CH<sub>3</sub>); <sup>13</sup>C NMR (100 MHz, (CD<sub>3</sub>)<sub>2</sub>SO) δ 176.4 (C=O), 165 (C=OEt), 150.4, 147.7, 132.3, 128.8, 128.1, 125.6, 112.3 (CCO<sub>2</sub>Et), 100.9 (CI), 61.4 (OCH<sub>2</sub>CH<sub>3</sub>), 14.2 (OCH<sub>2</sub>CH<sub>3</sub>); MS m/z (ES) [M + Na]<sup>+</sup> C<sub>12</sub>H<sub>10</sub>INO<sub>3</sub>Na requires 365.9603, found 365.9591; CHN for C<sub>12</sub>H<sub>10</sub>INO<sub>3</sub> requires C 42.01%, H 2.94%, N 4.08%, found C 42.17%, H 2.84%, N 3.95%.

1-Methyl-5-aminotetrazole (**52**) and 2-methyl-5-aminotetrazole (**53**)



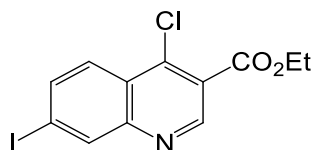
5-Amine-1H-tetrazole **51** (10.30 g; 121.00 mmol) was mixed in water (30mL) and aqueous sodium hydroxide 5M (≈30mL) was added, dropwise, until dissolution of **51**. The solution was kept at 50 °C and dimethyl sulphate (20.0 mL; 211.00 mmol) was added dropwise, keeping the pH around 14. The reaction mixture was stirred under reflux, at 100 °C, for 1 hour.

The mixture was cooled and kept inside the fridge. Compound **52** precipitated as crystals, which were collected by filtration and dried (3.07 g; 31.00 mmol; 26%). The aqueous residue was extracted with diethyl ether (2 x 30 ml), then with DCM (2 x 30 ml). The organic layers were combined, the solvent was removed under reduced pressure and the solid residue was recrystallized from ethanol (mixture kept inside the fridge) to afford **53** as white crystals (1.27 g; 12.82 mmol; 11%).

**52**: Melting range: 219-220 °C; <sup>1</sup>H NMR (400 MHz, (CD<sub>3</sub>)<sub>2</sub>SO) δ 6.62 (s, NH<sub>2</sub>), 3.69 (s, CH<sub>3</sub>); <sup>13</sup>C NMR (101 MHz, (CD<sub>3</sub>)<sub>2</sub>SO) δ 156.29 (CNH<sub>2</sub>), 31.93 (CH<sub>3</sub>); MS m/z (EI) [M]<sup>+</sup> C<sub>2</sub>H<sub>5</sub>N<sub>5</sub> requires 99.0545, found 99.0545 (and 57.0442: fragment N<sub>3</sub>CH<sub>3</sub>).

**53**: Melting range: 99-100 °C; <sup>1</sup>H NMR (400 MHz, (CD<sub>3</sub>)<sub>2</sub>SO) δ 5.94 (s, NH<sub>2</sub>), 4.06 (s, CH<sub>3</sub>); <sup>13</sup>C NMR (101 MHz, DMSO) δ 167.63 (C=NH<sub>2</sub>), 39.26 (CH<sub>3</sub>); MS m/z (EI) [M]<sup>+</sup> C<sub>2</sub>H<sub>5</sub>N<sub>5</sub> requires 99.0545, found 99.0545 (and 71.0475: fragment NH<sub>2</sub>CN<sub>2</sub>CH<sub>3</sub>).

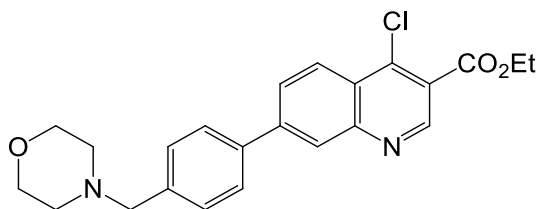
*Ethyl 4-chloro-7-iodo-quinoline-3-carboxylate (56)*



Ethyl 7-iodo-4-oxo-quinoline-3-carboxylate **46** (0.70 g; 2.04 mmol) was suspended in phosphoryl chloride (5 mL), under a nitrogen atmosphere, and the resulting mixture was refluxed at 97 °C overnight. The mixture was cooled to room temperature, poured into a beaker with ice, stirred for 1 hour and then extracted with chloroform. The organic layers were collected, dried over anhydrous MgSO<sub>4</sub>, filtered, and the solvent was removed by evaporation under reduced pressure to afford **56** as yellow solid (0.70 g, 1.94 mmol; 95%).

Melting range: 269-271 °C; <sup>1</sup>H NMR (400 MHz, CDCl<sub>3</sub>) δ 9.19 (s, CHN), 8.60 (s, 1H), 8.12 (d, 1H), 7.99 (d, 1H), 4.50 (q, OCH<sub>2</sub>CH<sub>3</sub>), 1.47 (t, OCH<sub>2</sub>CH<sub>3</sub>). <sup>13</sup>C NMR (100 MHz, CDCl<sub>3</sub>) δ 164.18, 150.95, 149.75, 138.69, 137.29, 126.59 (2C), 125.52, 123.33, 99.18 (CI), 62.28 (OCH<sub>2</sub>CH<sub>3</sub>), 14.25 (OCH<sub>2</sub>CH<sub>3</sub>); MS m/z (ES) [M + Na]<sup>+</sup> C<sub>12</sub>H<sub>9</sub>ClINO<sub>2</sub>Na requires 383.9264, found 383.9291; CHN for C<sub>12</sub>H<sub>9</sub>ClINO<sub>2</sub> requires C 39.86%, H 2.51%, N 3.87%, found C 39.28%, H 2.73%, N 3.56%.

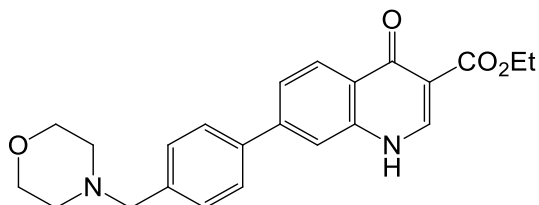
*Ethyl 4-chloro-7-(4-(morpholinomethyl)phenyl)-quinoline-3-carboxylate (59)*



A mixture of toluene:H<sub>2</sub>O (10 ml; 9:1) was added to a mixture of ethyl 4-chloro-7-iodo-quinoline-3-carboxylate **56** (0.42 g; 1.16 mmol), potassium carbonate (2.5 eq.), Pd(PPh<sub>3</sub>)<sub>4</sub> (5%) and 4-(4-morpholinomethyl)phenyl boronic acid pinacol ester **58** (1.1 eq.). The final mixture was refluxed at 100 °C for 24 hours, under a nitrogen atmosphere. The reaction mixture was cooled to room temperature and the inorganic solids were filtered through sand, silica and MgSO<sub>4</sub> and washed with ethyl acetate (around 250 ml). After filtration, the solution was concentrated to dryness by solvent evaporation under reduced pressure to provide the product **59** as a yellow solid (0.25 g; 0.60 mmol; 52%).

$^1\text{H}$  NMR (400 MHz,  $(\text{CD}_3)_2\text{SO}$ )  $\delta$  9.20 (s,  $\text{CHN}$ ), 8.47 (d, 1H), 8.42 (s, 1H), 8.23 (d, 1H), 7.91 (d, 2H), 7.51 (d, 2H), 4.45 (q,  $\text{OCH}_2\text{CH}_3$ ), 3.60 (m, 6H), 2.41 (m,  $\text{O}(\text{CH}_2\text{CH}_2)_2\text{N}$ ), 1.41 (t,  $\text{OCH}_2\text{CH}_3$ );  $^{13}\text{C}$  NMR (101 MHz,  $(\text{CD}_3)_2\text{SO}$ )  $\delta$  164.31, 150.76, 149.87, 144.08, 137.31, 137.23, 132.00, 130.26, 129.30, 129.18, 128.58, 127.74 (2C), 126.59, 126.26, 110.69 ( $\text{CCO}_2\text{Et}$ ), 66.69 (2C), 62.45 (2C), 53.69 (2C), 14.51 ( $\text{OCH}_2\text{CH}_3$ ); MS m/z (ES)  $[\text{M} + \text{H}]^+$   $\text{C}_{23}\text{H}_{24}\text{ClN}_2\text{O}_3$  requires 411.1475, found 411.1469.

*Ethyl 7-(4-(morpholinomethyl)phenyl)-4-oxo-quinoline-3-carboxylate (60)*

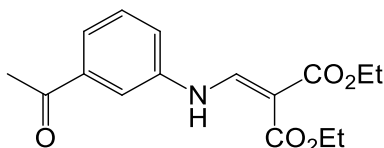


Ethyl 4-chloro-7-(4-(morpholinomethyl)phenyl)-quinoline-3-carboxylate **59** (0.25 g; 0.60 mmol) was added to DMF (10 ml) and the mixture was stirred for 15 min. A solution of  $\text{HCO}_2\text{H}$  (80%) in ethanol (5 ml) was added, and the resulting mixture was refluxed at  $145^\circ\text{C}$  for 18 hours. The reaction mixture was cooled to room temperature, DMF was removed by evaporation under reduced pressure and the residue was basified (with sodium bicarbonate) and extracted with a mixture of methanol (10%) in DCM (2 x 30 ml). The combined organic extracts were washed with brine and dried over  $\text{MgSO}_4$ . The organic solution was collected by filtration and concentrated by solvent evaporation under reduced pressure. The residue was purified by silica gel chromatography (eluting from 5% of methanol in DCM to 15% of methanol in DCM) to give a palid powder **60** (0.03 g; 0.08 mmol; 13%).

$^1\text{H}$  NMR (400 MHz,  $(\text{CD}_3)_2\text{SO}$ )  $\delta$  8.59 (s,  $\text{CHN}$ ), 8.22 (d, 1H), 7.83 (s, 1H), 7.73 (m, 3H), 7.47 (m, 2H), 4.23 (q,  $\text{OCH}_2\text{CH}_3$ ), 3.62 (m, 6H), 2.40 (m,  $\text{O}(\text{CH}_2\text{CH}_2)_2\text{N}$ ), 1.30 (t,  $\text{OCH}_2\text{CH}_3$ );  $^{13}\text{C}$  NMR data not obtained due to poor solubility in all available deuterated solvents; MS m/z (ES)  $[\text{M} + \text{Na}]^+$   $\text{C}_{23}\text{H}_{24}\text{N}_2\text{O}_4\text{Na}$  requires 415.1634, found 415.1620.

*Synthesis of 6- or 7-substituted 4-oxo-quinoline 3-esters; the issue of isomeric mixtures*

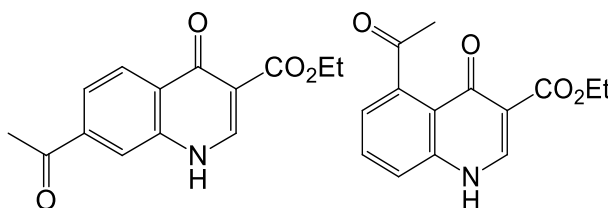
*Diethyl 2-(((3-acetylphenyl)amino)methylene)malonate (70)*



Synthesised according to the general method B, from 3-aminoacetophenone **61** (2.40 g; 17.76 mmol). The product precipitated in hexane, as a brown solid (5.41 g; 17.70 mmol; yield 99%).

Melting range: 79-80 °C;  $^1\text{H}$  NMR (400 MHz,  $(\text{CD}_3)_2\text{SO}$ )  $\delta$  10.72 (d, NH), 8.42 (d, CHNH), 7.88 (s, 1H), 7.71 (d, 1H), 7.62 (d, 1H), 7.53 (t, 1H), 4.20 (d, OCH<sub>2</sub>CH<sub>3</sub>), 4.12 (d, OCH<sub>2</sub>CH<sub>3</sub>), 2.59 (s, CH<sub>3</sub>), 1.24 (m, 2 x OCH<sub>2</sub>CH<sub>3</sub>);  $^{13}\text{C}$  NMR (100 MHz,  $(\text{CD}_3)_2\text{SO}$ )  $\delta$  198.04 (C=OCH<sub>3</sub>), 167.58 (CO<sub>2</sub>Et), 165.47 (CO<sub>2</sub>Et), 151.40 (CHNH), 140.45, 138.46, 130.51, 124.57, 122.40, 117.84, 94.44 [C(CO<sub>2</sub>Et)<sub>2</sub>], 60.20 (OCH<sub>2</sub>CH<sub>3</sub>), 60.05 (OCH<sub>2</sub>CH<sub>3</sub>), 27.38 (CH<sub>3</sub>), 14.73 (OCH<sub>2</sub>CH<sub>3</sub>), 14.66 (OCH<sub>2</sub>CH<sub>3</sub>); MS m/z (EI) [M]<sup>+</sup> C<sub>16</sub>H<sub>19</sub>NO<sub>5</sub> requires 305.1263, found 305.1266.

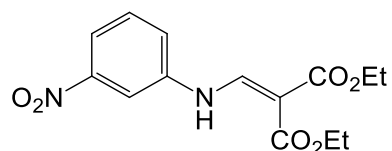
*Isomeric mixture: ethyl 7-acetyl-4-oxo-quinoline-3-carboxylate (79a) and ethyl 5-acetyl-4-oxo-quinoline-3-carboxylate (79b)*



Synthesised according to the general method C, from enamine **70** (0.61 g; 2.00 mmol) in 10 ml of Dowtherm A (3 hours). The products precipitated as a beige powder (0.09 g; 0.35 mmol; yield 18%) and were characterised as an isomeric mixture of **79a** and **79b**.

$^1\text{H}$  NMR (400 MHz,  $(\text{CD}_3)_2\text{SO}$ )  $\delta$  12.53 (s, 2 x NH)<sup>79a and 79b</sup>, 8.66 (s, CHNH)<sup>79b</sup>, 8.61 (s, CHNH)<sup>79a</sup>, 8.24 (d, 1H)<sup>79a</sup>, 8.19 (s, 1H)<sup>79a</sup>, 7.93 (d, 1H)<sup>79b</sup>, 7.75 (t, 1H)<sup>79b</sup>, 7.68 (d, 1H)<sup>79b</sup>, 7.15 (d, 1H)<sup>79a</sup>, 4.23 (dq, 2 x OCH<sub>2</sub>CH<sub>3</sub>), 2.51 (s, 2 x CH<sub>3</sub>CO), 1.29 (dt, 2 x OCH<sub>2</sub>CH<sub>3</sub>);  $^{13}\text{C}$  NMR data not obtained due to poor solubility in all available deuterated solvents; MS m/z (ES) [M + Na]<sup>+</sup> C<sub>14</sub>H<sub>13</sub>NO<sub>4</sub>Na requires 282.0742, found 282.0745; CHN for C<sub>14</sub>H<sub>13</sub>NO<sub>4</sub> requires C 64.86%, H 5.05%, N 5.4%, found C 64.81%, H 4.95%, N 5.21%.

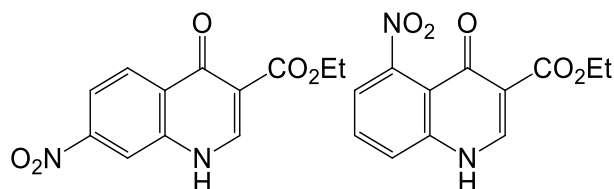
Diethyl 2-((3-nitrophenyl)amino)methylene)malonate (**71**)



Synthesised according to the general method B, from 3-nitroaniline **62** (3.00 g; 21.72 mmol). The product was recovered as yellow solid (6.69 g; 21.68 mmol; yield 99%) from precipitation in ethyl acetate, after slow evaporation at room temperature.

Melting range: 80-82 °C;  $^1\text{H}$  NMR (400 MHz,  $\text{CDCl}_3$ )  $\delta$  11.18 (d, NH), 8.52 (d, CHNH), 8.00 (m, 2H), 7.56 (t, 1H), 7.44 (d, 1H), 4.31 (dq, 2 x  $\text{OCH}_2\text{CH}_3$ ), 1.37 (dt, 2 x  $\text{OCH}_2\text{CH}_3$ );  $^{13}\text{C}$  NMR (101 MHz,  $\text{CDCl}_3$ )  $\delta$  169.21 ( $\text{CO}_2\text{Et}$ ), 165.61 ( $\text{CO}_2\text{Et}$ ), 151.04 (CHNH), 149.72 ( $\text{CNO}_2$ ), 140.94, 131.21, 123.07, 119.46, 111.87, 96.42 [ $\text{C}(\text{CO}_2\text{Et})_2$ ], 61.26 ( $\text{OCH}_2\text{CH}_3$ ), 60.93 ( $\text{OCH}_2\text{CH}_3$ ), 14.81 ( $\text{OCH}_2\text{CH}_3$ ), 14.64 ( $\text{OCH}_2\text{CH}_3$ ); MS  $m/z$  (ES)  $[\text{M} + \text{Na}]^+$   $\text{C}_{14}\text{H}_{16}\text{N}_2\text{O}_6\text{Na}$  requires 331.0906, found 331.0915.

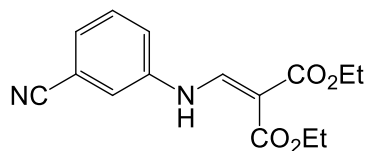
Isomeric mixture: ethyl 7-nitro-4-oxo-quinoline-3-carboxylate (**80a**) and ethyl 5-nitro-4-oxo-quinoline-3-carboxylate (**80b**)



Synthesised according to the general method C, from enamine **71** (1.00 g; 3.24 mmol) in 10 ml of Dowtherm A (3 hours). The product was recovered as a yellow solid (0.18 g; 0.70 mmol; yield 22%) as was characterised as a mixture of isomers **80a** and **80b**.

$^1\text{H}$  NMR (400 MHz,  $(\text{CD}_3)_2\text{SO}$ )  $\delta$  12.71 (s, 2 x NH)<sup>80a and 80b</sup>, 8.71 (s, CHNH)<sup>80a</sup>, 8.63 (s, CHNH)<sup>80b</sup>, 8.50 (s, 1H)<sup>80a</sup>, 8.35 (d, 1H)<sup>80a</sup>, 8.13 (d, 1H)<sup>80b</sup>, 7.82 (d, 2H)<sup>80a and 80b</sup>, 7.62 (t, 1H)<sup>80b</sup>, 4.20 (m, 2 x  $\text{OCH}_2\text{CH}_3$ ), 1.27 (m, 2 x  $\text{OCH}_2\text{CH}_3$ );  $^{13}\text{C}$  NMR data not obtained due to poor solubility in all available deuterated solvents; MS  $m/z$  (MALDI-TOF)  $[\text{M} + \text{H}]^+$   $\text{C}_{12}\text{H}_{11}\text{N}_2\text{O}_5$  requires 263.0668, found 263.0119; CHN for  $\text{C}_{12}\text{H}_{10}\text{N}_2\text{O}_5$  requires C 54.97%, H 3.84%, N 10.68%, found C 54.70%, H 3.73%, N 10.59%.

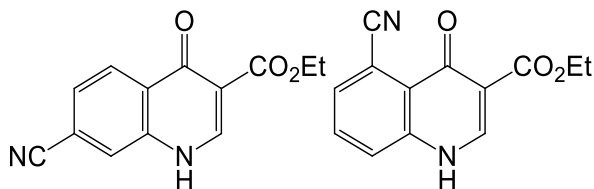
*Diethyl 2-(((3-cyanophenyl)amino)methylene)malonate (72)*



Synthesised according to the general method B, from 3-aminobenzonitrile **63** (3.00 g; 25.39 mmol). The product was recovered as a beige powder/crystal mixture (4.21 g; 14.60 mmol; yield 58%) from recrystallization in ethanol.

Melting range: 114-115 °C; <sup>1</sup>H NMR (400 MHz, CDCl<sub>3</sub>) δ 11.07 (d, NH), 8.46 (d, CHNH), 7.50 (t, 1H), 7.42 (m, 2H), 7.36 (d, 1H), 4.30 (dq, 2 x OCH<sub>2</sub>CH<sub>3</sub>), 1.36 (dt, 2 x OCH<sub>2</sub>CH<sub>3</sub>); <sup>13</sup>C NMR (101 MHz, CDCl<sub>3</sub>) δ 165.60 (CO<sub>2</sub>Et), 165.36 (CO<sub>2</sub>Et), 151.07 (CHNH), 140.57 (CNH), 131.24, 128.35, 121.69, 120.27, 118.29 (CN), 114.44 (CCN) 95.96 [C(CO<sub>2</sub>Et)<sub>2</sub>], 61.21 (OCH<sub>2</sub>CH<sub>3</sub>), 60.88 (OCH<sub>2</sub>CH<sub>3</sub>), 14.81 (OCH<sub>2</sub>CH<sub>3</sub>), 14.64 (OCH<sub>2</sub>CH<sub>3</sub>); MS m/z (ES) [M + Na]<sup>+</sup> C<sub>15</sub>H<sub>16</sub>N<sub>2</sub>O<sub>4</sub>Na requires 311.1008, found 311.1020.

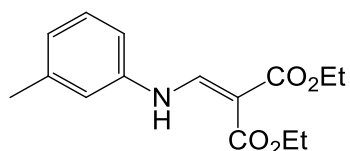
*Isomeric mixture: ethyl 7-cyano-4-oxo-quinoline-3-carboxylate (81a) and ethyl 5-cyano-4-oxo-quinoline-3-carboxylate (81b)*



Synthesised according to the general method C, from enamine **72** (1.03 g; 3.58 mmol), in 10 ml of Dowtherm A (3 hours). The product was recovered as a beige powder (0.17 g; 0.69 mmol; yield 19%) and was characterised as a mixture of isomers **81a** and **81b**.

<sup>1</sup>H NMR (400 MHz, (CD<sub>3</sub>)<sub>2</sub>SO) δ 12.60 (s, 2 x NH)<sup>81a and 81b</sup>, 8.66 (s, CHNH)<sup>81a</sup>, 8.61 (s, CHNH)<sup>81b</sup>, 8.27 (d, 1H)<sup>81a</sup>, 8.08 (s, 1H)<sup>81a</sup>, 7.88 (t, 2H)<sup>81b</sup>, 7.82 (d, 1H)<sup>81b</sup>, 7.76 (d, 1H)<sup>81a</sup>, 4.23 (m, 2 x OCH<sub>2</sub>CH<sub>3</sub>), 1.27 (m, 2 x OCH<sub>2</sub>CH<sub>3</sub>); <sup>13</sup>C NMR (101 MHz, (CD<sub>3</sub>)<sub>2</sub>SO) δ 172.19, 164.79, 145.59, 140.20, 133.55, 132.60, 127.32, 124.25, 119.02 (CN), 111.15, 109.92, 60.31 (OCH<sub>2</sub>CH<sub>3</sub>), 14.50 (OCH<sub>2</sub>CH<sub>3</sub>); MS m/z (MALDI-TOF) [M + H]<sup>+</sup> C<sub>13</sub>H<sub>11</sub>N<sub>2</sub>O<sub>3</sub> requires 243.0770, found 243.0695; CHN for C<sub>13</sub>H<sub>10</sub>N<sub>2</sub>O<sub>3</sub> requires C 64.46%, H 4.16%, N 11.56%, found C 64.11%, H 4.07%, N 11.51%.

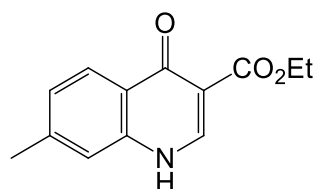
Diethyl 2-(((3-methylphenyl)amino)methylene)malonate (**73**)



Synthesised according to the general method B, from 3-methylaniline **64** (3.03 ml; 28.00 mmol). The product was recovered as brown oil (7.19 g; 25.90 mmol; yield 93%) after purification by silica gel column chromatography (eluting with DCM).

Melting range 38-39 °C;  $^1\text{H NMR}$  (400 MHz,  $(\text{CD}_3)_2\text{SO}$ )  $\delta$  10.63 (d, NH), 8.40 (d, CHNH), 7.25 (t, 1H), 7.18 – 7.06 (m, 2H), 6.96 (s, 1H), 4.14 (m, 2 x OCH<sub>2</sub>CH<sub>3</sub>), 2.29 (s, CH<sub>3</sub>), 1.23 (m, 2 x OCH<sub>2</sub>CH<sub>3</sub>);  $^{13}\text{C NMR}$  (101 MHz,  $(\text{CD}_3)_2\text{SO}$ )  $\delta$  167.95 (CO<sub>2</sub>Et), 165.40 (CO<sub>2</sub>Et), 151.50 (CHNH), 139.73, 139.64, 129.91, 125.82, 118.28, 114.99, 93.44 [C(CO<sub>2</sub>Et)<sub>2</sub>], 60.06 (OCH<sub>2</sub>CH<sub>3</sub>), 59.87 (OCH<sub>2</sub>CH<sub>3</sub>), 23.36 (CH<sub>3</sub>), 14.68 (OCH<sub>2</sub>CH<sub>3</sub>), 14.59 (OCH<sub>2</sub>CH<sub>3</sub>); MS m/z (EI) [M]<sup>+</sup> C<sub>15</sub>H<sub>19</sub>NO<sub>4</sub> requires 277.1314, found 277.1312; CHN for C<sub>15</sub>H<sub>19</sub>NO<sub>4</sub> requires C 64.97, H 6.91, N 5.05, found: C 65.07, H 6.95, N 4.77.

Ethyl 7-methyl-4-oxo-quinoline-3-carboxylate (**82a**)

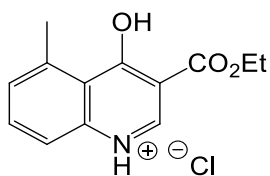


Synthesised according to the general method C, from enamine **73** (1.07 g; 3.86 mmol) in 10 ml of Dowtherm A (3 hours). The product was recovered as white powder (0.11 g; 0.48 mmol; yield 12%).

Melting range: 282-284 °C;  $^1\text{H NMR}$  (400 MHz,  $(\text{CD}_3)_2\text{SO}$ )  $\delta$  12.17 (s, NH), 8.49 (s, CHNH), 8.04 (d, 1H), 7.38 (s, 1H), 7.24 (d, 1H), 4.20 (m, OCH<sub>2</sub>CH<sub>3</sub>), 2.44 (s, CH<sub>3</sub>), 1.28 (t, OCH<sub>2</sub>CH<sub>3</sub>);  $^1\text{H NMR}$  (400 MHz, CDCl<sub>3</sub>)  $\delta$  12.20 (s, NH), 8.52 (s, CHNH), 8.26 (d, 1H), 7.38 (s, 1H), 7.25 (d, 1H), 4.35 (m, OCH<sub>2</sub>CH<sub>3</sub>), 2.48 (s, CH<sub>3</sub>), 1.39 (m, OCH<sub>2</sub>CH<sub>3</sub>);  $^{13}\text{C NMR}$  (101 MHz,  $(\text{CD}_3)_2\text{SO}$ )  $\delta$  176.02, 165.02, 143.52, 140.64, 140.02, 131.56, 127.42, 125.25, 116.96, 111.02, 59.58 (OCH<sub>2</sub>CH<sub>3</sub>), 23.42 (CH<sub>3</sub>), 14.35 (OCH<sub>2</sub>CH<sub>3</sub>); MS m/z (CI) [M + H]<sup>+</sup> C<sub>13</sub>H<sub>14</sub>NO<sub>3</sub> requires 232.0974, found 232.0977; CHN for C<sub>13</sub>H<sub>13</sub>NO<sub>3</sub> requires C 67.53, H 5.67, N 6.06; found: C 67.29, H 5.63, N 5.96.



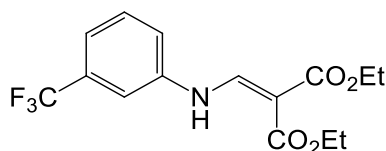
*Ethyl 4-hydroxy-5-methyl quinolinium chloride 3-carboxylate (82b·HCl)*



Synthesised according to the general method E, from enamine **73** (1.37 g; 4.94 mmol), in 15 ml of POCl<sub>3</sub>. The product was recovered as an orange powder/crystal mixture (0.25 g; 1.10 mmol; 22%).

Melting range 146-147 °C; <sup>1</sup>H NMR (400 MHz, (CD<sub>3</sub>)<sub>2</sub>SO) δ 8.38 (s, CHN), 7.49 (t, 1H), 7.44 (d, 1H), 7.10 (d, 1H), 4.18 (q, OCH<sub>2</sub>CH<sub>3</sub>), 2.78 (s, CH<sub>3</sub>), 1.26 (t, OCH<sub>2</sub>CH<sub>3</sub>); <sup>1</sup>H NMR (400 MHz, CDCl<sub>3</sub>) δ 9.26 (s, CHN), 8.51 (d, 1H), 7.91 (t, 1H), 7.59 (d, 1H), 4.58 (q, OCH<sub>2</sub>CH<sub>3</sub>), 3.01 (s, CH<sub>3</sub>), 1.50 (t, OCH<sub>2</sub>CH<sub>3</sub>); <sup>13</sup>C NMR (101 MHz, (CD<sub>3</sub>)<sub>2</sub>SO) δ 171.1, 171.1, 161.3, 144.6, 144.1, 140.1, 140.6, 132.0, 127.9, 117.3, 114.3, 60.1 (OCH<sub>2</sub>CH<sub>3</sub>), 23.9 (CH<sub>3</sub>), 14.8 (OCH<sub>2</sub>CH<sub>3</sub>); MS m/z (EI) [M]<sup>+</sup> C<sub>13</sub>H<sub>13</sub>NO<sub>3</sub> requires 231.0895, found 231.0899; CHN for C<sub>13</sub>H<sub>13</sub>NO<sub>3</sub> requires C 67.53, H 5.67, N 6.06; found: C 67.43, H 5.63, N 6.03.

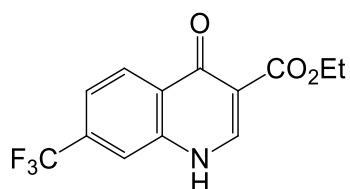
*Diethyl 2-(((3-(trifluoromethyl)phenyl)amino)methylene)malonate (74)*



Synthesised according to the general method B, from 3-aminobenzotrifluoride **65** (3.0 ml; 24.02 mmol). The product was recovered as white crystals (5.94 g; 17.90 mmol; yield 75%) after purification by silica gel column chromatography (eluting with 10% of ethyl acetate in hexane) and recrystallization from ethanol.

Melting range: 41-43 °C; <sup>1</sup>H NMR (400 MHz, (CD<sub>3</sub>)<sub>2</sub>SO) δ 10.71 (s, NH), 8.40 (s, CHNH), 7.79 (s, 1H), 7.67 (d, J 1H), 7.58 (t, 1H), 7.45 (d, 1H), 4.16 (m, 2 x OCH<sub>2</sub>CH<sub>3</sub>), 1.24 (t, 2 x OCH<sub>2</sub>CH<sub>3</sub>); <sup>13</sup>C NMR (100 MHz, (CD<sub>3</sub>)<sub>2</sub>SO) δ 167.35 (CO<sub>2</sub>Et), 165.42 (CO<sub>2</sub>Et), 151.12 (CHNH), 140.96 (CNH), 131.20, 130.85, 130.54, 121.66, 121.14, 115.28, 95.17 [C(CO<sub>2</sub>Et)<sub>2</sub>], 60.20 (2 x OCH<sub>2</sub>CH<sub>3</sub>), 14.68 (2 x OCH<sub>2</sub>CH<sub>3</sub>); MS m/z (ES) [M + Na]<sup>+</sup> C<sub>15</sub>H<sub>16</sub>F<sub>3</sub>NO<sub>4</sub>Na requires 354.0929, found 354.0928.

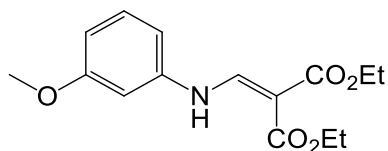
*Ethyl 7-trifluoromethyl-4-oxo-quinoline-3-carboxylate (83)*



Synthesised according to the general method C, from enamine **74** (1.03 g; 3.11 mmol), in 10 ml of Dowtherm A (3 hours). The product was recovered as a white powder (0.31 g; 1.10 mmol; yield 35%).

Melting range: 323-324 °C;  $^1\text{H NMR}$  (400 MHz,  $(\text{CD}_3)_2\text{SO}$ )  $\delta$  12.60 (s,  $\text{NH}$ ), 8.69 (s,  $\text{CHNH}$ ), 8.33 (d, 1H), 7.97 (s, 1H), 7.68 (d, 1H), 4.22 (q,  $\text{OCH}_2\text{CH}_3$ ), 1.28 (t,  $\text{OCH}_2\text{CH}_3$ );  $^{13}\text{C NMR}$  data not obtained due to poor solubility in all available deuterated solvents; MS  $m/z$  (MALDI-TOF)  $[\text{M} + \text{H}]^+$   $\text{C}_{13}\text{H}_{11}\text{F}_3\text{NO}_3$  requires 286.0691, found 286.0738; CHN for  $\text{C}_{13}\text{H}_{10}\text{F}_3\text{NO}_3$  requires C 54.74%, H 3.53%, N 4.91%, found C 54.77%, H 3.47%, N 4.81%.

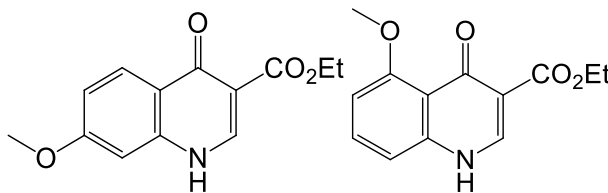
*Diethyl 2-(((3-methoxyphenyl)amino)methylene)malonate (75)*



Synthesised according to the general method B, from *m*-anisidine **66** (2.0 ml; 17.80 mmol). The product was obtained as a white solid (3.84 g; 13.11 mmol; yield 74%) after purification by silica gel column chromatography (eluting with 20% of ethyl acetate in hexane).

Melting range: 44-45 °C;  $^1\text{H NMR}$  (400 MHz,  $(\text{CD}_3)_2\text{SO}$ )  $\delta$  10.66 (d,  $\text{NH}$ ), 8.38 (d,  $\text{CHNH}$ ), 7.26 (t, 1H), 6.94 (s, 1H), 6.91 – 6.85 (d, 1H), 6.70 (d, 1H), 4.15 (dq, 2 x  $\text{OCH}_2\text{CH}_3$ ), 3.76 (s,  $\text{CH}_3$ ), 1.24 (dt, 2 x  $\text{OCH}_2\text{CH}_3$ );  $^{13}\text{C NMR}$  (101 MHz,  $(\text{CD}_3)_2\text{SO}$ )  $\delta$  167.80 ( $\text{CO}_2\text{Et}$ ), 165.40 ( $\text{CO}_2\text{Et}$ ), 160.82 ( $\text{COCH}_3$ ), 151.53 ( $\text{CHNH}$ ), 141.12 ( $\text{CNH}$ ), 131.03, 110.90, 109.78, 104.06, 93.72 [ $\text{C}(\text{CO}_2\text{Et})_2$ ], 60.13 ( $\text{OCH}_2\text{CH}_3$ ), 59.95 ( $\text{OCH}_2\text{CH}_3$ ), 55.76 ( $\text{H}_3\text{CO}$ ), 14.71 ( $\text{OCH}_2\text{CH}_3$ ), 14.65 ( $\text{OCH}_2\text{CH}_3$ ); MS  $m/z$  (MALDI-TOF)  $[\text{M}]^+$   $\text{C}_{15}\text{H}_{19}\text{NO}_5$  requires 293.1263, found 293.1171; CHN for  $\text{C}_{15}\text{H}_{19}\text{NO}_5$  requires C 61.42%, H 6.53%, N 4.78%, found C 61.26%, H 6.54%, N 4.59%.

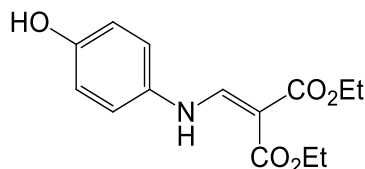
*Isomeric mixture: ethyl 7-methoxy-4-oxo-quinoline-3-carboxylate (84a) and ethyl 5-methoxy-4-oxo-quinoline-3-carboxylate (84b)*



Synthesised according to the general method C, from enamine **75** (1.50 g; 5.11 mmol), in 15 ml of Dowtherm A (3 hours). The product was recovered as a white powder (0.34 g; 1.41 mmol; yield 28%) and identified as a mixture of isomers **84a** and **84b**.

$^1\text{H NMR}$  (400 MHz,  $(\text{CD}_3)_2\text{SO}$ )  $\delta$  12.07 (s,  $\text{NH}$ ), 11.51 (?), 8.47 (s,  $\text{CHNH}$ ), 8.04 (d, 1H), 7.95 (?), 7.78 (?), 7.00 (d, 2H), 6.90 (?), 4.19 (q,  $\text{OCH}_2\text{CH}_3$ ), 3.85 (s,  $\text{CH}_3$ ), 1.26 (t,  $\text{OCH}_2\text{CH}_3$ );  $^{13}\text{C NMR}$  (101 MHz,  $(\text{CD}_3)_2\text{SO}$ )  $\delta$  176.90, 165.29, 162.73, 145.27, 142.23, 141.21, 139.49, 127.95, 127.25, 114.65, 113.60, 110.23, 109.04, 100.53, 99.49, 59.96 ( $\text{OCH}_2\text{CH}_3$ ), 56.05 ( $\text{H}_3\text{CO}$ ), 55.87 ( $\text{H}_3\text{CO}$ ), 14.80 ( $\text{OCH}_2\text{CH}_3$ ); CHN for  $\text{C}_{13}\text{H}_{13}\text{NO}_4$  requires C 63.15%, H 5.30%, N 5.67%, found C 62.89%, H 5.23%, N 5.55%.

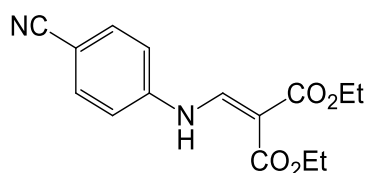
*Diethyl 2-(((4-hydroxyphenyl)amino)methylene)malonate (76)*



Synthesised according to the general method B, from 4-aminophenol **67** (2.00 g; 18.33 mmol). The product was obtained as yellow crystals (3.52 g; 12.59 mmol; yield 69%) after purification by silica gel column chromatography (eluting with DCM).

Melting range: 125-127 °C;  $^1\text{H NMR}$  (400 MHz,  $(\text{CD}_3)_2\text{SO}$ )  $\delta$  10.69 (d,  $\text{NH}$ ), 9.48 (s,  $\text{CHNH}$ ), 7.19 (d, 2H), 6.78 (d, 2H), 4.15 (dq, 2 x  $\text{OCH}_2\text{CH}_3$ ), 1.24 (dt, 2 x  $\text{OCH}_2\text{CH}_3$ );  $^{13}\text{C NMR}$  (101 MHz,  $(\text{CD}_3)_2\text{SO}$ )  $\delta$  168.11 ( $\text{CO}_2\text{Et}$ ), 165.47 ( $\text{CO}_2\text{Et}$ ), 155.45, 152.52, 131.84 ( $\text{CNH}$ ), 119.90 (2C), 116.50 (2C), 91.81 [ $\text{C}(\text{CO}_2\text{Et})_2$ ], 59.86 ( $\text{OCH}_2\text{CH}_3$ ), 59.67 ( $\text{OCH}_2\text{CH}_3$ ), 14.75 ( $\text{OCH}_2\text{CH}_3$ ), 14.69 ( $\text{OCH}_2\text{CH}_3$ ); MS  $m/z$  (ES)  $[\text{M} + \text{Na}]^+$   $\text{C}_{14}\text{H}_{17}\text{NO}_5\text{Na}$  requires 302.1004, found 302.0928; CHN for  $\text{C}_{14}\text{H}_{17}\text{NO}_5$  requires C 60.21%, H 6.14%, N 5.02%, found C 60.91%, H 6.95%, N 4.68%.

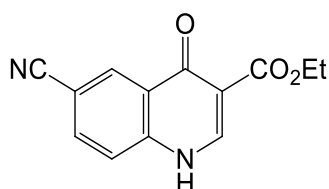
Diethyl 2-(((4-cyanophenyl)amino)methylene)malonate (**77**)



Synthesised according to the general method B, from 4-aminobenzonitrile **68** (4.00 g; 33.86 mmol). The product was obtained as white crystals (9.76 g; 33.80 mmol; yield 99%) from crystallization in DCM.

Melting range: 103-105 °C;  $^1\text{H NMR}$  (400 MHz,  $(\text{CD}_3)_2\text{SO}$ )  $\delta$  10.67 (s,  $\text{NH}$ ), 8.40 (s,  $\text{CHNH}$ ), 7.81 (d, 2H), 7.53 (d, 2H), 4.17 (dq, 2 x  $\text{OCH}_2\text{CH}_3$ ), 1.24 (m, 2 x  $\text{OCH}_2\text{CH}_3$ );  $^{13}\text{C NMR}$  (101 MHz,  $(\text{CD}_3)_2\text{SO}$ )  $\delta$  167.18 ( $\text{CO}_2\text{Et}$ ), 165.17 ( $\text{CO}_2\text{Et}$ ), 149.80 ( $\text{CHNH}$ ), 143.90 ( $\text{CNH}$ ), 134.34 (2C), 119.32 ( $\text{CN}$ ), 118.31 (2C), 106.38 ( $\text{CCN}$ ), 96.60 [ $\text{C}(\text{CO}_2\text{Et})_2$ ], 60.47 ( $\text{OCH}_2\text{CH}_3$ ), 60.28 ( $\text{OCH}_2\text{CH}_3$ ), 14.68 ( $\text{OCH}_2\text{CH}_3$ ), 14.60 ( $\text{OCH}_2\text{CH}_3$ ); MS  $m/z$  (ES)  $[\text{M} + \text{Na}]^+$   $\text{C}_{15}\text{H}_{16}\text{N}_2\text{O}_4\text{Na}$  requires 311.1008, found 311.1015.

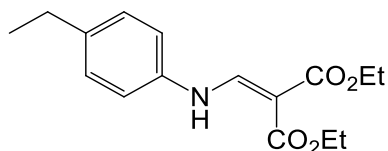
Ethyl 6-cyano-4-oxo-quinoline-3-carboxylate (**86**)



Synthesised according to the general method C, from enamine **77** (1.00 g; 3.47 mmol) in 10 ml of Dowtherm A (3 hours), to afford a yellow powder (0.15 g; 0.62 mmol; yield 18%).

Melting range: 325-326 °C;  $^1\text{H NMR}$  (400 MHz,  $(\text{CD}_3)_2\text{SO}$ )  $\delta$  12.66 (s,  $\text{NH}$ ), 8.65 (s, 1H), 8.49 (s, 1H), 8.05 (d, 1H), 7.78 (d, 1H), 4.21 (q,  $\text{OCH}_2\text{CH}_3$ ), 1.29 (t,  $\text{OCH}_2\text{CH}_3$ );  $^{13}\text{C NMR}$  data not obtained due to poor solubility in all available deuterated solvents.

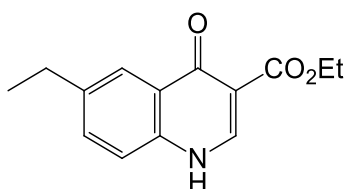
Diethyl 2-(((4-ethylphenyl)amino)methylene)malonate (**78**)



Synthesised according to the general method B, from 4-ethylaniline **69** (4.0 ml; 32.18 mmol). The product was recovered as a brown solid (9.28 g; 31.86 mmol; yield 99%) after purification by silica gel column chromatography (eluting with 20% of ethyl acetate in hexane).

Melting range: 30-31 °C; <sup>1</sup>H NMR (400 MHz, (CD<sub>3</sub>)<sub>2</sub>SO) δ 10.70 (d, NH), 8.37 (d, CHNH), 7.22 (dd, 4H), 4.14 (dq, 2 x OCH<sub>2</sub>CH<sub>3</sub>), 2.56 (q, CH<sub>2</sub>Ar), 1.23 (dt, 2 x OCH<sub>2</sub>CH<sub>3</sub>), 1.14 (t, CH<sub>3</sub>CH<sub>2</sub>Ar); <sup>13</sup>C NMR (101 MHz, (CD<sub>3</sub>)<sub>2</sub>SO) δ 168.03 (CO<sub>2</sub>Et), 165.37 (CO<sub>2</sub>Et), 151.77 (CHNH), 140.74, 137.61, 129.27 (2C), 117.92 (2C), 93.02 [C(CO<sub>2</sub>Et)<sub>2</sub>], 59.97 (OCH<sub>2</sub>CH<sub>3</sub>), 59.77 (OCH<sub>2</sub>CH<sub>3</sub>), 27.95 (CH<sub>3</sub>CH<sub>2</sub>Ar), 15.92 (CH<sub>3</sub>CH<sub>2</sub>Ar), 14.64 (OCH<sub>2</sub>CH<sub>3</sub>), 14.57 (OCH<sub>2</sub>CH<sub>3</sub>); MS m/z (ES) [M + Na]<sup>+</sup> C<sub>16</sub>H<sub>21</sub>NO<sub>4</sub>Na requires 314.1368, found 314.1208; CHN for C<sub>16</sub>H<sub>21</sub>NO<sub>4</sub> requires C 65.96%, H 7.27%, N 4.81%, found C 66.25%, H 7.41%, N 4.59%.

*Ethyl 6-ethyl-4-oxo-quinoline-3-carboxylate (87)*

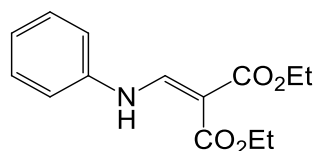


Synthesised according to the general method C, from enamine **78** (1.00 g; 3.43 mmol) in 10 ml of Dowtherm A (3 hours), to afford a yellow powder (0.11 g; 0.43 mmol; yield 13%).

Melting range: 262-264 °C; <sup>1</sup>H NMR (400 MHz, (CD<sub>3</sub>)<sub>2</sub>SO) δ 12.57 (s, NH), 8.51 (s, 1H), 7.97 (s, 1H), 7.56 (m, 2H), 4.22 (q, OCH<sub>2</sub>CH<sub>3</sub>), 2.73 (q, ArCH<sub>2</sub>), 1.29 (m, 2 x CH<sub>2</sub>CH<sub>3</sub>); <sup>13</sup>C NMR (101 MHz, (CD<sub>3</sub>)<sub>2</sub>SO) δ 173.83 (C=O), 165.34 (CO<sub>2</sub>Et), 144.88 (CHNH), 140.88, 137.65, 133.09, 127.71, 124.14, 119.28, 109.95, 59.96 (OCH<sub>2</sub>CH<sub>3</sub>), 28.31 (ArCH<sub>2</sub>CH<sub>3</sub>), 16.01 (ArCH<sub>2</sub>CH<sub>3</sub>), 14.81 (OCH<sub>2</sub>CH<sub>3</sub>).

*Synthesis of 4-oxo-quinoline core*

*Diethyl 2-((phenylamino)methylene)malonate (89)*

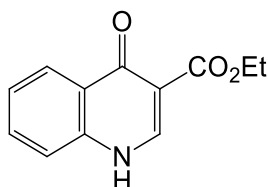


Synthesised according to the general method B, from aniline **88** (2.0 ml; 21.9 mmol). The product was recovered as an orange solid/crystal mixture (5.74 g; 21.80 mmol; yield 99%) after purification by silica gel column chromatography (eluting with 15% of ethyl acetate in hexane).

Melting range: 45-46 °C; <sup>1</sup>H NMR (400 MHz, (CD<sub>3</sub>)<sub>2</sub>SO) δ 10.72 (d, NH), 8.42 (d, CHNH), 7.44 – 7.35 (m, 4H), 7.17 (t, 1H), 4.17 (dq, 2 x OCH<sub>2</sub>CH<sub>3</sub>), 1.26 (m, 2 x

OCH<sub>2</sub>CH<sub>3</sub>); <sup>13</sup>C NMR (101 MHz, (CD<sub>3</sub>)<sub>2</sub>SO) δ 167.86 (C=O), 165.37 (C=O), 151.59 (CHNH), 139.84, 130.11 (2C), 125.09, 117.98 (2C), 93.90 [C(CO<sub>2</sub>Et)<sub>2</sub>], 60.09 (OCH<sub>2</sub>CH<sub>3</sub>), 59.90 (OCH<sub>2</sub>CH<sub>3</sub>), 14.69 (OCH<sub>2</sub>CH<sub>3</sub>), 14.63 (OCH<sub>2</sub>CH<sub>3</sub>); MS m/z (ES) [M + Na]<sup>+</sup> C<sub>14</sub>H<sub>17</sub>NO<sub>4</sub>Na requires 286.1055, found 286.1; CHN for C<sub>14</sub>H<sub>17</sub>NO<sub>4</sub> requires C 63.87%, H 6.51%, N 5.32%, found C 63.68%, H 6.58%, N 5.12%.

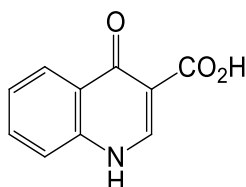
*Ethyl 4-oxo-quinoline-3-carboxylate (90)*



Synthesised according to the general method C, from enamine **89** (1.06 g; 4.01 mmol) in 10 ml of Dowtherm A (3 hours). The product was recovered as a white powder (0.27 g; 1.25 mmol; yield 31%).

Melting range > 350 °C; <sup>1</sup>H NMR (400 MHz, (CD<sub>3</sub>)<sub>2</sub>SO) δ 12.30 (s, NH), 8.53 (s, CHNH), 8.14 (d, 1H), 7.69 (t, 1H), 7.60 (d, 1H), 7.40 (t, 1H), 4.20 (q, OCH<sub>2</sub>CH<sub>3</sub>), 1.27 (t, OCH<sub>2</sub>CH<sub>3</sub>); <sup>13</sup>C NMR (101 MHz, (CD<sub>3</sub>)<sub>2</sub>SO) δ 173.89, 165.28, 145.35, 139.42, 132.86, 127.73, 126.09, 125.15, 119.24, 110.26, 60.02 (OCH<sub>2</sub>CH<sub>3</sub>), 14.80 (OCH<sub>2</sub>CH<sub>3</sub>); MS m/z (MALDI-TOF) [M + H]<sup>+</sup> C<sub>12</sub>H<sub>12</sub>NO<sub>3</sub> requires 218.0817, found 218.0973; CHN for C<sub>12</sub>H<sub>11</sub>NO<sub>3</sub> requires C 66.35%, H 5.10%, N 6.45%, found C 66.40%, H 5.03%, N 6.41%.

*4-Oxo-quinoline-3-carboxylic acid (91)*



Ethyl 4-oxo-quinoline-3-carboxylate **90** (0.20 g; 0.92 mmol) was suspended in methanol (5mL). Sodium hydroxide (10% aq, 7.5mL) was added and the mixture was heated at 100 °C, overnight. The resulting solution was cooled to room temperature and acidified by addition of HCl(aq) (10%; pH≈1). A precipitate was formed, filtered and washed with chloroform, methanol and hexane to give the product as a white powder (0.13 g; 0.69 mmol; 75%).

Melting range: 278-280 °C; <sup>1</sup>H NMR (400 MHz, (CD<sub>3</sub>)<sub>2</sub>SO) δ 15.34 (s, CO<sub>2</sub>H), 13.41 (s, NH), 8.89 (s, CHNH), 8.29 (d, 1H), 7.89 (t, 1H), 7.82 (d, 1H), 7.61 (t, 1H); <sup>13</sup>C NMR (101 MHz, (CD<sub>3</sub>)<sub>2</sub>SO) δ 178.82, 166.85 (C=O), 145.68, 139.93, 134.42, 126.69,

125.53, 124.88, 120.14, 108.06; MS m/z (MALDI-TOF)  $[M - H]^-$   $C_{10}H_6NO_3$  requires 188.0348, found 188.0562; CHN for  $C_{10}H_7NO_3$  requires C 63.49%, H 3.73%, N 7.40%, found C 63.02%, H 3.68%, N 7.23%.





---

# ***CHAPTER THREE***

---

## **RESULTS AND DISCUSSION**

### **Structural investigation of selected quinolone 3-esters**

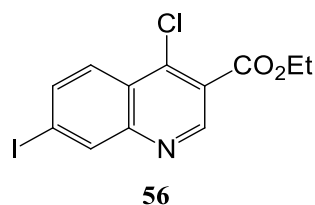


### 3.1. Structural, conformational and vibrational analysis of ethyl 4-chloro-7-iodoquinoline-3-carboxylate (**56**)

The work described in this section was included in the following publication:

P.C. Horta, M. S. C. Henriques, N. Kuş, J. A. Paixão, P. M. O'Neill, M. L. S. Cristiano and R. Fausto, "Synthesis, structural and conformational analysis, and IR spectra of ethyl 4-chloro-7-iodoquinoline-3-carboxylate", *Tetrahedron* (2015), volume 71, pages 7583-7592 (doi:10.1016/j.tet.2015.07.076).<sup>155</sup>

The solubility problems often exhibited by quinolones are reported in the literature and were also encountered along the work described in this thesis. To circumvent these problems, we were led to the synthesis of 4-chloroquinoline derivatives, expected to be more soluble than the corresponding 4-oxo precursors. One such example is compound **56**. This compound may act as a versatile building block, enabling the preparation of quinolone derivatives with chemical diversity at position 7. Additionally, the presence of chlorine at position 4 may allow to introduction of chemical diversity at the carbon 4, through nucleophilic displacement of halide.



The structure of 4-chloro-7-iodo-quinoline (**CIQC**) **56** was studied in the solid phase (crystalline and low-temperature amorphous phases), by X-ray crystallography and vibrational spectroscopy. The monomeric structure of **56** was studied experimentally, as isolated species in a cryogenic argon matrix (at around 15 K), using infrared spectroscopy as analytical method, and theoretically, using contemporary molecular orbital calculations (B3LYP/LANL2DZ+cc-pVDZ level of approximation).

#### 3.1.1. Theoretical calculations

The potential energy profile of **CIQC** was investigated. From analysis of the potential energy landscape obtained from rotation about the two C-O bonds (carboxylic and ester) and the C-C bond connecting the carboxylic ester to the C<sub>5</sub>N ring, different conformers may result. The results obtained from this study revealed that a *trans* conformation of the carboxylic ester moiety (O=C-O-C dihedral in the 180° region) is generally energetically unfavoured (higher energy forms) and, in this case, the higher

energy is also expected due to the steric hindrance resulting from the proximity between the ethyl-ester fragment and the substituents in *ortho* position (H, Cl).

Considering the generally more stable *cis* conformation (O=C–O–C dihedral in the 180° region), four main different minimum energy structures (Figure 3.1) have resulted from the scanning.

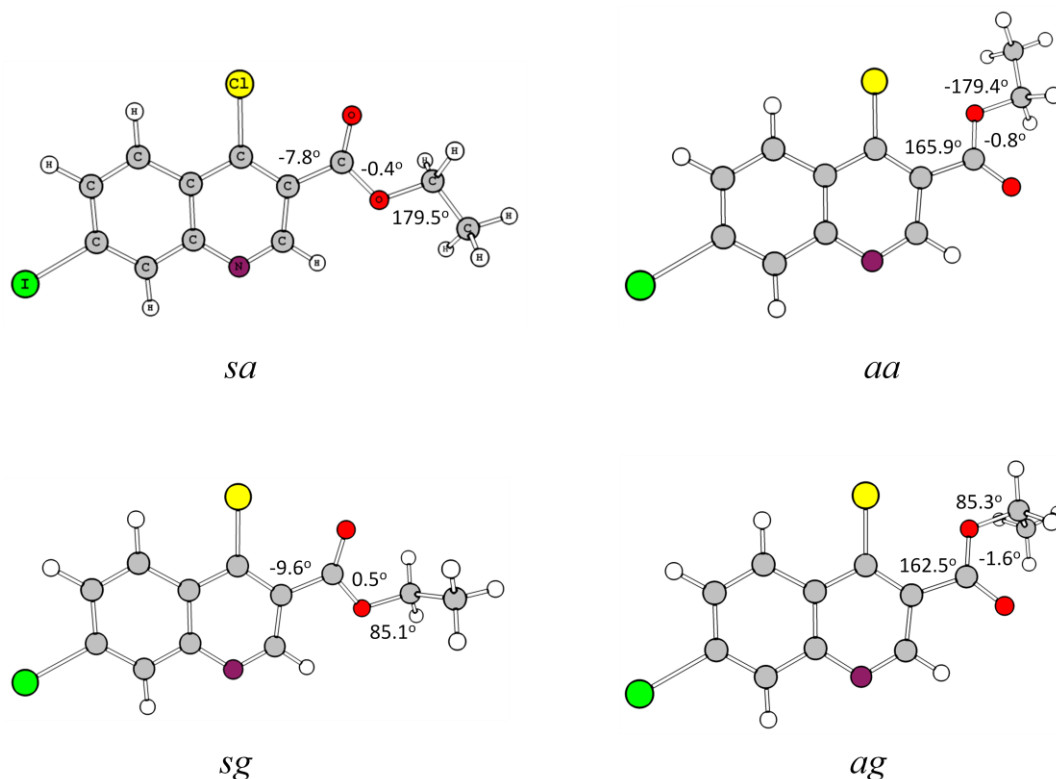


**Figure 3.1** - Optimized geometries (B3LYP/LANL2DZ+cc-pVDZ level of approximation) for the lower energy conformers of **56**. The atom numbering and the optimized values of the C–C–C=O, O=C–O–C and C–O–C–C dihedrals (°) are indicated.

Conformers **sa** and **sg** (with the carbonyl oxygen atom in the same side of the chlorine atom - *syn*) are slightly more stable than those with the chlorine atom facing the ester oxygen atom (**aa** and **ag** conformers - *anti*), indicating that the steric relevance of the ester oxygen atom is more important than that of to the carbonyl oxygen atom, in this context. For each pair of conformers, the structures with the ester group in *anti* conformation are more stable than the corresponding *gauche* forms, so the conformer **sa** is the most stable form of **56**. Nevertheless, the less stable conformer (**ag**) is just 0.92 kJ mol<sup>-1</sup> higher in energy than the most stable **sa** conformer (calculated electronic energies for the four conformers are rather similar, as shown in Table 3.1).

**Table 3.1** – B3LYP/LANL2DZ++cc-p VDZ calculated relative electronic energies ( $\Delta E$ : kJ mol<sup>-1</sup>) for minima of **56** and expected room temperature (298.15 K) gas phase populations (p<sub>298.15</sub>: %).

Conformer <sup>a</sup>	$\Delta E$	p <sup>298.15 b</sup>
<i>sa</i>	0.00	41.8
<i>aa</i>	0.61	15.7
<i>sg</i>	0.43	25.2
<i>ag</i>	0.92	17.3

All the conformers described can be expected to have significant populations in the room temperature gas phase equilibrium (298.15 K). These populations for **sa**, **aa**, **sg** and **ag** are, respectively 41.8, 15.7, 25.2 and 17.3% (Table 3.1).

The calculations yield minimum energy geometries for each conformer that are slightly non-planar and thus two equivalent-by-symmetry minima exist for each one. However, the energy difference between the found minima and the nearby structure exhibiting a planar skeleton is extremely small.

The barriers for interconversion between the conformers of **56** have also been calculated. With exception of the direct conversion between the equivalent-by-symmetry *gauche* forms, the energy barriers for conformational rotation between the various conformers are sufficiently low to be overpassed by warming of a cryogenic argon matrix of the compound to an experimentally accessible temperature (see Appendix 3 - Figure S11 and Figure S12).

Structure-activity relationship studies on the 4-oxo-quinoline 3-ester chemotype and docking studies performed *in silico* at the yeast Q<sub>o</sub> site of the bc<sub>1</sub> protein complex of *P. falciparum* indicated that both the 4-oxo-quinoline and the ethyl ester moieties are relevant for activity. The low barriers predicted for conformational isomerization around the ethyl ester moiety may be important to facilitate structural adjustments of the ethyl ester moiety in the enzyme pocket, to as to maximize drug-target interactions and, thus, to improve the pharmacodynamic profile.

### 3.1.2. Matrix isolation - Infrared spectroscopy studies

An interesting experimental strategy was used in this project, aiming to investigate spectroscopically solid samples of **CIQC** at cryogenic temperatures, under some conformation control.

Initially, an argon matrix of the compound to be studied, **CIQC**, was prepared. Then, the host inert gas matrix-atoms were allowed to evaporate, while the guest molecules could diffuse and form a thin film of the substance. This permits to know the conformational composition existing in the matrix immediately before the evaporation of the host atoms, which can be probed spectroscopically.

The experimental infrared spectrum of **56** isolated in an argon matrix (15 K) agrees with the simulated spectrum, assuming the room temperature equilibrium of the conformational mixture existing in the gas phase (Figure 3.2). This is particularly evident, for example, in the C=O stretching region, between 1700 and 1800  $\text{cm}^{-1}$ , where the experimental spectrum shows essentially a double-band structure (in opposition to the single band in the sole spectrum of the most stable conformer **sa**).

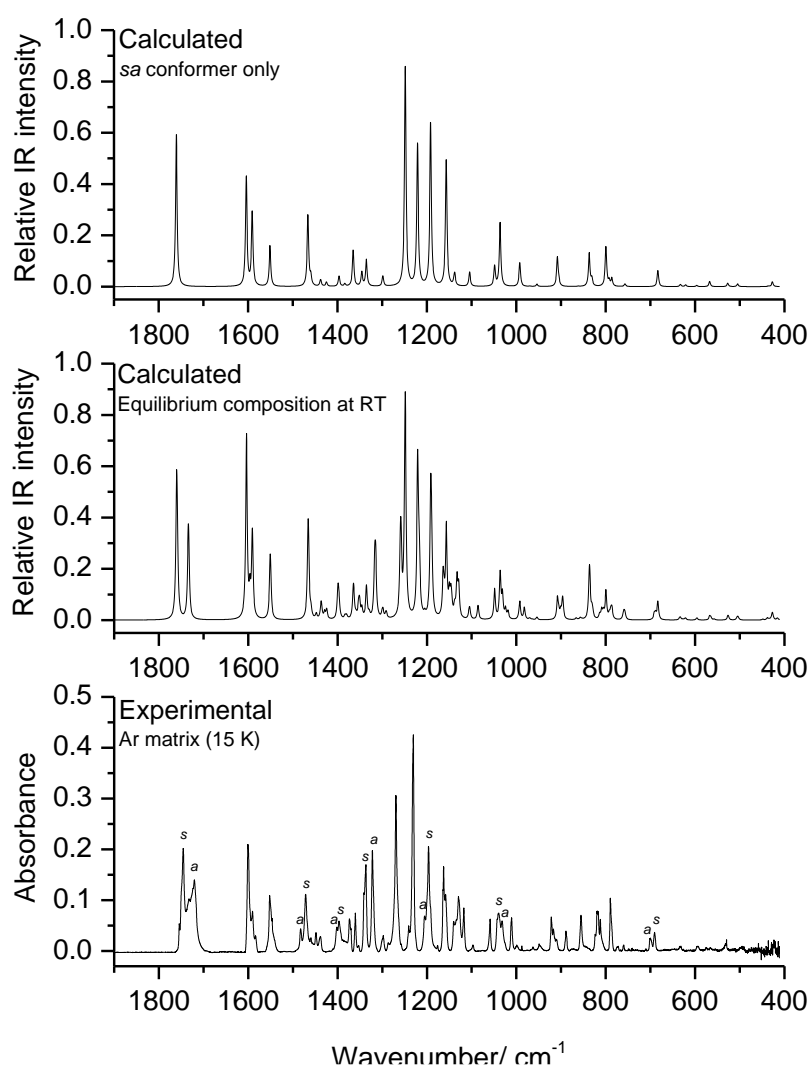


**Figure 3.2** - From top to bottom: simulated IR spectra (calculated at the B3LYP/LANL2DZ+cc-pVDZ level) for the most stable conformer (**sa**) and for the expected conformational equilibrium; observed IR spectrum of **56**, isolated in solid argon (15 K), from the vapor at room temperature (rt).

The same argon matrix of the compound **56**, used to demonstrate the results explained, was subjected to further warming. At 43 K (upon annealing) the matrix sample showed partial conversion (less than 10%) of the higher energy conformers into the most stable **sa** form, in consonance with the low predicted barriers for conformational isomerization. The assignment of the spectral bands to the different conformers is provided in Table S1 (Appendix 3).

In Figure 3.3 it is possible to see the evolution of the infrared spectrum of a sample of **56** along the performed thermal treatment. The selected spectral region corresponds to a characteristic feature of conformers exhibiting the *anti* orientation of the ethyl carboxylic ester substituent in relation to the ring system.

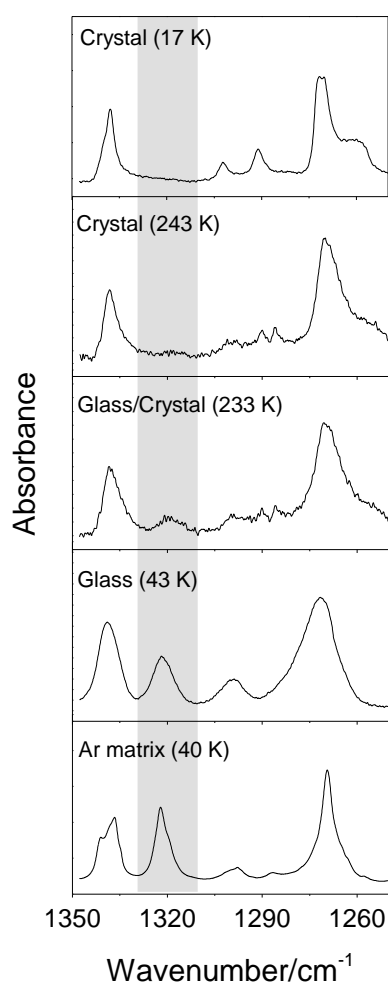


**Figure 3.3** - IR spectra of **56** obtained along the warming/cooling cycle. From bottom to top: spectrum of the argon matrix of the compound at 40 K, at 43 K (after evaporation of the argon) at 233 K, at 243 K and at 17 K (re-cooled crystal). The shadow calls the attention to the band at around 1320  $\text{cm}^{-1}$  (characteristic of **aa** and **ag** conformers).

When reaching the temperature of 233 K, spectral changes started being observed, which were completed when the temperature attained 243 K (generalized band narrowing

and disappearance of the bands which originate only in conformers other than the **sa** form). The sample was then heated to 270 K and re-cooled back to 17 K, to allow for a crystal relaxation. As expected, the spectrum predicted for the **sa** conformer reproduces well that of the re-cooled sample as single molecule (the amorphous state rearranged to the crystalline state).

### 3.1.3. Single crystal X-ray

The X-ray data performed at room temperature shows that, in the crystal, monomeric **56** has a geometry close to that of the conformer predicted theoretically as the most stable for the isolated molecule (**sa**) – see Figure S13 (Appendix 3) with an ORTEP plot of the molecule. The crystal structure consists of layers of molecules and, in each layer, the main packing motif consists of a group of 3 molecules joined together by a weak C-H $\cdots$ O (carbonyl) hydrogen-bond, with the chlorine atoms facing to the center of the group (see Figure S14 - Appendix 3). In the same plane, the interaction between groups occurs via a short contact between the iodine atom and an aromatic H atom of a neighbor molecule (Figure 3.4).

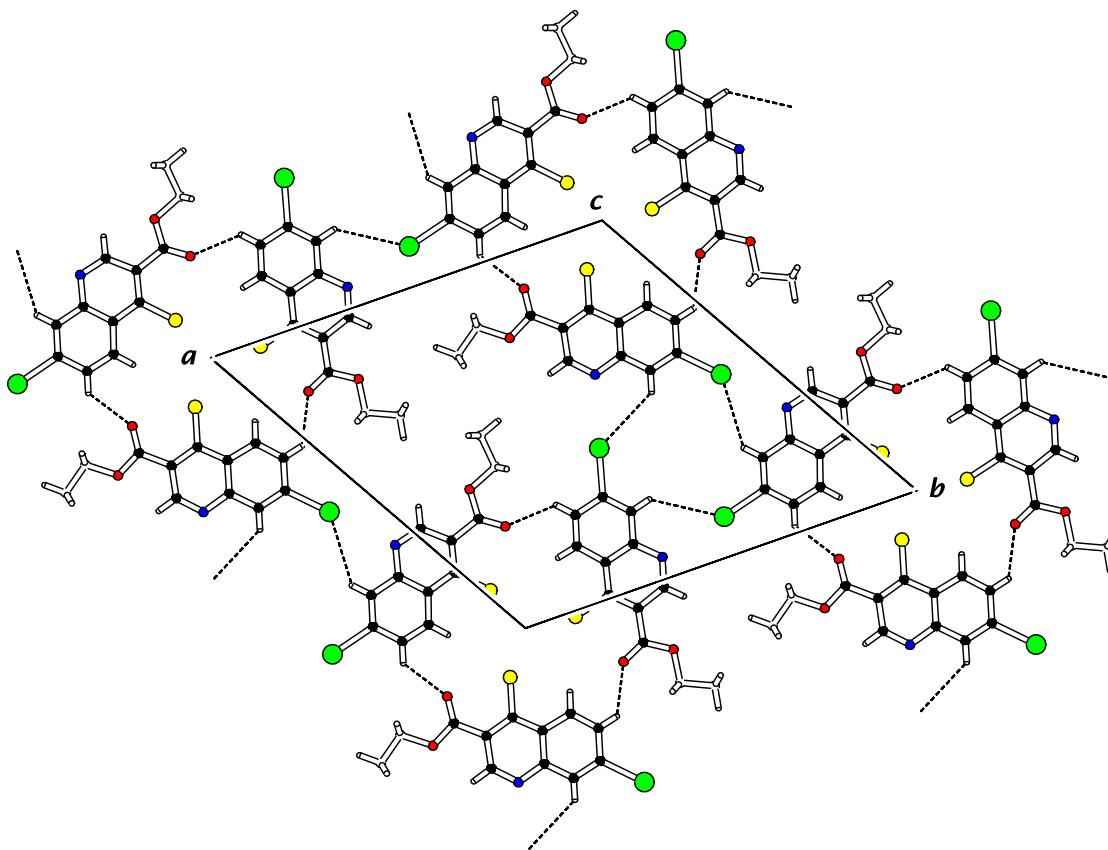


**Figure 3.4** - Intermolecular hydrogen-bond interactions between molecules of **56** in the same plane.



The oxygen carbonyl atom is placed in a position as to act as possible acceptor of the  $\pi$ -electron clouds of the aromatic rings of the molecules of the layers located above and below its own layer (weak intermolecular interactions between layers).

### 3.2. Investigation of the 4-oxo/4-hydroxy-quinoline tautomerism in quinolone 3-esters:

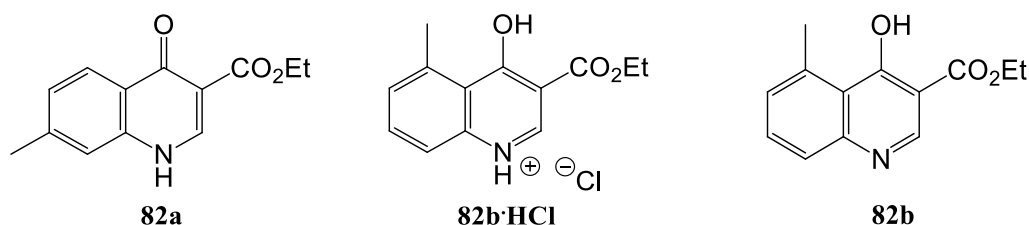
#### Structural, conformational and vibrational study of ethyl 7-methyl-4-oxo-quinoline-3-carboxylate (**82a**) and 4-hydroxy-5-methyl-quinoline-3-carboxylate (**82b**)

Part of the work described in this section was included in the following publication:

P.C. Horta, N. Kuş, M. S. C. Henriques, J. A. Paixão, L. Coelho, F. Nogueira, P. M. O'Neill, R. Fausto and M. L. S. Cristiano, "The quinolone-hydroxyquinoline tautomerism in quinolone 3-esters; preserving the 4-oxo-quinoline structure to retain antimalarial activity", *The Journal of Organic Chemistry* (2015), volume 80, pages 12244-12257 (doi: 10.1021/acs.joc.5b02169).<sup>162</sup>

As mentioned in the introduction, docking studies performed with yeast *bc1*<sup>120</sup> suggested an important role for the amino and 4-oxo functionalities in inhibition of the enzyme by quinolone 3-esters. In this section, we describe the results of our investigation on the 4-oxo/4-hydroxy-quinoline tautomerism in this chemotype, using ethyl 7-methyl-4-oxo-quinoline-3-carboxylate **82a** and ethyl 4-hydroxy-5-methyl-quinoline-3-carboxylate **82b** as model compounds.

As described in chapter 2, compound **82a** was obtained by thermal cyclisation from enamine **73**, in Dowtherm A, at 250 °C, and isolated as sole product. Because this quinolone presents poor solubility, an alternative synthetic approach was considered, involving the synthesis of the 4-chloroquinoline intermediate from enamine **73**. Surprisingly, cyclisation of **73** mediated by POCl<sub>3</sub> at 95 °C led to the isolation of a mixture of an amorphous powder and crystals, corresponding to the hydrochloride salt of one hydroxy-quinoline 3-ester isomer (**82b·HCl**).



Beyond the issue regarding the pattern of aromatic substitution (the synthesis may lead to 7- or 5-substituted quinolones, as previously discussed), the hydroxy-quinoline/oxo-quinoline tautomerism is, in this case, a real possibility, due to the isolation of the hydrochloride salt of **82b**. The tautomerism involving this ring system may be

compared to the equilibrium between 4-pyridones (oxo form) and 4-hydroxy-pyridines. For this system, it was found that the keto form is more stable in the crystal and in the liquid phase or in solution, while the enol form predominates in the vapor phase.<sup>163</sup>

N-substitution (present in quinolones used as antibacterial agents – *e.g.* nalidixic acid, ciprofloxacin and norfloxacin) hinders the possibility of tautomerism. However, it was suggested that the antimalarial activity of quinolone 3-esters requires the presence of N-H and 4-oxo groups in their structure, since the information from docking studies *in silico* at the yeast Q<sub>o</sub> site of the bc<sub>1</sub> protein complex establishes a relevant role for the 4-oxo and N-H groups in drug-target interactions.<sup>120</sup> As such, tautomerization will translate in alteration of chemical and physical properties, with consequences for pharmacokinetic and pharmacodynamic profiles, and should therefore be investigated.

The detailed structures (with emphasis on tautomer and conformer preferences) of 4-oxo and 4-hydroxy-quinoline 3-esters, **82a** and **82b**, were investigated experimentally: in solution, using NMR spectroscopy; in the solid state, using X-ray crystallography and FTIR spectroscopy; and in the monomeric state, using matrix isolation coupled with infrared spectroscopy. The structures of compounds **82a** and **82b** were also studied theoretically, through molecular orbital calculations, using DFT methods, at the B3LYP/6-311++G(d,p) level of approximation.

### **3.2.1. Single crystal X-ray of 82b·HCl**

The crystal structure of **82b·HCl** is presented in Figure 3.5 (and an ORTEP plot of the molecule is available in Appendix 3 - Figure S15). Two strong hydrogen bonds are evidenced, one between the amine group and the halide ion (NH<sup>+</sup>··Cl<sup>-</sup>) and the other between the hydroxyl substituent and the oxygen of the ester carbonyl group (OH··O). The major intermolecular interactions stabilizing the crystal structure are probably weak dispersion forces ( $\pi$ - $\pi$  type interactions) between the  $\pi$  electron clouds of the aromatic rings. The stacking of the molecules is such that the electron clouds of each N-substituted ring in one layer interact with the methyl-substituted phenyl rings in the adjacent layer.

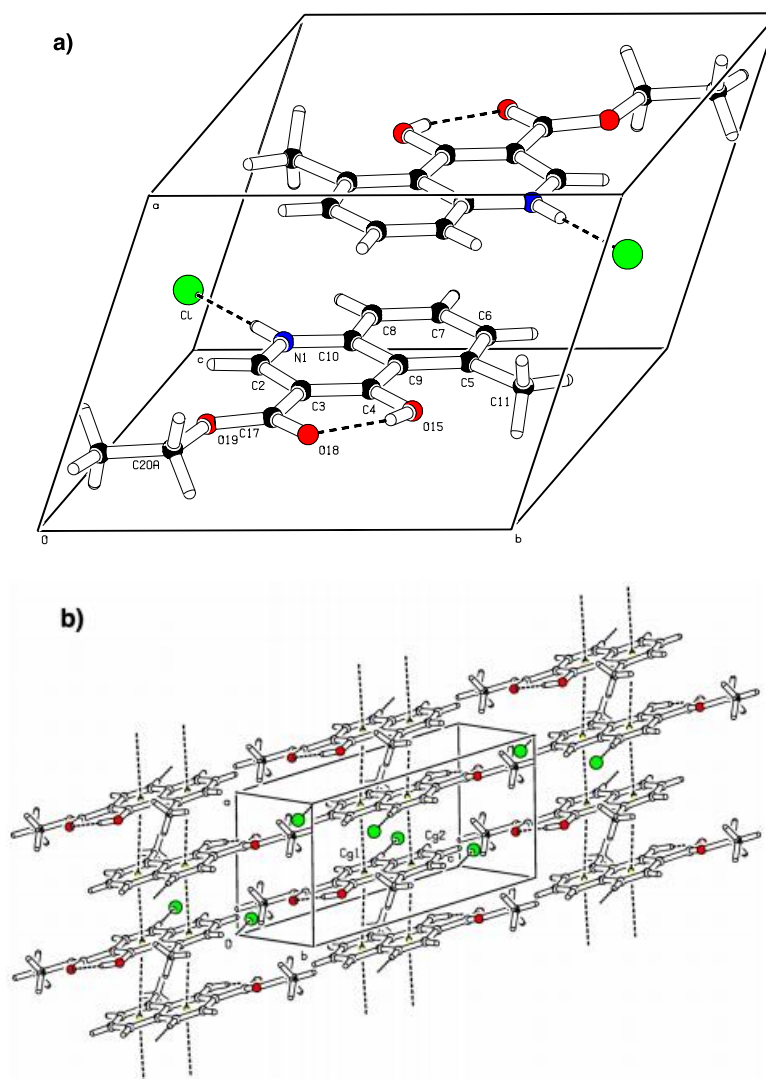


**Figure 3.5** - Crystal structure of ethyl 4-hydroxy-5-methyl quinolinium chloride 3-carboxylate (**82b·HCl**), showing (a) the intramolecular hydrogen-bonding pattern and (b) the molecular stacking and interactions between  $\pi$  electron clouds of aromatic rings.

### 3.2.2. NMR and FTIR spectroscopy

Compounds **82a** and **82b** are easily distinguished by  $^1\text{H}$  NMR and  $^{13}\text{C}$  NMR spectroscopy. In  $\text{D}_6\text{-DMSO}$ , **82a** is identified, in the  $^1\text{H}$  NMR spectrum (see Appendix 3 - Figure S16;  $^1\text{H}$  NMR spectrum of **82a** in D-Chloroform is also available - Appendix 3, Figure S18), by the presence of specific signals due to resonances of the N–H proton (bs,  $\delta = 12.17$  ppm) and of the proton at position 8 (s,  $\delta = 7.38$  ppm), and, in the  $^{13}\text{C}$  NMR spectrum (see Appendix 3 - Figure S17), by the resonance of the carbonyl carbon of the oxo-quinoline system, at position 4 ( $\delta = 176.02$  ppm). The expected NMR signals for the 4-hydroxy-quinoline tautomer of **82a** were not observed, indicating that the 4-oxo-quinoline tautomer was the sole compound present.

The  $^1\text{H}$ -NMR spectra of crystalline hydroxy-quinoline **82b·HCl**, in  $\text{D}_6$ -DMSO and in D-Chloroform (see Appendix 3 - Figure S19 and Figure S20, respectively), show the absence of a signal corresponding to the  $^1\text{H}$  resonance of N–H. In both solvents, the splitting patterns are compatible with the hydroxy-quinoline form with a methyl group at position 5. However, the  $^1\text{H}$ -chemical shifts were found to be different in  $\text{D}_6$ -DMSO and in D-Chloroform. This difference is more pronounced for signals due to resonances of the hydrogens linked to positions 2 and 8 of the quinolone core, with the proton resonances in D-Chloroform appearing downfield (H2, d,  $\delta = 9.26$  ppm; H8, s,  $\delta = 8.51$  ppm), compared to the corresponding resonances in  $\text{D}_6$ -DMSO (H2, d,  $\delta = 8.38$  ppm; H8, s,  $\delta = 7.44$  ppm). It appears reasonable to deduce that the differences in chemical shifts observed for **82b·HCl** in both solvents were due to loss of HCl from the salt, with formation of the free base **82b**, induced by the more polar media. The  $^{13}\text{C}$ -NMR spectrum, in  $\text{D}_6$ -DMSO (see Appendix 3 - Figure S20), shows characteristic signals for the hydroxy-quinoline form, namely a signal corresponding to the resonance of the carbon at position 4 at  $\delta = 171.1$  ppm (predicted at  $\delta = 184.2$  ppm for the quinolone tautomer), demonstrating the sole presence of the 4-hydroxy-quinoline tautomer in solution.

Structures of **82a** and **82b** may also be distinguished by FTIR spectroscopy (Figure 3.6). As it could have been anticipated, the two ATR spectra do not differ much, except in the characteristic regions of the OH group, present in **82b** and absent in **82a**, and for the carbonyl stretching mode of the quinolone carbonyl group of this latter compound, absent in the first. On the other hand, since the spectrum of **82b** corresponds to that of the HCl salt of the compound (**82b·HCl**), the quinolinic N is protonated and the vibration of this moiety is observed at a similar frequency than for **82a**.

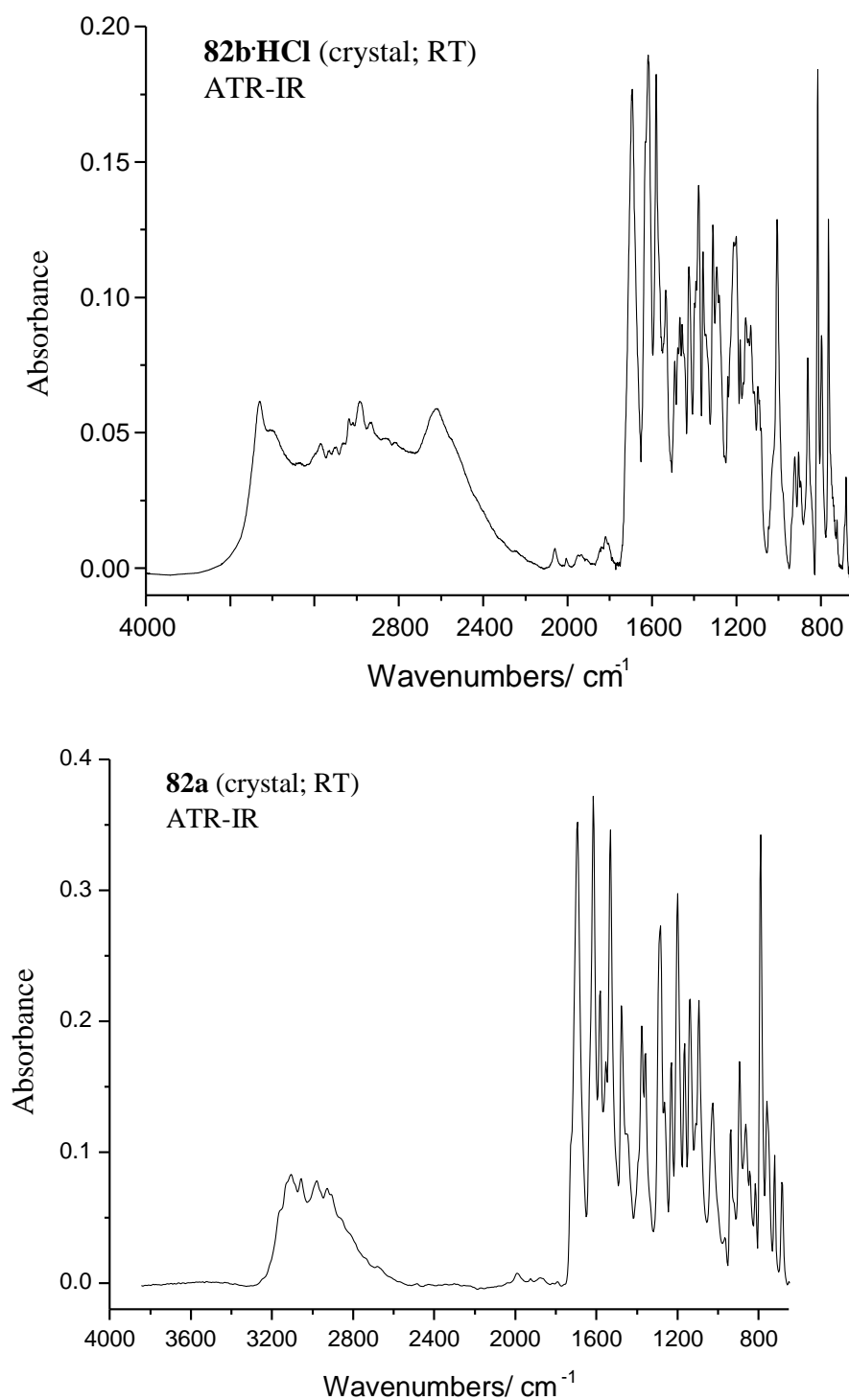


**Figure 3.6** - ATR-IR spectrum of crystalline **82b·HCl** – *top frame* – and **82a** – *bottom frame* – at room temperature.

The crystalline **82b·HCl** was washed with an aqueous solution of sodium bicarbonate. Analysis of the resulting compound revealed the presence of the corresponding keto form, **82c** (Figure 3.7), resulting from tautomerization of **82b** in basic

media. The ATR-IR spectrum of **82c** is similar to that of the **82a** (quinolone form with a methyl at position 7).

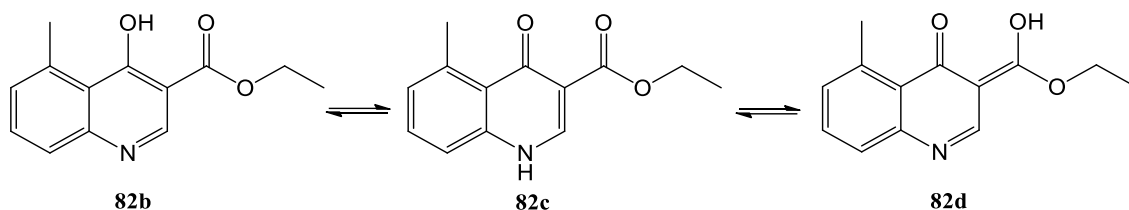


**Figure 3.7** – Structural representation of the tautomers of ethyl 4-hydroxy-5-methylquinoline-3-carboxylate (**82b**) considered in this work.

### 3.2.3. Theoretical calculations – Molecular structure, potential energy and aromaticity

In view of evaluating the tautomeric and conformations preferences of **82b** in the gas phase we considered the possibility of equilibrium between 3 tautomeric forms: 4-hydroxy-quinoline **82b**, 4-oxo-quinoline (or 4-quinolone) **82c** and 3-ethoxy(hydroxy)-4-oxo-quinoline **82d** (Figure 3.7). To assess the relative importance of the different tautomers of the compound as isolated species (or in the gas phase) we investigated the structure of monomeric compounds and the possibility of oxo-quinoline/hydroxy-quinoline equilibria, by theoretical methods (DFT/B3LYP/6-311++G(d,p)). The isomer **82a** (7-methyl-4-oxo-quinoline 3-ester) analogue was also investigated theoretically, at the same level of theory, for comparison.

The study of the potential energy surface of the tautomer **82b** yielded 8 non-equivalent-by-symmetry conformers, graphically depicted in Figure 3.8 and whose relative energies are given in Table 3.2.

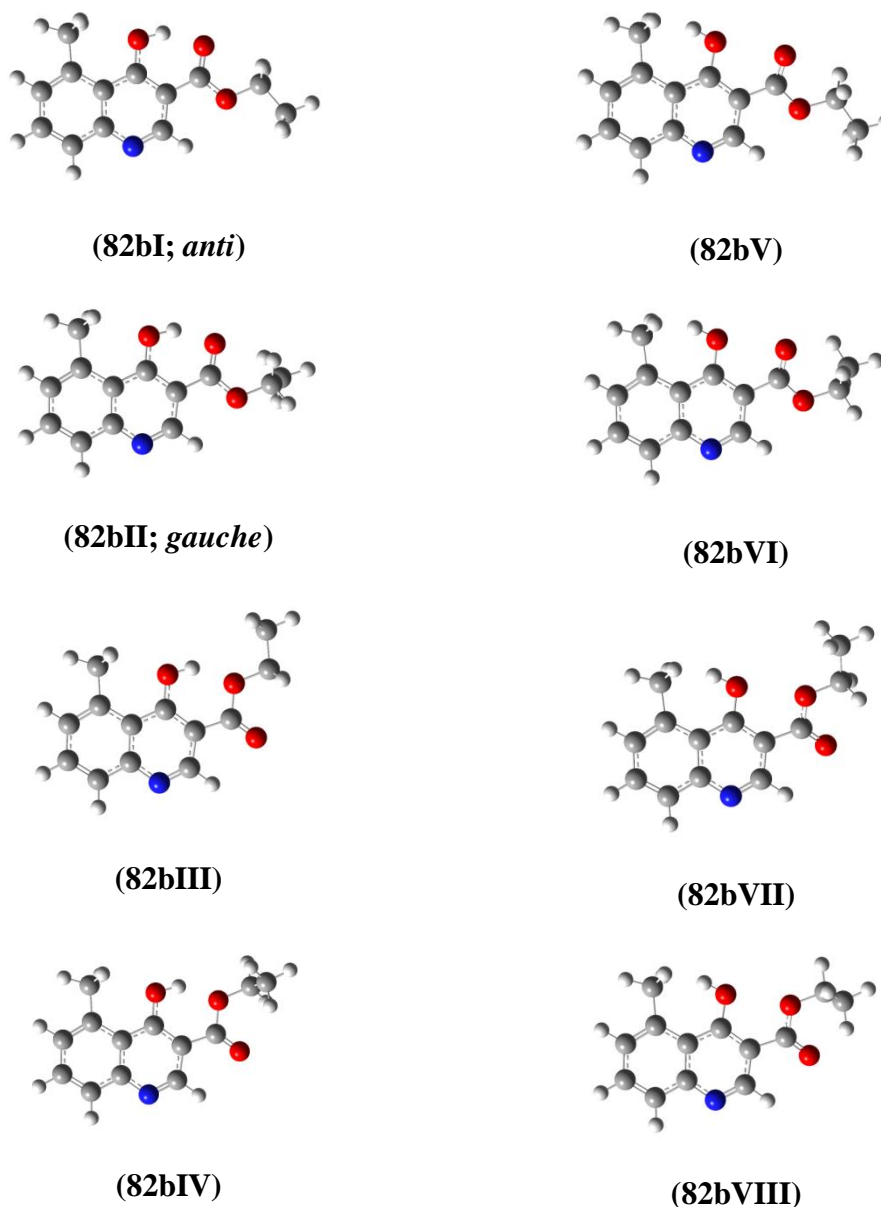


**Figure 3.8** – Representation of the conformers obtained for the 4-hydroxy-quinolone form of **82b** (DFT/B3LYP/6-311++G(d,p)).

Conformers **82bI** and **82bII** (**82bII** is higher in energy than **82bI** by only  $1.9 \text{ kJ mol}^{-1}$ ) have much lower energy than the other forms and shall represent around, respectively, 78% and 22% of the total population in the gas phase equilibrium at room temperature. The considerably lower energy of forms **82bI** and **82bII** can be correlated with the presence, in these forms, of the stabilizing  $\text{O}-\text{H}\cdots\text{O}_{(\text{carbonyl})}$  intramolecular H-bond interaction (Figure 3.8). The intermediate relative energies of forms **82bIII** and **82bIV** ( $\Delta E$  around  $18 \text{ kJ mol}^{-1}$ ) can be ascribed to the presence of the stabilizing  $\text{O}-\text{H}\cdots\text{O}_{(\text{ester})}$  (expected to be weaker than the  $\text{O}-\text{H}\cdots\text{O}_{(\text{carbonyl})}$ ) intramolecular H-bond interaction.



Conformers **82bV** to **82bVIII** do not evidence intramolecular H-bonds and the repulsive interactions between the OH and ester substituents dominate, justifying their much higher energies ( $\Delta E > 60 \text{ kJ mol}^{-1}$ ).

**Table 3.2** - Relative energies ( $\Delta E$ :  $\text{kJ mol}^{-1}$ ) of the relevant conformers for tautomeric forms **82b**, **82c** and **82d**.

Conformers of <b>82b</b> , <b>82c</b> and <b>82d</b>	$\Delta E$
<b>82b I</b> ( <i>anti</i> )	0.0
<b>82b II</b> ( <i>gauche</i> )	1.9
<b>82b III</b>	17.3
<b>82b IV</b>	18.3
<b>82b V</b>	61.3
<b>82b VI</b>	63.0
<b>82b VII</b>	60.6
<b>82b VIII</b>	62.3
<b>82c I</b>	26.6
<b>82c II</b>	28.7
<b>82c III</b>	34.4
<b>82c IV</b>	35.4
<b>82d I</b>	157.8
<b>82d II</b>	160.2

The calculated potential energy profile for internal rotation about the C-O-C-C dihedral, interconverting conformers **82bI** (around  $180^\circ$ ) and **82bII** at  $90^\circ$  (Figure 3.9), shows that this two conformers are separated by a small energy barrier ( $3.5 \text{ kJ mol}^{-1}$  in the **82bI**→**82bII** direction;  $1.6 \text{ kJ mol}^{-1}$  in the reverse direction). However, the direct interconversion between the two symmetry-equivalent gauche (**82bII**) implies crossing a large energy barrier ( $\sim 30 \text{ kJ mol}^{-1}$ ) corresponding to the highly sterically hindered transition state with C-O-C-C dihedral equal to  $0^\circ$ .

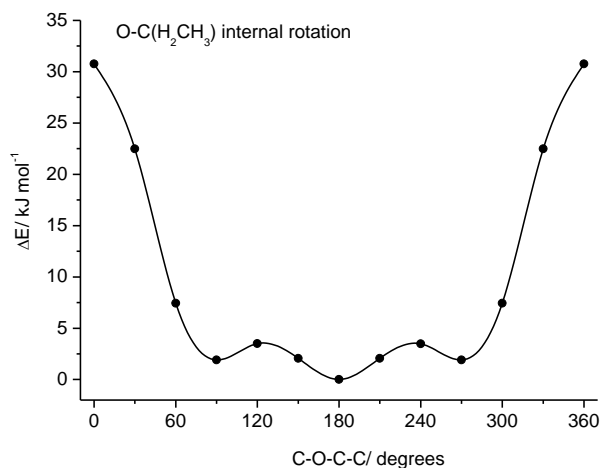


**Figure 3.9** – B3LYP/6-311++G(d,p) calculated relaxed potential energy profile for interconversion between conformers **I** and **II** of **82b**.

The conformers of **82c** and **82d**, calculated at the same level of theory, are represented in Figure 3.10 and Figure 3.11, respectively. The most stable conformer of **82c** (**I**) is higher in energy than the most stable conformer of the hydroxy-quinoline tautomer (**82bI**) by 27 kJ mol<sup>-1</sup>, while the two lowest energy conformers for **82d** have larger energies (more than 155 kJ mol<sup>-1</sup>) (Table 3.2).

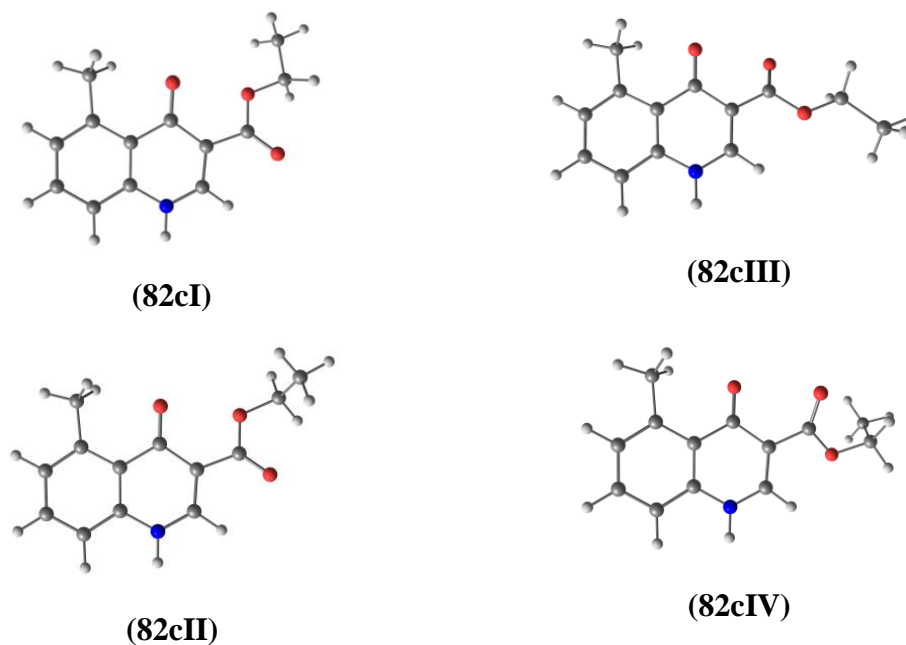


**Figure 3.10** – Representation of selected (lowest energy) conformers calculated for tautomer **82c** (DFT/B3LYP/6-311++G(d,p)).

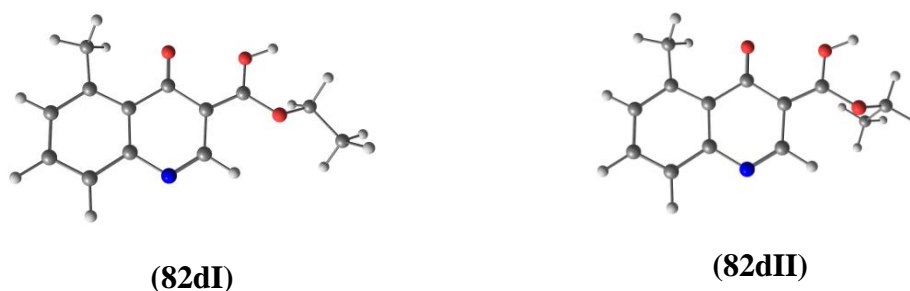


**Figure 3.11** – Representation of selected (lowest energy) conformers obtained for tautomer **82d** (DFT/B3LYP/6-311++G(d,p)).

The conformational and tautomeric preferences for monomeric 4-oxo-quinoline **82a** (7-methyl substituted quinolone) and its corresponding hydroxy-quinoline tautomer were also theoretically investigated, at the same level of theory, leading to the same conclusions as for compound **82b**. The hydroxy-quinoline form of **82a** is more stable in the gas phase than the oxo forms ( $\Delta E \sim 38.0 \text{ kJ mol}^{-1}$ ). Also the hydroxy-quinoline tautomer of **82a** has two low energy conformers exhibiting an  $\text{OH}\cdots\text{O}=\text{C}$  intramolecular H-bond (similar to the two most stable forms of **82b**).

Thus, the tautomeric and conformational patterns in the studied molecules, in the gas phase, are not significantly affected by the position of the methyl substituent on the benzenic ring of the quinoline moiety.

The aromaticity of the two rings in the 5-methyl substituted molecules (**82b**, **82c** and **82d**) has been estimated using two well-known aromaticity indexes: the harmonic oscillator measure of aromaticity (HOMA index), defined by Kruszewski and Krygowsky,<sup>164,165</sup> and the Bird index.<sup>166</sup>

Despite its simplicity, the HOMA index has been found to be one of the most effective structural indicators of aromaticity and a good measure of  $\pi$ -electron delocalization. If HOMA equals to 1 the ring is fully aromatic, if equals to 0 the ring is completely nonaromatic and if assumes a significantly negative value then the ring shows anti-aromaticity character.

The Bird index is another geometry-based quantity aimed at measuring aromaticity and the closer the Bird index is to 100 the stronger the aromaticity is.

**Table 3.3** – Calculated aromaticity indexes (HOMA and Bird) for tautomers **82b**, **82c** and **82d**.

		Tautomer		
		<b>82b</b>	<b>82c</b>	<b>82d</b>
<b>HOMA</b>	C <sub>5</sub> N-ring	0.73	0.04	-0.07
	C <sub>6</sub> -ring	0.76	0.90	0.89
<b>B<sub>I</sub></b>	C <sub>5</sub> N-ring	78.7	57.3	60.2
	C <sub>6</sub> -ring	80.0	88.3	88.1

The HOMA and  $B_I$  indexes for **82b**, **82c** and **82d** tautomers (Table 3.3), determined using the B3LYP/6-311++G(d,p) calculated bond lengths, agree with each other. For **82b**, both rings are aromatic, with the heteroaromatic ring being only slightly less aromatic than the benzenic ring. However for **82c** and **82d** the nitrogen-containing ring is essentially non-aromatic, while the benzenic ring is more aromatic than in **82b**. The reduced aromaticity of the heterocyclic ring for **82c** and **82d** can also be considered a relevant factor in rendering these species more energetic than **82b**.

#### 3.2.4. Matrix-isolation - IR spectroscopy and photostability studies

The structure of monomeric **82b** was studied using matrix isolation coupled to FTIR spectroscopy (upon sublimation of **82b**·HCl, HCl is evolved and sole the free base, **82b**, is isolated in the argon matrix).

Considering the theoretical results, prevalence of **82bI** and **82bII** in the gas phase should be expected. Also, there is the possibility of partial conversion of **82bII** into the most stable **82bI**, during preparation of the low temperature matrices, taking into account the low energy barrier for this conversion (conformational cooling). The matrices are prepared from deposition of a very diluted gaseous solution of the vapour of the compound in the noble gas onto the cold (15 K) IR transparent CsI optical substrate of the cryostat.<sup>167</sup> Since the gas phase population of **82bII** is already small (22%, according to the performed calculations) and its predicted IR spectrum is quite similar to those of **82bI**, the presence of **82bII** in the studied argon matrix could not be safely established.

Experimentally, the IR spectrum of **82b** isolated in solid argon can be fairly well reproduced by the calculated spectrum of conformer **I** alone (Figure 3.12).

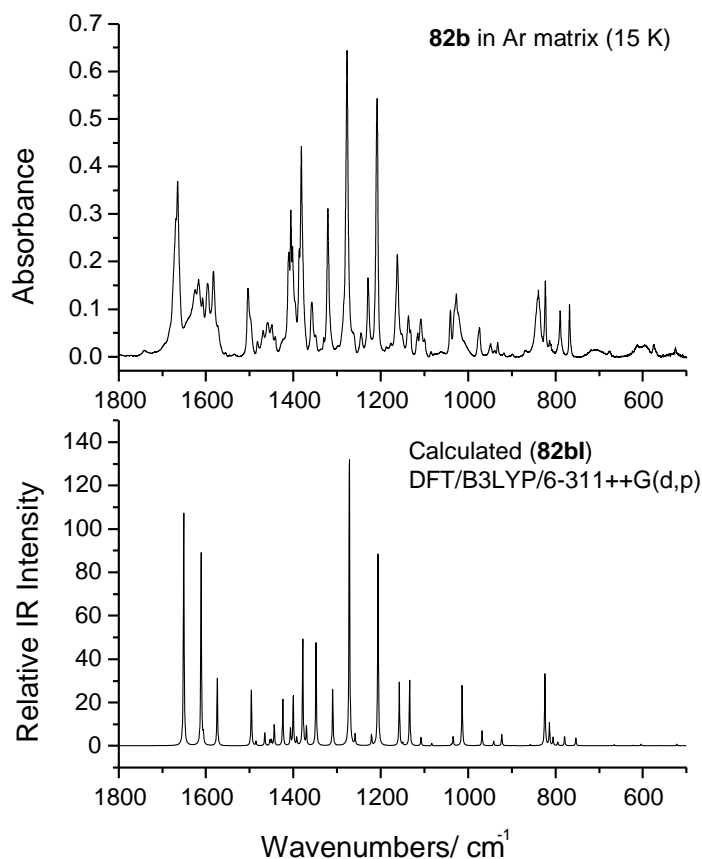


**Figure 3.12** – IR spectrum of the as-deposited argon matrix of **82b** (top) and calculated spectrum (B3LYP/6-311++G(d,p)) for conformer **82bI**.

Annealing of the matrix up to about 40 K led to small, but perceptible changes in the relative band intensities, indicating that conformer **82bII** could have partially survived to matrix deposition and had been converted into **82bI** upon the annealing.

The proposed assignments for the bands observed in the experimental spectrum (at 15 K) are summarized in Table S2 (Appendix 3). In this table, the theoretical wavenumbers and IR intensities for both conformers **82bI** and **82bII** are also provided.

It is worth mentioning that no traces of **82c** or **82d** tautomers were found in the experimental IR spectra, revealing that the species resulting from sublimation of the used hydrochloride salt (**82bHCl**) are solely HCl and **82b**, *i.e.*, the tautomeric species of the compound present in the crystalline solid did not convert to other tautomers upon sublimation (see Appendix 3 - Figure S22).

We prepared the quinolone form, **82c**, by alkaline washing of the salt, **82bHCl**. Matrix isolation studies on this sample show that, during sublimation the keto form **82c** converts extensively to the most stable hydroxy-quinoline form (**82b**). In fact, the infrared

spectrum of matrix-deposited **82c** is identical to that obtained upon deposition of the unwashed **82b**·HCl sample.

### 3.2.5. Evaluation of photostability; UV-induced photochemistry of matrix-isolated **82b**

The photostability of monomeric **82b** was assessed through an investigation of its UV-induced matrix photochemistry. Continuous broadband irradiation ( $\lambda > 220$  nm; 130 min) of the matrix led to only partial photodecomposition of **82b** (consumption of about 1/3 of the original compound), giving rise to an open-ring ketene isomeric species. The number of new bands detected in the spectra of the photolysed matrix was very small (Figure 3.13), indicating the formation of CO<sub>2</sub><sup>168</sup>, CO and ketene species.<sup>169–172</sup> Formation of ketenes has been observed for similar compounds isolated in matrices and subjected to similar irradiation conditions, for example, methyl *p*-hydroxybenzoic acid (methyl paraben) and triclosan.<sup>173,174</sup> The results obtained in the performed photochemical experiments indicate that **82b** appears to be relatively photostable.

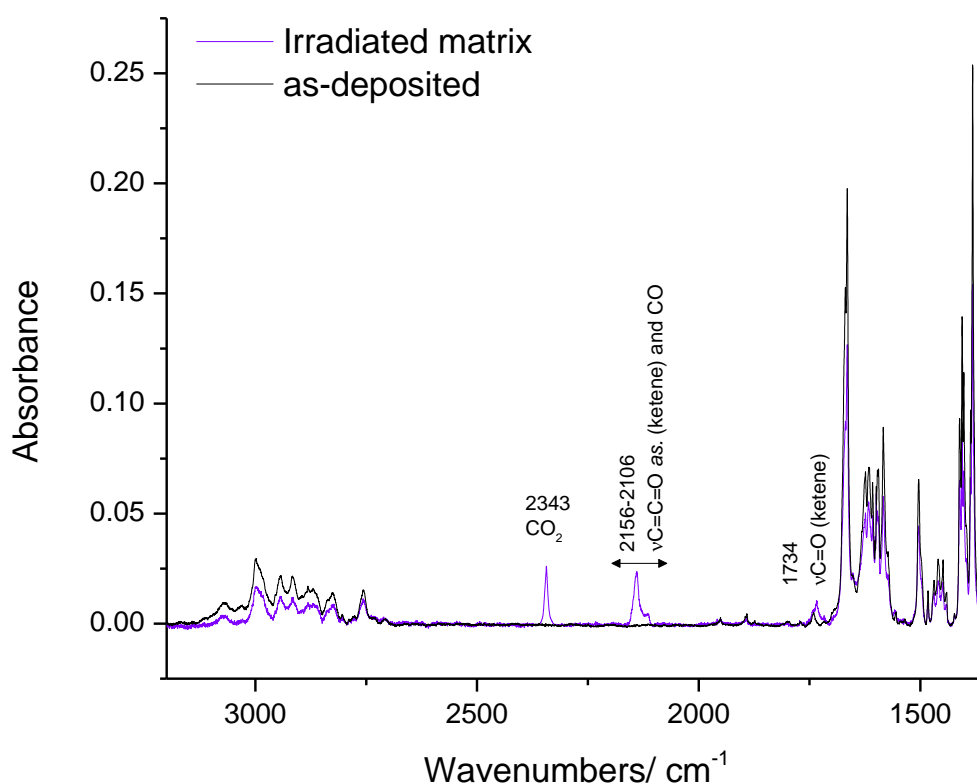


**Figure 3.13** – Fragment of the IR spectra showing photolysis ( $\lambda > 220$  nm; 130 min) of **82b** in argon matrix; in black: IR spectrum obtained prior to irradiation; in purple: IR spectrum obtained after irradiation; bands due to CO, CO<sub>2</sub> and ketene species are identified.

### 3.3. Investigation of 4-oxo/4-hydroxy-quinoline tautomerism using the unsubstituted 4-oxo-quinoline (92a) as model

To build a deeper understanding of the oxo-quinoline/hydroxy-quinoline tautomerism it was decided to study the unsubstituted quinolone core structure devoid of substituents, so as to exclude possible substituent effects on the tautomeric equilibrium. It is noteworthy that the ester substituent in position 3 of the quinolone structure affects the quinoline-hydroxyquinoline tautomerism in quinolone 3-esters and introduces the possibility of another tautomeric form. We intended to conduct a brief structural study of quinolone core in order to gather information regarding its tautomeric equilibrium and those preferences, using contemporary computational methods, by performing molecular orbital calculations.

The quinolone scaffold **92a** (4-oxo-quinoline) was thus considered and its tautomeric equilibrium studied theoretically (Figure 3.14), using DFT methods.

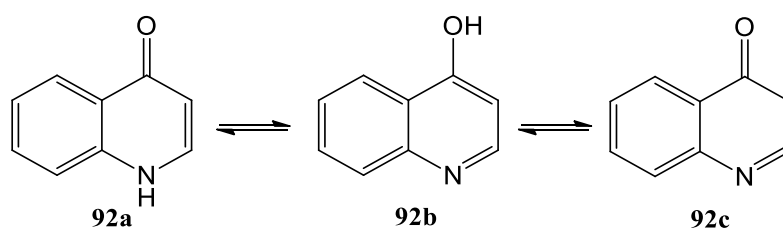


**Figure 3.14** – Structural representation of the possible tautomers of 4-oxo-quinoline (**92a**) considered in the theoretical investigation (B3LYP/6-311++G(d,p)).

Considering the planarity relatively of the quinolone core, the presence of conformers for tautomer **92a** and **92c** was not considered in this study. As represented in Figure 3.15, from rotation of the hydroxyl in compound **92b**, two conformational minima were calculated (H-O-C-C dihedral equal to  $0^\circ$  or to  $180^\circ$ ).

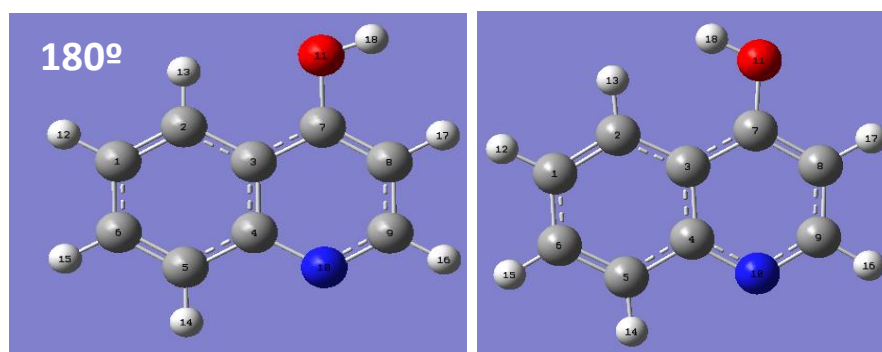


**Figure 3.15** – Structural representation of the two conformational minima, **92b180** and **92b0**, calculated from the scanning for conformational evaluation of **92b** (B3LYP/6-311++G(d,p)).

The minima energies for optimized structures of **92a**, **92b180**, **92b0** and **92c** were determined by using different functional and basis functions (selected from a study about theoretical structure and vibrational spectra of ciprofloxacin).<sup>175</sup> Results obtained with the various levels of theory proved to follow a similar trend, with the quinolone **92a** as the most stable structure, while **92c** is the most unstable (with an average of relative energy of about 265.92 kJ mol<sup>-1</sup>). The absence of an ester carbonyl at position 3 of the quinolone core abrogates the advantageous stabilization of the hydroxyl group of **92b**, when compared with the more stable form, the tautomer **92a**. However, the two minima of **92b** show energies relatively close together and also relatively close to **92a** ( $\Delta E = 44.76$  kJ mol<sup>-1</sup> for **92b0**; and  $\Delta E = 34.44$  kJ mol<sup>-1</sup> for **92b180**, in average). Thus, all these three forms, tautomer **92a** and both conformers of **92b**, can coexist and contribute to the equilibrium populations at room temperature.



### 3.4. Summary and conclusions

The low intrinsic solubility of 4-oxo-quinoline 3-esters drove us to consider the synthesis of 4-chloroquinoline derivatives (for example compound **56**) as intermediate compounds. 4-Chloroquinolines derivatives steamed as versatile building blocks for the preparation of 4-oxo-quinolines, with the possibility of introducing chemical diversity at positions 4, 6 and/or 7 of the quinoline core structure. Theoretical calculations ((B3LYP/6-311++G(d,p)) predicted four different conformers of 4-chloroquinoline **56**, at room temperature. These conformers are related with the ester moiety but show low predicted barriers for conformational interconversion. The same four conformers were found in the as-deposited argon-matrix of the compound, in relative amounts close to those predicted by theory.

Structure-activity relationship studies on the quinolone 3-ester chemotype and docking studies performed *in silico* at the yeast Q<sub>o</sub> site of the *bc*<sub>1</sub> protein complex of *P. falciparum* indicated that both the 4-oxo-quinoline and the ethyl ester moieties are relevant for activity. The present work shows that the barriers predicted for conformational isomerization around the ethyl ester moiety are low and this may be important to facilitate structural adjustments of the ethyl ester moiety in the enzyme pocket, so as to maximize drug-target interactions, thereby improving the pharmacodynamic profile.

Conventional quinolones (*e.g.* nalidixic acid, ciprofloxacin and norfloxacin) that are widely used in medicine as antibacterial agents are N-alkyl substituted, and the N-substituent hinders the possibility of tautomerism. However, this strategy cannot be applied in the development of quinolones antimalarials directed to the *bc*<sub>1</sub> protein complex, since the docking studies indicated that the 4-oxo and N-H groups in the quinolone core appear to be important to the antimalarial activity of quinolone 3-esters. Hence, the possibility of tautomerism between 4-oxo-quinoline and 4-hydroxy-quinoline forms should not be neglected. Tautomerization translates in an alteration of chemical and physical properties, with consequences for pharmacokinetic and pharmacodynamic profiles.

For the compounds in study (**82** series), calculations show a difference between the lowest energy hydroxy-quinoline and quinolone forms of 27 and 38 kJ mol<sup>-1</sup>, for 5-substituted and 7-substituted compounds, respectively. The preference for the hydroxy-quinoline form can be correlated with the presence in these forms of a O-H...O(ester

carbonyl) stabilizing intramolecular H-bond interaction. Calculations of aromaticity for the two rings of each compound in study by HOMA and  $B_I$  indexes afford results that are in keeping with the observed preference for the enol forms, and the aromaticity can thus be considered a relevant factor in defining structural preferences.

Sublimation of the hydroxy-quinoline salt followed by its deposition to form a cryogenic matrix and analysis by FTIR spectroscopy allowed collection of data showing that the tautomeric species of the compound present in the crystalline solid (hydroxy-quinoline) did not convert to another tautomer upon sublimation. On the contrary, when the solid 4-oxo-quinoline (keto) form was used as starting material in the matrix isolation experiments, extensive tautomerization of the compound was observed, resulting in the sole observation of the 4-hydroxy-quinoline tautomeric form.

To understand the effect of the 3-ester substituent on the quinolone structure, a brief computational study was conducted on the quinolone scaffold (**92** series), calculating the structure and energy of its tautomeric equilibrium species. The results obtained highlighted the keto form as the most stable compound, in the unsubstituted 4-oxo-quinoline, since the absence of an ester carbonyl at position 3 of the quinolone core abrogates the possibility of advantageous stabilization of the hydroxyl group at position 4. However, the energy barriers between the 4-hydroxy-quinoline and 4-oxo-quinoline forms are relatively close together and all these tautomers can coexist and contribute to the equilibrium populations.

### **3.5. Experimental**

#### *X-ray diffraction studies*

The single crystal X-ray diffraction (XRD) study was performed at room temperature on a Bruker APEXII diffractometer using graphite monochromatized Mo K $\alpha$  radiation ( $\lambda = 0.71073 \text{ \AA}$ ). Bond lengths and angles are within the expected range of values. The crystal structure have been deposited at the Cambridge Crystallographic Data Centre (deposition numbers: CCDC 1406711 for **56** and 1039599 for **82b·HCl**) and further details on data collection, structure refinement and full tables of interatomic distances, valence and torsion angles are available therein.

#### *Matrix preparation, IR spectroscopy and photostability studied*

Isolation of the compound in solid argon was achieved by sublimating the solid compound in a specialized thermoelectrically-heatable mini-oven assembled inside the cryostat, and co-depositing its vapors with argon (N60, supplied by Air Liquide), coming out from a separate line, onto a CsI window kept at 15 K. The obtained matrices were enough diluted (matrix:sample ratio >1000), so that they contain only monomers of the compound. Annealing of the matrices was undertaken in steps of 1 degree, until evaporation of the argon host (at 40-43 K), and in steps of 5 degrees, after that temperature.

Evaporation of the host matrix atoms allowed obtaining an amorphous solid, which could later be crystallized at a temperature of ~233-243 K. The crystal was then re-cooled down to 17 K and its infrared spectrum collected.

The low temperature set up used includes, as main component, an APD Cryogenics closed-cycle helium refrigeration system, with a DE-202A expander. The temperature was measured directly at the sample holder, using a silicon diode sensor connected to a digital temperature controller (Scientific Instruments, Model 9650-1), which provides accuracy of 0.1 degree.

The IR spectra were recorded in the 4000-400 cm $^{-1}$  range with 0.5 cm $^{-1}$  resolution, on a Thermo Nicolet 6700 Fourier-transform infrared (FTIR) spectrometer, equipped with a deuterated triglycine sulfate (DTGS) detector and a KBr beamsplitter.

UV-irradiation of the matrices was done through the outer quartz window of the cryostat, using a HBO200 high-pressure Hg(Xe) lamp.

The ATR-FTIR spectra were obtained using a germanium crystal in a Nicolet iN10 MX infrared system with a MCT-A detector and a KBr/Germanium optics. The

spectral resolution used was  $2\text{ cm}^{-1}$ , with an aperture of 80 and number of scans of and 64.

*Theoretical calculations*

The quantum chemical calculations were performed using Gaussian 09.<sup>176</sup> Geometries were fully optimized at the DFT/B3LYP level of approximation.<sup>177-179</sup>

The potential energy profiles for internal rotation were calculated with the driving coordinate incrementally fixed and all the other geometrical parameters optimized.

The harmonic vibrational wavenumbers were obtained at the same level of theory and scaled by 0.978, to correct them for the shortcomings of the applied methodology (mainly for anharmonicity). The scaled calculated frequencies, together with the calculated intensities, were used to produce the simulated spectra.

---

# ***CHAPTER FOUR***

---

## **RESULTS AND DISCUSSION**

**Docking studies, CLogP calculations and  
evaluation of antimalarial activity**



#### **4.1.Lipophilicity/solubility evaluation – CLogP calculation**

To reach its target, a drug must pass through several membranes, beginning with the absorption in the stomach and small and large intestine, if orally administered. To pass across most membranes, the drug must be relatively non polar. However the drug must be solubilized in biological media and, for that, it should possess some polar characteristics. The polarity of a substance is measured by its partition coefficient in a two phase system consisting of 1-octanol (mimicking the cell membrane) and water (mimicking the extracellular fluid), where P is the ratio between the amount of drug in octanol and the amount in water. Usually, in medicinal chemistry, the logarithm of the partition coefficient (LogP) is used to assess the drug-likeness of a given molecule, as it is a well-established measure for the compound's hydrophilicity and/or hydrophobicity.<sup>180</sup>

Partition coefficients have a strong influence on pharmacokinetic properties of drugs and are thus useful to estimate the absorption and distribution of drugs within the body and also to predict how rapidly they are metabolized and excreted. For a drug to be orally absorbed, it normally must first pass through lipid bilayers in the intestinal epithelium and must be hydrophobic enough (high LogP values), but not so hydrophobic since the drug must be previously dissolved, and once it is in the bilayer should not partition out again.<sup>181</sup> On the other hand, in terms of pharmacodynamic profile, hydrophobic drugs tend to be more toxic because, in general, they are retained for longer periods and have a wider distribution within the body.<sup>182</sup>

However, LogP is not an accurate determinant of lipophilicity for ionisable compounds, because it only describes the partition coefficient of neutral molecules. This limitation can affect the research, since approximately 80% of the drugs are ionisable and are subject to the changing pH environments in the body.<sup>180-182</sup>

Nowadays, there are computer programs available to calculate the LogP (CLogP) values from the structure of compounds. In this work we have used ALog PS 2.1 (available from Virtual Computation Chemistry Laboratory – [www.vcclab.org/lab/alogps/](http://www.vcclab.org/lab/alogps/)), considered to be the most accurate program to predict lipophilicity and aqueous solubility of molecules.

Christopher Lipinski developed the “Rule of five” based on the observation that most orally administered drugs are relatively small (with molecular weight of less than or equal to 500 g mol<sup>-1</sup>), not too polar (five or fewer hydrogen-bond donors and up to 10

hydrogen-bond acceptors) and are moderately lipophilic (not too hydrophobic nor too hydrophilic), with an intermediate LogP value (between 2 and 5).<sup>183</sup>

#### 4.1.1. Evaluation of CLogP

As pointed out in the previous chapter, changes in the structure of 4-oxo-quinoline 3-esters (due for example to tautomeric and conformational preferences) will translate in changes of chemical and physical properties (like solubility) and may have impact on pharmacokinetic and pharmacodynamic profiles. Considering the possibility of keto-enol tautomerism in the chemotype investigated<sup>162</sup> and also the fact that, in some cases, an isomeric mixture (5 and 7-substituted) was obtained from the cyclisation step due to the possibility of various aromatic substitution patterns, the LogP values were calculated for the library of quinolones studied and for the corresponding tautomers and isomers (Table 4.1).

**Table 4.1** - CLogP values for ethyl 4-oxo-quinoline-3-carboxylates, substituted at positions 5 or 7, and for the corresponding tautomers. (a) calculated by ALog PS2.1.

Compound	Substituent	CLogP value <sup>(a)</sup>			
		Position 7, keto form	Position 5, keto form	Position 7, enol form	Position 5, enol form
13	Benzoyloxy-	2.95±0.39	3.04±0.42	3.88±0.42	3.91±0.40
14	Benzyloxy-	3.02±0.45	3.12±0.39	4.02±0.61	4.01±0.61
31	Benzisothiazoloxo-	2.40±0.67	2.53±0.60	3.41±0.95	3.38±0.96
33	Hydroxyl-	1.11±0.49	1.50±0.41	1.96±0.28	2.09±0.37
43	Fluorine-	1.69±0.43	1.80±0.32	2.67±0.44	2.68±0.44
46	Iodine-	2.44±0.41	2.54±0.35	3.41±0.60	3.40±0.60
60	4-morpholino methyl-phenyl	2.70±0.45	2.75±0.44	3.62±0.61	3.61±0.61
79	Acetyl-	1.40±0.44	1.56±0.32	2.32±0.42	2.22±0.37
80	Nitro-	1.44±0.41	1.52±0.31	2.40±0.41	2.31±0.34
81	Nitrile-	1.31±0.41	1.36±0.29	2.23±0.39	2.23±0.39
82	Methyl-	1.90±0.40	1.99±0.31	2.88±0.51	2.87±0.51
83	Trifluoromethyl-	2.47±0.46	2.56±0.33	3.34±0.51	3.35±0.50
84	Methoxy-	1.56±0.34	1.54±0.38	2.37±0.40	2.48±0.63

Analysis of Table 4.1 shows that the keto forms have a lower CLogP than the corresponding enol forms for all the examples investigated, predicting a higher aqueous solubility for 4-oxo-quinolines, but also a reduced lipophilicity that can lead to a decrease



in the passage through biological membranes. Thus, the CLogP values exhibited by the 4-hydroxy-quinoline derivatives appear more adequate from a bioavailability viewpoint (higher than 2 and lower than 5).

On the other hand, the presence of the substituent at positions 7 or 5 does not appear to affect significantly the CLogP value, predicting that the pattern of substitution on the carboxylic part of the quinolone structure may not interfere significantly with the pharmacokinetic profile for the range of substituents considered in this work.

## **4.2. Biological activity**

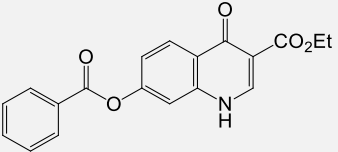
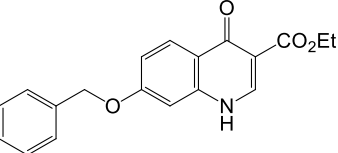
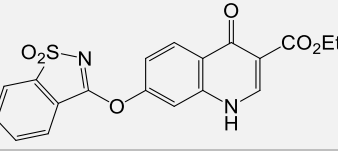
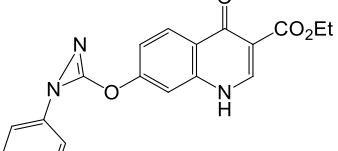
Following Lipinski's rule (Rule of 5), the lipophilicity/solubility of the synthesized quinoline derivatives (expressed by their CLogP values), molecular weight (in  $\text{g mol}^{-1}$ ) and the number of hydrogen-bond donors and acceptors were considered as part of a preliminary test for the drug-likeness of the compounds (see number of violations of Lipinski's rule at column Rof5 violations in Table 4.2). Considering the results, it appears clear that, in general, the quinolones synthesized do not violate the parameters of Lipinski's rule. The exception is compound **45b** that presents a molecular weight higher than 500 g/mol and a CLogP value higher than 5 (2 violations).

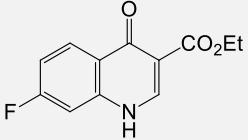
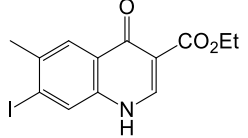
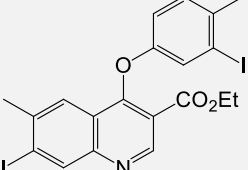
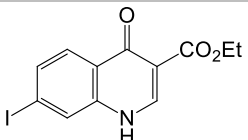
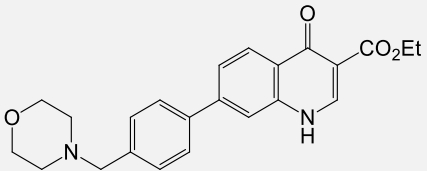
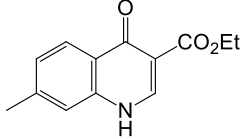
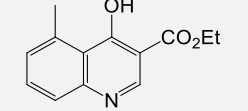
The soluble quinolines were evaluated for their activities against laboratory-adapted chloroquine and mefloquine-resistant *Plasmodium falciparum* Dd2 and/or for 3D7 chloroquine sensitive strains (Table 4.2). Compounds **45a** and **87** demonstrated the best antiplasmodial activities, showing  $\text{IC}_{50}$  values for sensitive strains of 323 nM and 398 nM, respectively. For chloroquine/mefloquine-resistant strains it is noteworthy the  $\text{IC}_{50}$  value of compound **87** (335 nM).

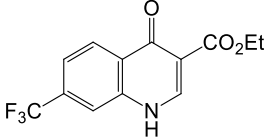
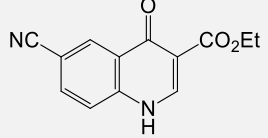
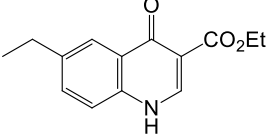
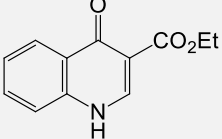
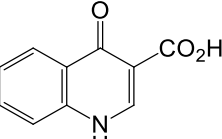
Since compounds **14**, **43**, **46**, **83** and **86** were not soluble in DMSO, they could not be tested against 3D7 and Dd2 strains and their potential as antimalarial drugs could not be evaluated. Also, the poor solubility of some of the quinolones synthesized (for example compounds **31** and **32b**) may have influenced results obtained for biological activities. In the case of quinolone **31** the biological test has failed and it was not possible to obtain an optimal curve to determine an  $\text{IC}_{50}$  value. Compound **32b** was tested in duplicate (contrary to the other compounds in study, which were tested in triplicate) and the results were not coherent, since the biological activity (measured in terms of  $\text{IC}_{50}$  values) of **32b** against 3D7 strain in the first assay was 2.7  $\mu\text{M}$  while in the second one was around 16.2  $\mu\text{M}$ , resulting in the large standard deviation observed for this compound ( $9.476 \pm 9.525 \mu\text{M}$ ).

Quinolones **13** and **60** showed weak activity against the sensitive strain of *Plasmodium* (8.7  $\mu\text{M}$  and 5.4  $\mu\text{M}$ , respectively) and, therefore, these compounds were not tested against the resistant strain Dd2.

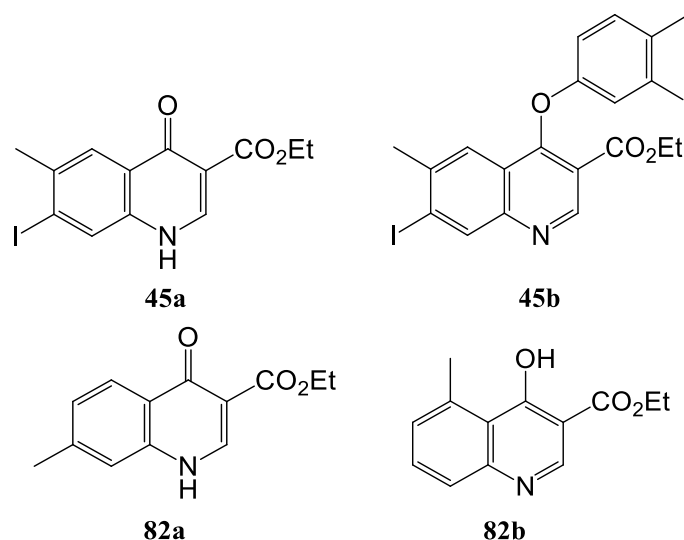
**Table 4.2** – Final step yield, drug-likeness properties (MW, CLogP values, number of hydrogen-bond donors and acceptors atoms in each structure and number of violations to the Rule of 5) and *in vitro* antimalarial activity for chloroquine and mefloquine and for synthesized quinolines. (a) calculated by ALog PS2.1.

Compound	Structural representation	Yield (%)	MW (g/mol)	CLogP <sup>(a)</sup> ± SD	Donors	Acceptors	Rof5 (violations)	Antiplasmodial activity (IC <sub>50</sub> ; μM) Average ± SD	
								3D7	Dd2
<b>Chloroquine</b>	Chloroquine	n.a.	319.87	5.28±0.68	1	3	1	0.023±0.006	0.270±0.071
<b>Mefloquine</b>	Mefloquine	n.a.	378.31	3.10±0.41	2	9	0	0.030±0.012	0.094±0.004
<b>13</b>		73	337.33	2.95±0.39	1	6	0	8.715±1.691	n.d.
<b>14</b>		17	323.34	3.02±0.45	1	5	0	Not soluble	Not soluble
<b>31</b>		48	398.39	2.40±0.67	1	8	0	Poor solubility	n.d.
<b>32b</b>		22	349.34	3.30±0.45	1	7	0	9.476±9.525 (Poor solubility)	n.d.

<b>43</b>		44	235.21	1.69±0.43	1	5	0	Not soluble	Not soluble
<b>45a</b>		62	357.14	2.79±0.37	1	4	0	0.323±0.060	1.013±0.088
<b>45b</b>		12	573.16	6.18±0.79	0	4	2	0.743±0.124	1.553±0.201
<b>46</b>		44	343.12	2.44±0.41	1	4	0	Not soluble	Not soluble
<b>60</b>		13	392.45	2.70±0.45	1	6	0	5.396±1.065	n.d.
<b>82a</b>		12	231.25	1.90±0.40	1	4	0	n.d.	3.034±0.347
<b>82b</b>		22	231.25	2.87±0.51	1	4	0	n.d.	5.891±1.542

<b>83</b>		35	285.22	2.47±0.46	1	7	0	Not soluble	Not soluble
<b>86</b>		18	242.23	1.41±0.39	1	5	0	Not soluble	Not soluble
<b>87</b>		13	245.27	2.33±0.46	1	4	0	0.398±0.155	0.335±0.058
<b>90</b>		31	217.22	1.51±0.40	1	4	0	3.423±0.274	n.d.
<b>91</b>		75	189.17	0.89±0.47	2	4	0	4.844±0.849	n.d.

Considering the results from docking studies performed for 4-oxo-quinoline 3-esters on Q<sub>o</sub> site<sup>120</sup> and the evidence of tautomerism in some cases,<sup>162</sup> it could be expected that the 4-oxo-quinoline 3-ester form, with the N–H and 4-oxo groups involved in important interactions inside the enzyme pocket, presents a much better pharmacological profile as *P. falciparum* bc<sub>1</sub> inhibitor than its 4-hydroxy-quinoline 3-ester tautomer. From the chemical diversity of our library of compounds, we could evaluate and compare the *in vitro* activities of 4-oxo-quinoline and of its derivatives without the N-H and 4-oxo groups (**45a** vs **45b**; and **82a** vs **82b**).



The 4-hydroxy-quinoline **82b** exhibited activity against *P. falciparum* Dd2 at micromolar concentrations, with an IC<sub>50</sub> of 5.891 μM (against Dd2 strain), while its isomer, 4-oxo-quinoline **82a**, showed antiplasmodial Dd2 activity slightly higher than **82b** (IC<sub>50</sub> of 3.034 μM) - Table 4.2. Isomers **82a** and **82b** are not true tautomers. However, since it was not possible to isolate the 4-hydroxy-quinoline of **82a** and the 4-oxo-quinoline of **82b**, we compared the antimalarial activities for these two compounds although they bear the methyl substituent at different positions. The activity results may look somewhat surprising if we consider published results from docking studies: the activity profile of **82b** as inhibitor of the *P. falciparum* bc<sub>1</sub> complex is expected to be less favourable and a bigger difference in its activity was expected, comparing with **82a**.

We could presuppose that the better pharmacodynamic performance of **82a** may be offset by its poor bioavailability, considering the lower value of CLogP for **82a** compared to **82b**. However, we consider that further investigations are required to understand the micromolar activity of **82b**.

Similar results were obtained to **45a** and **45b**. These compounds demonstrated slightly different antimalarial activities against the multiresistant strain Dd2, with IC<sub>50</sub> values of 1.013 μM and 1.553 μM respectively.

In order to test the importance of the ethyl ester group at position 3 of the quinolone core, the ethyl ester of compound **90** was hydrolysed to afford the corresponding carboxylic acid **91**. The antimalarial results support the idea that compounds with an ethyl ester group have slightly increased potency *in vitro* relatively to the analogues with a carboxylic acid at the same position (IC<sub>50</sub> for **90** against 3D7 is around 3.4 μM, while for **91** is around 4.8 μM).

### **4.3. Docking simulations – binding of 4-oxo-quinolines to the Q<sub>i</sub> site of cytochrome *bc*<sub>1</sub> complex**

The Q-cycle requires two distinct binding sites for the reduction of ubiquinone and the oxidation of ubiquinol. Both sites are located within cytochrome *b*: the Q<sub>o</sub> site acts to oxidize ubiquinol near the intermembrane space and the Q<sub>i</sub> site reduces ubiquinone near the mitochondrial matrix.<sup>50</sup>

Atovaquone binds to cytochrome *bc*<sub>1</sub> at the Q<sub>o</sub> site. However, several mutations have been reported, giving rise to atovaquone-resistant strains of *P. falciparum*. These mutations arise in the Q<sub>o</sub> pocket and prevent atovaquone from binding.

Many different classes of compounds have been investigated as potential drugs and much work has focused on the inhibition of the Q<sub>o</sub> site.<sup>85</sup> Among these, selected quinolones have been investigated, in view of finding suitable inhibitors targeting the Q<sub>o</sub> site of *P. falciparum*. Although exhibiting activity at low nanomolar concentrations, some of these compounds have clearly not avoided the issues that resulted in atovaquone resistance, demonstrating some cross resistance with atovaquone. However, when tested in atovaquone resistant strains, only a 92 fold drop in potency was observed, representing a distinct improvement over the 760-fold decrease in potency observed for atovaquone in the same atovaquone-resistant parasite strain. These results may indicate a mode of action different from the intended Q<sub>o</sub> inhibition.<sup>59,120,184</sup>

Also, the results described in the previous section, concerning the antimalarial activity exhibited by the 4-oxo-quinoline/4-hydroxy-quinoline pair, prompted us to hypothesize that the quinolone chemotype may bind to the Q<sub>i</sub> site of the *bc*<sub>1</sub> complex.

Taken together, the evidence exposed above encouraged us to investigate the possibility of drug-target interactions with the Q<sub>i</sub> site of the *bc*<sub>1</sub> complex, using docking studies. An additional stimulus comes from the fact that the Q<sub>i</sub> site of cytochrome *bc*<sub>1</sub> has been far less explored than the Q<sub>o</sub> site in the search for antimalarial compounds and only the binding of a few compounds has been visualized directly.<sup>67,185,186</sup>

The 4(1H)-pyridone chemotype has been optimized for antiplasmodial activity. From this effort, compounds **GW844520** and **GSK932121** (Figure 4.1), produced by GSK, emerged as promising leads, exhibiting excellent antimalarial properties, even against atovaquone-resistant parasites. However, these compounds had to be withdrawn from development due to unexpected toxicity, attributed to cardiotoxicity and possibly due to the inhibition of the mammalian *bc*<sub>1</sub> complex.<sup>55,73,85</sup>



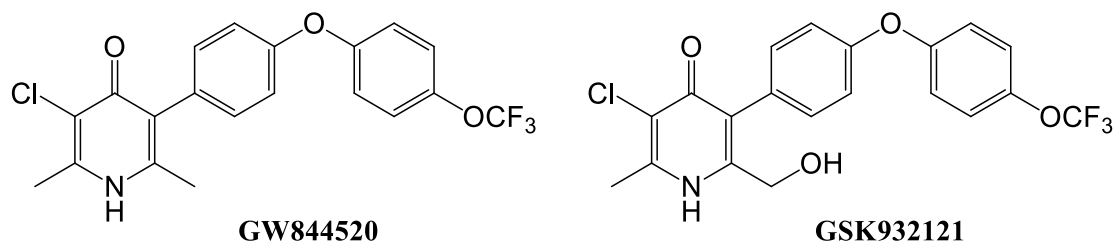


**Figure 4.1** – Representation of the chemical structures of 4(1H)-pyridones **GW844520** and **GSK932121** docked for the  $Q_i$  site of cytochrome  $bc_1$  in a previous study.

Co-crystallization of the cytochrome  $bc_1$  complex with compounds **GSK932121** and **GW844520** revealed that these inhibitors do not bind at the  $Q_o$  site but, instead, bind at the  $Q_i$  site, providing a molecular explanation for the cardiotoxicity and for the ability of this class to overcome parasite  $Q_o$ -based atovaquone resistance.<sup>85,102,103</sup>

In our docking simulations, we will investigate the hypothesis that some of the quinolones from our library bind to the  $Q_i$  site, as observed for the 4(1H)-pyridones.

#### 4.3.1. Software available for protein-ligand docking

Computational chemistry has greatly improved, providing various tools that may be successfully applied in strategies for drug design and optimization. Ligand docking is nowadays a standard method for exploring the way in which small molecules bind to specific sites of proteins or other biological macromolecular targets. It is possible to determine the structures that would lead to optimized interactions (virtual screening) or rationalize the results obtained from random screening of compounds previously synthesized, helping the analysis of structure-activity relationships required to lead optimization.

There are several options of available docking software, including the GOLD (Genetic Optimization for Ligand Docking) suite of programs elected for this study. GOLD performs molecular docking using a genetic algorithm in which the molecules to be docked are modeled and the strength of binding is predicted according to the non-covalent interactions observed between the ligand and the protein.<sup>187–189</sup> Predicted poses are scored (GoldScore) according to factors such as hydrogen bonding and van der Waals energies, ligand strain and steric clashes, to generate a figure intending to show the optimal ligand-protein pose and demonstrating the most probable docking pose for a given protein-ligand complex. The reported pose with the highest GoldScore is considered to be the more favorable pose for the results of that search.<sup>188,190</sup>

All molecular docking simulations conducted in the work described herein were performed using GOLD docking suite version 5.2. A genetic algorithm (GA) using piecewise linear potential (PLP) as the fitness function was used for all docking calculations. Ten independent GA runs were performed for each ligand. Default settings were used, except the “allow early termination” setting, that was turned off.

#### 4.3.2. Protein – Co-crystallized structure of bovine *bc*<sub>1</sub>

Since an atomic structure for *P. falciparum bc*<sub>1</sub> is not available, the compounds selected for this study were modeled *in silico* using the coordinates of the crystal structure of bovine heart cytochrome *bc*<sub>1</sub> protein (Protein Data Bank accession code 4D6U), where the ligand **GSK932121** is bound in the Q<sub>i</sub> site. Using GOLD, this ligand can be removed and other compounds docked into the Q<sub>i</sub> site.<sup>85</sup>

Although not identical to the parasite *bc*<sub>1</sub> complex, the protein sequence alignment of bovine, human and *P. falciparum* cytochrome *b* shows a fairly conserved Q<sub>i</sub> binding site. However, some differences are shown between the mammalian and *Plasmodium* proteins, especially in the N-terminal region of cytochrome *bc*<sub>1</sub> (Figure 4.2).<sup>85</sup>

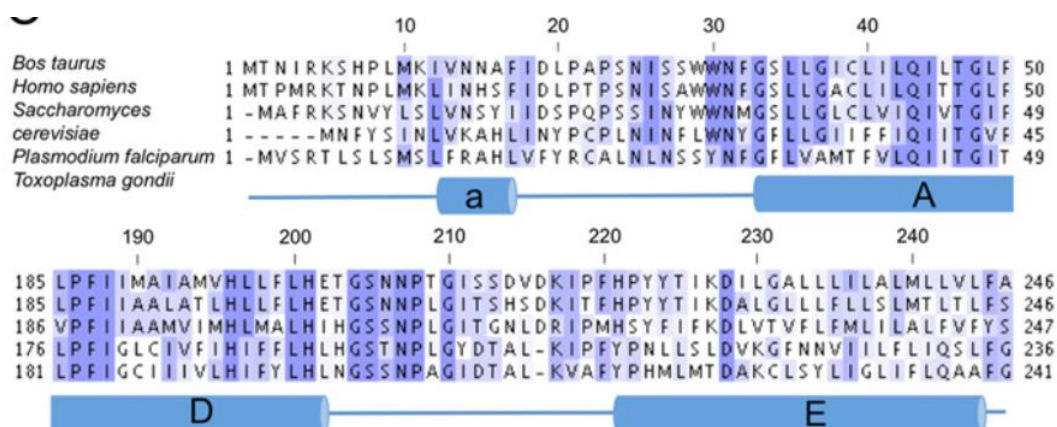


**Figure 4.2** – Representation of protein sequence alignments of bovine (*B. taurus*), human (*H. sapiens*), *S. cerevisiae*, *P. falciparum* and *T. gondii*, showing conservation in the Q<sub>i</sub> binding site. The scale at the top is numbered according to the bovine sequence. Residues fully conserved are colored in deep blue, partially conserved in light blue and unconserved in white.<sup>85</sup>

#### 4.3.3. Binding of pyridone GSK932121 to the Q<sub>i</sub> site of cytochrome *bc*<sub>1</sub>

The binding modes of the antimalarial 4(1H)-pyridones to the Q<sub>i</sub> site of cytochrome *bc*<sub>1</sub> have been previously published (Figure 4.3).<sup>85</sup> The pyridone ring of **GSK932121** is oriented in a way to place the amine of the pyridone and the N of His201 on helix D within bonding range (separated by 3.3 Å). The same study has demonstrated that the carbonyl of this compound was within 3.5 Å of both Ser35 on loop A and Asp228 on loop E, to allow formation of hydrogen bonds. The formation of hydrogen bonds

between several residues and the head group indicates that this pyridone is strongly bound at the Q<sub>i</sub> site.

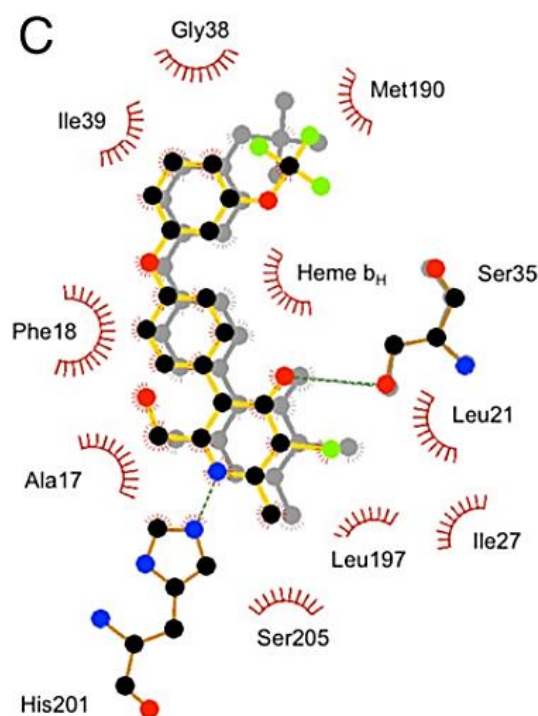


**Figure 4.3** – Representation of interactions between the Q<sub>i</sub> binding site and compounds **GSK932121** (in the foreground) and **GW844520** (in gray, in the rear). Carbons are colored in black, oxygens in red, nitrogens in blue and halogens in green.<sup>85</sup>

Additionally, the trifluoromethyl tail group is positioned between Met190 and Met194. The residues Phe18, Leu21 and Leu197 form a hydrophobic pocket around the aromatic rings of the pyridone tail, while Phe220 forms a stacking interaction with the head group (hydrophobic interactions provide a large part of the binding energy). These stacking interactions may help to fix the pyridone compounds in place, as opposed to the ubiquinone, explaining the increased strength of binding to the pyridones, compared with ubiquinone.

These data indicate that the Q<sub>i</sub> site of the *bc*<sub>1</sub> complex may be a target for a number of ubiquinone-mimicking antimalarials that are not cross-resistant with atovaquone.

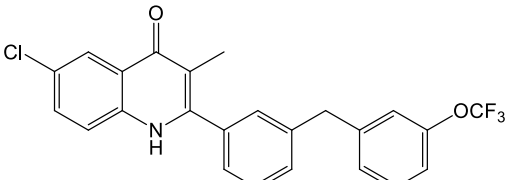
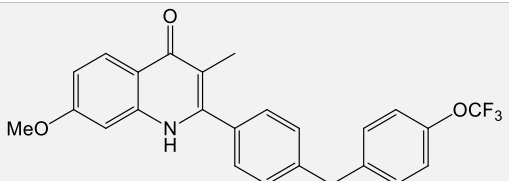
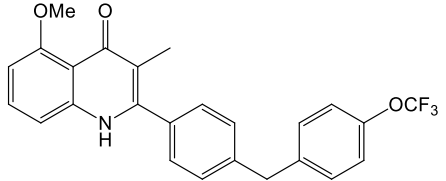
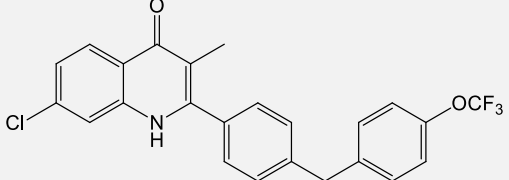
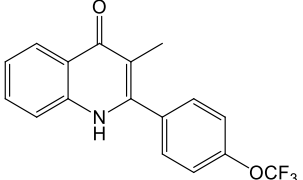
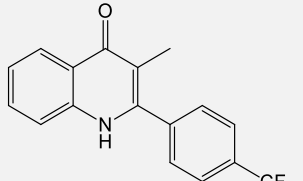
#### 4.3.4. Selection of quinolone ligands

From some papers published by the groups of Roman Manetsch<sup>191</sup> and Paul O'Neill<sup>118</sup> and considering the structure of 3-aryl substituted 4(1H)-pyridones **GSK932121** and **GW844520**, a library of 25 quinolones (compound **93** to **117**) with antimalarial activity was selected for docking studies. This selection includes aryl substitution at positions 2 or 3 of the quinolone core (Table 4.3 and Table 4.4, respectively)

and, for each group, compounds with IC<sub>50</sub> values ranging from 1nM to more than 1μM are included.

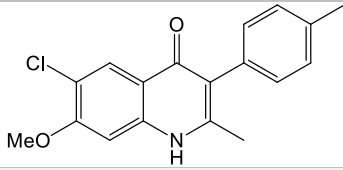
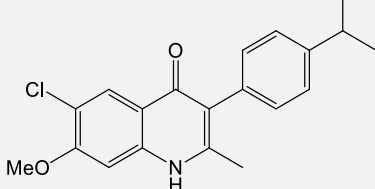
**Table 4.3** – Structural representations of 2-aryl substituted quinolones selected for docking and corresponding *in vitro* activities against the *P. falciparum* strains 3D7 and C2B.

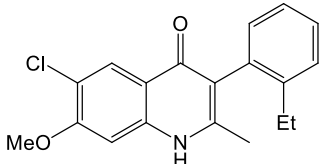
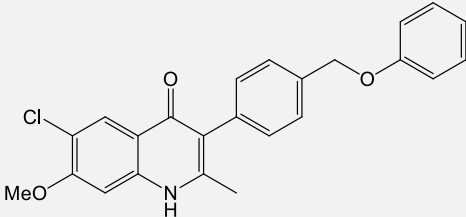
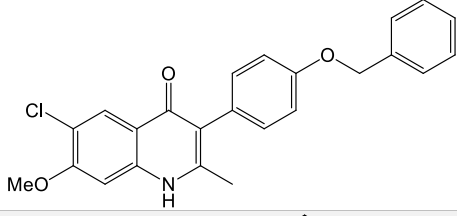
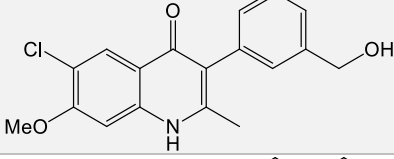
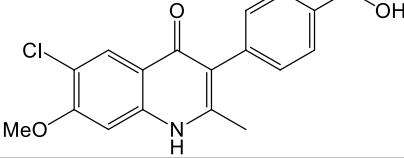
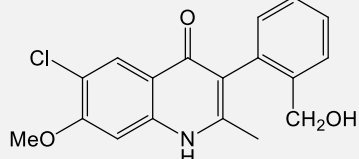
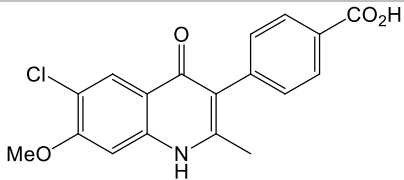
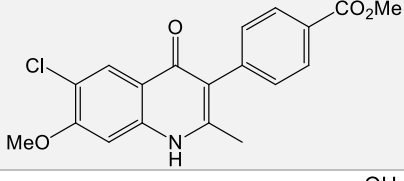
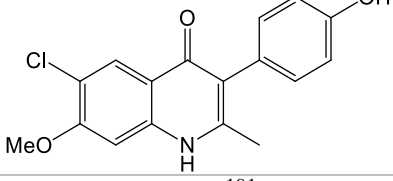
Compound	Structural representation	Antiplasmodial activity (IC <sub>50</sub> ; nM) <sup>a</sup>	
		3D7	C2B
93		26	92
94		73	274
95		212	n.d.
96		408	n.d.
97		465	n.d.
98		139	n.d.
99		105	552
100		24	n.d.

101		8.4	31
102		8	n.d.
103		664	n.d.
104		36	178
105		+1000	n.d.
106		752	n.d.

<sup>a</sup> Values extracted from the literature.<sup>118</sup>

**Table 4.4** - Structural representations of 3-aryl substituted quinolones selected for docking and corresponding *in vitro* activities against the *P. falciparum* strains W2 and C2B.

Compound	Structural representation	Antiplasmodial activity (IC <sub>50</sub> ; nM) <sup>a</sup>	
		W2	C2B
107		24.5	7.33
108		6.65	2.67

109		61.7	160
110		1.30	0.638
111		10.6	1.28
112		5400	829
113		154	93.9
114		258	277
115		517	73.1
116		777	48.4
117		2860	467

<sup>a</sup> Values extracted from the literature.<sup>191</sup>

The minimum energy structures of ligands were determined using Merck molecular force field (MMFF) 94, within the SPARTAN '08.<sup>192</sup> The files were then

uploaded to the GOLD protein-ligand docking suite and docked into the Q<sub>i</sub> site using the protein configuration previously described (where compound **GSK932121** was docked). For each ligand docked, 10 independent results of GoldScore and distinct poses were registered, for visual comparison and analysis.

#### **4.3.5. Docking of selected compounds – GoldScore vs IC<sub>50</sub> correlation**

From the docking results obtained for 2-aryl (Table 4.5) and 3-aryl substituted (Table 4.6) quinolones it is possible to conclude that the 2-aryl substituted compounds exhibit a higher GoldScore range (64.4-80.8) than their 3-aryl substituted counterparts (53.5-67.8). However, these results only describe the predicted strengths of interaction between the protein and the compound for a given docking pose, not accounting for many other factors that influence the activity of the compounds, such as membrane permeability, solubility or plasma half-life. These factors must also be considered when predicting how efficacious a compound is. Furthermore, in the docking simulation the receptor model of the protein is a rigid system with the amino acid fixed in the crystallized position, while in a biological setting the protein is a flexible structure that can adapt to its environment.<sup>188,189,192,193</sup> Thus, although important, results from docking must be cautiously interpreted and, for the present case, one cannot assume that 2-aryl substituted quinolones are more antimalarially active than their 3-aryl substituted analogues on the sole basis of results from docking simulations.

**Table 4.5** – GoldScore results obtained from the docking of 2-aryl substituted quinolones to the Q<sub>i</sub> site of *P. falciparum* bc<sub>1</sub> complex.

Ligand	GoldScore		
	Highest	Average ± SD	GS/nonH
<b>93</b>	79,9	71,8 ± 6,5	2,052569
<b>94</b>	78,6	77,9 ± 0,6	2,513118
<b>95</b>	75,8	67,9 ± 4,8	1,995819
<b>96</b>	70,7	69,2 ± 0,9	2,036004
<b>97</b>	75,3	73,5 ± 1,2	2,371305
<b>98</b>	76,7	75,0 ± 0,7	2,418851
<b>99</b>	78,9	77,8 ± 0,8	2,881419
<b>100</b>	82,5	79,5 ± 1,6	2,483531
<b>101</b>	82,7	80,3 ± 2,1	2,589522
<b>102</b>	80,1	79,0 ± 0,6	2,469841
<b>103</b>	83,5	80,8 ± 2,0	2,524687
<b>104</b>	78,7	77,1 ± 1,3	2,486014
<b>105</b>	65,5	64,4 ± 0,7	2,801977
<b>106</b>	65,2	64,8 ± 0,4	2,945663

**Table 4.6** – GoldScore results obtained from the docking of 3-aryl substituted quinolones to the Q<sub>i</sub> site of *P. falciparum* bc<sub>1</sub> complex.

Ligand	GoldScore		
	Highest	Average ± SD	GS/nonH
<b>107</b>	55,2	53,7 ± 0,8	2,441261
<b>108</b>	59,8	57,9 ± 1,8	2,412066
<b>109</b>	57,5	55,1 ± 1,8	2,396792
<b>110</b>	71,6	67,8 ± 1,7	2,336793
<b>111</b>	70,4	66,5 ± 1,8	2,291618
<b>112</b>	59,4	58,6 ± 0,6	2,548302
<b>113</b>	59,9	57,7 ± 1,6	2,507608
<b>114</b>	60,9	58,9 ± 2,0	2,563028
<b>115</b>	57,3	56,0 ± 0,7	2,334175
<b>116</b>	58,7	56,7 ± 1,4	2,364318
<b>117</b>	57,1	53,5 ± 1,3	2,430855

In an attempt to examine if there is a correlation between GoldScore and antimalarial activity (expressed as IC<sub>50</sub>) for the 2 sets of compounds, the values of log (1/IC<sub>50</sub>) were plotted against the GoldScore average or against a parameter that considers



the molecular size (GS/nonH – division of GoldScore by the number of non-hydrogen atoms). When considering the molecular size (GS/nonH), for 2- and 3-aryl substituted derivatives, and the GoldScore average for 3-aryl substituted derivatives (Chart 4.1), the correlation with the antimalarial activities were somewhat deviated from linearity. However, some correlation between the GoldScore average and  $\log(1/IC_{50})$  values for the 2-aryl series could be observed (Chart 4.2), when considering the antimalarial activities against the 3D7 strain.

**Chart 4.1** - Correlation between the GoldScore average and  $\log(1/IC_{50})$ , for 3-aryl substituted ligands selected, considering their antimalarial activities against the 3D7 strain. See Table 4.4, for structures and corresponding activities, and Table 4.6, for GoldScore average values.

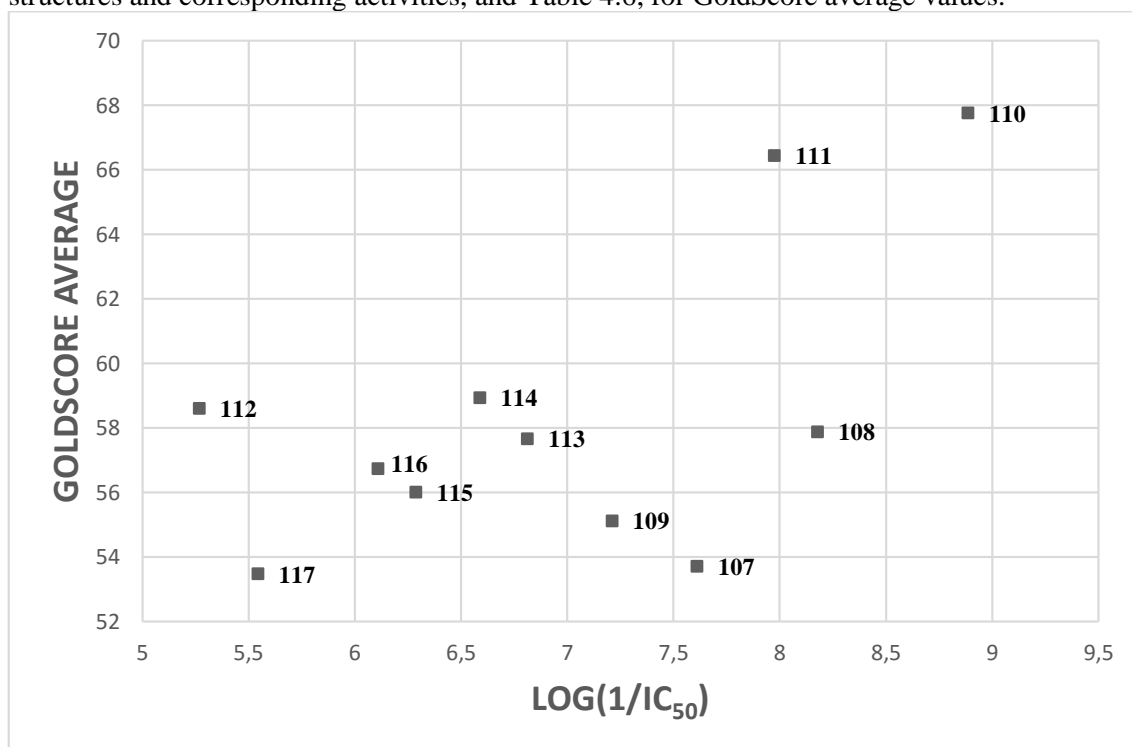
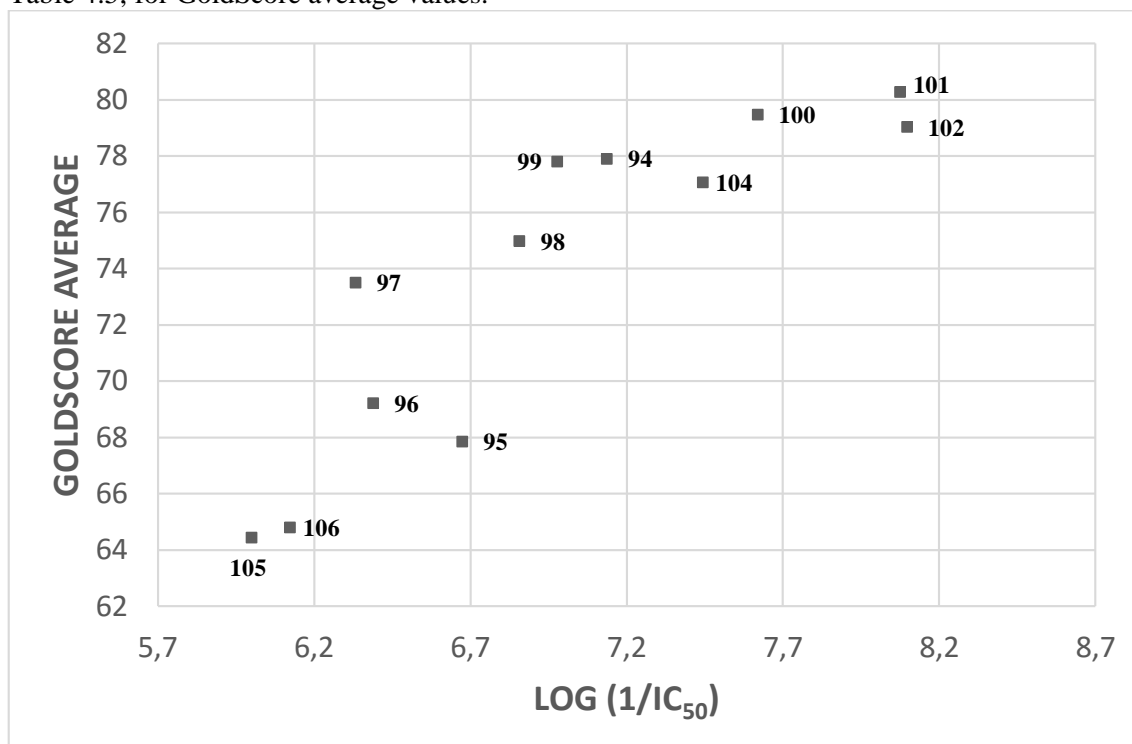


**Chart 4.2** - Correlation between the GoldScore average and  $\log(1/IC_{50})$ , for 2-aryl substituted ligands selected, considering the antimalarial activities against the 3D7 strain.  $R^2 = 0.7668$ . Compound **103** was not included, as it is an outlier and it is the only compound of the 2-aryl series with a methoxy group at position 5. See Table 4.3, for structures and corresponding activities, and Table 4.5, for GoldScore average values.



These evidence of possible or no correlation between the GoldScore and the antimalarial activity has to be interpreted taking in consideration that the GoldScore only gives indication of the predicted strength of protein-ligand interaction (pharmacodynamics), not taking in account other variables adjacent to the pharmacological activity and also the possibility of multiple-targets which give the phenotypic readout.<sup>188,189,192,193</sup>

#### 4.3.6. Docking pose of selected quinolones in the Q<sub>i</sub> site

Compound **110** exhibited the highest *in vitro* activities against W2 and C2B strains of *P. falciparum* and has also shown the highest GoldScore average among selected members of the 3-aryl series. Therefore, **110** can be considered of most importance with regard to modeling interpretation. However, comparison of the docking poses results shows that other 3-aryl substituted compounds studied in this project exhibit similar results, with the key structural features located in the similar positions for all ligands docked. The differences are only observed in their precise alignment with the protein residues, orientating the compounds such that the quinolone “head” and the phenyl ring of the tail are in a similar position along the series (Figure 4.4).

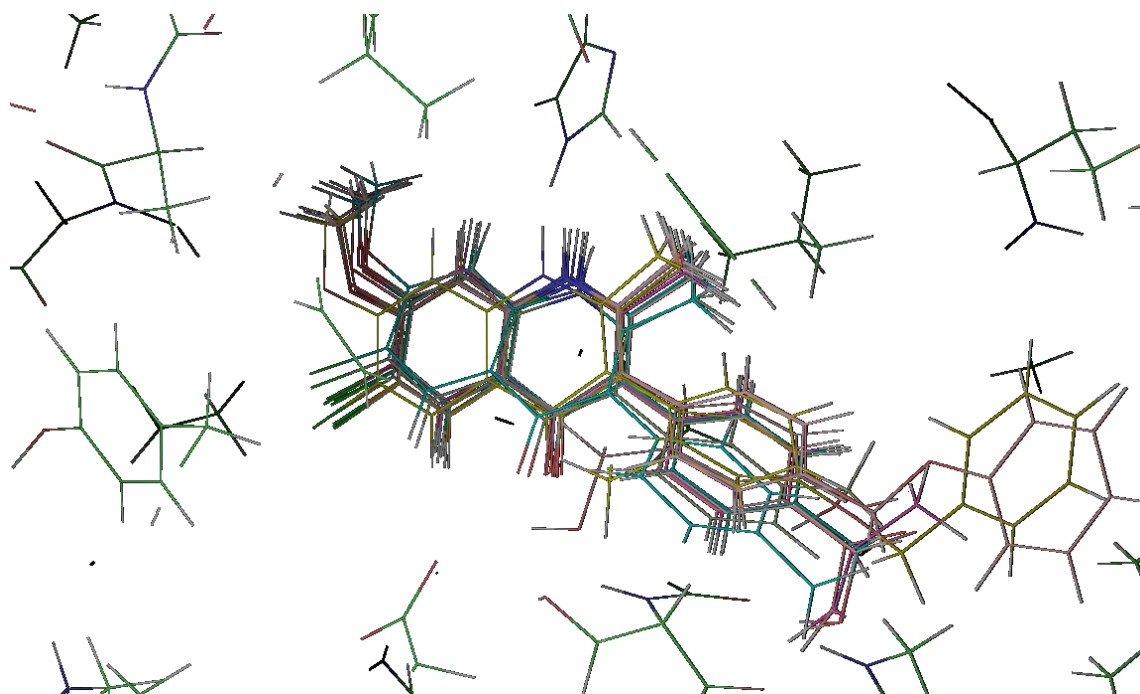


**Figure 4.4** - Image of the  $Q_i$  site showing the highest scoring docking pose for each of the 3-aryl substituted compounds studied.

The GoldScore results for **110** across the 10 distinct docking poses vary by less than 6 units (Table 4.7) and this compound is orientated in a similar manner to the reference ligand (**GSK932121**) in the  $Q_i$  binding pocket.<sup>85</sup> Between all the 10 distinct docking poses of **110**, only small differences are visible in the position assumed by the aryl tail in position 3 (related to a slow alignment with the protein residues).

**Table 4.7** – Results for docking of **110** in the  $Q_i$  site, expressed as GoldScore.

Docking pose	1	2	3	4	5	6	7	8	9	10
GoldScore	65,9	65,9	67,1	68,9	71,6	67,0	66,3	69,1	67,5	69,1

The orientation of the quinolone core of **110** promotes the formation of key hydrogen-bonds between the inhibitor and the amino acids Asp228/Ser205 and His201 (Figure 4.5). The quinolone N1 forms a hydrogen bond with the Nε2 of His201 and the two atoms are separated by 2.4Å, while Ser205 and Asp228 on helix E are 2.7Å and 3.3Å, respectively, apart from the carbonyl group, allowing formation of hydrogen bonds. Phe220 appears to form a stacking interaction with the aromatic quinolone core, while residues Phe18, Leu21, Leu197, Ile42, Leu41, Met190 and Met194 form a tight hydrophobic pocket around the aromatic rings of the quinolone tail (Figure 4.5), suggesting that these hydrophobic interactions provide a contribution to the binding

energy. A stacking interaction between the phenyl rings of the tail and Phe18 can also be perceived, which may help to fix the quinolone 3-aryl substituted compounds in place.

The same residues were also found to interact directly with the head of the reference ligands **GSK932121** and **GW844520**, with antimycin (compound known to bind to the  $Q_i$  site) and with ubiquinone (natural substrate of  $Q_i$  site), which lie in a similar position deep within this cavity.<sup>67,85,185,186</sup> Considering that the stacking interaction described between Phe18 and the tail of our compound was not seen in ubiquinone-bound structures,<sup>67</sup> due to the absence of an aryl substituent in this natural substrate, it may be postulated that this difference contributes to an increased strength of binding in the quinolones compared with ubiquinone.

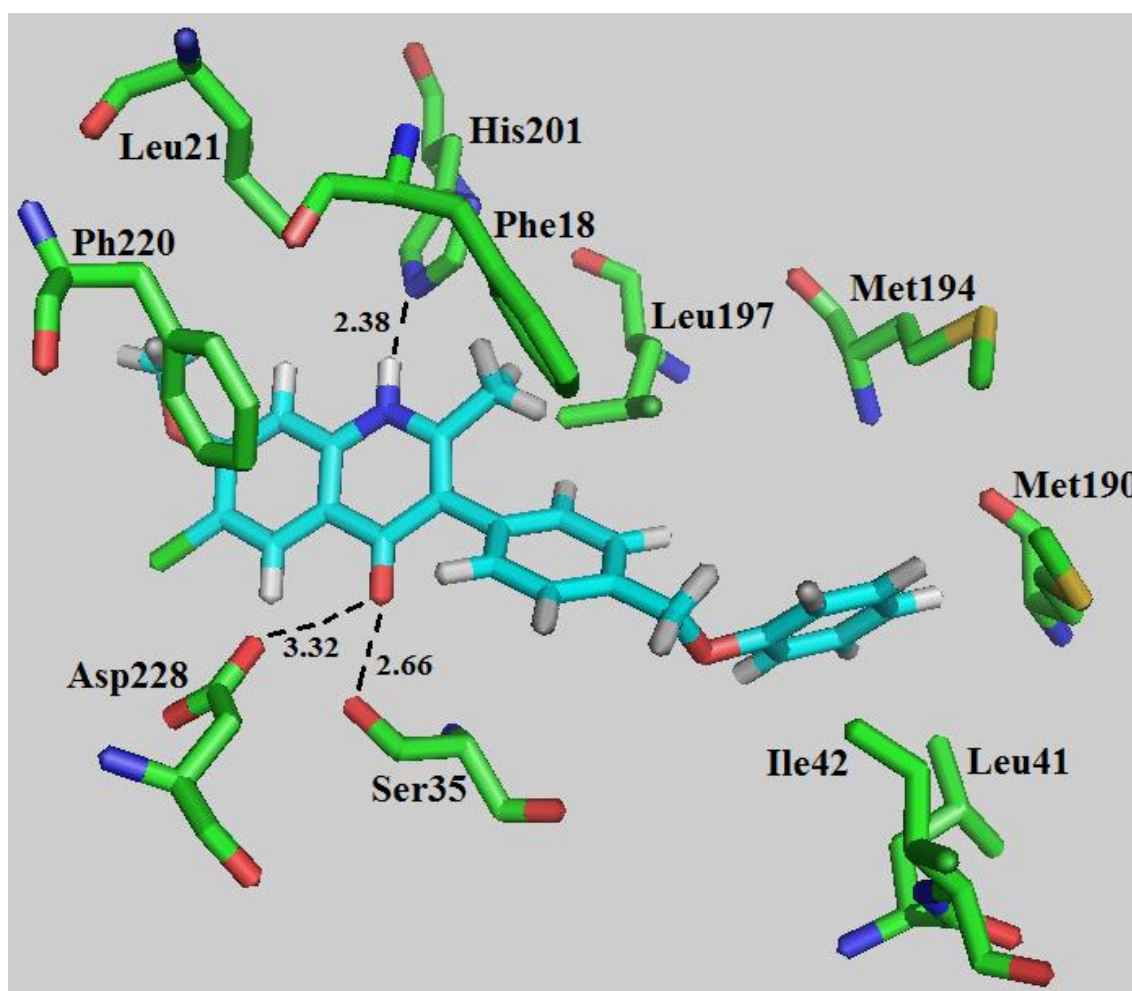


**Figure 4.5** – Image representing the  $Q_i$  site interactions with the quinolone core of compound **110**. The key protein residues are highlighted and the potential H-bond interactions indicated in black. H-bond lengths indicated are expressed in Å. Molecules are rendered as sticks colored by atom type (ligand structure, cyan; hydrogens, white; protein residues, green; oxygens, red; nitrogens, blue; and sulphurs, yellow).

Among the compounds of the 2-aryl series selected, compound **102** exhibited the highest *in vitro* activity against 3D7 strain and also one of the highest GoldScore values.

Results across the 10 distinct docking poses for **102** vary by less than 3 units (Table 4.8). The other 2-aryl substituted compounds studied in this project have shown similar results, *i.e.* similar positions for protein-interactions, with only minor deviations.

**Table 4.8** – Results for docking of **102** in the Q<sub>i</sub> site, expressed as GoldScore.

Docking pose	1	2	3	4	5	6	7	8	9	10
GoldScore	79,1	79,1	78,3	79,6	78,0	80,1	79,4	79,2	78,5	79,1

When comparing the orientation of the 2-aryl substituted quinolones with that exhibited by the 3-aryl substituted analogues and the reference ligand **GSK932121**,<sup>85</sup> an inversion of the quinolone core in the Q<sub>i</sub> binding pocket is easily perceived. This inversion of the quinolone core in the 2-aryl substituted quinolones may enable an increase in strength of interaction between the protein and the compound for a given docking pose, and may explain the higher GoldScore results observed, compared to the 3-aryl series (64.4-80.8 for the 2-aryl series vs 53.5-67.8 for the 3-aryl series).

For the 3-aryl substituted quinolones, the quinolone core promotes the formation of hydrogen bonds between quinolone-N1 and His201 and also between the C4 carbonyl oxygen and Ser205/Asp228. However, for example for **102** it is possible to observe that the quinolone-N1 hydrogen binds to Ser205 and Asp228 on helix E, with donor and acceptor separated by 2.1Å and 2.3Å, respectively, while the C4 carbonyl oxygen interacts with the Ne2 of His201, with donor and acceptor separated by 3.0Å (Figure 4.6).

Between all the 10 distinct docking poses of **102**, only minor differences are perceived in the position of the 2-aryl tail (related to a slow alignment with the protein residues). The aromatic rings of the quinolone tail may force the inversion of the quinolone core, to keep the interactions between the ligand and the hydrophobic pocket. Considering that **102** bears an aromatic tail at the position 2, inversion of the quinolone core places the aromatic ring in position for optimized stacking interaction with Phe18, while favoring other hydrophobic interactions with the residues Leu21, Leu197, Ile42, Leu41, Met190 and Met194 that form a hydrophobic pocket around the aromatic rings of the quinolone tail (Figure 4.6). These interactions between the tail and the hydrophobic channel can also be observed for the reference ligand **GSK932121**.<sup>85</sup>

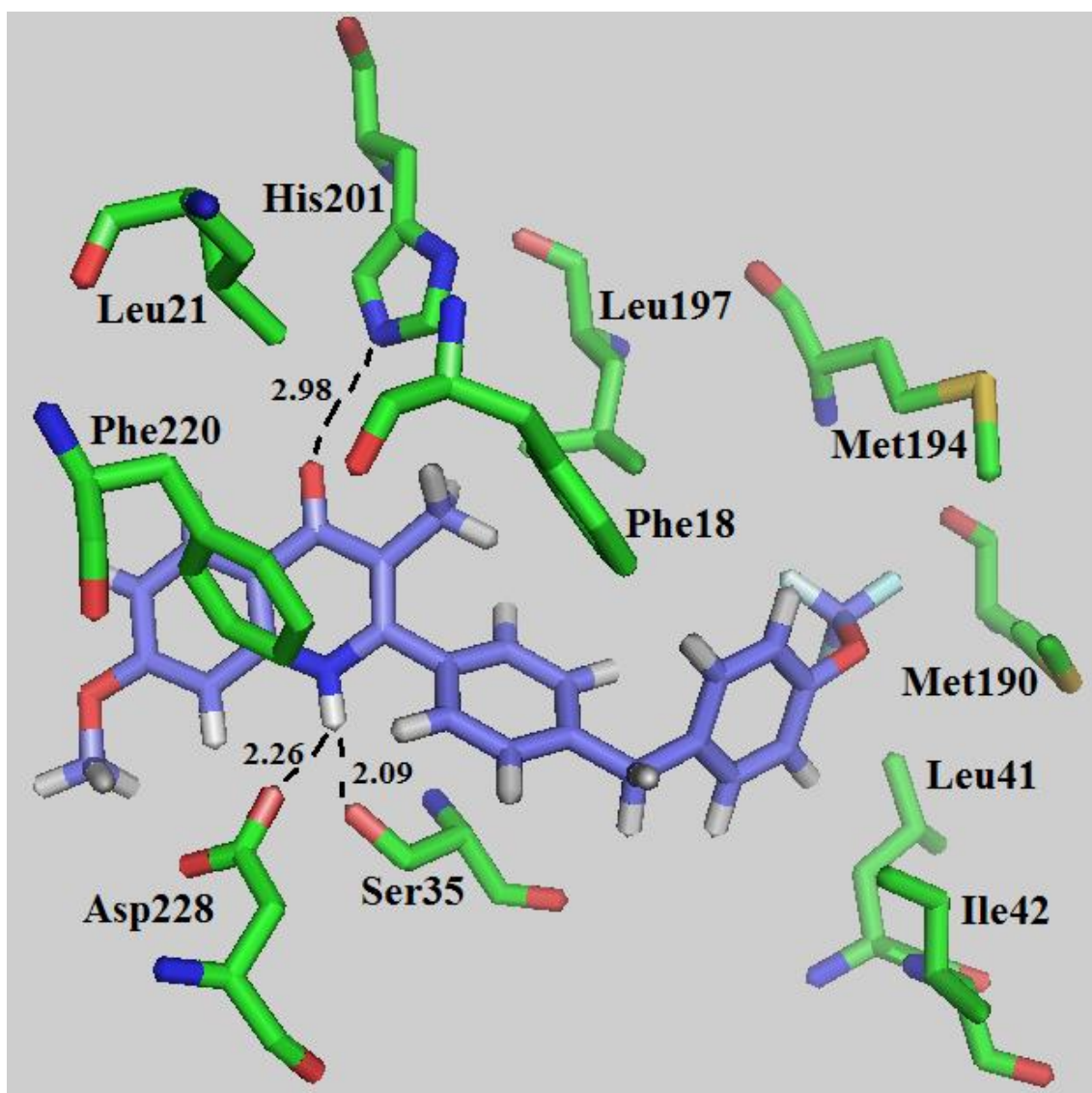


**Figure 4.6** - Image representing the  $Q_i$  site interactions with the quinolone core of compound **102**. The key protein residues are highlighted and the potential H-bond interactions indicated in black. H-bond lengths indicated are expressed in Å. Molecules are rendered as sticks colored by atom type (ligand structure, lilac; hydrogens, white; protein residues, green; oxygens, red; nitrogens, blue; and sulphurs, yellow).

Also, as evidenced for compounds of the 3-aryl series, **GSK932121**, **GW844520**, antimycin and ubiquinone,<sup>67,85,185,186</sup> in the 2-aryl series Phe220 appears to form a stacking interaction with the aromatic core, suggesting that the hydrophobic interactions contribute substantially to the binding energy.

From these docking results, it may be extracted that the residues that intervene in the binding ligand-protein and that are non-conserved (Phe18, Leu21 and Leu197) are from the hydrophobic pocket around the aromatic tail of the quinolones in study (these are replaced with Leu, Tyr and Ile, respectively, in *P. falciparum*). The residues involved in interactions with the quinolone core, by hydrogen bonds and by stacking (His201,

Asp228, Ser205 and Phe220), are mainly conserved across cytochrome *b* sequences.<sup>85</sup> The differences observed between the bovine heart *bc*<sub>1</sub> and the *P. falciparum* *bc*<sub>1</sub> sequences also may contribute to the observed fragility in the correlations between GoldScore and IC<sub>50</sub> values.

Along with the docking simulations carried out for 2- and 3-aryl substituted quinolone derivatives, ten independent GA runs were performed for atovaquone binding at the Q<sub>i</sub> site. However, atovaquone did not produce consistent docking poses at the Q<sub>i</sub> site. No similarities were observed when overlapping the figure pose for all the 10 runs. These results are consistent with some previous studies reported<sup>85</sup> and support the idea that atovaquone binds to the Q<sub>o</sub>, not binding to Q<sub>i</sub> site and, consequently, not overcoming the phenomenon of parasite resistance associated to Q<sub>o</sub>-mutations.

#### **4.4. Summary, conclusions and future work**

It is generally accepted that changes in the structure of compounds (for example by tautomeric and conformational preferences) may translate in changes of chemical and physical properties (like solubility). In drugs, those changes may impact on the pharmacokinetic and pharmacodynamic profiles.

For the range of 4-oxo-quinoline 3-esters prepared in this work, the possibility of keto-enol tautomerism and the different patterns of aromatic substitution obtained during the synthesis of quinolone derivatives, led us to calculate the ClogP values as an estimation of solubility. Results indicate that the pattern of substitution on the quinoline core structure (substituent at position 7 or 5) does not appear to alter the ClogP values (thus, possibly with a minor impact on the pharmacokinetic profile). However, regarding tautomerism, the differences are substantial, with the 4-hydroxy-quinoline derivatives demonstrating CLogP values that appear more adequate from a bioavailability viewpoint. In fact, the keto forms have a consistently lower CLogP than their enol isomers, predicting a higher aqueous solubility for 4-oxo-quinolines, but also have a lower lipophilicity that can translate in a decrease in the passage through biological membranes.

On the side of pharmacodynamics, the 4-oxo-quinoline 3-ester forms were expected to present a much better pharmacological profile as *P. falciparum*  $bc_1$  inhibitors than their 4-hydroxy-quinoline 3-ester isomers, with the N-H and 4-oxo groups involved in important interactions inside the enzyme pocket. However, the 4-oxo-quinoline derivatives studied have shown to be only slightly more active than their 4-hydroxy-quinoline isomers.

Then, we may conclude that the better pharmacodynamic performance of quinolone derivatives may be offset by their poorer bioavailability (considering the lower value of CLogP). Alternatively, it may be postulated that 4-hydroxy-quinoline 3-esters bind differently to the same site ( $Q_o$ ) or switch to the  $Q_i$  site of the  $bc_1$  complex.

Other factors supporting the hypothesis of binding to  $Q_i$  site are the capacity exhibited by selected quinolone derivatives to partially overcome the atovaquone resistance (no cross-resistance observed) and the evidence that 4(1H)-pyridones bind to this site.

The docking studies performed in this project demonstrated that the 2-aryl and 3-aryl selected compounds can bind at the  $Q_i$  site, as observed for 4(1H)-pyridones, which may explain the ability of some of them overcome parasite  $Q_o$ -based atovaquone



resistance. Results indicate that the 2-aryl and 3-aryl substituted compounds occupy similar positions in the protein-site, keeping the hydrophobic interactions. The quinolone core establishes key H-bonding interactions with the residues His201, Ser205 and Asp228 and these are conserved along the range of compounds studied.

However, attempts to establish a correlation between GoldScore results and observed antimalarial activities did not yield good results, probably due to the following reasons: GoldScore data reflects the mode and strength of ligand-protein interactions; the study only considered one target (the compounds studied may bind to Q<sub>i</sub> and Q<sub>o</sub>); the docking results do not account for many conditions influencing the activity of the compounds (such as membrane permeability or solubility); the receptor model of the protein is a rigid system with the amino acid residues fixed in a crystallized position (while in a biological setting the protein is a flexible structure that can adapt to its environment); and there are differences between the bovine heart *bc*<sub>1</sub> (protein used for this study) and the *P. falciparum* *bc*<sub>1</sub>, especially in the hydrophobic pocket. Compounds of the 2-aryl series demonstrated higher GoldScore results (64.4-80.8) than those of the 3-aryl series (53.5-67.8), indicating a stronger interaction between the protein and the compound at the Q<sub>i</sub> pocket. However, this may not mean that the 2-aryl substituted compounds tested are more active as antimalarial agents than their 3-aryl analogues.

Future work should be performed to optimize a homology model of *P. falciparum* *bc*<sub>1</sub> (Q<sub>i</sub> site) and the inhibition may be evaluated directly in the complex (not only accounting the *in vivo* antimalarial activity in specific strains) to provide a better correlation between the GoldScore and the IC<sub>50</sub>. Considering the cardiotoxicity revealed for 4(1H)-pyridones and the possibility that some of the quinolone derivatives tested bind to the same site pocket, additional studies regarding the cardiotoxicity of these compounds should be performed.

## 4.5. Experimental

### CLogP calculations

CLogP calculations were performed using ALog PS2.1, available in <http://www.vcclab.org/lab/alogps/>.

### Biological activity

Laboratory-adapted chloroquine and mefloquine-resistant *Plasmodium falciparum* Dd2 and chloroquine sensitive *P. falciparum* 3D7 were continuously cultured. Staging and parasitaemia were determined by light microscopy of Giemsa-stained thin blood smears. Antimalarial activity of the compounds was determined using the SYBR Green I assay with modifications. Briefly, early ring stage parasites (> 90% of rings, 3% haematocrit and 1% parasitaemia) were tested in triplicate in a 96-well plate and incubated with the compounds for 48h (37 °C, 5% CO<sub>2</sub>), parasite growth was assessed with SYBR Green I. Each compound was tested at concentrations ranging from 10-0.002 µM. Fluorescence intensity was measured with a multi-mode microplate reader (Dynex Triad, Alfacene), with excitation and emission wavelengths of 485 and 535 nm, respectively, and analysed by nonlinear regression using GraphPad Prism 5 demo version to determine IC<sub>50</sub>.

### Docking simulations

Compounds for docking simulations were selected from published papers by the groups of Roman Manetsch<sup>191</sup> and Paul O'Neill<sup>118</sup>. The structures were built in ChemDraw and the three-dimensional minimum energy structures were created via energy minimization using the Merck molecular force field (MMFF) 94, within the SPARTAN '08.<sup>192</sup>

Each compound was modelled *in silico* using the crystal structure of bovine heart cytochrome *bc*<sub>1</sub> protein (Protein Data Bank accession code 4D6U). The structure of **GSK932121**, bound in the Q<sub>i</sub> site of protein 4D6U, was removed using GOLD and the compound in study was then docked.

All molecular docking experiments were performed by GOLD docking suite version 5.2 using piecewise linear potential (PLP) as the fitness function. Ten independent GA runs were performed for each ligand. Default settings were used, except the “allow early termination” setting (in the “fitness and search option”) that was “turned off”.

---

# ***CHAPTER FIVE***

---

## **RESULTS AND DISCUSSION**

**Synthesis of selected quinolone  
derivatives and evaluation of activity  
against *M. tuberculosis***



## 5.1. Tuberculosis and malaria co-infection

Tuberculosis (TB) and some parasitic diseases in humans, such as malaria, exhibit an extensive distribution and are endemic in many regions of the world, especially in developing countries, and the co-infection with the two pathogens is common. Some studies have showed that the immune response in the co-infection situation is modified, resulting in increased complexity of control and prevention of tuberculosis and of malaria.<sup>194,195</sup>

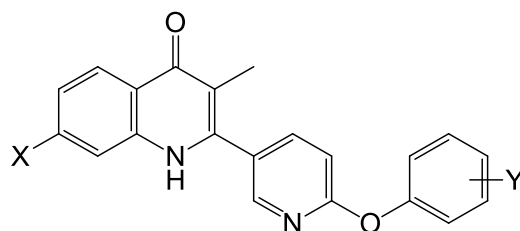
TB is an infectious bacterial disease caused by *Mycobacterium tuberculosis* that most commonly affects the lungs causing cough (sometimes with sputum or blood), chest pain, weakness, weight loss, fever and night sweats. Despite available treatments for this disease, the tuberculosis treatment is a global health problem since the pathogen agent has demonstrated an increased prevalence of multi and extensive drug-resistant strains (MDR and XDR, respectively). The resistance phenomenon may result, mostly, from the misuse of current antituberculosis chemotherapeutic regimens. These involve the use of combinations of, at least, three different drugs, must be taken for six months or longer and possess some characteristic side effects. So, the development of new and effective antimycobacterial agents, able to shorten the treatment duration and to treat MDR and XDR tuberculosis infections, is a priority.<sup>117,196</sup>

Over the past years, several subclasses of quinoline derivatives, incorporating various substituents in the structure of the quinoline core, have demonstrated diverse bioactivities, including high activity against bacterial pathogens. Among these studies, one publication on some quinolone derivatives as promising scaffolds for the development of new antituberculosis agents came to light<sup>117</sup> encouraging us to explore further the quinolone chemotype in the context of TB chemotherapeutics.

Thus, in parallel to the study of quinolone 3-esters directed to the plasmodial cytochrome *bc*<sub>1</sub> of *P. falciparum*, the author of this thesis was involved in a research project, in cooperation with members of the O'Neill research group, directed to the synthesis of a small library of quinolones with potential activity against *M. tuberculosis*, acting as inhibitors of the mitochondrial electron transport chain of this bacillus.

## 5.2. Quinolones with potential antituberculosis activity

Based in the structure of previously synthesized quinolones targeting the therapeutic target *Pf*NDH<sub>2</sub><sup>118,119</sup>, a similar template structure was considered and the synthetic routes were adapted for the synthesis of compound **128**.



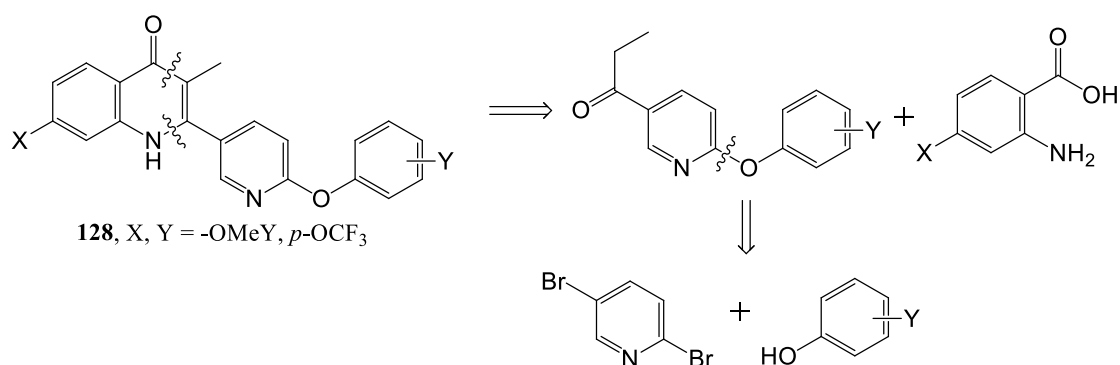
**128**, X, Y = -OMeY, *p*-OCF<sub>3</sub>

Some results of this investigation were included in a publication submitted to Journal of Medicinal Chemistry:

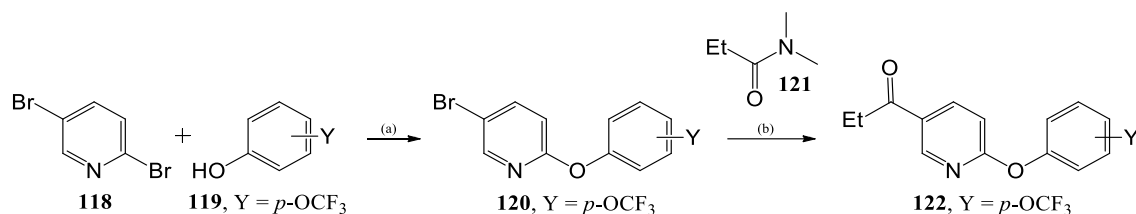
Nixon, G. L.; Gibbons, P. D.; Leung, S. C.; Hong, W. D.; Amewu, R.; Stocks, P. A.; Stachulski, A.; Horta, P.; Cristiano, M. L. S.; Shone, A. E.; Moss, D.; Ardrey, A.; Sharma, R.; Warman, A. J.; Bedingfield, P.; Fisher, N. E.; Aljayyousi, G.; Mead, S.; Caws, M.; Berry, N. G.; Ward, S. A.; Biagini, G. A.; O'Neill, P. M.: "Rational design, synthesis and biological evaluation of heterocyclic quinolones; targeting the respiratory chain of *Mycobacterium Tuberculosis*", April (2016).

### 5.2.1. Synthesis of quinolone **128** and of its prodrug **129**

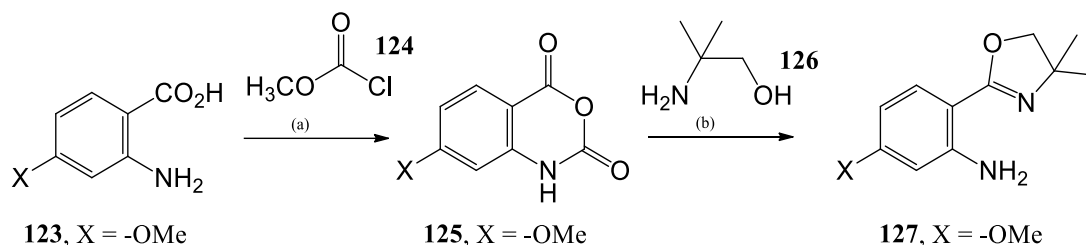
The proposed retrosynthetic approach to quinolone **128** is depicted in Scheme 5.1. Considering a convergent synthesis, the preparation of the two main blocks, ketone **122** (Scheme 5.2) and oxazoline derivative **127** (Scheme 5.3), was undertaken. Thereafter, these two blocks were coupled through a cyclisation reaction, to afford the desired quinolone scaffold **128** (Scheme 5.4). The versatility of the starting materials enable the possibility to incorporate different functionalities (Y and X), allowing for the synthesis of several other quinolone derivatives, based on structure **128**.



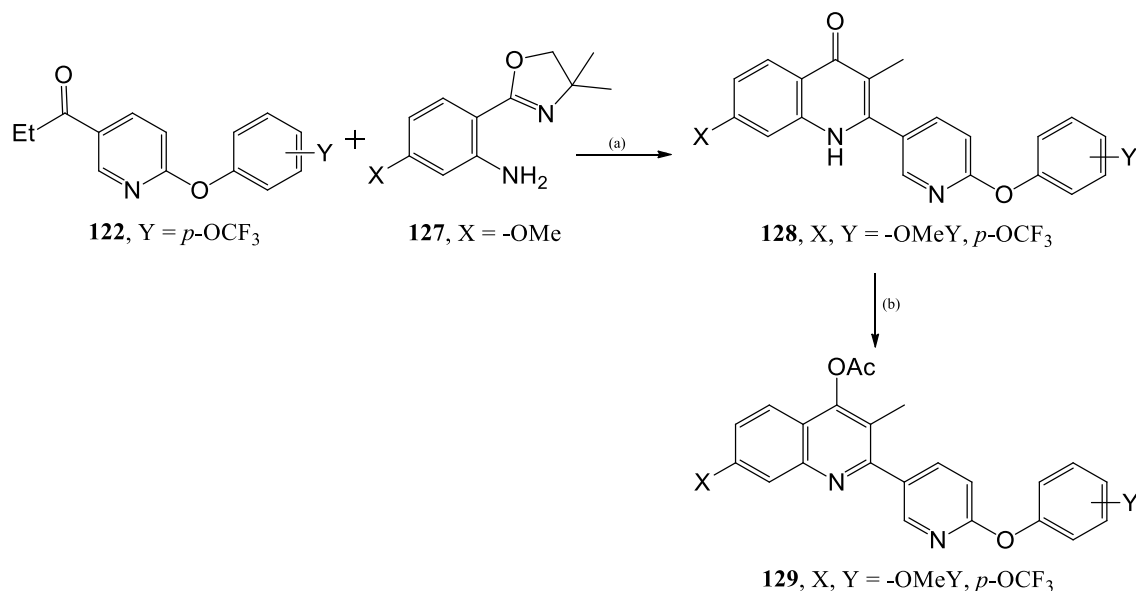
**Scheme 5.1** – Retrosynthetic analysis of quinolone derivative **128**.



**Scheme 5.2** – Preparation of synthetic block 1. Representation of the synthetic approach followed to afford ketone **122**. Conditions: (a) CuI, TMEDA, Cs<sub>2</sub>CO<sub>3</sub>, DMSO, 110 °C, 24 hours; (b) Dry diethyl ether, *n*-BuLi (2.5M in hexane), -78 °C to room temperature, 3 hours.



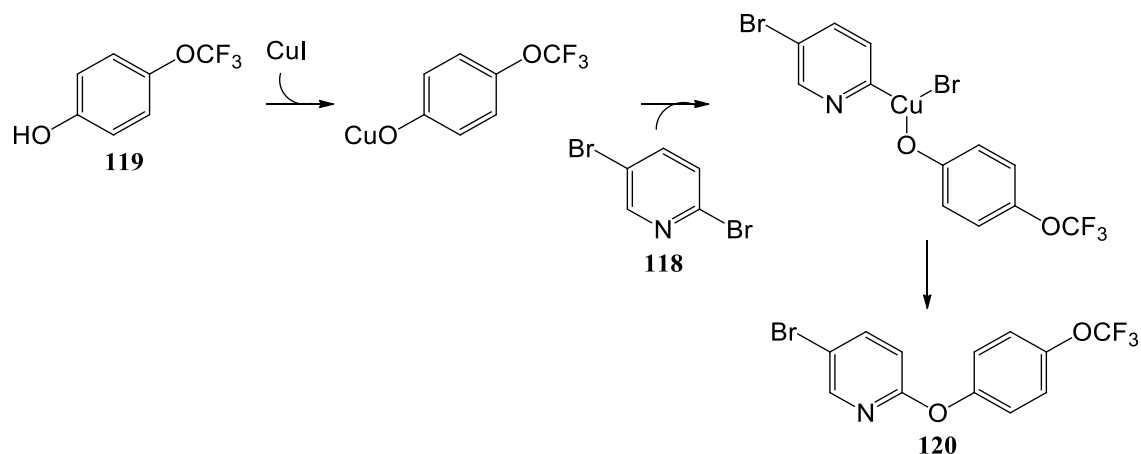
**Scheme 5.3** – Preparation of synthetic block 2. Representation of the synthetic approach followed to afford oxazoline **127**. Conditions: (a) THF:H<sub>2</sub>O (1:1), 0 °C to room temperature, 3 hours; (b) Chlorobenzene, ZnCl<sub>2</sub>, 140 °C, 18 hours.



**Scheme 5.4** – Representation of the synthetic approach to the preparation of quinolone **128** and of its prodrug **129**. Conditions: (a) TFSA, *n*-butanol, 130 °C, 2 days; (b) *t*ButOK, dry THF, acetyl chloride, room temperature, 90 minutes.

The reaction conditions for coupling the phenol derivative **119** to 2,5-dibromopyridine **118** were improved, from an yield of around 17%, using sodium hydride and DMF (where some quantities of a side product from the reaction between **118** and DMF has resulted) to an yield of around 90%. This improvement was achieved following the Ullmann reaction (Scheme 5.5), a copper-catalysed coupling between an aryl iodide

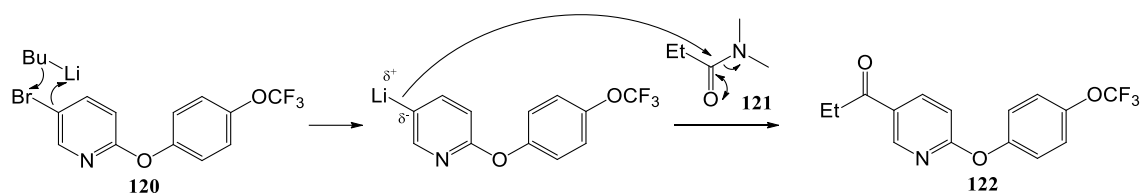
or bromide (**118**) and a phenol (**119**) to afford diaryl ether (**120**). Most copper salts are insoluble in organic solvents and the reactions require higher temperatures (125–220 °C), limiting the utility of this methodology. Hence, new methods have been developed to synthesize diaryl ethers under relatively mild reaction conditions (110–120 °C), for example by adding a base ( $\text{Cs}_2\text{CO}_3$ ) and/or a ligand for metal ions (TMEDA - tetramethylethylenediamine) that forms stable and soluble complexes in organic solvents.<sup>197,198</sup>



**Scheme 5.5** – Schematic representation of the mechanism proposed for the coupling reaction, following the Ullmann methodology.<sup>197,198</sup>

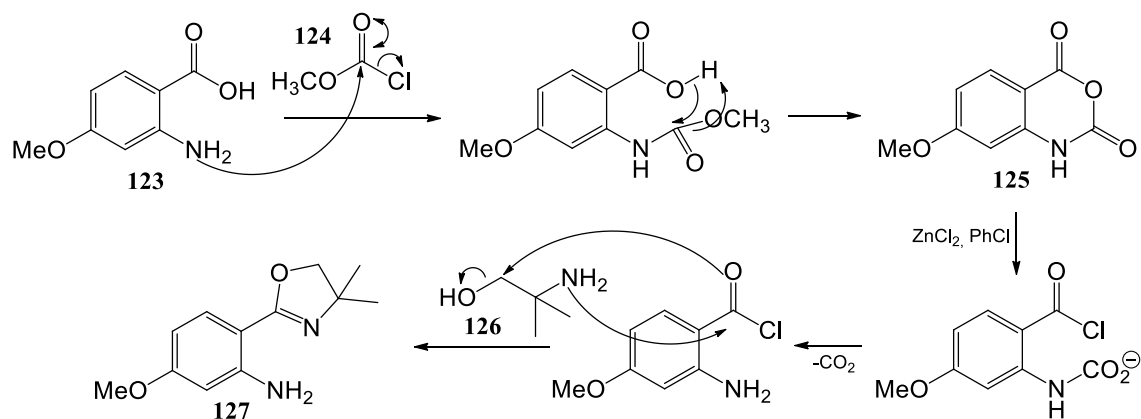
Ketone **122** was then synthesized, in good yield (59%), by first treating **120** with  $n\text{-BuLi}$  to generate an aryl-lithium intermediate, which further reacted with  $N,N$ -dimethylpropionamide. Henry Gilman found an important organolithium transformation and described the lithium-halogen exchange<sup>199,200</sup> that may explain the formation of the intermediate 5-lithio-2-(4-(trifluoromethoxy)phenoxy)pyridine. However, the mechanism for the formation of the lithium intermediate is not fully understood. As for Grignard reagents, aryl-lithium compounds, are rarely isolated (they are formed in solution and used immediately in the desired reaction). The organometallic compound formed from **120** has a strongly polarized carbon-metal bond ( $\text{C}^{\delta-}\text{-Li}^{\delta+}$ ), turning the carbon from an electrophilic carbon into a nucleophilic centre that can attack the carbonyl carbon of the  $N,N$ -dimethylpropionamide **121**.<sup>153</sup> The mechanism proposed for this step is represented in Scheme 5.6.





**Scheme 5.6** – Schematic representation of the mechanism proposed for the synthesis of ketone **122**, from the bromide derivative **120**.<sup>153,199,200</sup>

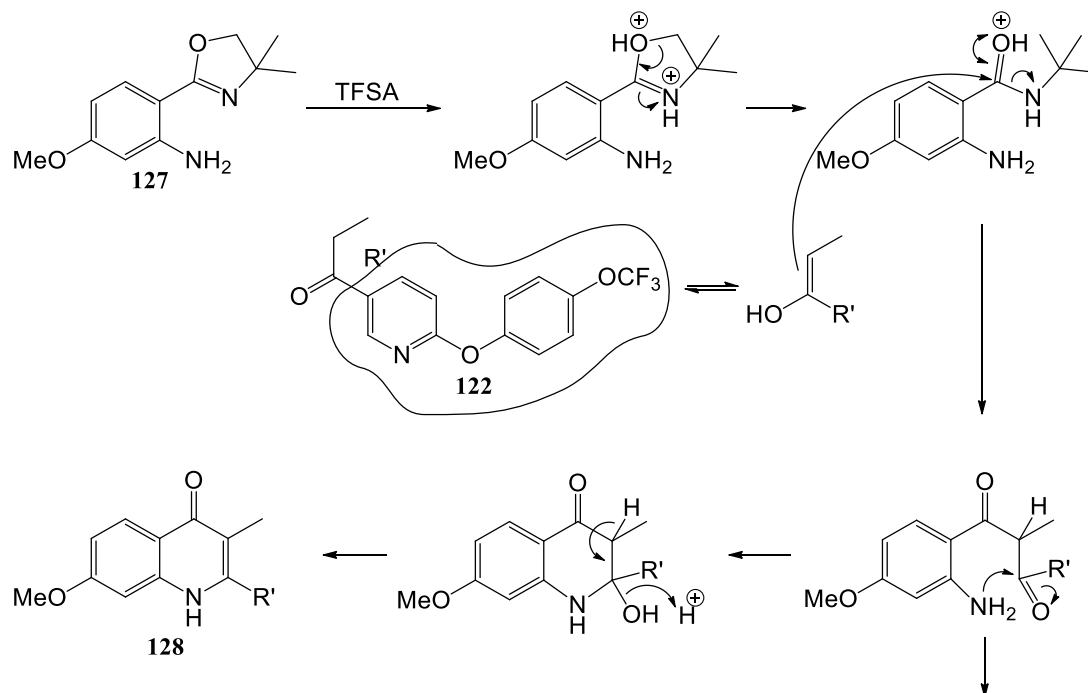
Oxazoline **127** was synthesised (76% yield) from the isatoic anhydride **125**, previously obtained from 4-methoxy anthranilic acid **123** (85% yield). Isatoic anhydride is a very useful intermediate in synthesis and there are different methodologies commonly used for its preparation. Among them, the cyclisation of anthranilic acid with a carbonic acid derivative (*e.g.* ethyl chloroformate, phosgene or phosgene derivatives) was chosen for this project. Diphosgene is related to phosgene (a chemical weapon during World War I) and is comparably toxic. Although its handling required the observation of several safety measures, diphosgene is more conveniently handled than phosgene, since it is a liquid whereas phosgene is a gas. The reaction of an anthranilic acid derivative with phosgene is well documented in the literature and can be adapted for the reaction with diphosgene.<sup>201</sup> From the isatoic anhydride synthesized, and in the presence of anhydrous zinc chloride (a moderate-strength Lewis acid) in dry chlorobenzene, formation of the desired oxazoline **127** occurred, following the mechanism proposed in Scheme 5.7.<sup>202</sup>



**Scheme 5.7** – Schematic representation of the mechanism proposed for the synthesis of isatoic anhydride **125** and for its conversion into the oxazoline derivative **127**.<sup>201,202</sup>

The strategy followed for the coupling of the synthetic blocks **1** (**122**) and **2** (**127**), to afford the target quinolone derivative **128**, is an adaptation of Friedländer synthesis, an acid-catalysed reaction (using trifluoromethanesulfonic acid – TFSA). Quinolone **128** was recovered with a yield of 39%. Several mechanisms were proposed to describe this reaction.<sup>135,203</sup> Scheme 5.8 presents one of these mechanisms. It is proposed that, initially,

the oxazoline **127** is protonated twice in TFSA and the resulting intermediate undergoes a ring-opening reaction to produce a reactive dicationic species that further reacts with the ketone **122**, or more specifically with its enol form, following the Friedländer methodology.<sup>204</sup>

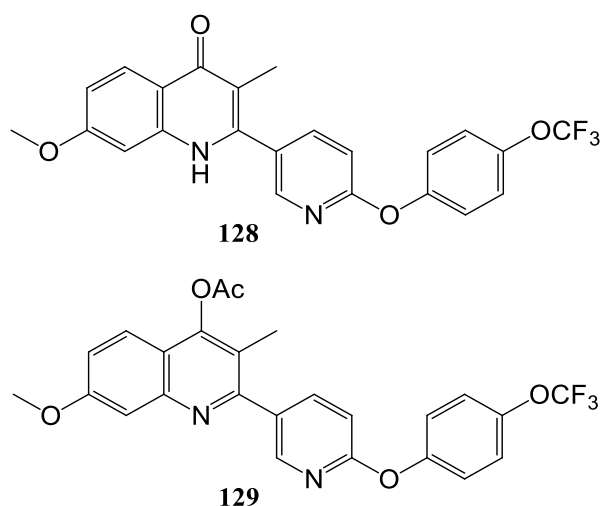


**Scheme 5.8** – Schematic representation of the mechanism proposed for the synthesis of quinolone derivative **128**.<sup>135,201–204</sup>

Due to the poor solubility of **128** and considering some biological results (discussed below), an acetate prodrug of **128** (**129**) was synthesized by esterification of acetyl chloride with the keto/enol form of quinolone **128**, in 56% yield (Scheme 5.4).

### 5.2.2. Investigation of antituberculous activity

At the Liverpool School of Tropical Medicine, the quinolone **128** was tested *in vitro* against *Mycobacterium tuberculosis* (H37Rv strain) and its pharmacokinetic profile was evaluated *in vivo* (Wistar rats). The antituberculous activity of **128** was screened using the mycobacteria growth indicator tube (MGIT) assay, where a specific compound is converted to a fluorescent compound in presence of *M. tuberculosis*.



The MGIT assay result for compound **128** (Figure 5.2) was compared to those exhibited by isoniazid and rifampicin (antituberculostatic drugs), under the same conditions. From the analysis, it was possible to conclude that quinolone **128** has demonstrated an activity profile that overlaps with the “no drug” assay. This data could mean that the quinolone **128** is not active against *M. tuberculosis* or, alternatively, the apparent lack of activity could result from solubility problems. Another quinolone derivative (**130**, **MTC420**, Figure 5.1) synthesized by a member of Paul O'Neill's group, was tested in the same conditions and demonstrated much better activity with potency approaching that of isoniazid.

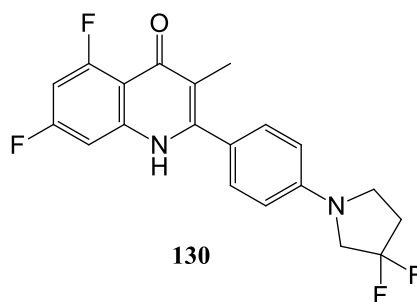
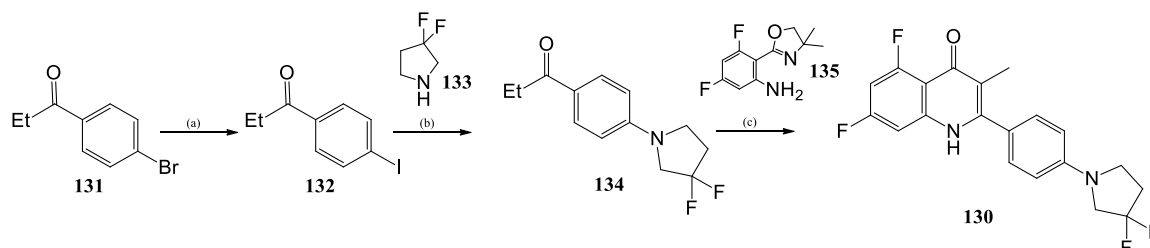


**Figure 5.1** – Structural representation of quinolone derivative (**130**), synthesized by a member of Paul O'Neill's group and screened for antituberculosic activity together with compounds **128** and **129**.

Therefore, the project was directed to the synthesis and optimisation of analogues of **130**. The synthetic approach to compound **130** is present in Scheme 5.9.

For the synthesis of **130**, 4-bromopropiophenone **131** was first converted to a more reactive 4-iodopropiophenone **132** by an aromatic substitution catalysed by copper(I) iodide in combination with *N,N*-dimethyl-1,2-diaminoethane. The amination of **132** was performed following the Buchwald-Hartwig methodology, using tris(dibenzylidene-acetone)dipalladium(0) [(Pd<sub>2</sub>(dba)<sub>3</sub>] and Xantphos (4,5-

bis(diphenylphosphino)-9,9-dimethylxanthene) to afford the ketone side chain **134**. Oxazoline **135** was synthesized following the methodology used for the synthesis of **127**. The strategy followed for the coupling of **134** and **135**, to afford the target quinolone derivative **130**, is similar to that one used for the synthesis of **128** (Friedländer synthesis – see Scheme 5.8 as example).



**Scheme 5.9** – Representation of the synthetic approach to the preparation of quinolone **130**. Conditions: (a) CuI, *N,N*-dimethyl-1,2-diaminoethane, NaI, 1,4-dioxane, 110°C, 24 hours; (b) Pd<sub>2</sub>(dba)<sub>3</sub>, Xantphos, NaOtBu, 1,4-dioxane, 110°C, 24 hours; (c) CF<sub>3</sub>SO<sub>3</sub>H, *n*-BuOH, N<sub>2</sub>, 130 °C, 24 hours.

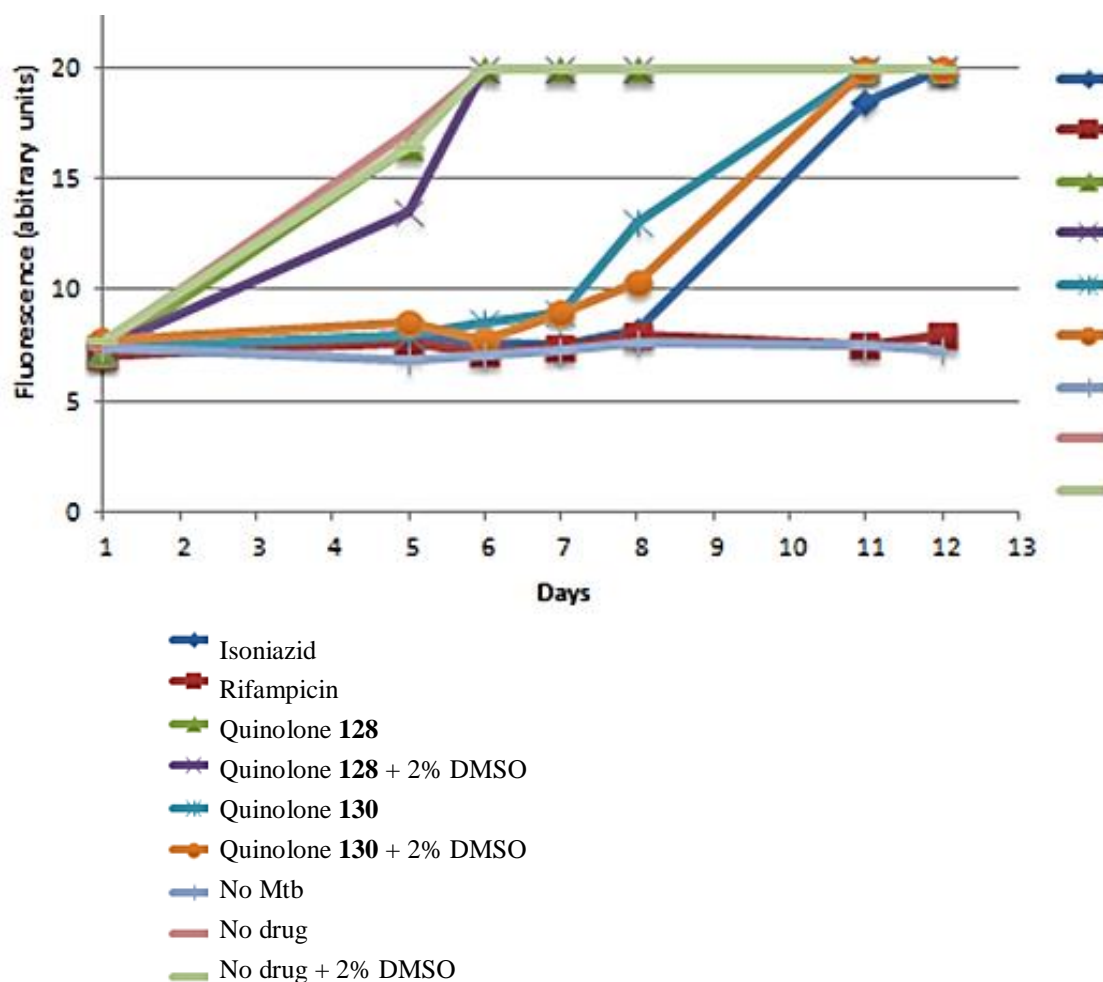


**Figure 5.2** – Results of the MGIT assay for quinolones **128** and **130**.

Additionally, the antiplasmodial activities of **128** and its prodrug (**129**) were also evaluated and the results are promising, both against sensitive and chloroquine/mefloquine-resistant strains (see Table 5.1).

**Table 5.1** - *In vitro* antimalarial activities for quinolone **128** (parent quinolone) and for its acetate prodrug **129**.

Compound	Antiplasmodial activity (IC <sub>50</sub> ; $\mu$ M); Average $\pm$ SD	
	3D7	Dd2
<b>128</b>	0.018 $\pm$ 0.009	0.017 $\pm$ 0.002
<b>129</b>	0.070 $\pm$ 0.046	0.048 $\pm$ 0.002

In addition to the solubility issues exhibited by quinolone **128**, pharmacokinetic analysis shown in Figure 5.3 shows that an increasing dose of **128** (from 10 mg/kg to 50 mg/kg) did not translate into increase of exposure. However, a 10-fold increase was observed when using the acetate prodrug **129** at 10 mg/kg and an increase of over 30-fold at 50 mg/kg, compared to the exposure of **128**. The exposure has increased 5-6 times on increasing the dose of **129** from 10 mg/kg to 50 mg/kg.

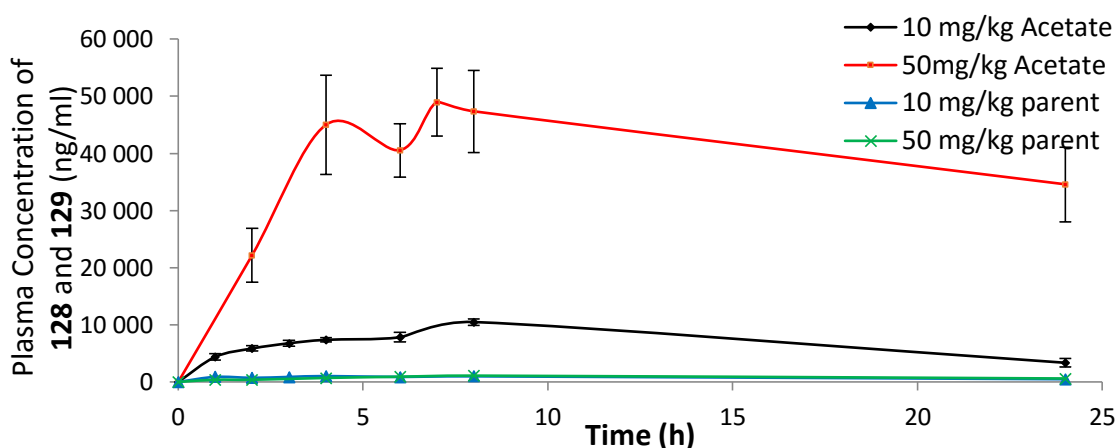


**Figure 5.3** – Pharmacokinetic profiles of quinolone **128** (parent quinolone) and of its acetate prodrug **129**.

The CYP450 inhibition by compounds **128** and **130** was also tested, using an assay where a substrate for each P450 is provided and the oxidation (metabolism) of this substrate results in the formation of a fluorescent metabolite. For each CYP450 isoform assay study, only one specific isoform is expressed. The results were compared with the data obtained for the incubation with the vehicle control (where maximum fluorescence intensity is observed) and for the positive controls using 10  $\mu$ M ketoconazole (a known CYP3A4 inhibitor - Figure 5.4 and Figure 5.5), 30  $\mu$ M sulfaphenazole (a known CYP2C9

inhibitor - Figure 5.6 and Figure 5.7) and 10  $\mu\text{M}$  montelukast (a known CYP2C8 inhibitor - Figure 5.8 and Figure 5.9).

The results (Figure 5.4 and Figure 5.5) indicate that **128** and **130** did not lead to inhibition of CYP3A4 at the three concentrations in study. The fluorescence measured for both compounds is higher than for the vehicle controls and these results are not well understood since the pre-incubation of the drugs showed no inherent compound fluorescence. These compounds did not exhibited inhibition for CYP3A5 (results not shown).

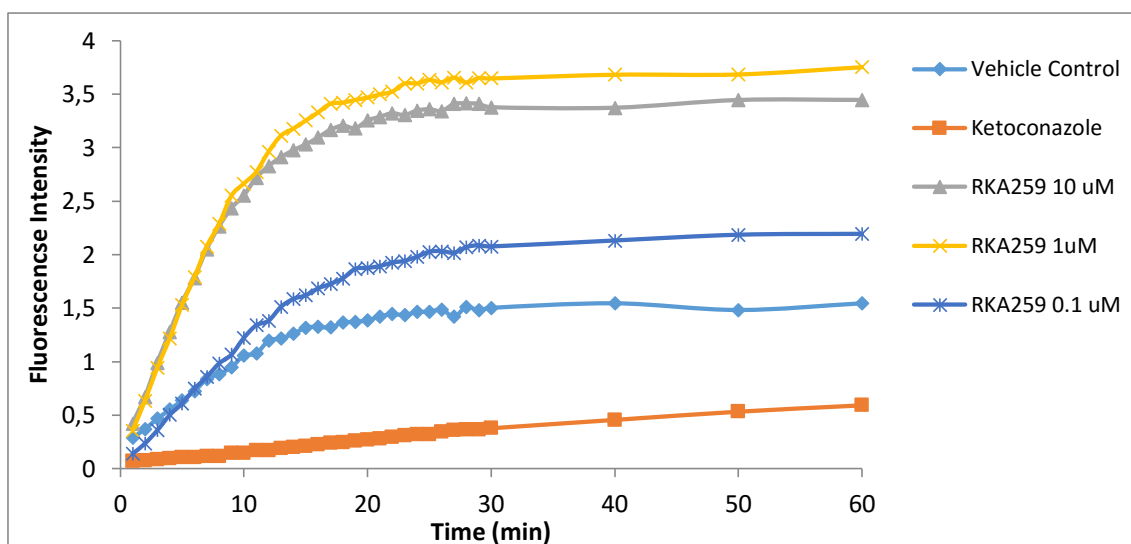


**Figure 5.4** – CYP3A4 inhibition assay for quinolone **128** at 0.1  $\mu\text{M}$ , 1  $\mu\text{M}$  and 10  $\mu\text{M}$  (here defined as RKA259), considering ketoconazole (10  $\mu\text{M}$ ) as positive control.

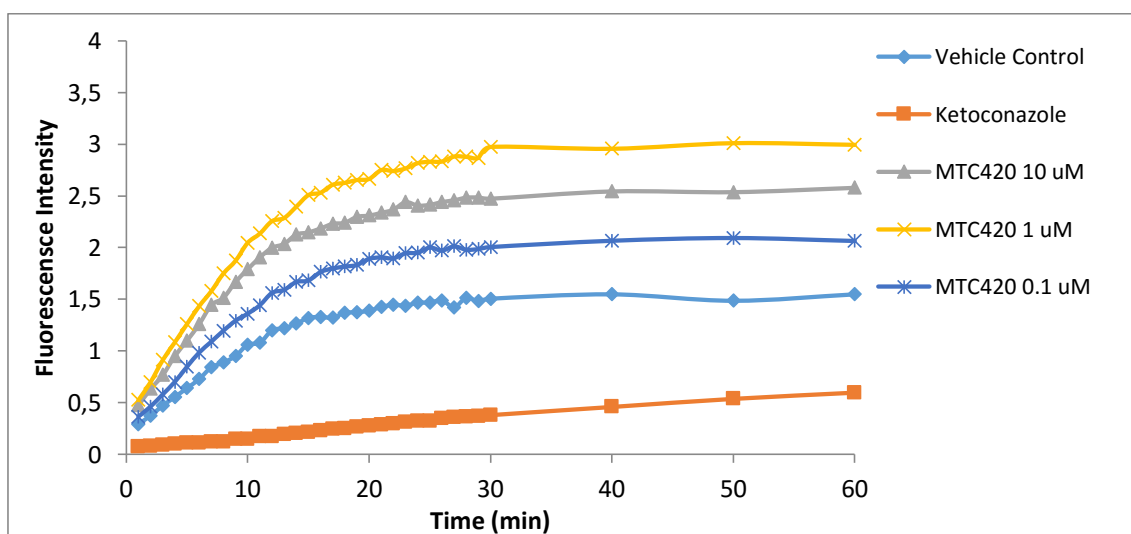


**Figure 5.5** – CYP3A4 inhibition assay for quinolone **130** at 0.1  $\mu\text{M}$ , 1  $\mu\text{M}$  and 10  $\mu\text{M}$  (here defined as MTC420), considering ketoconazole (10  $\mu\text{M}$ ) as positive control.

The quinolone **130** resulted in little or no inhibition of CYP2C9 (Figure 5.7), while **128** exhibited an inhibitory capacity dependent on dose, decreasing the activity of this isoform by 43% at 10  $\mu\text{M}$  concentration (Figure 5.6).

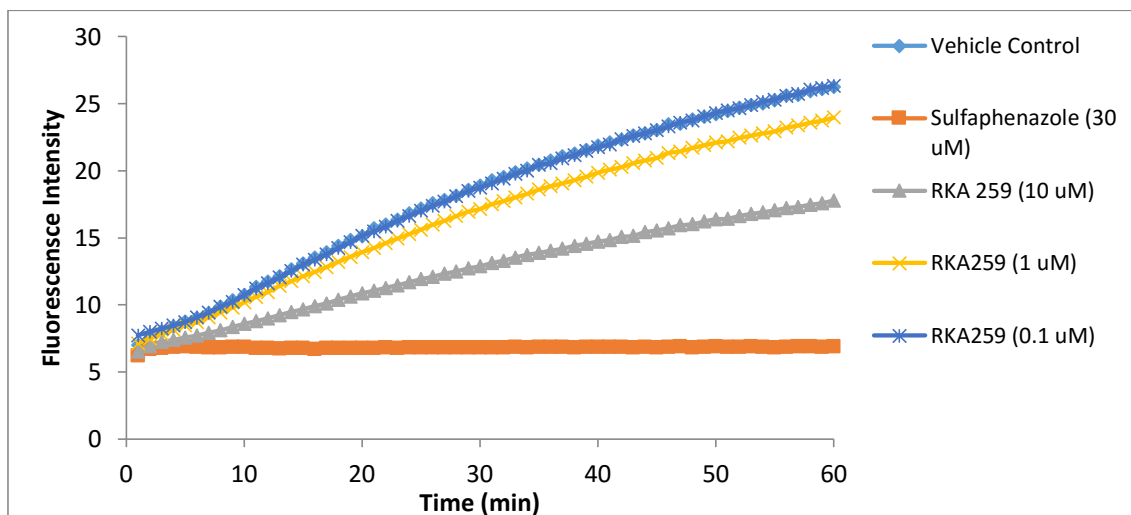


**Figure 5.6** – CYP2C9 inhibition assay for quinolone **128** at 0.1  $\mu\text{M}$ , 1  $\mu\text{M}$  and 10  $\mu\text{M}$  (here defined as RKA259), considering sulfaphenazole (30  $\mu\text{M}$ ) as positive control.

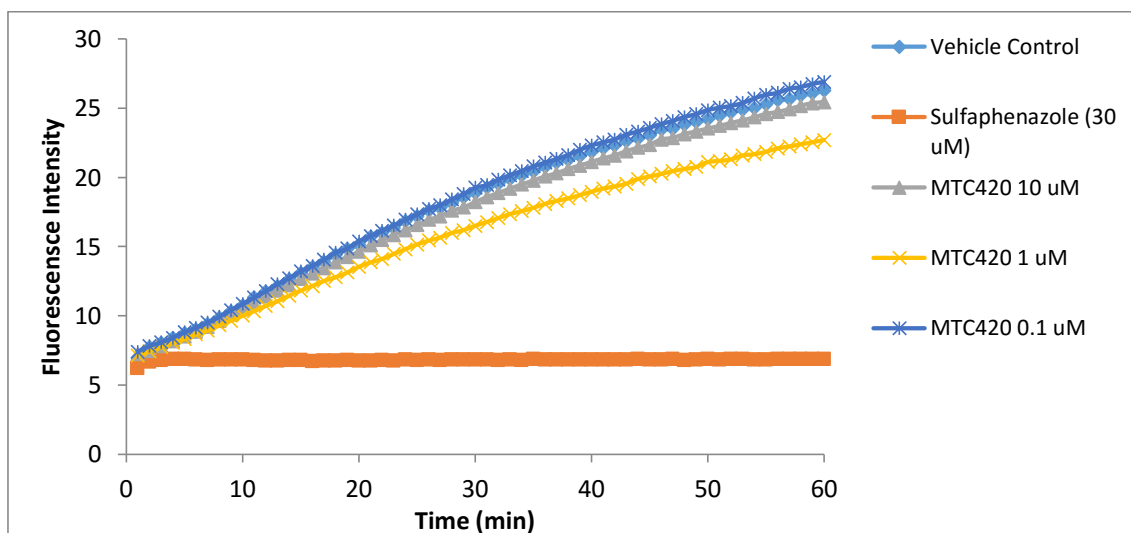


**Figure 5.7** – CYP2C9 inhibition assay for quinolone **130** at 0.1  $\mu\text{M}$ , 1  $\mu\text{M}$  and 10  $\mu\text{M}$  (here defined as MTC420), considering sulfaphenazole (30  $\mu\text{M}$ ) as positive control.

While **128** showed strong inhibitory capacity (Figure 5.8), **130** only exhibited moderate inhibition on CYP2C8 (Figure 5.9), reducing the activity of this isoform in 60% at 10  $\mu\text{M}$  of **128** and in 39% at 10  $\mu\text{M}$  of **130**. In contrast, atovaquone (10  $\mu\text{M}$ ) did not evidence inhibition capacity towards CYP2C8.

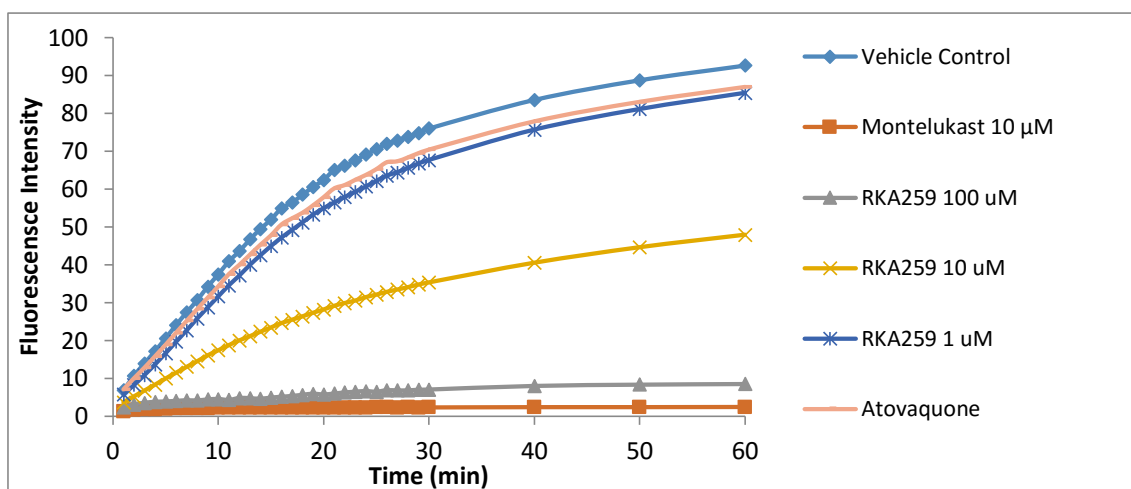


**Figure 5.8** – CYP2C8 inhibition assay for quinolone **128** at 1 μM, 10 μM and 100 μM (here defined as RKA259), and for atovaquone (10 μM), considering montelukast (10 μM) as positive control.

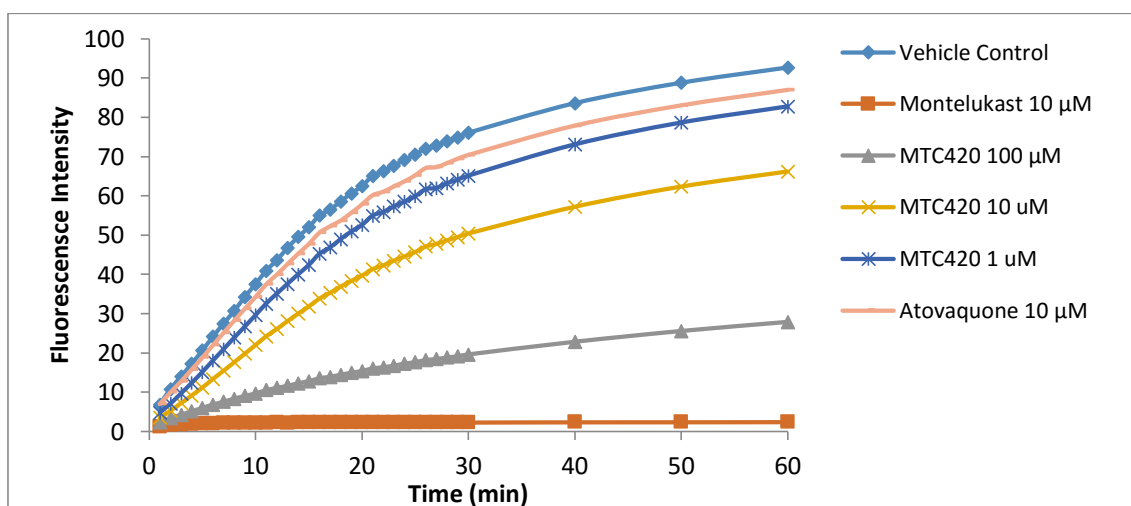


**Figure 5.9** – CYP2C8 inhibition assay for quinolone **130** at 1 μM, 10 μM and 100 μM (here defined as MTC420), and for atovaquone (10 μM), considering montelukast (10 μM) as positive control.



### 5.3. Summary, conclusions and future work

In general, the reaction conditions followed in the synthetic steps required for the preparation of quinolone derivatives **128** and **129** (with potential activity against *M. tuberculosis*) were optimized. However, considering the hazards inherent to some reagents used on these synthetic routes, some alternatives should be considered.

As described for many of the quinolone 3-esters discussed in the previous chapter, also the quinolones proposed in this section have demonstrated solubility problems and these may contribute to the negligible activity of compound **128**. Quinolone derivative **130** has activity close to isoniazid *versus M. tuberculosis* and, therefore, synthesis of some derivatives should be considered, in view of selecting analogues with improved properties for development.

The solubility liabilities demonstrated for quinolone **128** reflected in a poor pharmacokinetic profile, but this problem was solved with the synthesis and use of the acetate prodrug **129**.

Quinolone **128** did not inhibit CYP3A4 and CYP3A5, but exhibited some potential inhibitory capacity towards CYP2C9 and strong inhibitory capacity towards CYP2C8, while **130** did not inhibit CYP3A4, CYP3A5 and CYP2C9 but exhibited moderate inhibitory capacity towards CYP2C8.

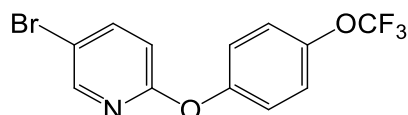
## 5.4. Experimental

Solvents, reagents and other compounds; Monitoring and purification; Spectroscopic analysis; and other analysis

These specifications are found in the experimental section of the previous chapter (Synthesis of quinolone 3-esters with potential activity against *P. falciparum*).

### Preparation of the synthetic block 1: synthesis of ketone 122

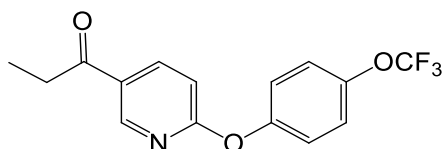
#### *5-Bromo-2-(4-(trifluoromethoxy)phenoxy)pyridine (120)*



2,5-dibromopyridine **118** (2.00 g; 8.44 mmol; 1 eq.), 4-(trifluoromethoxy)-phenol **119** (1 eq.), copper (II) iodide (0.1 eq.), tetramethylethylenediamine (0.1 eq.) and cesium carbonate were mixed in DMSO (15 mL), under a nitrogen atmosphere. The reaction was stirred at 110 °C for 24 hours. The mixture was cooled to room temperature and filtered by using Celite to remove the inorganic residues. From the extraction in DCM and brine, the organic layer was dried under MgSO<sub>4</sub> anhydrous, filtered, concentrated under vacuum and purified by column chromatography in silica gel (eluting with 30% of DCM in hexane), to afford the desired product as a yellow oil (2.55 g; 7.63 mmol; 90%).

<sup>1</sup>H NMR (400 MHz, CDCl<sub>3</sub>) δ 8.21 (s, 1H), 7.80 (d, 1H), 7.24 (d, 2H), 7.15 (dd, 2H), 6.89 (d, 1H); <sup>13</sup>C NMR (101 MHz, CDCl<sub>3</sub>) δ 162.45, 152.38, 148.68 (2C), 142.58, 122.80 (2C), 122.72 (2C), 114.38, 113.71 (2C); MS m/z (ES) [M + H]<sup>+</sup> C<sub>12</sub>H<sub>8</sub>NO<sub>2</sub>F<sub>3</sub>Br requires 333.9690, found 333.9689.

#### *1-(6-(4-(trifluoromethoxy)phenoxy)pyridin-3-yl)propan-1-one (122)*



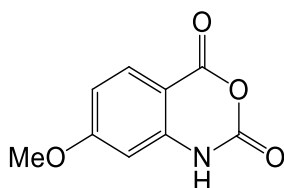
To a solution of 5-bromo-2-(4-(trifluoromethoxy)phenoxy)pyridine **120** (2.00 g; 5.99 mmol) in dry diethyl ether (40 mL), at -78 °C, and under nitrogen atmosphere, was added, slowly, a 2.5M solution of n-butyl lithium in hexane (2.88 mL; 1.2 eq.). After 1 hour, at -78 °C, *N,N*-dimethylpropanamide **121** (1.2 eq) was added and the reaction temperature was allowed to rise to room temperature, under stirring, for 2 hours. The reaction mixture was quenched with saturate NH<sub>4</sub>Cl solution, the organic layer was

separated and the aqueous layer extracted with diethyl ether (2 x 30 mL). The organic layers were combined, washed with brine and dried over MgSO<sub>4</sub>, filtered and concentrated under vacuum. The crude product was purified by column chromatography (eluting with 70% of DCM in hexane) to give the pure product as yellow oil (1.10 g; 3.55 mmol; 59%).

<sup>1</sup>H NMR (400 MHz, CDCl<sub>3</sub>) δ 8.77 (s, 1H), 8.30 (d, 1H), 7.32 – 7.27 (m, 2H), 7.22 – 7.17 (m, 2H), 7.00 (d, 1H), 2.96 (q, CH<sub>3</sub>CH<sub>2</sub>CO), 1.23 (t, CH<sub>3</sub>CH<sub>2</sub>CO); <sup>13</sup>C NMR (101 MHz, CDCl<sub>3</sub>) δ 198.50 (CH<sub>3</sub>CH<sub>2</sub>CO), 166.09, 151.89, 149.24 (2C), 139.75, 128.62, 123.17 (2C), 122.78 (2C), 111.91 (2C), 32.21 (CH<sub>3</sub>CH<sub>2</sub>CO), 8.36 (CH<sub>3</sub>CH<sub>2</sub>CO); MS m/z (ES) [M + H]<sup>+</sup> C<sub>15</sub>H<sub>13</sub>F<sub>3</sub>NO<sub>3</sub> requires 312.0848, found 312.0857.

Preparation of the synthetic block 2: synthesis of oxazoline 127

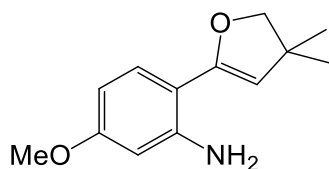
*4-Methoxy-isatoic anhydride (125)*



4-methoxy anthranilic acid **123** (3.00 g; 17.95 mmol) was dissolved in a mixture of THF:H<sub>2</sub>O (1:1; 60mL), under stirring, at 0 °C. Trichloromethyl chloroformate **124** (1.5 eq.) was added drop-by-drop, very carefully and slowly. The reaction temperature was allowed to rise to room temperature and the mixture was kept stirring for 3 hours. The organic solvent was carefully removed under reduced pressure to leave the water solution and some precipitate, that was filtrated, carefully washed with water and dried under vacuum to give the product as an off-white solid (2.94 g; 15.20 mmol; 85%).

<sup>1</sup>H NMR (400 MHz, (CD<sub>3</sub>)<sub>2</sub>SO) δ 7.84 (d, 1H), 6.84 (d, 1H), 6.59 (s, 1H), 3.86 (s, OCH<sub>3</sub>); <sup>13</sup>C NMR (101 MHz, (CD<sub>3</sub>)<sub>2</sub>SO) δ 166.23, 159.29, 147.79, 143.99, 131.41, 112.00, 103.25, 98.87, 56.27 (OCH<sub>3</sub>); MS m/z (CI) [M + H + NH<sub>3</sub>]<sup>+</sup> C<sub>9</sub>H<sub>11</sub>N<sub>2</sub>O<sub>4</sub> requires 211.0718, found 211.0820.

*2-(4,4-dimethyl-4,5-dihydrooxazol-2-yl)-5-methoxyaniline (127)*

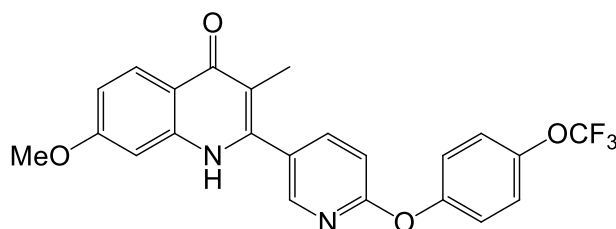


4-methoxy-isatoic anhydride **125** (2.31 g; 11.98 mmol) was suspended in chlorobenzene (30 mL), under nitrogen, and stirred for 15 minutes. 2-amino-2-methylpropan-1-ol **126** (1.4 eq) was added to the suspension via a syringe, followed by zinc chloride (0.1 eq). The mixture was refluxed at 140 °C for 18 hours. The solvent was removed under reduced pressure and the residue extracted with ethyl acetate (2 x 25 mL), washed with brine, dried over MgSO<sub>4</sub>, filtered and concentrated under vacuum. Purification by column chromatography, eluting with 15% of ethyl acetate in hexane, gave the desired oxazoline **127** as a white solid (2.00 g; 9.06 mmol; 76%).

<sup>1</sup>H NMR (400 MHz, CDCl<sub>3</sub>) δ 7.64 (s, 1H), 6.26 (d, 1H), 6.17 (d, 1H), 4.00 (s, CH<sub>2</sub>), 3.79 (s, OCH<sub>3</sub>), 1.37 (s, C(CH<sub>3</sub>)<sub>2</sub>); <sup>13</sup>C NMR (101 MHz, CDCl<sub>3</sub>) δ 163.09, 162.29, 150.43 (CNH<sub>2</sub>), 131.50, 103.97, 103.05, 99.69 (2C), 67.88, 55.53 (OCH<sub>3</sub>), 29.12 (2C); MS m/z (CI) [M + H]<sup>+</sup> C<sub>12</sub>H<sub>17</sub>N<sub>2</sub>O<sub>2</sub> requires 221.1290, found 221.1281.

*Coupling of synthetic blocks 1 and 2: cyclisation reaction to give the desired quinolone scaffold 128*

*7-methoxy-3-methyl-2-(6-(4-(trifluoromethoxy)phenoxy)pyridin-3-yl)-4-oxo-quinoline (128)*

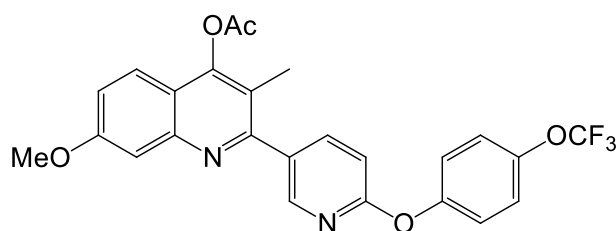


2-(4,4-dimethyl-4,5-dihydrooxazol-2-yl)-5-methoxyaniline (oxazoline **127**; 0.82 g; 3.72 mmol) was added to a solution of ketone **122** (1 eq.) and trifluoromethanesulfonic acid (TFSA, 1.4 eq.) in n-butanol (10 mL). The reaction mixture was heated to 130 °C, under nitrogen, and stirred for 2 days. The solvent was removed under reduced pressure and water (20 mL) was added. The aqueous solution was extracted with ethyl acetate (3 x 20 mL), dried over MgSO<sub>4</sub>, filtered and concentrated under vacuum. The product was

purified by column chromatography (eluting with 75% of ethyl acetate in hexane) to give the desired quinolone **128** as a white solid (0.64 g; 1.45 mmol; 39%).

$^1\text{H}$  NMR (400 MHz,  $(\text{CD}_3)_2\text{SO}$ )  $\delta$  11.49 (s,  $\text{NH}$ ), 8.36 (d, 1H), 8.10 (d, 1H), 8.02 (d, 1H), 7.48 (d, 2H), 7.36 (d, 1H), 7.35 (d, 1H), 7.30 (d, 1H), 6.96 (d, 1H), 6.91 (d, 1H), 3.83 (s,  $\text{OCH}_3$ ), 2.51 (s,  $\text{CH}_3$ );  $^{13}\text{C}$  NMR data not obtained due to poor solubility in all available deuterated solvents; MS  $m/z$  (ES)  $[\text{M} + \text{Na}]^+$   $\text{C}_{23}\text{H}_{17}\text{F}_3\text{N}_2\text{O}_4\text{Na}$  requires 465.1038, found 415.1036; CHN for  $\text{C}_{23}\text{H}_{17}\text{F}_3\text{N}_2\text{O}_4$  requires C 62.43%, H 3.88%, N 6.33%, found C 62.24%, H 3.96%, N 6.32%.

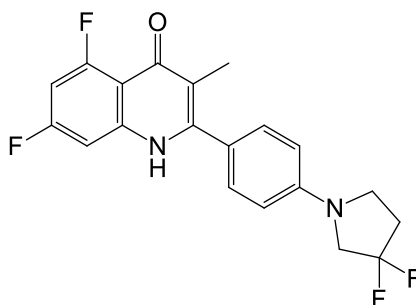
*Acetate 7-methoxy-3-methyl-2-(6-(4-(trifluoromethoxy)phenoxy)pyridin-3-yl)-4-yl-quinoline (129)*



A mixture of quinolone **128** (0.40 g; 0.90 mmol) and potassium *tert*-butoxide (1.25 eq.) in anhydrous THF (30 mL) was stirred for 1 hour at room temperature. Acetyl chloride (2.0 eq) was added and the mixture was stirred 30 min. The reaction was quenched with water (approximately 10 mL) and the mixture was concentrated under reduced pressure. Water (approximately 10 mL) was added to the residue and the product was extracted with ethyl acetate (3 x 20 mL). The combined organic layers were dried over  $\text{MgSO}_4$ , filtered and concentrated. The resulting residue was purified by column chromatography (eluting with 40% of ethyl acetate in hexane) to give the desired ester as a white solid (0.24 g; 0.50 mmol; 56%).

$^1\text{H}$  NMR (400 MHz,  $\text{CDCl}_3$ )  $\delta$  8.44 (s, 1H), 7.68 (d, 1H), 7.31 – 7.26 (m, 4H), 7.26 – 7.20 (m, 3H), 7.10 (d, 1H), 3.96 (s,  $\text{OCH}_3$ ), 2.53 (s,  $\text{CH}_3$ ), 2.28 (s,  $\text{COCH}_3$ );  $^{13}\text{C}$  NMR data not obtained due to poor solubility in all available deuterated solvents; MS  $m/z$  (ES)  $[\text{M} + \text{H}]^+$   $\text{C}_{25}\text{H}_{20}\text{F}_3\text{N}_2\text{O}_5$  requires 485.1324, found 485.1342; CHN for  $\text{C}_{25}\text{H}_{19}\text{F}_3\text{N}_2\text{O}_5$  requires C 61.71%, H 4.35%, N 5.76%, found C 62.36%, H 4.15%, N 5.80%.

*Preparation and characterization of 2-(4-(3,3-difluoropyrrolidin-1-yl)phenyl)-5,7-difluoro-3-methyl-4-oxo-quinoline (130)*



For the synthesis of **130**, 4-bromopropiophenone **131** was first converted to a more reactive 4-iodopropiophenone **132** by an aromatic reaction catalysed by copper(I) iodide in combination with *N,N*-dimethyl-1,2-diaminoethane. The amination of **132** was performed following the Buchwald-Hartwig methodology using tris(dibenzylideneacetone)dipalladium(0) [(Pd<sub>2</sub>(dba)<sub>3</sub>] and Xantphos (4,5-bis(diphenylphosphino)-9,9-dimethylxanthene) to afford the ketone side chain **134**.

Oxazoline **135** (1 eq.), previously synthesized following the same methodology than the used for the synthesis of **127**, was added to a solution of ketone **134** (1 eq.) and trifluoromethanesulfonic acid (TFSA, 0.2 eq.) in anhydrous *n*-butanol (10 mL). The reaction mixture was heated to 130 °C, under nitrogen, and stirred for 24 hours. The final mixture was cooled and the solvent removed under reduced pressure. Saturated NaHCO<sub>3</sub> solution was added and the resulting aqueous solution was extracted with ethyl acetate (3 × 20 mL). The combined organic layers were washed with brine, dried over MgSO<sub>4</sub>, filtered and concentrated under vacuum. The product was purified by trituration to give the desired quinolone **130** as a white solid (56%).

Melting range: 316-317 °C; <sup>1</sup>H NMR (400 MHz, (CD<sub>3</sub>)<sub>2</sub>SO) δ 7.41 (d, 2H), 7.17 (d, 1H), 7.01 (m, 1H), 6.78 (d, 2H), 3.79 (t, 1H), 3.56 (t, 1H), 2.59 (tt, 1H), 1.87 (s, 1H); <sup>13</sup>C NMR (101 MHz, (CD<sub>3</sub>)<sub>2</sub>SO) δ 175.38, 164.09, 148.09, 147.72, 142.82, 130.34, 129.16, 126.71, 122.79, 116.32, 111.98, 111.61, 99.37, 98.82, 54.96, 45.75, 33.72, 12.54; MS *m/z* (ES) [M + H]<sup>+</sup> C<sub>20</sub>H<sub>16</sub>F<sub>4</sub>N<sub>2</sub>ONa requires 399.1096, found 399.1093.

*Biological activity – Mycobacteria growth indicator tube*

Cultures of *M. tuberculosis* H37Rv were continuously cultured until a mid-log growth phase was reached, in a liquid growth medium specially used for culture of *Mycobacterium* (Middlebrook 7H9 Broth) with addition of 10% albumin–dextrose–

catalase solution (Becton Dickinson), glycerol and Tween 80. The antituberculous activity was determined using the mycobacteria growth indicator tube (MGIT) assay, where a specific compound is converted to a fluorescent compound in presence of *M. tuberculosis*. Each compound was tested at concentrations ranging from 10  $\mu\text{M}$  to 0.08  $\mu\text{M}$  and was co-incubated with replicating *Mycobacterium tuberculosis* (7 days, 37°C) using a microplate Alamarblue assay (MABA). Measurements of well absorbance at 570 and 600 nm recorded using an Opsys MR plate reader were determined to calculate IC<sub>50</sub> values for the compounds tested.

#### *In vitro* CYP450 inhibition

CYP450 VIVID® inhibition kits were purchased from Invitrogen Life Technologies™. Briefly, compounds were tested at a final concentration of 10, 1 and 0.1  $\mu\text{M}$  alongside with a relevant positive control for the isoform of interest and a solvent control. The assay utilised a substrate, specific to the isoform, which produced a fluorescent metabolite as it underwent oxidation by the P450 enzyme. Inhibition of the enzyme led to reduced fluorescent output. The assay was carried out in kinetics mode, with readings taken every minute, during 1 hour.

#### *Pharmacokinetic studies in Male Wistar rats*

Male Wistar rats (180 – 250 g) (n=4) were purchased from Charles River Laboratories, UK and allowed to acclimatise for 1 week in controlled conditions (temperature 23  $\pm$  3 °C; relative humidity 50  $\pm$  10 %; light-dark cycle 12 h). The animals were provided with feed pellet and filtered water *ad libitum*. Each rat received an oral dose of the relevant compound (10 or 50 mg/kg) in PEG400 (100 %) (5 mL/kg) via gavage needle. At various time-points, the rats were anaesthetised using isoflurane and a blood sample (< 300  $\mu\text{L}$ ) was taken from a superficial vein in the tail. The blood was properly treated, an aliquot of plasma was removed (100  $\mu\text{L}$ ) and then the plasma concentration of drug was determined.





---

# *Conclusions*

---

## Conclusions

---

## *Conclusions*

---

General synthetic approaches to afford quinolone 3-esters with chemical diversity were devised and optimized, generally using nitro arenes as starting compounds. Reaction conditions for the reduction of nitro arenes (*ortho* and/or *meta* substituted) and for the coupling of the corresponding anilines with DEEMM were optimized to give high yield of the desired products (anilines and  $\alpha,\beta$ -unsaturated ester, respectively).

The cyclisation step of the enamine derivatives to afford the quinolone scaffolds, following the thermally driven Gould-Jacobs intramolecular cyclisation methodology, posed some problems. The yields of this step varied from 3% to 62% and for some of the enamines derivatives no product was recovered. The reaction proved to be dependent on concentration. The poor solubility of the quinolone derivatives rendered difficult their isolation, purification and characterization. The high temperatures required for this step and the high boiling point of the solvent (Dowtherm A) may lead to the degradation of susceptible groups and to side reactions, as well as to difficulties in the removal of the solvent.

To overcome those problems, the synthesis of 4-chloroquinoline derivatives (with improved solubility) mediated by  $\text{POCl}_3$  was considered. However, as for the Gould-Jacob methodology, the possibility of obtaining a mixture of structural isomers from the cyclisation reaction of the enamine, due to different patterns of aromatic substitution, and to the possibility of oxo-quinoline/hydroxy-quinoline tautomerism should not be neglected.

4-Chloroquinoline derivatives steamed as versatile building blocks for the preparation of 4-oxo-quinolines, enabling the introduction of chemical diversity at positions 6 and/or 7 of the quinoline prior to conversion into the corresponding quinolone structure. The structure of a 4-chloroquinoline derivative (compound **56**) was elucidated. Four conformers were predicted by theoretical calculations and found in the as-deposited argon-matrix. These conformers, related to rotations in the ester moiety, show low predicted barriers for conformational interconversion what may facilitate structural adjustments of the ethyl ester moiety in the enzyme pocket, maximizing drug-target interactions and improving the pharmacodynamic profile.

## Conclusions

Considering that the quinolone derivatives studied in this thesis are not N1 substituted (contrary to the conventional quinolone antibacterials – ciprofloxacin, norfloxacin and levofloxacin), the possibility of tautomerization is a reality. In the compounds under investigation tautomerism may translate in alteration of chemical and physical properties, with consequences for pharmacokinetic and pharmacodynamic profiles, especially because the N-H and 4-oxo groups are believed to be involved in important interactions inside the Q<sub>o</sub> site of the enzyme pocket.

From a detailed study of tautomerism in the **82** series (quinolone 3-esters with a methyl group at position 7 or 5), the preference for the hydroxy-quinoline form was evident. The lower energy of the hydroxy-quinoline form is related to the presence of an intramolecular H-bond interaction, O–H···O(ester carbonyl), and to the highest aromatic character exhibited by the heterocyclic ring of quinoline in the enol form. When evaluating compound without a 3-ester group (**92** series), the keto form was considered as the most stable form but the energy barriers between the 4-hydroxy-quinoline and 4-oxo-quinoline forms were found to be relatively close together, so these tautomers can coexist and contribute to the equilibrium populations.

While the substitution pattern on the carbocyclic part of the quinolone bicyclic structure (7- or 5-substituted derivatives) does not appear to interfere with the lipophilicity/solubility profile within the range of compounds studied, tautomerism does interfere. The 4-hydroxy-quinoline forms appear more adequate from a bioavailability viewpoint but, on the other side, it is expected that the 4-oxo-quinoline 3-ester forms present a much better pharmacological profile as *P. falciparum* bc<sub>1</sub> inhibitors acting at the Q<sub>o</sub> site. However, the activity results showed that the 4-oxo-quinoline derivatives were only slightly more active than their 4-hydroxy-quinoline analogues.

These results may support the hypothesis of quinolone binding to another site (for example to Q<sub>i</sub> site). It was reported that some quinolones partially overcome the atovaquone resistance and, additionally, reports that selected 4(1H)-pyridones (with similar structure to quinolone derivative) bind to Q<sub>i</sub> site also came to light. The docking simulation performed during our studies demonstrated that the quinolones selected can bind at the Q<sub>i</sub> site, as observed for 4(1H)-pyridones. The quinolone core appears to be positioned to enable formation of key hydrogen bonds with the residues His201, Ser205 and Asp228.

2-Aryl quinolones were synthesized and tested against *M. tuberculosis*. The solubility liabilities demonstrated for quinolone **128** reflected in a poor pharmacokinetic

profile, which was solved through the synthesis of its acetate prodrug (compound **129**). Although promising, quinolone **130** demonstrated to be as active as isoniazid against *M. tuberculosis* and, therefore, synthesis of some derivatives should be considered, in view of identifying optimised leads. In general, **128** and **130** did not evidence inhibitory capacity towards cytochromes P450 isoforms, the exception being the CYP2C8 isoform (with strong and moderate inhibitory capacity observed for **128** and **130**, respectively).

Quinolone derivative **130** has activity close to isoniazid *versus M. tuberculosis* and, therefore, synthesis of some derivatives should be considered, in view of selecting analogues with improved properties for development.

## Conclusions

---

# *References*

---

## References



---

## References

---

- (1) *World Malaria Report 2014*; World Health Organization, 2014.
- (2) Poinar, G. *Syst. Parasitol.* 2005, 61 (1), 47–52.
- (3) Canali, S. *Med. Secoli* 2008, 20 (3), 827–846.
- (4) Centers for Disease Control Prevention - Malaria <http://www.cdc.gov/malaria> (accessed Jan 14, 2015).
- (5) Cox, F. E. *Parasit. Vectors* 2010, 3 (1), 5.
- (6) Sherman, I. W. *The Malaria Genome Projects: Promise, Progress, and Prospects*; World Scientific, 2012.
- (7) Holt, R. A.; Subramanian, G. M.; Halpern, A.; Sutton, G. G.; Charlab, R.; Nusskern, D. R.; Wincker, P.; Clark, A. G.; Ribeiro, J. M. C.; Wides, R.; Salzberg, S. L.; Loftus, B.; Yandell, M.; Majoros, W. H.; Rusch, D. B.; Lai, Z.; Kraft, C. L.; Abril, J. F.; Anthouard, V.; Arensburger, P.; Atkinson, P. W.; Baden, H.; de Berardinis, V.; Baldwin, D.; Benes, V.; Biedler, J.; Blass, C.; Bolanos, R.; Boscus, D.; Barnstead, M.; Cai, S.; Center, A.; Chaturverdi, K.; Christophides, G. K.; Chrystal, M. A.; Clamp, M.; Cravchik, A.; Curwen, V.; Dana, A.; Delcher, A.; Dew, I.; Evans, C. A.; Flanigan, M.; Grundschober-Freimoser, A.; Friedli, L.; Gu, Z.; Guan, P.; Guigo, R.; Hillenmeyer, M. E.; Hladun, S. L.; Hogan, J. R.; Hong, Y. S.; Hoover, J.; Jaillon, O.; Ke, Z.; Kodira, C.; Kokoza, E.; Koutsos, A.; Letunic, I.; Levitsky, A.; Liang, Y.; Lin, J.-J.; Lobo, N. F.; Lopez, J. R.; Malek, J. A.; McIntosh, T. C.; Meister, S.; Miller, J.; Mobarry, C.; Mongin, E.; Murphy, S. D.; O’Brochta, D. A.; Pfannkoch, C.; Qi, R.; Regier, M. A.; Remington, K.; Shao, H.; Sharakhova, M. V.; Sitter, C. D.; Shetty, J.; Smith, T. J.; Strong, R.; Sun, J.; Thomasova, D.; Ton, L. Q.; Topalis, P.; Tu, Z.; Unger, M. F.; Walenz, B.; Wang, A.; Wang, J.; Wang, M.; Wang, X.; Woodford, K. J.; Wortman, J. R.; Wu, M.; Yao, A.; Zdobnov, E. M.; Zhang, H.; Zhao, Q.; Zhao, S.; Zhu, S. C.; Zhimulev, I.; Coluzzi, M.; della Torre, A.; Roth, C. W.; Louis, C.; Kalush, F.; Mural, R. J.; Myers, E. W.; Adams, M. D.; Smith, H. O.; Broder, S.; Gardner, M. J.; Fraser, C. M.; Birney, E.; Bork, P.; Brey, P. T.; Venter, J. C.; Weissenbach, J.; Kafatos, F. C.; Collins, F. H.; Hoffman, S. L. *Science* 2002, 298 (5591), 129–149.
- (8) Gardner, M. J.; Hall, N.; Fung, E.; White, O.; Berriman, M.; Hyman, R. W.; Carlton, J. M.; Pain, A.; Nelson, K. E.; Bowman, S.; Paulsen, I. T.; James, K.; Eisen, J. A.; Rutherford, K.; Salzberg, S. L.; Craig, A.; Kyes, S.; Chan, M.-S.; Nene, V.; Shallom, S. J.; Suh, B.; Peterson, J.; Angiuoli, S.; Pertea, M.; Allen, J.; Selengut, J.; Haft, D.; Mather, M. W.; Vaidya, A. B.; Martin, D. M. A.; Fairlamb, A. H.; Fraunholz, M. J.; Roos, D. S.; Ralph, S. A.; McFadden, G. I.; Cummings, L. M.; Subramanian, G. M.; Mungall, C.; Venter, J. C.; Carucci, D. J.; Hoffman, S. L.; Newbold, C.; Davis, R. W.; Fraser, C. M.; Barrell, B. *Nature* 2002, 419 (6906), 498–511.
- (9) Carlton, J. M.; Adams, J. H.; Silva, J. C.; Bidwell, S. L.; Lorenzi, H.; Caler, E.; Crabtree, J.; Angiuoli, S. V.; Merino, E. F.; Amedeo, P.; Cheng, Q.; Coulson, R. M. R.; Crabb, B. S.; Del Portillo, H. A.; Essien, K.; Feldblyum, T. V.; Fernandez-Becerra, C.; Gilson, P. R.; Gueye, A. H.; Guo, X.; Kang’a, S.; Kooij, T. W. A.; Korsinczky, M.; Meyer, E. V.-S.; Nene, V.; Paulsen, I.; White, O.; Ralph, S. A.; Ren, Q.; Sargeant, T. J.; Salzberg, S. L.; Stoeckert, C. J.; Sullivan, S. A.; Yamamoto, M. M.; Hoffman, S. L.; Wortman, J. R.; Gardner, M. J.; Galinski, M. R.; Barnwell, J. W.; Fraser-Liggett, C. M. *Nature* 2008, 455 (7214), 757–763.
- (10) Sachs, J.; Malaney, P. *Nature* 2002, 415 (6872), 680–685.
- (11) Shetty, N.; Tang, J. W.; Andrews, J. *Infectious Disease: Pathogenesis, Prevention and Case Studies*; John Wiley & Sons, 2009.
- (12) Satoskar, A. R.; Simon, G.; Hotez, P. J.; Tsuji, M. *Medical Parasitology*; Landes

## References

- Bioscience, 2009.
- (13) Kats, L. M.; Black, C. G.; Proellocks, N. I.; Coppel, R. L. *Trends Parasitol.* 2006, 22 (6), 269–276.
- (14) Leventhal, R.; Cheadle, R. F. *Medical Parasitology: A Self-instructional Text*, 6th ed.; F.A. Davis Company, 2012.
- (15) Pasvol, G. *Nat. Genet.* 2010, 42 (4), 284–285.
- (16) Alam, A. *Interdiscip. Perspect. Infect. Dis.* 2014, 2014, 453186.
- (17) Costa, M. da S.; Kiralj, R.; Ferreira, M. M. C. *Quim. Nova* 2007, 30 (1), 25–31.
- (18) Sturm, A.; Amino, R.; van de Sand, C.; Regen, T.; Retzlaff, S.; Renneberg, A.; Krueger, A.; Pollok, J.-M.; Menard, R.; Heussler, V. T. *Science* 2006, 313 (5791), 1287–1290.
- (19) Malaguarnera, L.; Musumeci, S. *Lancet Infect. Dis.* 2002, 2 (8), 472–478.
- (20) Kumar, V.; Abbas, A. K.; Aster, J. C. *Robbins Basic Pathology*, 9th ed.; Elsevier Health Sciences, 2012.
- (21) *Martindale: The Complete Drug Reference*, 36th ed.; Sweetman, Sean C. (BPharm, Frp., Ed.); Pharmaceutical Press, 2009.
- (22) Goodman, L. S. *Goodman and Gilman Manual of Pharmacology and Therapeutics*, 2nd ed.; McGraw Hill Professional, 2013.
- (23) Katzung, B.; Masters, S.; Trevor, A. *Basic and Clinical Pharmacology*, 11th ed.; McGraw Hill Professional, 2009.
- (24) Ridley, R. G. *Nature* 2002, 415 (6872), 686–693.
- (25) *Antimalarial Chemotherapy - Mechanisms of Action, Resistance, and New Directions in Drug Discovery*; Rosenthal, P. J., Ed.; Springer Science & Business Media, 2001.
- (26) Bray, P. G.; Martin, R. E.; Tilley, L.; Ward, S. A.; Kirk, K.; Fidock, D. A. *Mol. Microbiol.* 2005, 56 (2), 323–333.
- (27) Ehrhardt, S.; Meyer, C. G. *Ther. Clin. Risk Manag.* 2009, 5, 805–815.
- (28) Nzila, A.; Ward, S. A.; Marsh, K.; Sims, P. F. G.; Hyde, J. E. *Trends Parasitol.* 2005, 21 (7), 334–339.
- (29) Martinelli, A.; Henriques, G.; Cravo, P.; Hunt, P. *Int. J. Parasitol.* 2011, 41 (2), 165–171.
- (30) Cortes, S.; Albuquerque, A.; Cabral, L. I. L.; Lopes, L.; Campino, L.; Cristiano, M. L. S. *Antimicrob. Agents Chemother.* 2015, 59 (8), 5032–5035.
- (31) Njuguna, N. M.; Ongarora, D. S. B.; Chibale, K. *Expert Opin. Ther. Pat.* 2012, 22 (10), 1179–1203.
- (32) Acton, N.; Roth, R. J. *J. Org. Chem.* 1992, 57 (13), 3610–3614.
- (33) Yadav, N.; Sharma, C.; Awasthi, S. K. *RSC Adv.* 2014, 4 (11), 5469.
- (34) ClinicalTrials.gov <https://clinicaltrials.gov/ct2/> (accessed May 26, 2015).
- (35) Charman, S. A.; Arbe-Barnes, S.; Bathurst, I. C.; Brun, R.; Campbell, M.; Charman, W. N.; Chiu, F. C. K.; Chollet, J.; Craft, J. C.; Creek, D. J.; Dong, Y.; Matile, H.; Maurer, M.; Morizzi, J.; Nguyen, T.; Papastogiannidis, P.; Scheurer, C.; Shackelford, D. M.; Sriraghavan, K.; Stingelin, L.; Tang, Y.; Urwyler, H.; Wang, X.; White, K. L.; Wittlin, S.; Zhou, L.; Vennerstrom, J. L. *Proc. Natl. Acad. Sci. U. S. A.* 2011, 108 (11), 4400–4405.
- (36) Valecha, N.; Looareesuwan, S.; Martensson, A.; Abdulla, S. M.; Krudsood, S.; Tangpukdee, N.; Mohanty, S.; Mishra, S. K.; Tyagi, P. K.; Sharma, S. K.; Moehrle, J.; Gautam, A.; Roy, A.; Paliwal, J. K.; Kothari, M.; Saha, N.; Dash, A. P.; Björkman, A. *Clin. Infect. Dis.* 2010, 51 (6), 684–691.
- (37) O'Neill, P. M.; Barton, V. E.; Ward, S. A. *Molecules* 2010, 15 (3), 1705–1721.
- (38) Pandey, K. C.; Wang, S. X.; Sijwali, P. S.; Lau, A. L.; McKerrow, J. H.; Rosenthal, P. J. *Proc. Natl. Acad. Sci. U. S. A.* 2005, 102 (26), 9138–9143.
- (39) Wyatt, D. M.; Berry, C. *FEBS Lett.* 2002, 513 (2-3), 159–162.
- (40) Banerjee, R.; Liu, J.; Beatty, W.; Pelosof, L.; Klemba, M.; Goldberg, D. E. *Proc. Natl. Acad. Sci.* 2002, 99 (2), 990–995.
- (41) Gero, A. M.; Weis, A. L. 2001, 367–384.
- (42) Wengelnik, K.; Vidal, V.; Ancelin, M. L.; Cathiard, A.-M.; Morgat, J. L.; Kocken, C. H.; Calas, M.; Herrera, S.; Thomas, A. W.; Vial, H. J. *Science* 2002, 295 (5558), 1311–1314.
- (43) Perozzo, R.; Kuo, M.; Sidhu, A. bir S.; Valiyaveetil, J. T.; Bittman, R.; Jacobs, W. R.; Fidock, D. A.; Sacchettini, J. C. *J. Biol. Chem.* 2002, 277 (15), 13106–13114.

- (44) Eastman, R. T.; Buckner, F. S.; Yokoyama, K.; Gelb, M. H.; Van Voorhis, W. C. *J. Lipid Res.* 2006, 47 (2), 233–240.
- (45) Banumathy, G.; Singh, V.; Pavithra, S. R.; Tatu, U. *J. Biol. Chem.* 2003, 278 (20), 18336–18345.
- (46) Péroval, M.; Péry, P.; Labbé, M. *Int. J. Parasitol.* 2006, 36 (10-11), 1205–1215.
- (47) Woodard, C. L.; Li, Z.; Kathcart, A. K.; Terrell, J.; Gerena, L.; Lopez-Sanchez, M.; Kyle, D. E.; Bhattacharjee, A. K.; Nichols, D. A.; Ellis, W.; Prigge, S. T.; Geyer, J. A.; Waters, N. C. *J. Med. Chem.* 2003, 46 (18), 3877–3882.
- (48) Cameron, A.; Read, J.; Tranter, R.; Winter, V. J.; Sessions, R. B.; Brady, R. L.; Vivas, L.; Easton, A.; Kendrick, H.; Croft, S. L.; Barros, D.; Lavandera, J. L.; Martin, J. J.; Risco, F.; García-Ochoa, S.; Gamo, F. J.; Sanz, L.; Leon, L.; Ruiz, J. R.; Gabarró, R.; Mallo, A.; Gómez de las Heras, F. *J. Biol. Chem.* 2004, 279 (30), 31429–31439.
- (49) Martin, W.; Müller, M. *Nature* 1998, 392 (6671), 37–41.
- (50) Painter, H. J.; Morrissey, J. M.; Mather, M. W.; Vaidya, A. B. *Nature* 2007, 446 (7131), 88–91.
- (51) Embley, T. M.; Martin, W. *Nature* 2006, 440 (7084), 623–630.
- (52) Nagy, M.; Lacroute, F.; Thomas, D. *Proc. Natl. Acad. Sci. U. S. A.* 1992, 89 (19), 8966–8970.
- (53) Vaidya, A. B.; Mather, M. W. *Annu. Rev. Microbiol.* 2009, 63, 249–267.
- (54) Rodrigues, T.; Lopes, F.; Moreira, R. *Curr. Med. Chem.* 2010, 17 (10), 929–956.
- (55) Nixon, G. L.; Pidathala, C.; Shone, A. E.; Antoine, T.; Fisher, N.; O'Neill, P. M.; Ward, S. A.; Biagini, G. A. *Future Med. Chem.* 2013, 5 (13), 1573–1591.
- (56) Takeo, S.; Kokaze, A.; Ng, C. S.; Mizuchi, D.; Watanabe, J.; Tanabe, K.; Kojima, S.; Kita, K. *Mol. Biochem. Parasitol.* 2000, 107 (2), 191–205.
- (57) Ke, H.; Morrissey, J. M.; Ganesan, S. M.; Painter, H. J.; Mather, M. W.; Vaidya, A. B. *Eukaryot. Cell* 2011, 10 (8), 1053–1061.
- (58) Wrenger, C.; Müller, I. B.; Butzloff, S.; Jordanova, R.; Lunev, S.; Groves, M. R. *Acta Crystallogr. Sect. F. Struct. Biol. Cryst. Commun.* 2012, 68 (Pt 6), 659–662.
- (59) Biagini, G. A.; Viriyavejakul, P.; O'Neill, P. M.; Bray, P. G.; Ward, S. A. *Antimicrob. Agents Chemother.* 2006, 50 (5), 1841–1851.
- (60) Fisher, N.; Bray, P. G.; Ward, S. A.; Biagini, G. A. *Trends Parasitol.* 2007, 23 (7), 305–310.
- (61) Fisher, N.; Warman, A. J.; Ward, S. A.; Biagini, G. A. *Type II NADH: quinone oxidoreductases of Plasmodium falciparum and Mycobacterium tuberculosis kinetic and high-throughput assays.*; 2009; Vol. 456.
- (62) Mráček, T.; Drahotka, Z.; Houštěk, J. *Biochim. Biophys. Acta* 2013, 1827 (3), 401–410.
- (63) Ou, X.; Ji, C.; Han, X.; Zhao, X.; Li, X.; Mao, Y.; Wong, L.-L.; Bartlam, M.; Rao, Z. *J. Mol. Biol.* 2006, 357 (3), 858–869.
- (64) Brandt, U.; Trumpower, B. *Crit. Rev. Biochem. Mol. Biol.* 1994, 29 (3), 165–197.
- (65) Solmaz, S. R. N.; Hunte, C. *J. Biol. Chem.* 2008, 283 (25), 17542–17549.
- (66) Zara, V.; Conte, L.; Trumpower, B. L. *FEBS J.* 2009, 276 (7), 1900–1914.
- (67) Gao, X.; Wen, X.; Esser, L.; Quinn, B.; Yu, L.; Yu, C.-A.; Xia, D. *Biochemistry* 2003, 42 (30), 9067–9080.
- (68) Mitchell, P. *FEBS Lett.* 1975, 59 (2), 137–139.
- (69) Link, T. A.; Haase, U.; Brandt, U.; von Jagow, G. *J. Bioenerg. Biomembr.* 1993, 25 (3), 221–232.
- (70) Trumpower, B. L. *J. Biol. Chem.* 1990, 265 (20), 11409–11412.
- (71) Hunte, C.; Palsdottir, H.; Trumpower, B. L. *FEBS Lett.* 2003, 545 (1), 39–46.
- (72) Fisher, N.; Meunier, B. *FEMS Yeast Res.* 2008, 8 (2), 183–192.
- (73) Barton, V.; Fisher, N.; Biagini, G. A.; Ward, S. A.; O'Neill, P. M. *Curr. Opin. Chem. Biol.* 2010, 14 (4), 440–446.
- (74) Brasseur, G.; Saribaş, A. S.; Daldal, F. *Biochim. Biophys. Acta - Bioenerg.* 1996, 1275 (1-2), 61–69.
- (75) Link, T. A.; Iwata, M.; Björkman, J.; Spoel, D.; Stocker, A.; Iwata, S. In *Chemistry of Crop Protection: Progress and Prospects in Science and Regulation*; Voss, G., Ramos,

## References

- G., Eds.; Wiley-VCH Verlag GmbH & Co. KGaA: Weinheim, FRG, 2002; pp 110–127.
- (76) Esser, L.; Quinn, B.; Li, Y.-F.; Zhang, M.; Elberry, M.; Yu, L.; Yu, C.-A.; Xia, D. *J. Mol. Biol.* 2004, *341* (1), 281–302.
- (77) Mather, M. W.; Darrouzet, E.; Valkova-Valchanova, M.; Cooley, J. W.; McIntosh, M. T.; Daldal, F.; Vaidya, A. B. *J. Biol. Chem.* 2005, *280* (29), 27458–27465.
- (78) Bulusu, V.; Jayaraman, V.; Balaram, H. *J. Biol. Chem.* 2011, *286* (11), 9236–9245.
- (79) Fieser, L. F.; Berliner, E.; Bondhus, F. J.; Chang, F. C.; Dauben, W. G.; Ettliger, M. G.; Fawaz, G.; Fields, M.; Fieser, M.; Heidelberger, C.; Heymann, H.; Seligman, A. M.; Vaughan, W. R.; Wilson, A. G.; Wilson, E.; Wu, M.; Leffler, M. T.; Hamlin, K. E.; Hathaway, R. J.; Matson, E. J.; Moore, E. E.; Moore, M. B.; Rapala, R. T.; Zaugg, H. E. *J. Am. Chem. Soc.* 1948, *70* (10), 3151–3155.
- (80) Nixon, G. L.; Moss, D. M.; Shone, A. E.; Laloo, D. G.; Fisher, N.; O'Neill, P. M.; Ward, S. A.; Biagini, G. A. *J. Antimicrob. Chemother.* 2013, *68* (5), 977–985.
- (81) Fieser, L. F.; Heymann, H.; Seligman, A. M. *J. Pharmacol. Exp. Ther.* 1948, *94* (2), 112–124.
- (82) Biagini, G. A.; Fisher, N.; Shone, A. E.; Mubarak, M. A.; Srivastava, A.; Hill, A.; Antoine, T.; Warman, A. J.; Davies, J.; Pidathala, C.; Amewu, R. K.; Leung, S. C.; Sharma, R.; Gibbons, P.; Hong, D. W.; Pacorel, B.; Lawrenson, A. S.; Charoensutthivarakul, S.; Taylor, L.; Berger, O.; Mbekeani, A.; Stocks, P. A.; Nixon, G. L.; Chadwick, J.; Hemingway, J.; Delves, M. J.; Sinden, R. E.; Zeeman, A.-M.; Kocken, C. H. M.; Berry, N. G.; O'Neill, P. M.; Ward, S. A. *Proc. Natl. Acad. Sci. U. S. A.* 2012, *109* (21), 8298–8303.
- (83) Zsila, F.; Fitos, I. *Org. Biomol. Chem.* 2010, *8* (21), 4905–4914.
- (84) Cheung, T. W. *AIDS* 1999, *13* (14), 1984–1985.
- (85) Capper, M. J.; O'Neill, P. M.; Fisher, N.; Strange, R. W.; Moss, D.; Ward, S. A.; Berry, N. G.; Lawrenson, A. S.; Hasnain, S. S.; Biagini, G. A.; Antonyuk, S. V. *Proc. Natl. Acad. Sci.* 2015, *112* (3), 201416611.
- (86) Patel, S. N.; Kain, K. C. *Expert Rev. Anti. Infect. Ther.* 2005, *3* (6), 849–861.
- (87) Kessl, J. J.; Meshnick, S. R.; Trumpower, B. L. *Trends Parasitol.* 2007, *23* (10), 494–501.
- (88) Kessl, J. J.; Ha, K. H.; Merritt, A. K.; Lange, B. B.; Hill, P.; Meunier, B.; Meshnick, S. R.; Trumpower, B. L. *J. Biol. Chem.* 2005, *280* (17), 17142–17148.
- (89) Hughes, L. M.; Covian, R.; Gribble, G. W.; Trumpower, B. L. *Biochim. Biophys. Acta* 2010, *1797* (1), 38–43.
- (90) Kessl, J. J.; Lange, B. B.; Merbitz-Zahradnik, T.; Zwicker, K.; Hill, P.; Meunier, B.; Pálsdóttir, H.; Hunte, C.; Meshnick, S.; Trumpower, B. L. *J. Biol. Chem.* 2003, *278* (33), 31312–31318.
- (91) Peters, J. M.; Chen, N.; Gatton, M.; Korsinczky, M.; Fowler, E. V.; Manzetti, S.; Saul, A.; Cheng, Q. *Antimicrob. Agents Chemother.* 2002, *46* (8), 2435–2441.
- (92) Sutherland, C. J.; Laundry, M.; Price, N.; Burke, M.; Fivelman, Q. L.; Pasvol, G.; Klein, J. L.; Chiodini, P. L. *Malar. J.* 2008, *7* (1), 240.
- (93) Korsinczky, M.; Chen, N.; Kotecka, B.; Saul, A.; Rieckmann, K.; Cheng, Q. *Antimicrob. Agents Chemother.* 2000, *44* (8), 2100–2108.
- (94) Srivastava, I. K.; Morrissey, J. M.; Darrouzet, E.; Daldal, F.; Vaidya, A. B. *Mol. Microbiol.* 1999, *33* (4), 704–711.
- (95) Schwobel, B.; Alifrangis, M.; Salanti, A.; Jelinek, T. *Malar. J.* 2003, *2* (1), 5.
- (96) Fivelman, Q.; Butcher, G.; Adagu, I.; Warhurst, D.; Pasvol, G. *Malar. J.* 2002, *1* (1), 1.
- (97) Berry, A.; Senescau, A.; Lelièvre, J.; Benoit-Vical, F.; Fabre, R.; Marchou, B.; Magnaval, J. F. *Trans. R. Soc. Trop. Med. Hyg.* 2006, *100* (10), 986–988.
- (98) Beteck, R. M.; Smit, F. J.; Haynes, R. K.; N'Da, D. D. *Malar. J.* 2014, *13* (1), 339.
- (99) Teixeira, C.; Vale, N.; Pérez, B.; Gomes, A.; Gomes, J. R. B.; Gomes, P. *Chem. Rev.* 2014, *114* (22), 11164–11220.
- (100) El Hage, S.; Ane, M.; Stigliani, J.-L.; Marjorie, M.; Vial, H.; Baziard-Mouysset, G.; Payard, M. *Eur. J. Med. Chem.* 2009, *44* (11), 4778–4782.
- (101) Hughes, L. M.; Lanteri, C. A.; O'Neil, M. T.; Johnson, J. D.; Gribble, G. W.; Trumpower, B. L. *Mol. Biochem. Parasitol.* 2011, *177* (1), 12–19.

- (102) Xiang, H.; McSurdy-Freed, J.; Moorthy, G. S.; Hugger, E.; Bambal, R.; Han, C.; Ferrer, S.; Gargallo, D.; Davis, C. B. *J. Pharm. Sci.* 2006, *95* (12), 2657–2672.
- (103) Yeates, C. L.; Batchelor, J. F.; Capon, E. C.; Cheesman, N. J.; Fry, M.; Hudson, A. T.; Pudney, M.; Trimming, H.; Woolven, J.; Bueno, J. M.; Chicharro, J.; Fernández, E.; Fiandor, J. M.; Gargallo-Viola, D.; Gómez de las Heras, F.; Herreros, E.; León, M. L. *J. Med. Chem.* 2008, *51* (9), 2845–2852.
- (104) Dorn, A.; Scovill, J.; Ellis, W.; Matile, H.; Ridley, R.; Vennerstrom, J. *Am J Trop Med Hyg* 2001, *65* (1), 19–20.
- (105) Biagini, G. A.; Fisher, N.; Berry, N.; Stocks, P. A.; Meunier, B.; Williams, D. P.; Bonar-Law, R.; Bray, P. G.; Owen, A.; O'Neill, P. M.; Ward, S. A. *Mol. Pharmacol.* 2008, *73* (5), 1347–1355.
- (106) Winter, R. W.; Kelly, J. X.; Smilkstein, M. J.; Dodean, R.; Hinrichs, D.; Riscoe, M. K. *Exp. Parasitol.* 2008, *118* (4), 487–497.
- (107) Winter, R. W.; Kelly, J. X.; Smilkstein, M. J.; Dodean, R.; Bagby, G. C.; Rathbun, R. K.; Levin, J. I.; Hinrichs, D.; Riscoe, M. K. *Exp. Parasitol.* 2006, *114* (1), 47–56.
- (108) Kelly, J. X.; Smilkstein, M. J.; Brun, R.; Wittlin, S.; Cooper, R. A.; Lane, K. D.; Janowsky, A.; Johnson, R. A.; Dodean, R. A.; Winter, R.; Hinrichs, D. J.; Riscoe, M. K. *Nature* 2009, *459* (7244), 270–273.
- (109) Sissi, C.; Palumbo, M. *Curr. Med. Chem. Anticancer. Agents* 2003, *3* (6), 439–450.
- (110) Kim, O. K.; Ohemeng, K.; Barrett, J. F. *Expert Opin. Investig. Drugs* 2001, *10* (2), 199–212.
- (111) Nakamura, S.; Kozuka, M.; Bastow, K. F.; Tokuda, H.; Nishino, H.; Suzuki, M.; Tatsuzaki, J.; Morris Natschke, S. L.; Kuo, S.-C.; Lee, K.-H. *Bioorg. Med. Chem.* 2005, *13* (14), 4396–4401.
- (112) Tedesco, R.; Shaw, A. N.; Bambal, R.; Chai, D.; Concha, N. O.; Darcy, M. G.; Dhanak, D.; Fitch, D. M.; Gates, A.; Gerhardt, W. G.; Halegoua, D. L.; Han, C.; Hofmann, G. A.; Johnston, V. K.; Kaura, A. C.; Liu, N.; Keenan, R. M.; Lin-Goerke, J.; Sarisky, R. T.; Wiggall, K. J.; Zimmerman, M. N.; Duffy, K. J. *J. Med. Chem.* 2006, *49* (3), 971–983.
- (113) Kumar, D. V.; Rai, R.; Brameld, K. A.; Somoza, J. R.; Rajagopalan, R.; Janc, J. W.; Xia, Y. M.; Ton, T. L.; Shaghafi, M. B.; Hu, H.; Lehoux, I.; To, N.; Young, W. B.; Green, M. *J. Bioorg. Med. Chem. Lett.* 2011, *21* (1), 82–87.
- (114) Serrao, E.; Debnath, B.; Otake, H.; Kuang, Y.; Christ, F.; Debyser, Z.; Neamati, N. *J. Med. Chem.* 2013, *56* (6), 2311–2322.
- (115) Dorow, R. L.; Herrinton, P. M.; Hohler, R. A.; Maloney, M. T.; Mauragis, M. A.; McGhee, W. E.; Moeslein, J. A.; Strohbach, J. W.; Veley, M. F. *Org. Process Res. Dev.* 2006, *10* (3), 493–499.
- (116) Sultana, N.; Naz, A.; Khan, B.; Arayne, M. S.; Mesaik, M. A. *Med. Chem. Res.* 2009, *19* (9), 1210–1221.
- (117) Kathrotiya, H. G.; Patel, M. P. *Eur. J. Med. Chem.* 2013, *63*, 675–684.
- (118) Pidathala, C.; Amewu, R.; Pacorel, B.; Nixon, G. L.; Gibbons, P.; Hong, W. D.; Leung, S. C.; Berry, N. G.; Sharma, R.; Stocks, P. A.; Srivastava, A.; Shone, A. E.; Charoensutthivarakul, S.; Taylor, L.; Berger, O.; Mbekeani, A.; Hill, A.; Fisher, N. E.; Warman, A. J.; Biagini, G. A.; Ward, S. A.; O'Neill, P. M. *J. Med. Chem.* 2012, *55* (5), 1831–1843.
- (119) Leung, S. C.; Gibbons, P.; Amewu, R.; Nixon, G. L.; Pidathala, C.; Hong, W. D.; Pacorel, B.; Berry, N. G.; Sharma, R.; Stocks, P. A.; Srivastava, A.; Shone, A. E.; Charoensutthivarakul, S.; Taylor, L.; Berger, O.; Mbekeani, A.; Hill, A.; Fisher, N. E.; Warman, A. J.; Biagini, G. A.; Ward, S. A.; O'Neill, P. M. *J. Med. Chem.* 2012, *55* (5), 1844–1857.
- (120) Cowley, R.; Leung, S.; Fisher, N.; Al-Helal, M.; Berry, N. G.; Lawrenson, A. S.; Sharma, R.; Shone, A. E.; Ward, S. A.; Biagini, G. A.; O'Neill, P. M. *Medchemcomm* 2012, *3* (1), 39–44.
- (121) O'Donnell, J. A.; Gelone, S. P. *Infect. Dis. Clin. North Am.* 2000, *14* (2), 489–513.
- (122) Bisacchi, G. S. *J. Med. Chem.* 2015.
- (123) Divo, A. A.; Sartorelli, A. C.; Patton, C. L.; Bia, F. J. *Antimicrob. Agents Chemother.*

## References

- 1988, 32 (8), 1182–1186.
- (124) Watt, G.; Shanks, G. D.; Edstein, M. D.; Pavanand, K.; Webster, H. K.; Wechgritaya, S. *J. Infect. Dis.* 1991, 164 (3), 602–604.
- (125) McClean, K. L.; Hitchman, D.; Shafran, S. D. *J. Infect. Dis.* 1992, 165 (5), 904–907.
- (126) Salzer, W.; Timmler, H.; Andersag, H. *Chem. Ber.* 1948, 81 (1), 12–19.
- (127) Casey, A. C. 1974.
- (128) Ryley, J. F.; Peters, W. *Ann. Trop. Med. Parasitol.* 1970, 64 (2), 209–222.
- (129) Winter, R.; Kelly, J. X.; Smilkstein, M. J.; Hinrichs, D.; Koop, D. R.; Riscoe, M. K. *Exp. Parasitol.* 2011, 127 (2), 545–551.
- (130) Cross, R. M.; Monastyrskiy, A.; Mutka, T. S.; Burrows, J. N.; Kyle, D. E.; Manetsch, R. *J. Med. Chem.* 2010, 53 (19), 7076–7094.
- (131) Nilsen, A.; LaCrue, A. N.; White, K. L.; Forquer, I. P.; Cross, R. M.; Marfurt, J.; Mather, M. W.; Delves, M. J.; Shackelford, D. M.; Saenz, F. E.; Morrissey, J. M.; Steuten, J.; Mutka, T.; Li, Y.; Wirjanata, G.; Ryan, E.; Duffy, S.; Kelly, J. X.; Sebayang, B. F.; Zeeman, A.-M.; Noviyanti, R.; Sinden, R. E.; Kocken, C. H. M.; Price, R. N.; Avery, V. M.; Angulo-Barturen, I.; Jiménez-Díaz, M. B.; Ferrer, S.; Herreros, E.; Sanz, L. M.; Gamo, F.-J.; Bathurst, I.; Burrows, J. N.; Siegl, P.; Guy, R. K.; Winter, R. W.; Vaidya, A. B.; Charman, S. A.; Kyle, D. E.; Manetsch, R.; Riscoe, M. K. *Sci. Transl. Med.* 2013, 5 (177), 177ra37.
- (132) da Cruz, F. P.; Martin, C.; Buchholz, K.; Lafuente-Monasterio, M. J.; Rodrigues, T.; Sönnichsen, B.; Moreira, R.; Gamo, F.-J.; Marti, M.; Mota, M. M.; Hannus, M.; Prudêncio, M. *J. Infect. Dis.* 2012, 205 (8), 1278–1286.
- (133) Skraup, Z. H. *Monatshefte für Chemie - Chem. Mon.* 1880, 1 (1), 316–318.
- (134) Edinger, A. *Berichte der Dtsch. Chem. Gesellschaft* 1896, 29 (3), 2456–2460.
- (135) Friedländer, P.; Gohring, C. F. *Berichte der Dtsch. Chem. Gesellschaft* 1883, 16 (2), 1833–1839.
- (136) Doebner, O.; v. Miller, W. *Berichte der Dtsch. Chem. Gesellschaft* 1881, 14 (2), 2812–2817.
- (137) Pfitzinger, W. *J. für Prakt. Chemie* 1886, 33 (1), 100–100.
- (138) Povarov, L. S. *Russ. Chem. Rev.* 1967, 36 (9), 656–670.
- (139) Tois, J.; Vahermo, M.; Koskinen, A. *Tetrahedron Lett.* 2005, 46 (5), 735–737.
- (140) Mitsos, C.; Zografos, A.; Igglessi-Markopoulou, O. *Chem. Pharm. Bull. (Tokyo)*. 2000, 48 (2), 211–214.
- (141) Camps, R. *Berichte der Dtsch. Chem. Gesellschaft* 1899, 32 (3), 3228–3234.
- (142) Niementowski, S. *Berichte der Dtsch. Chem. Gesellschaft* 1894, 27 (2), 1394–1403.
- (143) Stern, E.; Millet, R.; Depreux, P.; Hénichart, J.-P. *Tetrahedron Lett.* 2004, 45 (50), 9257–9259.
- (144) Conrad, M.; Limpach, L. *Berichte der Dtsch. Chem. Gesellschaft* 1887, 20 (1), 944–948.
- (145) Boteva, A. A.; Krasnykh, O. P. *Chem. Heterocycl. Compd.* 2009, 45 (7), 757–785.
- (146) Zilberberg, I.; Pelmeshikov, A.; Mcgrath, C. J.; Davis, W.; Leszczynska, D.; Leszczynski, J. *Int. J. Mol. Sci.* 2002, 3 (7), 801–813.
- (147) Hudlicky, M. *Reductions in Organic Chemistry*, Ellis Horw.; 1984.
- (148) Agrawal, A.; Tratnyek, P. G. *Environ. Sci. Technol.* 1996, 30 (1), 153–160.
- (149) Gould, R. G.; Jacobs, W. A. *J. Am. Chem. Soc.* 1939, 61 (10), 2890–2895.
- (150) Stadlbauer, W.; Badawey, E.-S.; Hojas, G.; Roschger, P.; Kappe, T. *Molecules* 2001, 6 (4), 338–352.
- (151) Hubbard, P.; Brittain, W. J. *J. Org. Chem.* 1998, 63 (3), 677–683.
- (152) Williamson, A. *Philos. Mag. Ser. 3* 1850, 37 (251), 350–356.
- (153) Vollhardt, K. P. C.; Schore, N. E. *Organic Chemistry*, 6th ed.; W. H. Freeman, 2010.
- (154) Brigas, A. F.; Fonseca, C. S. C.; Johnstone, R. A. W. *J. Chem. Res.* 2002, No. 6, 2.
- (155) Horta, P. C.; Henriques, M. S. C.; Kuş, N.; Paixão, J. a.; O'Neill, P. M.; Cristiano, M. L. S.; Fausto, R. *Tetrahedron* 2015, 71 (40), 7583–7592.
- (156) Henry, R. A.; Finnegan, W. G. *J. Am. Chem. Soc.* 1954, 76 (3), 923–926.
- (157) Ismael, A.; Paixão, J. A.; Fausto, R.; Cristiano, M. L. S. *J. Mol. Struct.* 2012, 1023, 128–142.

- (158) Guram, A. S.; Buchwald, S. L. *J. Am. Chem. Soc.* 1994, *116* (17), 7901–7902.
- (159) Paul, F.; Patt, J.; Hartwig, J. F. *J. Am. Chem. Soc.* 1994, *116* (13), 5969–5970.
- (160) Miyaura, N.; Yamada, K.; Suzuki, A. *Tetrahedron Lett.* 1979, *20* (36), 3437–3440.
- (161) Willard, A. K.; Smith, R. L.; Cragoe, E. J. *J. Org. Chem.* 1981, *46* (19), 3846–3852.
- (162) Horta, P.; Kuş, N.; Henriques, M. S. C.; Paixão, J. A.; Coelho, L.; Nogueira, F.; O'Neill, P. M.; Fausto, R.; Cristiano, M. L. S. *J. Org. Chem.* 2015.
- (163) Smith, M. B.; March, J. *March's Advanced Organic Chemistry: Reactions, Mechanisms, and Structure*; 2007.
- (164) Kruszewski, J.; Krygowski, T. M. *Tetrahedron Lett.* 1972, *13* (36), 3839–3842.
- (165) Krygowski, T. M. *J. Chem. Inf. Model.* 1993, *33* (1), 70–78.
- (166) Bird, C. W. *Tetrahedron* 1985, *41* (7), 1409–1414.
- (167) Reva, I. D.; Lopes Jesus, A. J.; Rosado, M. T. S.; Fausto, R.; Ermelinda Eusébio, M.; Redinha, J. S. *Phys. Chem. Chem. Phys.* 2006, *8* (45), 5339.
- (168) Lakhlifi, A.; Chabbi, H.; Dahoo, P. R.; Teffo, J. L. *Eur. Phys. J. D* 2000, *12* (3), 435–448.
- (169) Dubost, H.; Abouaf-Marguin, L. *Chem. Phys. Lett.* 1972, *17* (2), 269–273.
- (170) Raducu, V.; Gauthier-Roy, B.; Dahoo, R.; Abouaf-Marguin, L.; Langlet, J.; Caillet, J.; Allavena, M. *J. Chem. Phys.* 1996, *105* (22), 10092.
- (171) Kuş, N.; Breda, S.; Reva, I.; Tasal, E.; Ogretir, C.; Fausto, R. *Photochem. Photobiol.* 2007, *83* (5), 1237–1253.
- (172) Breda, S.; Reva, I.; Lapinski, L.; Fausto, R. *Phys. Chem. Chem. Phys.* 2004, *6* (5), 929.
- (173) Kuş, N.; Bayarı, S. H.; Fausto, R. *J. Phys. Chem. B* 2013, *117* (43), 13543–13555.
- (174) Kuş, N.; Reva, I.; Bayarı, S.; Fausto, R. *J. Mol. Struct.* 2012, *1007*, 88–94.
- (175) Yang, Y.; Gao, H. *Spectrochim. Acta. A. Mol. Biomol. Spectrosc.* 2013, *102*, 134–141.
- (176) Frisch, M. J.; Trucks, G. W.; Schlegel, H. B.; Scuseria, G. E.; Robb, M. A.; Cheeseman, J. R.; Scalmani, G.; Barone, V.; Mennucci, B.; Petersson, G. A.; Nakatsuji, H.; Caricato, M.; Li, X.; Hratchian, H. P.; Izmaylov, A. F.; Bloino, J.; Zheng, G.; Sonnenberg, J. L.; Hada, M.; Ehara, M.; Toyota, K.; Fukuda, R.; Hasegawa, J.; Ishida, M.; Nakajima, T.; Honda, Y.; Kitao, O.; Nakai, H.; Vreven, T.; Montgomery, J. A., Jr.; Peralta, J. E.; Ogliaro, F.; Bearpark, M.; Heyd, J. J.; Brothers, E.; Kudin, K. N.; Staroverov, V. N.; Kobayashi, R.; Normand, J.; Raghavachari, K.; Rendell, A.; Burant, J. C.; Iyengar, S. S.; Tomasi, J.; Cossi, M.; Rega, N.; Millam, J. M.; Klene, M.; Knox, J. E.; Cross, J. B.; Bakken, V.; Adamo, C.; Jaramillo, J.; Gomperts, R.; Stratmann, R. E.; Yazyev, O.; Austin, A. J.; Cammi, R.; Pomelli, C.; Ochterski, J. W.; Martin, R. L.; Morokuma, K.; Zakrzewski, V. G.; Voth, G. A.; Salvador, P.; Dannenberg, J. J.; Dapprich, S.; Daniels, A. D.; Farkas, O.; Foresman, J. B.; Ortiz, J. V.; Cioslowski, J.; Fox, D. J. *Gaussian 09, Revision A.02*; Gaussian, Inc.: Wallingford, CT, 2009.
- (177) Becke, A. D. *Phys. Rev. A* 1988, *38* (6), 3098–3100.
- (178) Lee, C.; Yang, W.; Parr, R. G. *Phys. Rev. B* 1988, *37* (2), 785–789.
- (179) Vosko, S. H.; Wilk, L.; Nusair, M. *Can. J. Phys.* 1980, *58* (8), 1200–1211.
- (180) Leeson, P. D.; Springthorpe, B. *Nat. Rev. Drug Discov.* 2007, *6* (11), 881–890.
- (181) Kubinyi, H. *Farmacolo. Sci.* 1979, *34* (3), 248–276.
- (182) Pliška, V.; Testa, B.; Waterbeemd, H. van de. *Lipophilicity in Drug Action and Toxicology*; John Wiley & Sons Ltd: New York, 1996.
- (183) Lipinski, C. A. *Drug Discov. Today. Technol.* 2004, *1* (4), 337–341.
- (184) Hammond, D. J.; Burchell, J. R.; Pudney, M. *Mol. Biochem. Parasitol.* 1985, *14* (1), 97–109.
- (185) Li, H.; Zhu, X.-L.; Yang, W.-C.; Yang, G.-F. *Chem. Biol. Drug Des.* 2014, *83* (1), 71–80.
- (186) Berry, E. A.; Huang, L.-S.; Lee, D.-W.; Daldal, F.; Nagai, K.; Minagawa, N. *Biochim. Biophys. Acta* 2010, *1797* (3), 360–370.
- (187) Cole, J. C.; Nissink, J. W. M.; Taylor, R. In *Virtual Screening in Drug Discovery*; Alvarez, J., Schoichet, B., Eds.; 2005; pp 379–415.
- (188) Verdonk, M. L.; Cole, J. C.; Hartshorn, M. J.; Murray, C. W.; Taylor, R. D. *Proteins* 2003, *52* (4), 609–623.
- (189) Verdonk, M. L.; Chessari, G.; Cole, J. C.; Hartshorn, M. J.; Murray, C. W.; Nissink, J. W. M.; Taylor, R. D.; Taylor, R. *J. Med. Chem.* 2005, *48* (20), 6504–6515.

## References

- (190) Friesner, R. A.; Banks, J. L.; Murphy, R. B.; Halgren, T. A.; Klicic, J. J.; Mainz, D. T.; Repasky, M. P.; Knoll, E. H.; Shelley, M.; Perry, J. K.; Shaw, D. E.; Francis, P.; Shenkin, P. S. *J. Med. Chem.* 2004, 47 (7), 1739–1749.
- (191) Cross, R. M.; Flanigan, D. L.; Monastyrskyi, A.; LaCrue, A. N.; Sáenz, F. E.; Maignan, J. R.; Mutka, T. S.; White, K. L.; Shackelford, D. M.; Bathurst, I.; Fronczek, F. R.; Wojtas, L.; Guida, W. C.; Charman, S. A.; Burrows, J. N.; Kyle, D. E.; Manetsch, R. *J. Med. Chem.* 2014, 57 (21), 8860–8879.
- (192) Shao, Y.; Molnar, L. F.; Jung, Y.; Kussmann, J.; Ochsenfeld, C.; Brown, S. T.; Gilbert, A. T. B.; Slipchenko, L. V.; Levchenko, S. V.; O'Neill, D. P.; DiStasio, R. A.; Lochan, R. C.; Wang, T.; Beran, G. J. O.; Besley, N. A.; Herbert, J. M.; Lin, C. Y.; Van Voorhis, T.; Chien, S. H.; Sodt, A.; Steele, R. P.; Rassolov, V. A.; Maslen, P. E.; Korambath, P. P.; Adamson, R. D.; Austin, B.; Baker, J.; Byrd, E. F. C.; Dachsel, H.; Doerksen, R. J.; Dreuw, A.; Dunietz, B. D.; Dutoi, A. D.; Furlani, T. R.; Gwaltney, S. R.; Heyden, A.; Hirata, S.; Hsu, C.-P.; Kedziora, G.; Khalliulin, R. Z.; Klunzinger, P.; Lee, A. M.; Lee, M. S.; Liang, W.; Lotan, I.; Nair, N.; Peters, B.; Proynov, E. I.; Pieniazek, P. A.; Rhee, Y. M.; Ritchie, J.; Rosta, E.; Sherrill, C. D.; Simmonett, A. C.; Subotnik, J. E.; Woodcock, H. L.; Zhang, W.; Bell, A. T.; Chakraborty, A. K.; Chipman, D. M.; Keil, F. J.; Warshel, A.; Hehre, W. J.; Schaefer, H. F.; Kong, J.; Krylov, A. I.; Gill, P. M. W.; Head-Gordon, M. *Phys. Chem. Chem. Phys.* 2006, 8 (27), 3172–3191.
- (193) Perola, E.; Walters, W. P.; Charifson, P. S. *Proteins* 2004, 56 (2), 235–249.
- (194) Wiwanitkit, V. *J. Vector Borne Dis.* 2006, 43 (4), 195–197.
- (195) Li, X.-X.; Zhou, X.-N. *Parasit. Vectors* 2013, 6 (1), 79.
- (196) Ballell, L.; Bates, R. H.; Young, R. J.; Alvarez-Gomez, D.; Alvarez-Ruiz, E.; Barroso, V.; Blanco, D.; Crespo, B.; Escribano, J.; González, R.; Lozano, S.; Huss, S.; Santos-Villarejo, A.; Martín-Plaza, J. J.; Mendoza, A.; Rebollo-Lopez, M. J.; Remuñan-Blanco, M.; Lavandera, J. L.; Pérez-Herran, E.; Gamo-Benito, F. J.; García-Bustos, J. F.; Barros, D.; Castro, J. P.; Cammack, N. *ChemMedChem* 2013, 8 (2), 313–321.
- (197) Gujadhur, R. K.; Bates, C. G.; Venkataraman, D. *Org. Lett.* 2001, 3 (26), 4315–4317.
- (198) Ma, D.; Cai, Q. *Org. Lett.* 2003, 5 (21), 3799–3802.
- (199) Gilman, H.; Jacoby, A. L. *J. Org. Chem.* 1938, 03 (2), 108–119.
- (200) Bailey, W. F.; Luderer, M. R.; Jordan, K. P. *J. Org. Chem.* 2006, 71 (7), 2825–2828.
- (201) Peet, N. P.; Sunder, S. *J. Org. Chem.* 1974, 39 (13), 1931–1935.
- (202) Button, K. M.; Gossage, R. A. *J. Heterocycl. Chem.* 2003, 40 (3), 513–517.
- (203) Shaabani, A.; Soleimani, E.; Badri, Z. *Synth. Commun.* 2007, 37 (4), 629–635.
- (204) Klumpp, D. A.; Rendy, R.; McElrea, A. *Tetrahedron Lett.* 2004, 45 (42), 7959–7961.
- (205) Zalibera, L.; Milata, V.; Ilavský, D. *Magn. Reson. Chem.* 1998, 36 (9), 681–684.



---

# *Appendix*

---

Appendix

---

## *Appendix – List of Figures and Tables*

---

<b>Figure S1</b> – Mass spectrum of ethyl 7-benzoyloxy-4-oxo-quinoline-3-carboxylate ( <b>13</b> ).....	243
<b>Figure S2</b> – <sup>1</sup> H-NMR spectrum of ethyl 7-benzoyloxy-4-oxo-quinoline-3-carboxylate ( <b>13</b> ) (400 MHz; D <sub>6</sub> -DMSO) and structural representation of the compound showing the chemical shifts (ppm) predicted for <sup>1</sup> H-NMR.....	243
<b>Figure S3</b> – <sup>13</sup> C-NMR spectrum of ethyl 7-benzoyloxy-4-oxo-quinoline-3-carboxylate ( <b>13</b> ) (101 MHz; D <sub>6</sub> -DMSO) and structural representation of the compound showing the chemical shifts (ppm) predicted for <sup>13</sup> C-NMR.....	244
<b>Figure S4</b> – <sup>1</sup> H-NMR spectra (range of chemical shifts for aromatic protons) of ethyl 7-benzothiazoloxo-4-oxo-quinoline-3-carboxylate ( <b>31</b> ) and Dowtherm A, superimposed (400 MHz; D <sub>6</sub> -DMSO). Structural representation of <b>31</b> showing the chemical shifts (ppm) predicted for <sup>1</sup> H-NMR.....	244
<b>Figure S5</b> – Mass spectrum (by EI) of ethyl 7-(1-phenyl-1H-diazirin-3-yl)oxy-4-oxo-quinoline-3-carboxylate ( <b>32b</b> ).....	245
<b>Figure S6</b> – <sup>13</sup> C-NMR spectrum (from 165 to 100 ppm) of ethyl 7-(1-phenyl-1H-diazirin-3-yl)oxy-4-oxo-quinoline-3-carboxylate ( <b>32b</b> ) (101 MHz; D <sub>6</sub> -DMSO). Structural representations of <b>32b</b> and <b>32c</b> showing the chemical shifts (ppm) predicted for <sup>13</sup> C-NMR.....	245
<b>Figure S7</b> – ORTEPII plot of ethyl 3-((3,4-difluorophenyl)amino)-2-((3,4-difluorophenyl)carbonyl)acrylate ( <b>44b</b> ), in the crystal (from single crystal XRD data).....	246
<b>Figure S8</b> – ORTEPII plot of 1,3-bis(3,4-difluorophenyl)urea ( <b>44c</b> ), in the crystal (from single crystal XRD data).....	246
<b>Figure S9</b> – Mass spectra of 1-methyl-5-aminotetrazole ( <b>52</b> ) and 2-methyl-5-aminotetrazole ( <b>53</b> ) with a representation of the fragmentation patterns.....	247
<b>Figure S10</b> – <sup>13</sup> C-NMR spectrum of the isomeric mixture of ethyl 7-methoxy-4-oxo-quinoline-3-carboxylate ( <b>84a</b> ) and ethyl 5-methoxy-4-oxo-quinoline-3-carboxylate ( <b>84b</b> ) (101 MHz; D <sub>6</sub> -DMSO). Structural representations of <b>84a</b> and <b>84b</b> showing the chemical shifts (ppm) predicted for <sup>13</sup> C-NMR.....	247
<b>Figure S11</b> - Calculated relaxed potential energy profiles for internal rotation around the C–O ester bond of <b>56</b> .....	249
<b>Figure S12</b> - Calculated relaxed potential energy profiles for internal rotation around the C–C bond connecting the ester substituent to the ring system of <b>56</b> .....	250
<b>Figure S13</b> - ORTEP drawing of <b>56</b> , showing the atom numbering scheme.....	254
<b>Figure S14</b> - Projection of the crystal structure along the c-axis, showing the molecular packing diagram, and along the a-axis.....	254
<b>Figure S15</b> - ORTEPII plot of ethyl 4-hydroxy-5-methyl quinolinium chloride 3-carboxylate ( <b>82b·HCl</b> ) in the crystal of the compound.....	255
<b>Figure S16</b> - <sup>1</sup> H-NMR spectrum of ethyl 7-methyl-4-oxo-quinoline-3-carboxylate ( <b>82a</b> ) (400 MHz; D <sub>6</sub> -DMSO). Atoms identification (A) and predicted chemical shifts (ppm) for <sup>1</sup> H-NMR (B).....	255
<b>Figure S17</b> - <sup>13</sup> C-NMR spectrum of ethyl 7-methyl-4-oxo-quinoline-3-carboxylate ( <b>82a</b> ) (101 MHz; D <sub>6</sub> -DMSO). Atoms identification (A) and predicted chemical shifts (ppm) for <sup>13</sup> C-NMR (B).....	256

## Appendix

<b>Figure S18</b> - $^1\text{H}$ -NMR spectrum of ethyl 7-methyl-4-oxo-quinoline-3-carboxylate ( <b>82a</b> ) (400 MHz; D-Chloroform) .....	256
<b>Figure S19</b> - $^1\text{H}$ -NMR spectrum of ethyl 4-hydroxy-5-methylquinoline-3-carboxylate ( <b>82b</b> ) (400 MHz; D <sub>6</sub> -DMSO). Atoms identification ( <b>A</b> ) and predicted chemical shifts (ppm) for $^1\text{H}$ -NMR ( <b>B</b> ) .....	257
<b>Figure S20</b> - $^{13}\text{C}$ -NMR spectrum of ethyl 4-hydroxy-5-methylquinoline-3-carboxylate ( <b>82b</b> ) (101 MHz; D <sub>6</sub> -DMSO). Atoms identification ( <b>A</b> ) and predicted chemical shifts (ppm) for $^{13}\text{C}$ -NMR ( <b>B</b> ) .....	257
<b>Figure S21</b> - $^1\text{H}$ -NMR spectrum of ethyl 4-hydroxy-5-methylquinoline-3-carboxylate ( <b>82b</b> ) (400 MHz; D-Chloroform) .....	258
<b>Figure S22</b> - Comparison of the calculated IR spectra of the most stable conformers of <b>82b</b> , <b>82c</b> and <b>82d</b> , with the experimental IR spectrum of compound <b>82b</b> , obtained in argon matrix (15 K) .....	261
<b>Table S1</b> - Assignment of the infrared spectra for matrix isolated <b>56</b> (15 K), as well as for the neat solid glassy state and crystalline compound .....	251
<b>Table S2</b> - Observed IR frequencies for <b>82b</b> in argon matrix (15 K) and B3LYP/6-311++G(d,p) calculated frequencies and IR intensities for conformers <b>82bI</b> and <b>82bII</b> .....	259

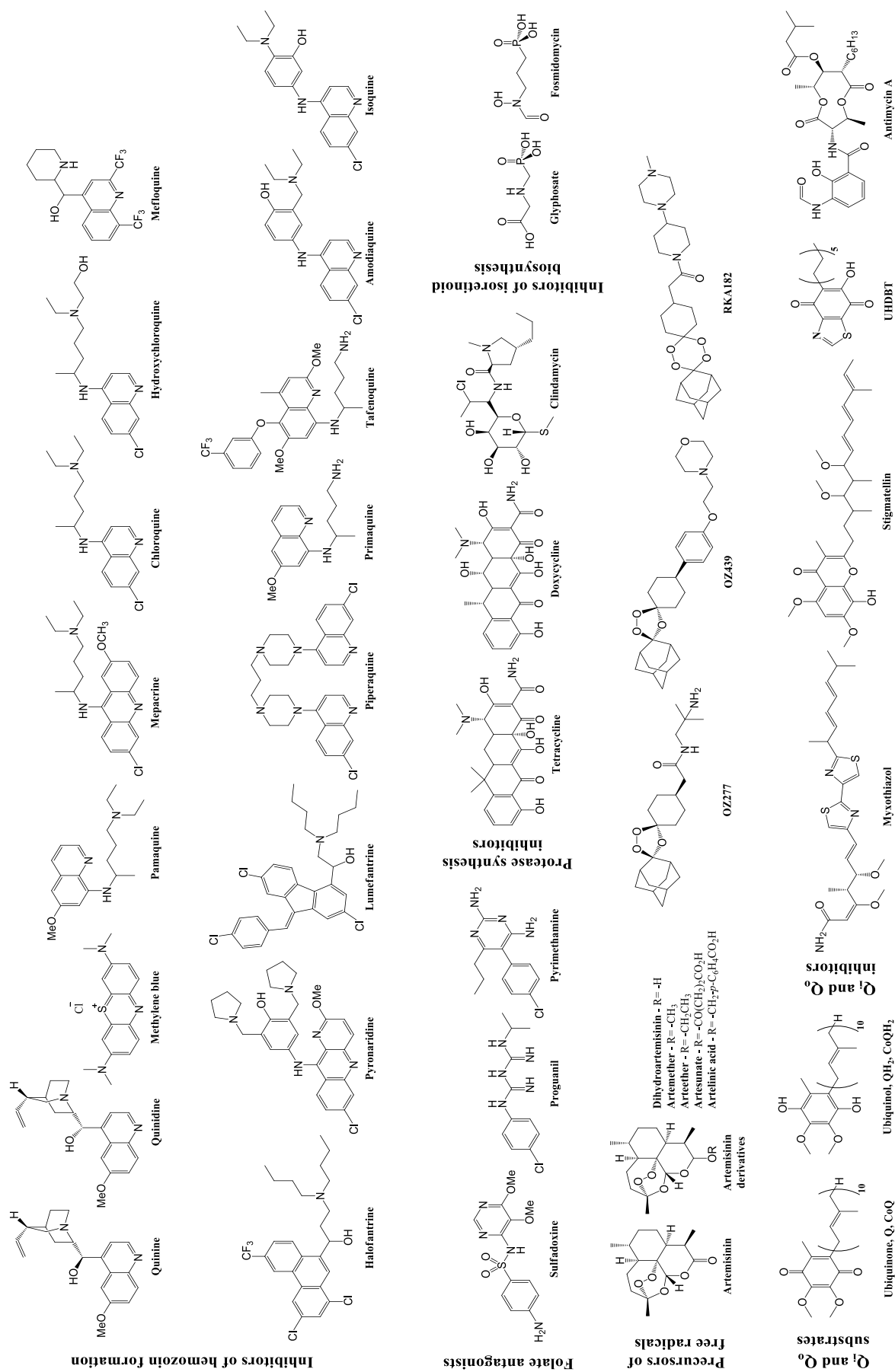
## Appendix 1 - Chemical structures

- Chapter one: Structural representation of chemotherapeutic agents; compounds mentioned in the section related to introduction and “*state of the art*” .....229
- Chapter two: Structural representation of compounds **1 – 92a** (mentioned in the section related to the synthesis of quinolones as potential antimalarials) .....233
- Chapter three: Structural representation of compounds **56, 82** and **92** and their derivatives and conformers (mentioned in the section related to structural investigations).....237
- Chapter four: Structural representation of quinolone derivatives evaluated for *in vitro* activity and by CLogP values; Structural representation of compound studied by docking simulations (**93 – 117**) .....239
- Chapter five: Structural representation of compounds **118 – 130** (mentioned in the section related to the synthesis of quinolones as potential antituberculosis agents).....241

Appendix

## Appendix 1 - Chemical structures

- Chapter one: Structural representation of chemotherapeutic agents; compounds mentioned in the section related to introduction and “state of the art”.

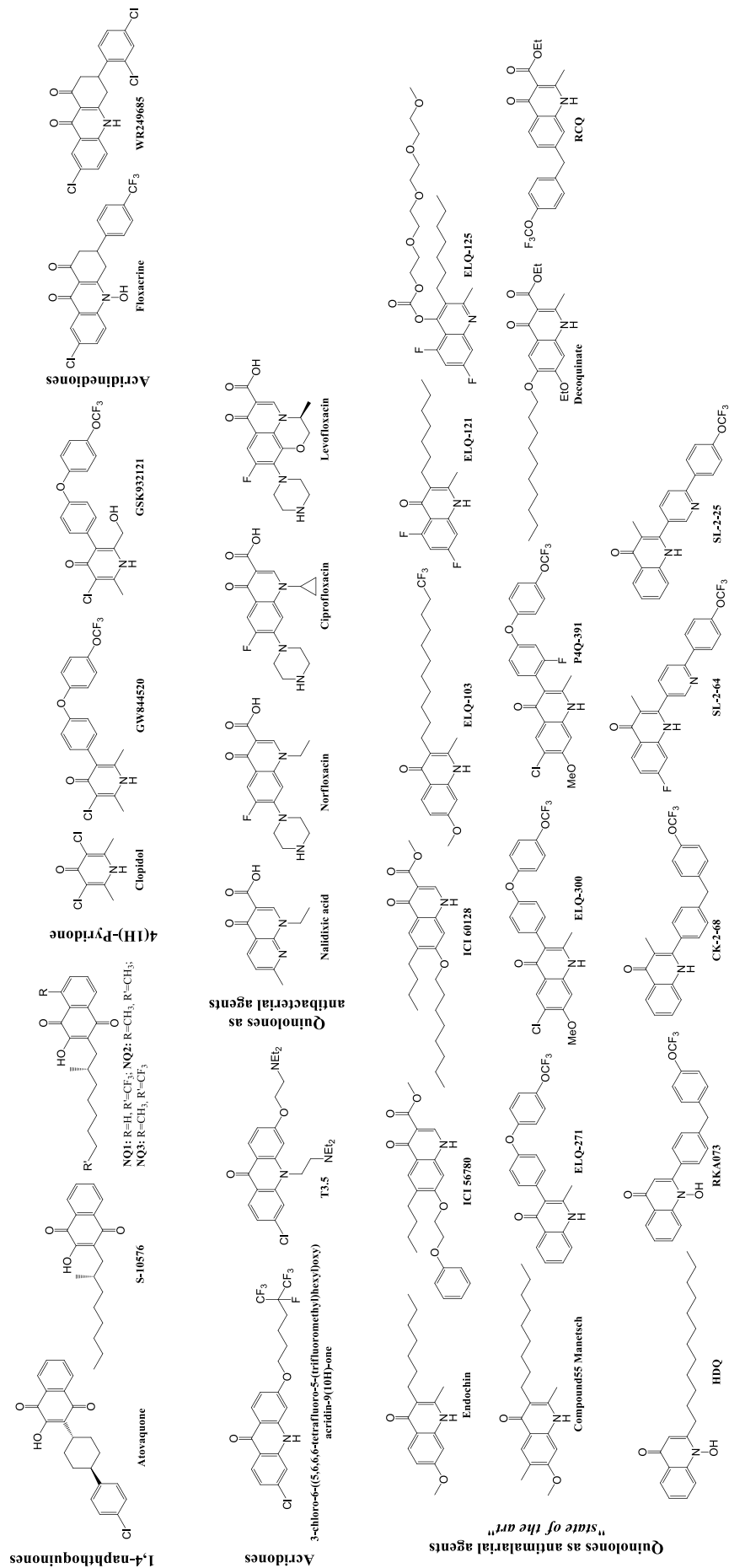


Appendix



## Appendix 1 - Chemical structures

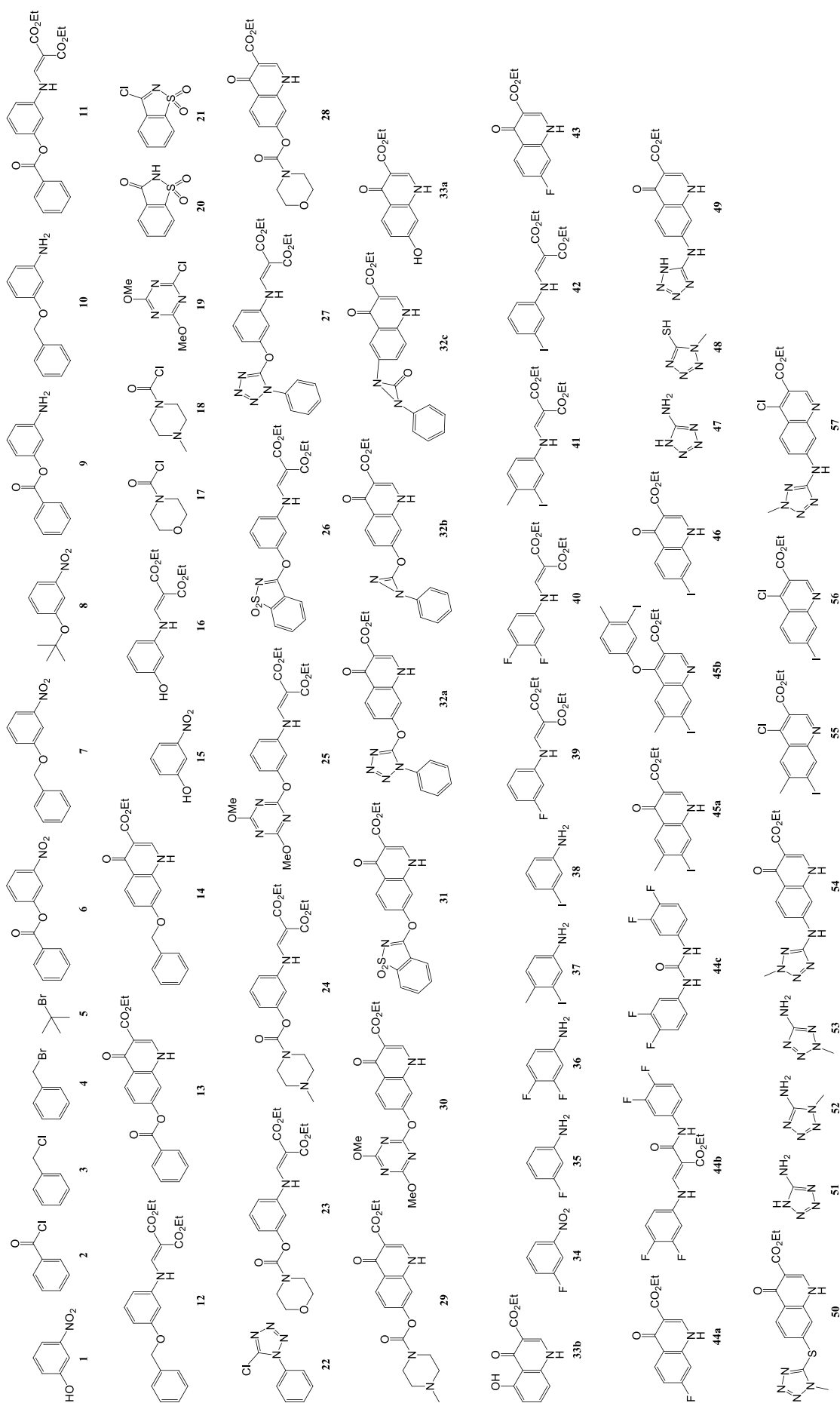
- Chapter one: Structural representation of chemotherapeutic agents; compounds mentioned in the section related to introduction and “state of the art”.



Appendix

## Appendix 1 - Chemical structures

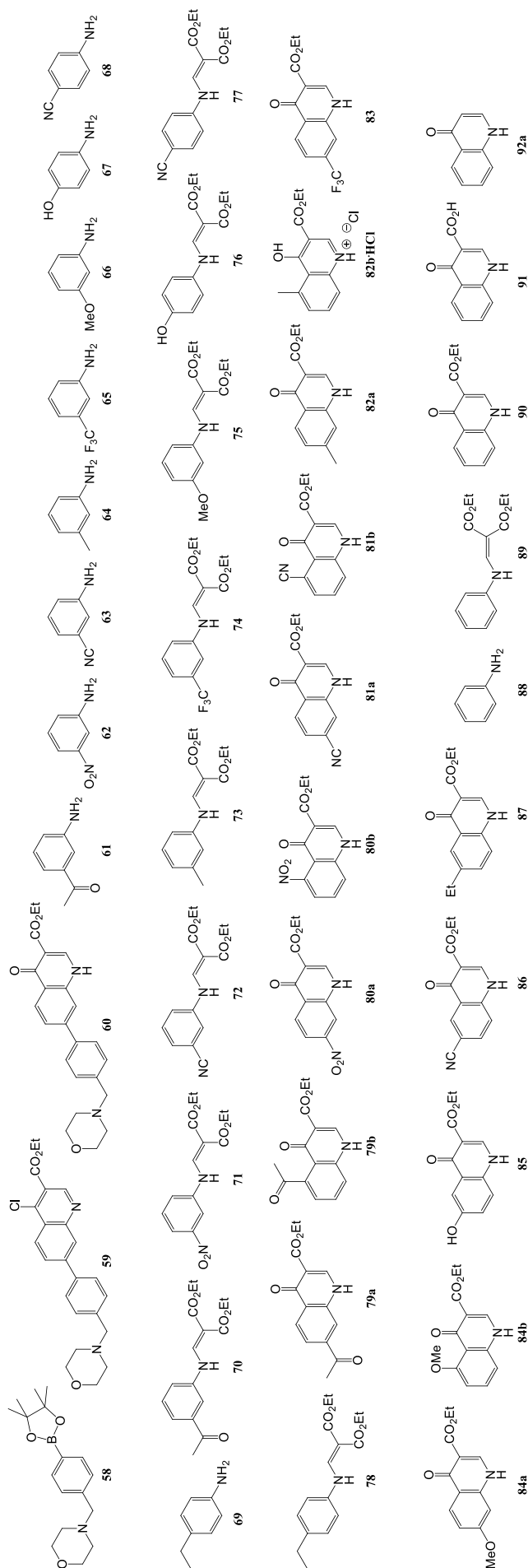
- Chapter two: Structural representation of compounds **1** – **92a** (mentioned in the section related to the synthesis of quinolones as potential antimicrobials).



Appendix

## Appendix 1 - Chemical structures

- Chapter two: Structural representation of compounds **1 – 92a** (mentioned in the section related to the synthesis of quinolones as potential antimicrobials).



Appendix

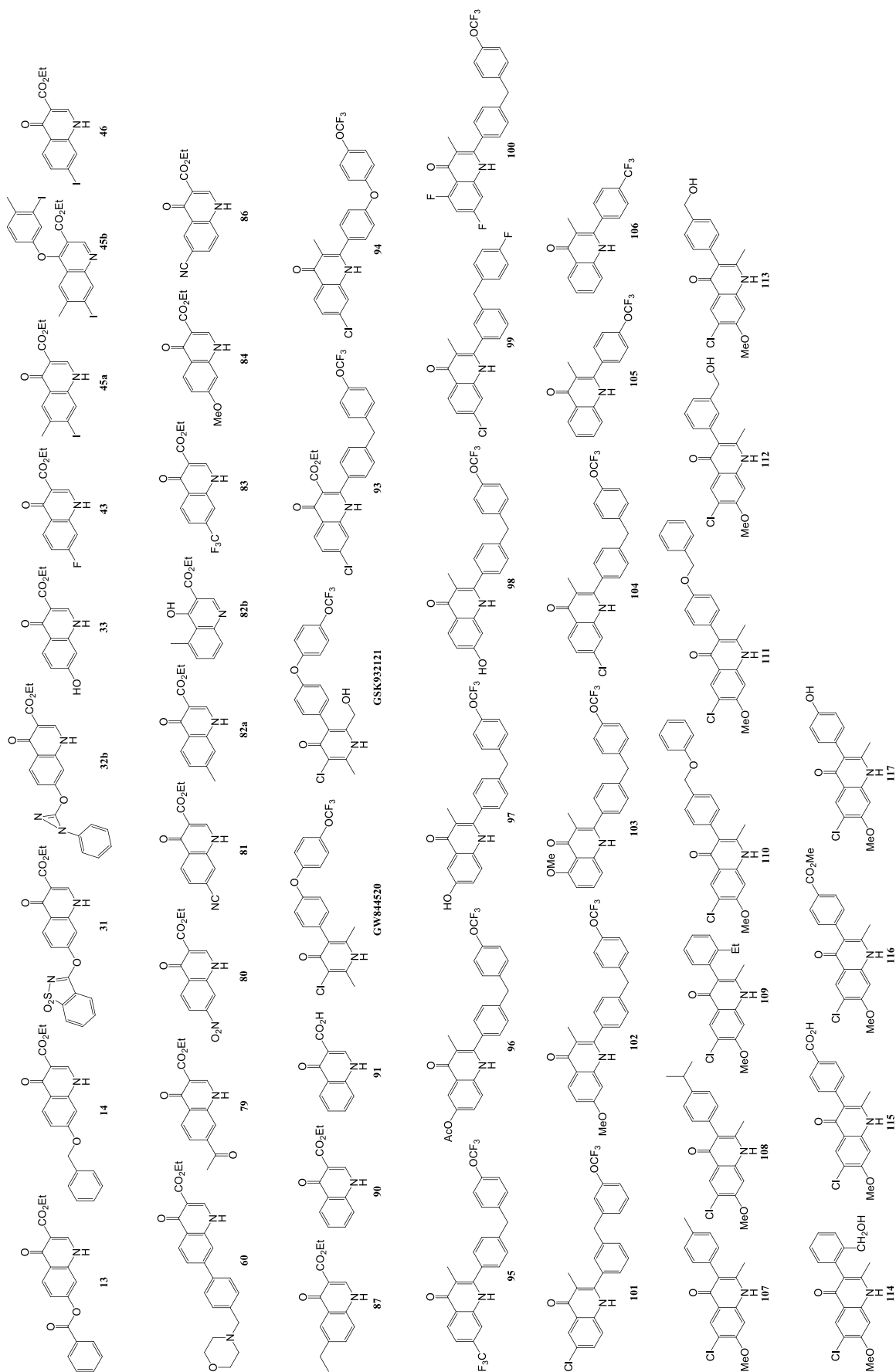


Appendix



## Appendix 1 - Chemical structures

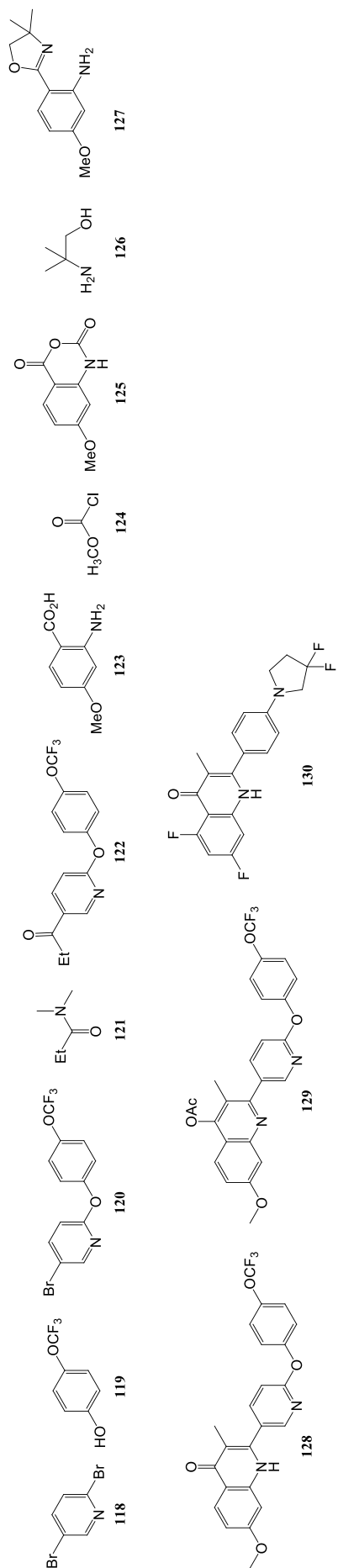
- Chapter four: Structural representation of quinolone derivatives evaluated for in vitro activity and by CLogP values; Structural representation of compound studied by docking simulations (93 – 117).



Appendix

## Appendix 1 - Chemical structures

- Chapter five: Structural representation of compounds **118** – **130** (mentioned in the section related to the synthesis of quinolones as potential antituberculosis agents).



Appendix

## Appendix 2 – Chemical characterization of compounds synthesized in this project and described in Chapter two.

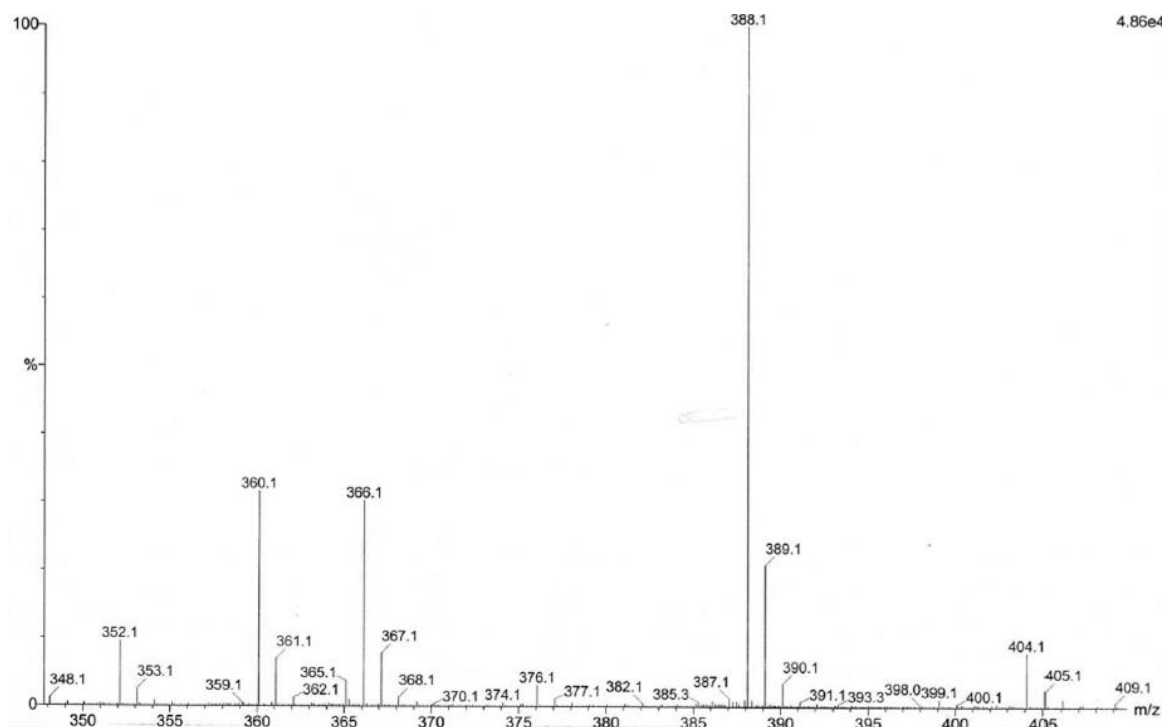


**Figure S1** – Mass spectrum of ethyl 7-benzoyloxy-4-oxo-quinoline-3-carboxylate (**13**).

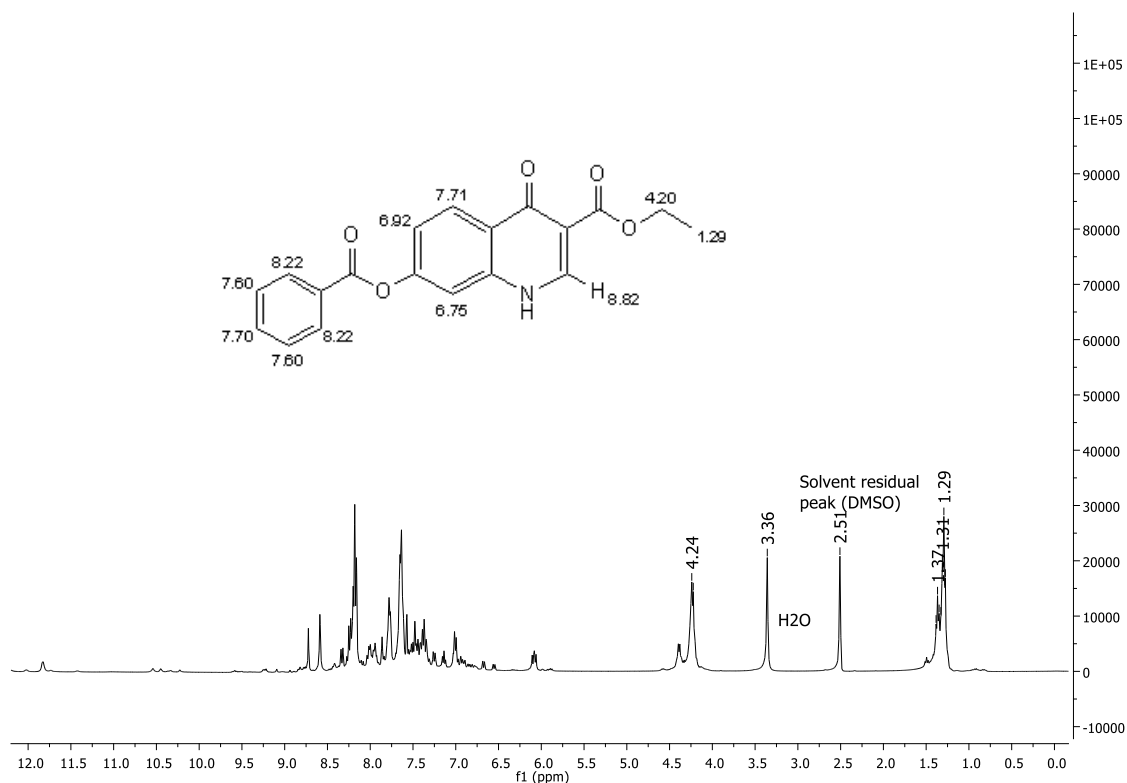


**Figure S2** –  $^1\text{H-NMR}$  spectrum of ethyl 7-benzoyloxy-4-oxo-quinoline-3-carboxylate (**13**) (400 MHz;  $\text{D}_6\text{-DMSO}$ ) and structural representation of the compound showing the chemical shifts (ppm) predicted for  $^1\text{H-NMR}$ , obtained using MestReNova software.

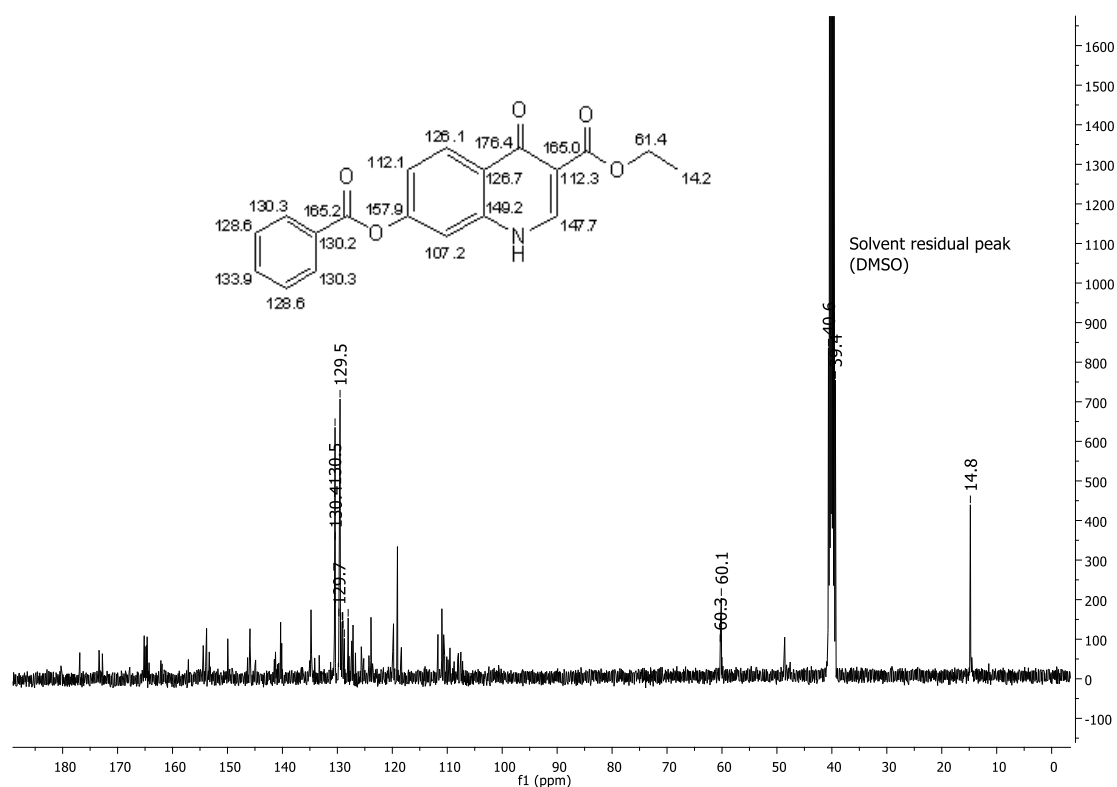


**Figure S3** –  $^{13}\text{C}$ -NMR spectrum of ethyl 7-benzoyloxy-4-oxo-quinoline-3-carboxylate (**13**) (101 MHz;  $\text{D}_6$ -DMSO) and structural representation of the compound showing the chemical shifts (ppm) predicted for  $^{13}\text{C}$ -NMR, obtained using MestReNova software.

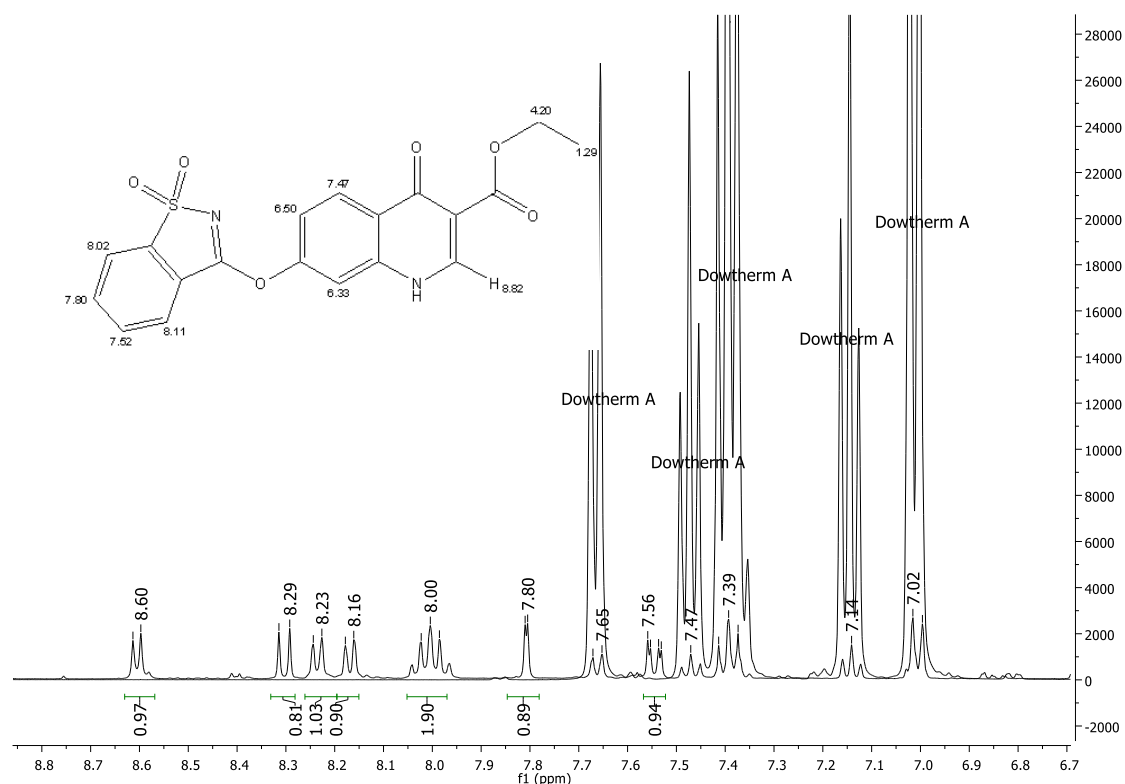


**Figure S4** –  $^1\text{H}$ -NMR spectra (range of chemical shifts for aromatic protons) of ethyl 7-benzothiazoloxo-4-oxo-quinoline-3-carboxylate (**31**) and Dowtherm A, superimposed (400 MHz;  $\text{D}_6$ -DMSO). Structural representation of **31** showing the chemical shifts (ppm) predicted for  $^1\text{H}$ -NMR, obtained using MestReNova software.

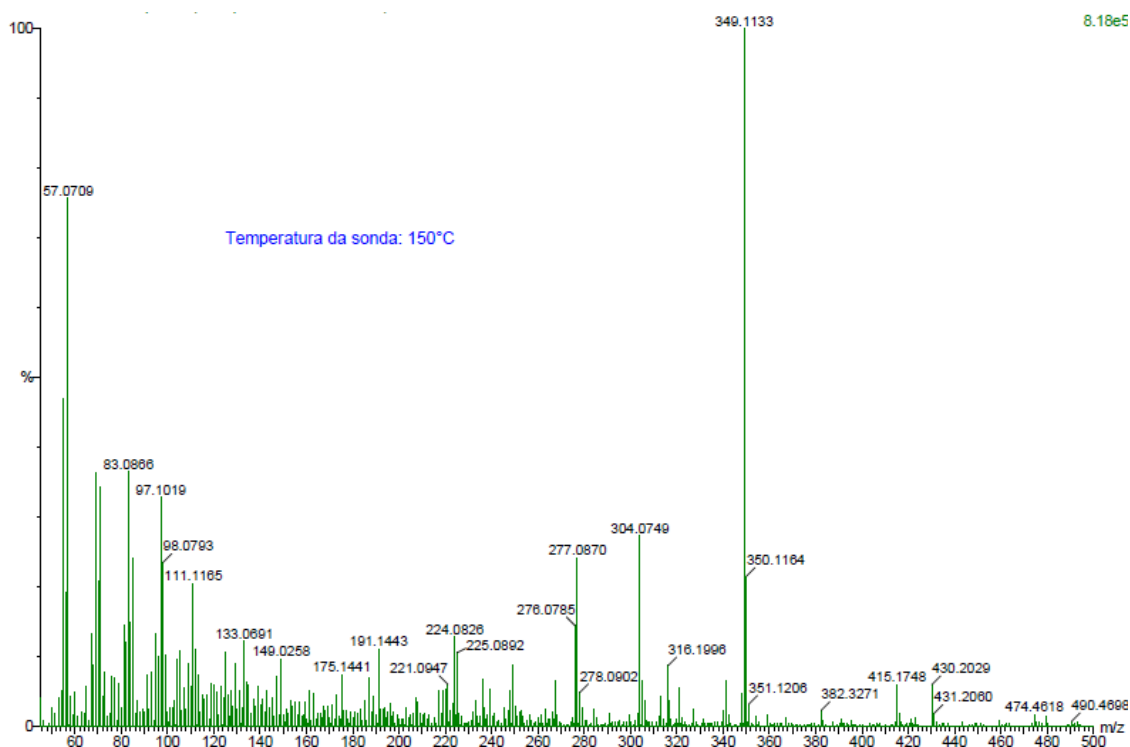


**Figure S5** – Mass spectrum (by EI) of ethyl 7-(1-phenyl-1H-diazirin-3-yl)oxy-4-oxo-quinoline-3-carboxylate (**32b**).

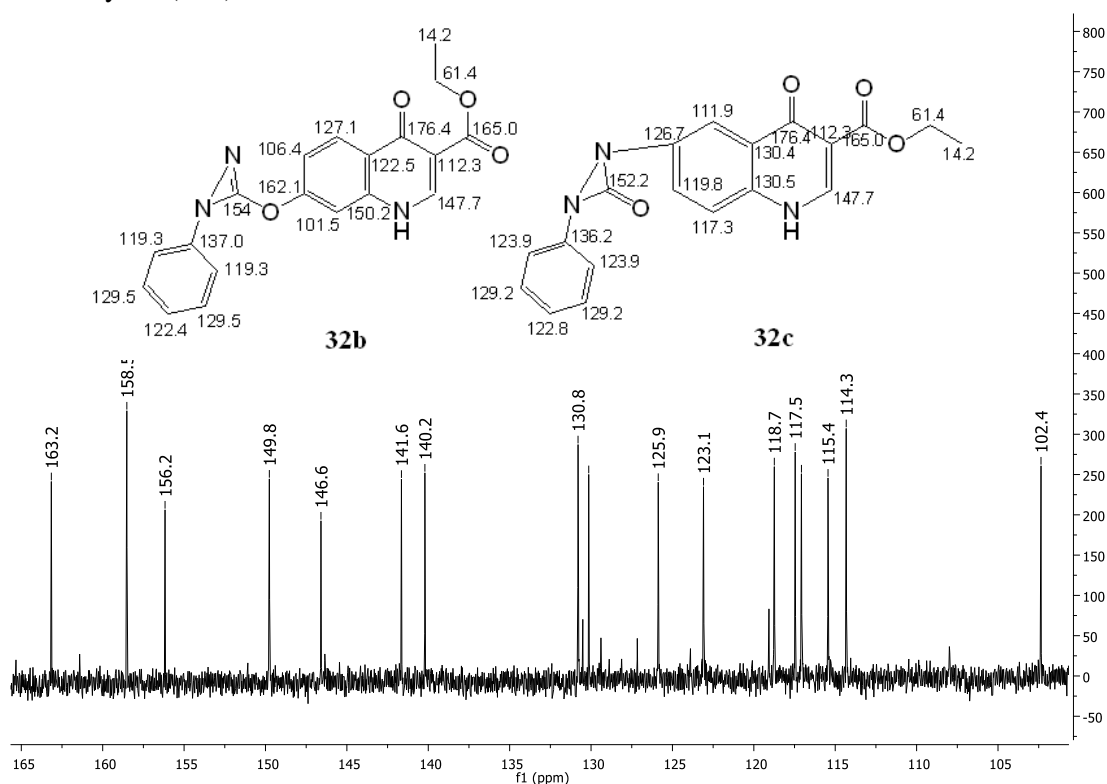


**Figure S6** –  $^{13}\text{C}$ -NMR spectrum (from 165 to 100 ppm) of ethyl 7-(1-phenyl-1H-diazirin-3-yl)oxy-4-oxo-quinoline-3-carboxylate (**32b**) (101 MHz;  $\text{D}_6$ -DMSO). Structural representations of **32b** and **32c** showing the chemical shifts (ppm) predicted for  $^{13}\text{C}$ -NMR, obtained using MestReNova software.

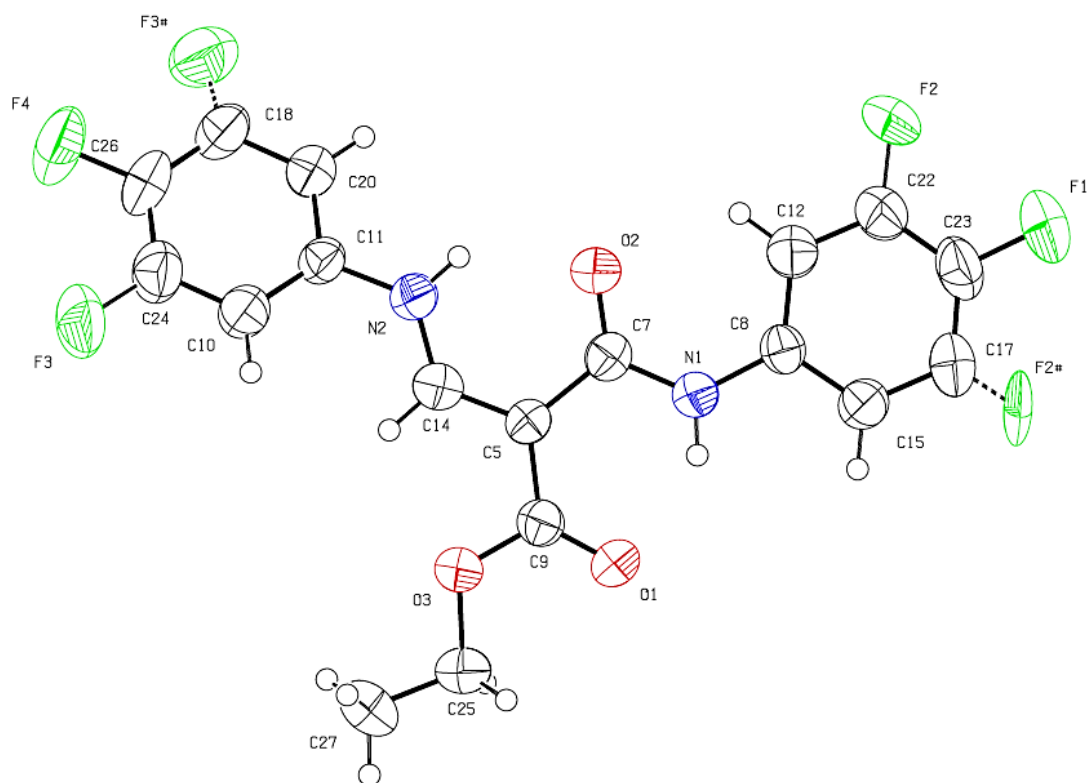


**Figure S7** – ORTEPII plot of ethyl 3-((3,4-difluorophenyl)amino)-2-((3,4-difluorophenyl)carbamoyl) acrylate (**44b**), in the crystal (from single crystal XRD data). Atoms F2# and F3# are, approximately, 20% of F2 and F3 atoms and 80% of H atoms. Fluorinated benzene rings have rotational through dihedrals C10-C11-N2-C14 and C7-N1-C8-C12.

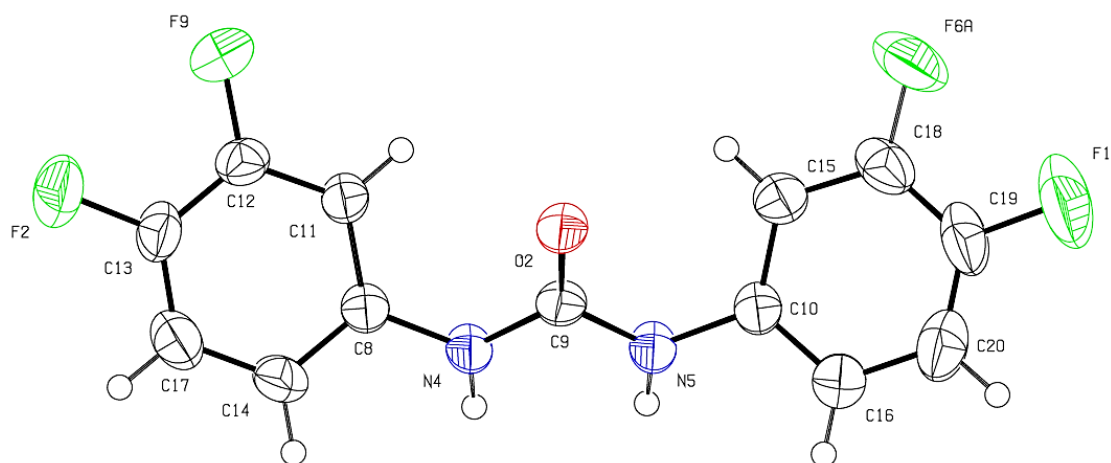


**Figure S8** – ORTEPII plot of 1,3-bis(3,4-difluorophenyl)urea (**44c**), in the crystal (from single crystal XRD data).



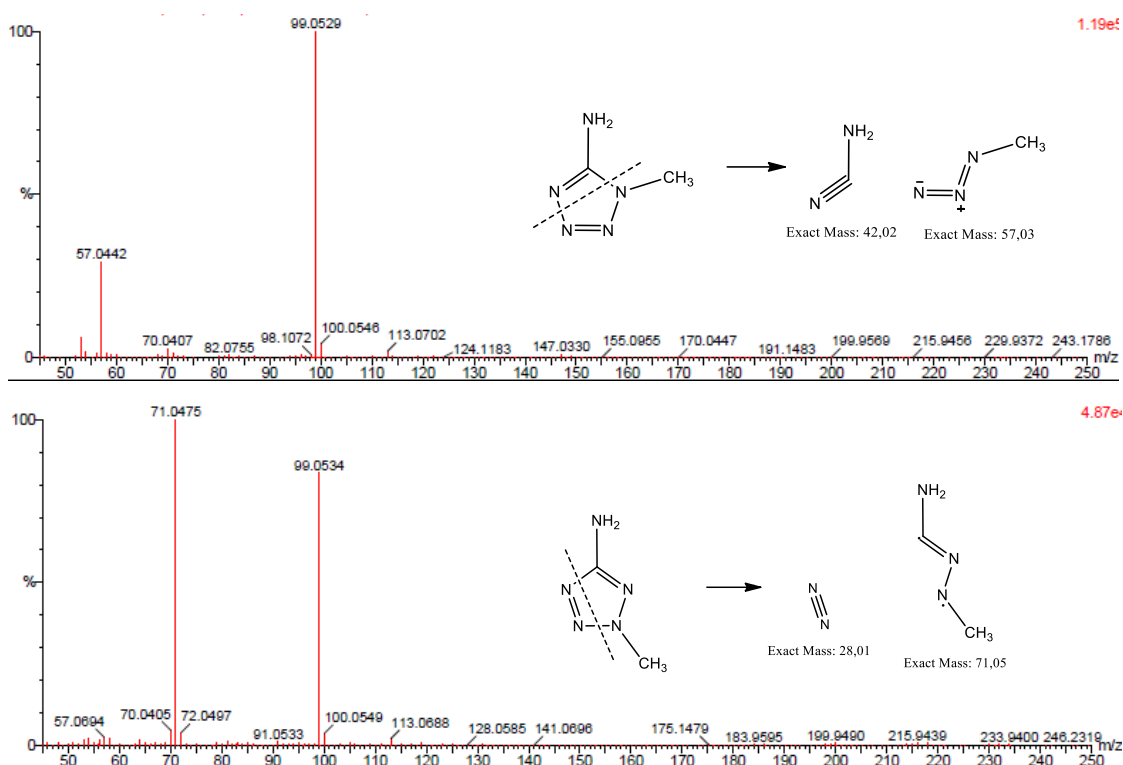


**Figure S9** – Mass spectra of 1-methyl-5-aminotetrazole (**52**) – *top frame* – and 2-methyl-5-aminotetrazole (**53**) – *bottom frame* – with a representation of the fragmentation patterns.

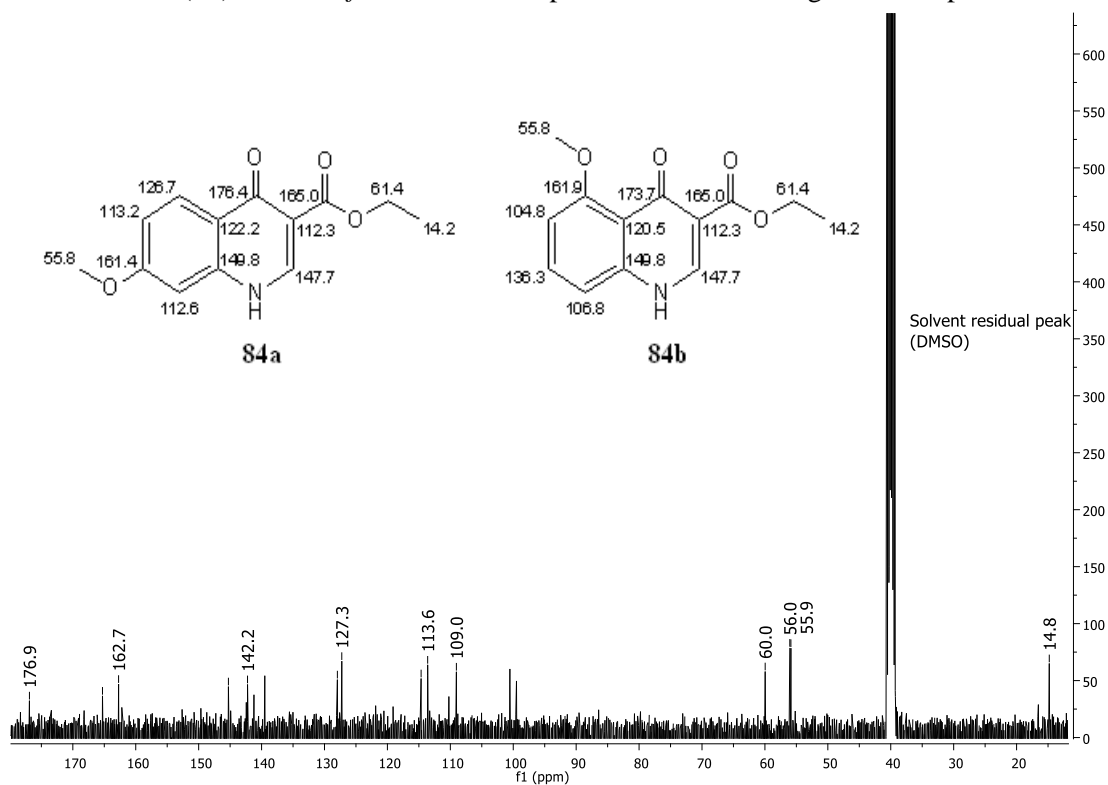


**Figure S10** – <sup>13</sup>C-NMR spectrum of the isomeric mixture of ethyl 7-methoxy-4-oxo-quinoline-3-carboxylate (**84a**) and ethyl 5-methoxy-4-oxo-quinoline-3-carboxylate (**84b**) (101 MHz; D<sub>6</sub>-DMSO). Structural representations of **84a** and **84b** showing the chemical shifts (ppm) predicted for <sup>13</sup>C-NMR, obtained using MestReNova software.

Appendix

**Appendix 3 – Structural investigation of selected quinolone derivatives, as discussed in Chapter three.**

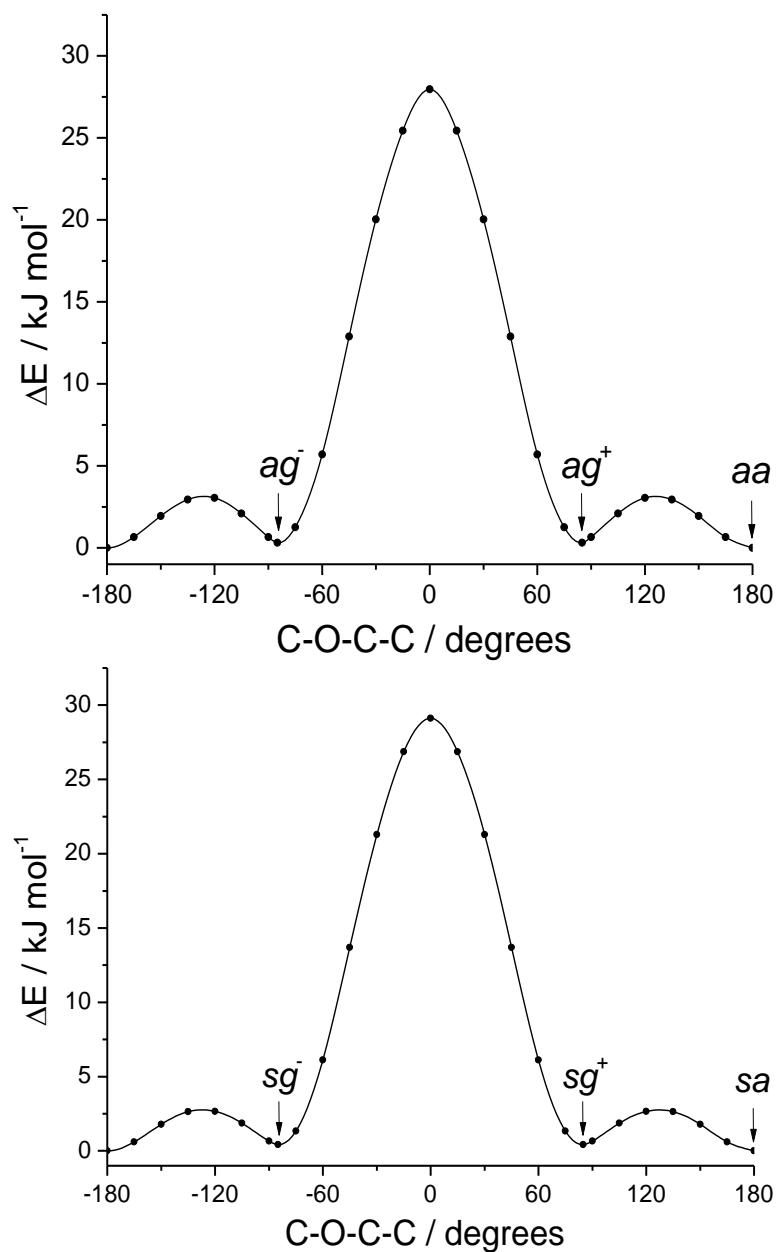


**Figure S11** - B3LYP/LANL2DZ+cc-pVDZ calculated relaxed potential energy profiles for internal rotation around the C–O ester bond of **56**, showing interconversion pathways between conformers **aa** and  $ag^\pm$  (*top*), and between **sa** and  $sg^\pm$  (*bottom*).

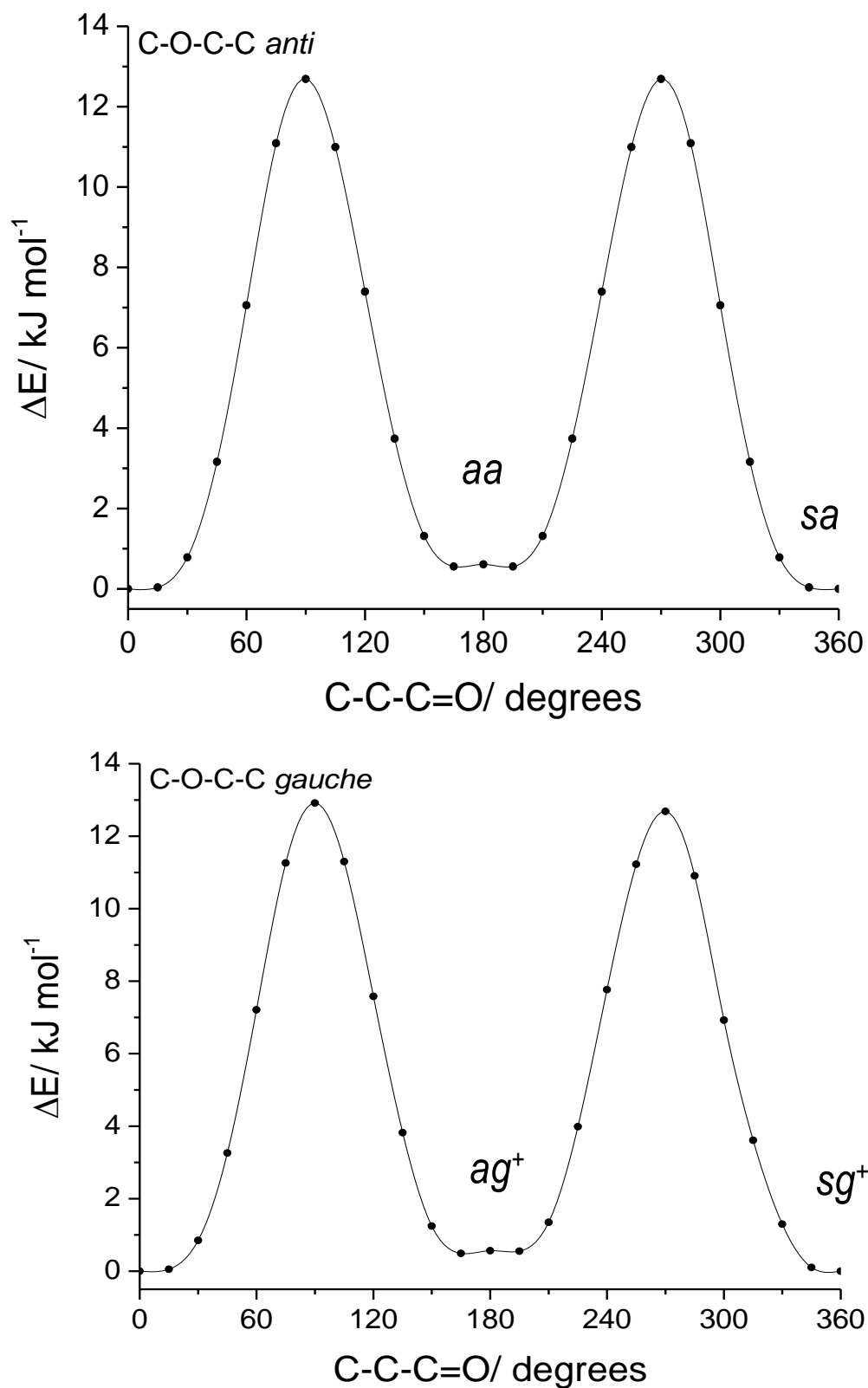


**Figure S12** - B3LYP/LANL2DZ+cc-pVDZ calculated relaxed potential energy profiles for internal rotation around the C–C bond connecting the ester substituent to the ring system of **56**, showing the interconversion pathways between conformers *aa* and *sa* (top), and between *ag*<sup>+</sup> and *sg*<sup>+</sup> (bottom). A similar potential energy profile to this latter exists for the interconversion between *ag*<sup>-</sup> and *sg*<sup>-</sup>.

**Table S1** - Assignment of the infrared spectra for matrix isolated **56** (15 K), as well as for the neat solid glassy state and crystalline compound. <sup>a</sup>

Approximate Description <sup>b</sup>	Experimental	Glass (43 K)	Crystal (17 K) <sup>c</sup>	Calculated							
	Ar matrix (15 K) v			<i>sa</i> v I <sup>IR</sup>		<i>aa</i> v I <sup>IR</sup>		<i>sg</i> v I <sup>IR</sup>		<i>ag</i> v I <sup>IR</sup>	
vCH <sub>2</sub> <i>s</i> Ph	3098.4	3097.4	3105.0	3157.2	1.1	3156.5	1.2	3157.6	1.1	3157.7	0.7
vCH Ph	3098.4	3097.4	3105.0	3153.0	0.3	3155.0	0.3	3154.3	0.3	3155.6	0.8
vCH <sub>2</sub> <i>as</i> Ph	3071.7	3068.8	3088.1	3140.0	1.2	3138.0	1.1	3141.1	1.2	3139.6	1.0
vCH Py	3071.7	3068.8	3088.1	3132.9	2.3	3119.6	0.5	3132.7	2.2	3118.3	0.5
vCH <sub>3</sub> <i>as</i> "	3003.4	2984.3						3074.2	21.5	3075.1	19.5
	2998.3	2984.3	2991.0	3057.9	31.3	3060.5	29.5				
vCH <sub>3</sub> <i>as</i> '	2991.8	2984.3	2980.3	3051.8	22.8	3052.8	23.1	3054.4	6.9	3055.0	5.8
vCH <sub>2</sub> <i>as</i>	2991.8	2984.3						3045.0	23.3	3046.0	23.4
	2967.4	2945.2	2938.8	3025.7	7.0	3028.4	6.9				
vCH <sub>2</sub> <i>s</i>	2950.8	2945.2						3007.0	32.1	3007.5	27.4
	2940.0	2932.4	2928.0	2985.8	18.5	2987.6	18.0				
vCH <sub>3</sub> <i>s</i>	2920.5	2908.9	2913.1	2975.1	17.2						
	2917.0	2908.9				2976.6	15.3	2973.8	17.8	2974.1	17.8
vC=O	1754.8/1749.0/1747.4	1743.8						1759.0	216.4		
	1753.4/1744.8/1740.7/1738.3	1732.7	1733.9/1727.8	1760.7	224.5					1733.4	270.2
	1732.6/1723.9/1720.2	1715.2				1734.7	280.2				
vC=C Ph	1602.1	1597.2				1603.8	151.9	1604.2	160.0	1604.0	152.9
	1595.8/1590.0	1591.5	1597.8/1590.1	1604.2	160.4						
vC=N Py	1599.6	1582.8				1596.6	63.2	1590.9	111.0	1596.3	66.4
	1581.4	1582.8	1584.4/1577.4	1590.9	107.5						
vC=C Ph	1551.8	1548.9	1552.0/1548.7	1551.2	59.7	1550.1	60.8	1551.1	59.4	1550.0	60.8
vC=C Py	1484.0	1479.8				1464.9	59.3			1464.9	55.3
	1471.3	1471.0	1466.1	1466.3	104.4			1465.9	114.6		
δCH <sub>2</sub>	1460.5	1471.0	1456.2	1459.8	13.7	1459.3	2.4				
	1455.7	1448.0						1447.6	7.2	1448.2	15.4
δCH <sub>3</sub> <i>as</i> '	1448.2	1438.5	1436.6	1438.3	6.9	1438.5	1.2	1429.5	13.1	1436.6	33.4
vCC Ph	1448.2	1438.5	1436.6	1437.3	3.3	1436.1	28.1	1437.1	8.6	1429.0	15.1
δCH <sub>3</sub> <i>as</i> "	1438.9	n.obs	1430.7	1424.8	6.3	1424.5	6.5	1424.8	10.6	1424.4	11.4
vC=C Ph	1401.4	1395.0				1399.8	88.3			1398.7	87.7
	1397.1	1389.7	1391.0	1396.7	15.2			1396.4	15.8		
δCH <sub>3</sub> <i>s</i>	1387.8	1389.7	1385.0	1383.7	3.6	1383.6	8.7				
	1383.6	1389.7						1380.3	10.0	1379.3	4.8

δCH Ph	1374.1	1372.2	1372.0/1370.0	1365.1	53.4			1363.6	43.6		
	1371.4	1372.2				1360.1	3.1			1358.7	12.6
	1361.5	1359.9				1351.3	68.0	1350.4	13.6	1353.3	54.1
wCH <sub>2</sub>	1359.7	1359.9	1357.2/1353.8	1345.7	20.4						
δCH Py	1340.9	1339.2	1337.9	1335.5	39.1			1335.7	45.2		
	1337.0	1321.7				1329.2	10.5			1329.6	14.0
νCC Py	1322.4	1321.7				1314.9	280.2			1317.1	248.4
	1297.8	1299.6	1302.3/1291.1	1298.7	15.1			1300.5	14.7		
tw CH <sub>2</sub>	1287.9	1299.6						1292.2	15.3	1290.7	15.4
νC-O	1270.3	1282.8				1259.6	305.7			1258.1	253.8
tw CH <sub>2</sub>	n.obs.	n.obs.	n.obs.	1252.6	1.1	1253.1	1.1				
δCH Ph	1266.7	1271.3	1271.7/1262.6	1248.5	321.3			1249.5	267.3		
δCH <sub>2</sub> Ph	1235.8	1232.0 <sup>d</sup>	1228.2/1217.1	1221.1	208.9			1220.8	172.6		
	1232.1					1218.4	154.4			1216.8	149.6
δCH <sub>2</sub> Ph	1206.5					1205.1	3.0			1204.9	14.4
νC-O	1201.6/1195.5	1199.1	1197.9	1191.8	240.6						
	1196.0/1192.3	1199.1						1189.6	202.3		
γCH <sub>2</sub>	1164.7	1174.2						1164.0	127.5	1161.9	65.7
δCH <sub>2</sub> Ph	1163.0	1162.7 <sup>d</sup>	1165.8	1156.8	184.5						
	1157.9					1150.1	118.8	1146.7	66.5	1144.8	49.1
γCH <sub>2</sub>	1143.4	1160.1	1161.2	1139.6	4.0	1138.6	4.5				
νCC Ph	1140.0	1135.1 <sup>d</sup>	1142.2	1137.9	16.4						
	1129.0					1132.5	95.7	1133.3	76.1		
	1119.6									1129.1	149.2
νC-CH <sub>3</sub>	1117.6	1116.5	1118.2	1104.5	20.9	1106.4	21.7				
	1097.4	1095.9						1086.0	35.7	1085.7	17.7
νCC Ph	1058.2	1059.7	1063.8	1048.6	29.4	1048.3	22.1	1049.2	27.1	1048.5	22.5
νO-C	1042.5	1033.7 <sup>d</sup>	1034.3	1036.3	93.5						
	1040.7							1031.2	80.4		
	1031.6					1024.3	54.0				
	1025.4									1018.7	37.0
δring Py	1011.7	1009.8	1012.8	992.2	35.2	994.0	11.3				
	999.9	1009.8						982.0	31.4	982.8	15.7
γCH <sub>2</sub> <i>as</i> Ph	963.1	998.5	1005.8	969.9	0.6	971.2	3.9	969.7	0.6	969.4	3.5
γCH Py	951.0	998.5				965.0	0.6			963.9	1.7
	949.1	944.6	940.4	953.9	3.5			954.4	3.5		
νC-C(=O)	921.6	922.4	922.4	908.1	42.3						

$\gamma$ CH Ph	917.9	915.8	917.0	904.9	5.9	905.7	6.2	905.5	5.8	905.8	6.1
$\nu$ C-C(=O)	911.1	910.0				900.9	40.5				
	889.0	885.8						896.7	49.4	895.9	40.8
$\gamma$ CH <sub>3</sub> '	872.0	885.8				866.2	9.2				
	857.8	854.6	856.0	861.1	0.5						
	855.2	846.9						853.3	1.7	856.9	9.4
$\nu$ C-Cl	819.7	825.0	838.4/824.6	836.9	48.9			836.6	47.5		
	817.1	819.5/816.2				835.7	52.9			835.6	52.4
$\gamma$ CH <sub>2</sub> <i>s</i> Ph	811.9	812.8	812.8	831.0	10.4	829.1	10.7	830.8	10.4	828.9	10.6
$\delta$ OCC	790.0	785.5	790.8	799.6	57.8	805.3	38.8	809.2	30.5	813.7	22.5
$\gamma$ CH <sub>3</sub> "	783.9	774.5	788.7	792.2	7.9	792.8	3.8				
$\tau$ ring Ph	776.0	759.7	760.1	786.3	11.6	785.7	16.0	789.1	18.5	787.5	19.9
$\tau$ ring Ph	760.0	755.9						759.1	17.3	760.9	18.4
$\gamma$ C=O		755.9	741.5	756.9	3.9	757.6	4.5	756.8	9.1	758.3	4.3
$\delta$ ring Py	699.2	698.3				691.4	30.4			688.5	27.5
	691.7	689.5	689.4	683.3	23.6			683.5	22.9		
$\delta$ ring Ph	634.1	635.1	635.1	632.8	3.2	634.5	3.5	633.3	2.9	635.4	3.3
$\nu$ C-I	n. obs.	631.5	631.5	621.2	2.7	627.6	2.1	622.6	3.4	627.1	1.6
$\gamma$ CCl	595.6	593.5	593.4/589.5	596.3	1.8	595.0	1.8	596.4	2.2	595.7	2.3
$\delta$ CC=O	573.6	n.obs.	579.3	567.4	7.6			564.9	7.9		
	567.0	n.obs.				556.9	2.7			557.6	2.2
$\delta$ CCl	532.0	534.6	534.6	527.0	5.0	525.5	4.2	525.4	4.6	526.2	3.7

<sup>a</sup> Wavenumbers ( $\nu$ ) in  $\text{cm}^{-1}$ ; calculated intensities ( $I^{\text{IR}}$ ) in  $\text{km mol}^{-1}$ ; the calculated wavenumbers were scaled by 0.978. <sup>b</sup>  $\nu$ , stretching;  $\delta$ , bending;  $\gamma$ , rocking;  $w$ , wagging;  $tw$ , twisting;  $\tau$ , torsion; Py, pyridine ring; Ph, Phenyl ring;  $s$ , symmetric;  $as$ , anti-symmetric. <sup>c</sup> Assignments refer to the  $sa$  conformer, which constitutes the molecular unit in the crystal. <sup>d</sup> Bands observed for the glassy phase at 1232.0, 1162.7, 1135.1 and 1033.7  $\text{cm}^{-1}$  exhibit very broad profiles and shall correspond to superposition of several bands belonging to different conformers present in this phase (in the Table the frequencies of these bands are presented in the first row of the set of rows to which they correspond, to avoid extensive repetition).

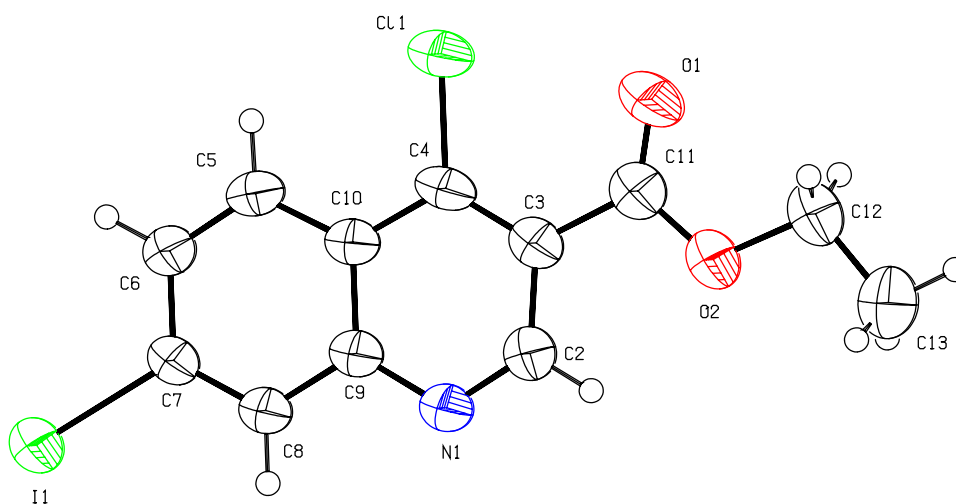


**Figure S13** - ORTEP drawing of **56**, showing the atom numbering scheme. Ellipsoids were drawn at the 50% probability level.

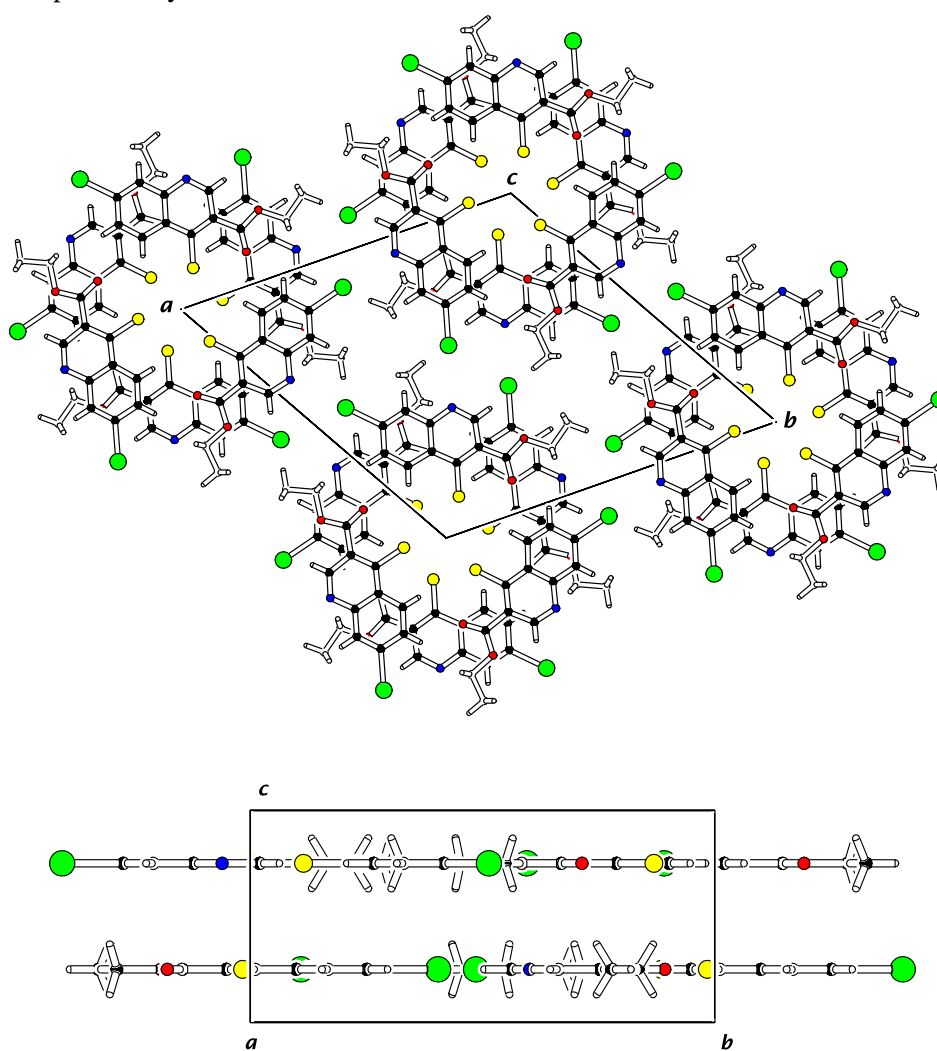


**Figure S14** - Projection of the crystal structure along the c-axis, showing the molecular packing diagram (*top*), and along the a-axis (*bottom*), highlighting the layered nature of the molecular packing.



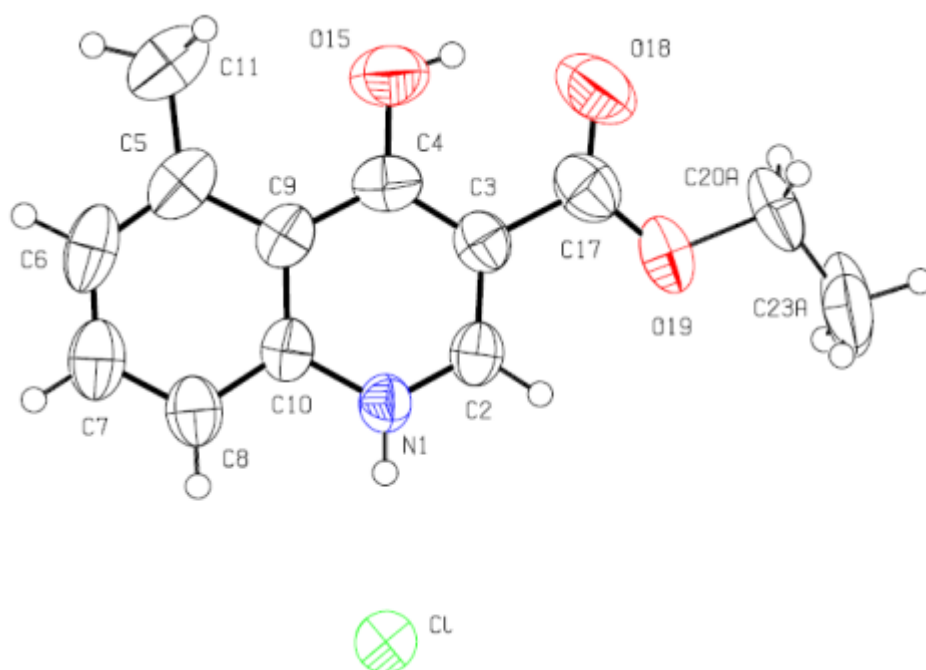


**Figure S15** - ORTEP plot of ethyl 4-hydroxy-5-methyl quinolinium chloride 3-carboxylate (**82b·HCl**) in the crystal of the compound, showing the anisotropic displacement ellipsoids drawn at the 50% probability level. For clarity, only the major component of the disordered ethyl group is shown.

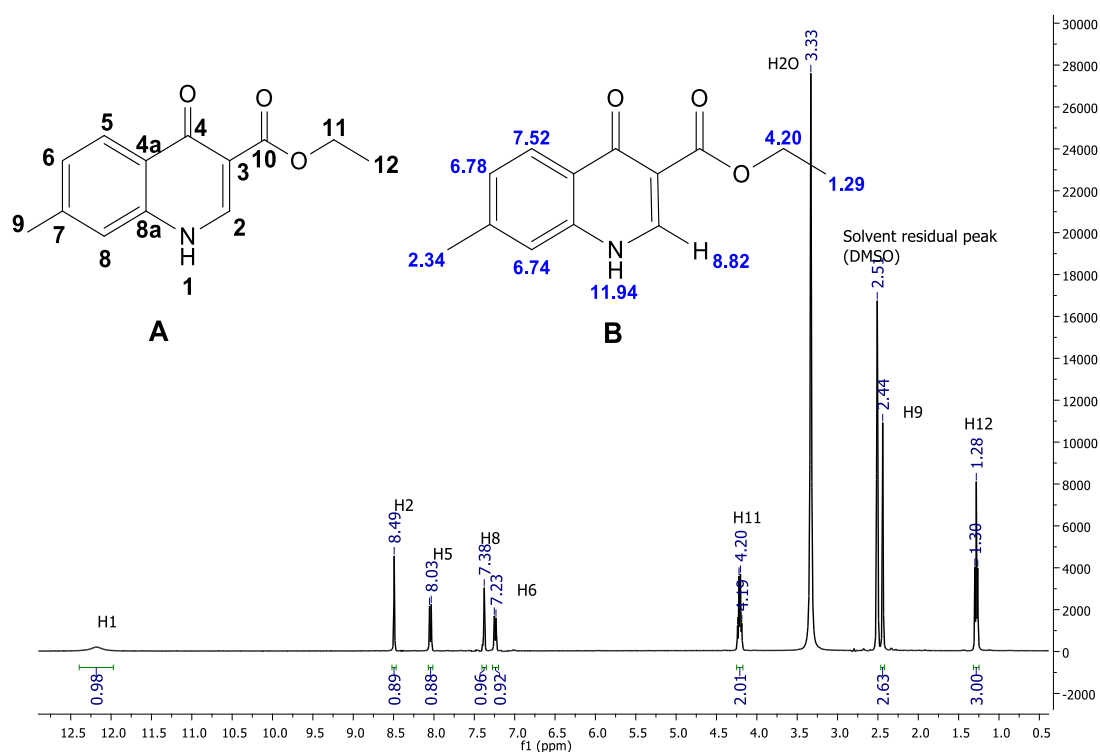


**Figure S16** -  $^1\text{H-NMR}$  spectrum of ethyl 7-methyl-4-oxo-quinoline-3-carboxylate (**82a**) (400 MHz;  $\text{D}_6\text{-DMSO}$ ). Atoms identification (A) and predicted chemical shifts (ppm) for  $^1\text{H-NMR}$  (B), obtained using MestReNova software and considering the literature,<sup>205</sup> are shown.

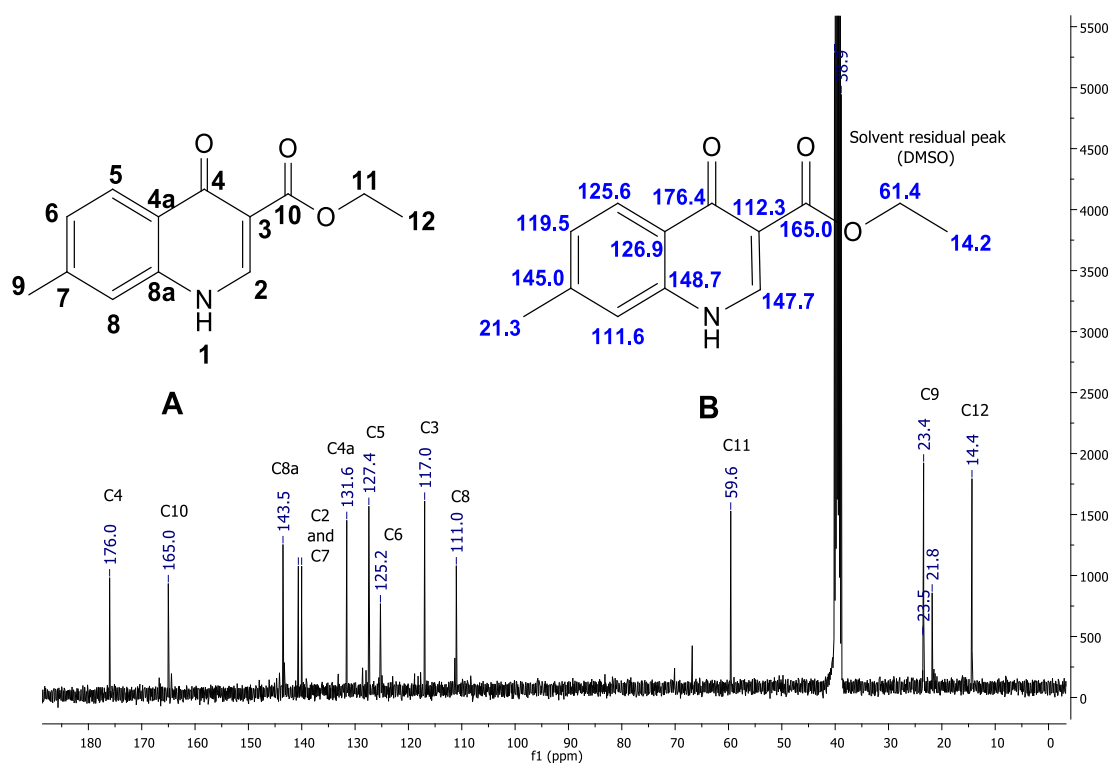


**Figure S17** -  $^{13}\text{C}$ -NMR spectrum of ethyl 7-methyl-4-oxo-quinoline-3-carboxylate (**82a**) (101 MHz;  $\text{D}_6$ -DMSO). Atoms identification (A) and predicted chemical shifts (ppm) for  $^{13}\text{C}$ -NMR (B), obtained using MestReNova software, are shown.

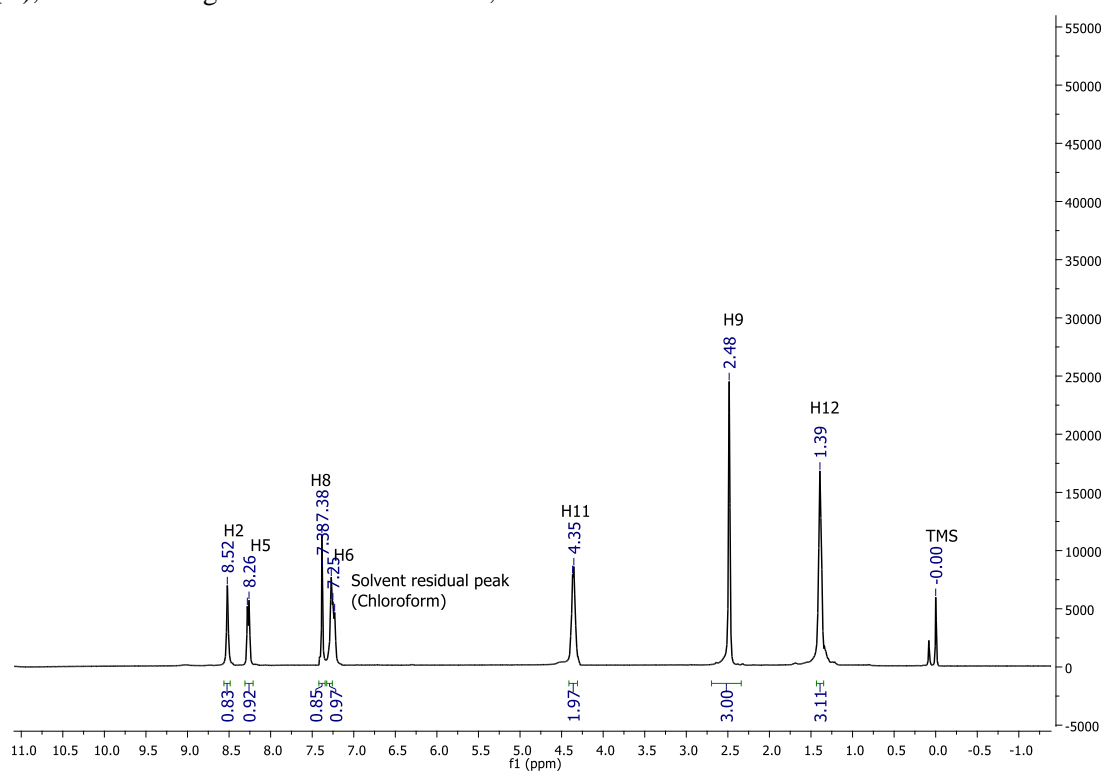


**Figure S18** -  $^1\text{H}$ -NMR spectrum of ethyl 7-methyl-4-oxo-quinoline-3-carboxylate (**82a**) (400 MHz;  $\text{D}$ -Chloroform). H1 was observed around 12.20, but after calibration by TMS it was not possible to show this peak.

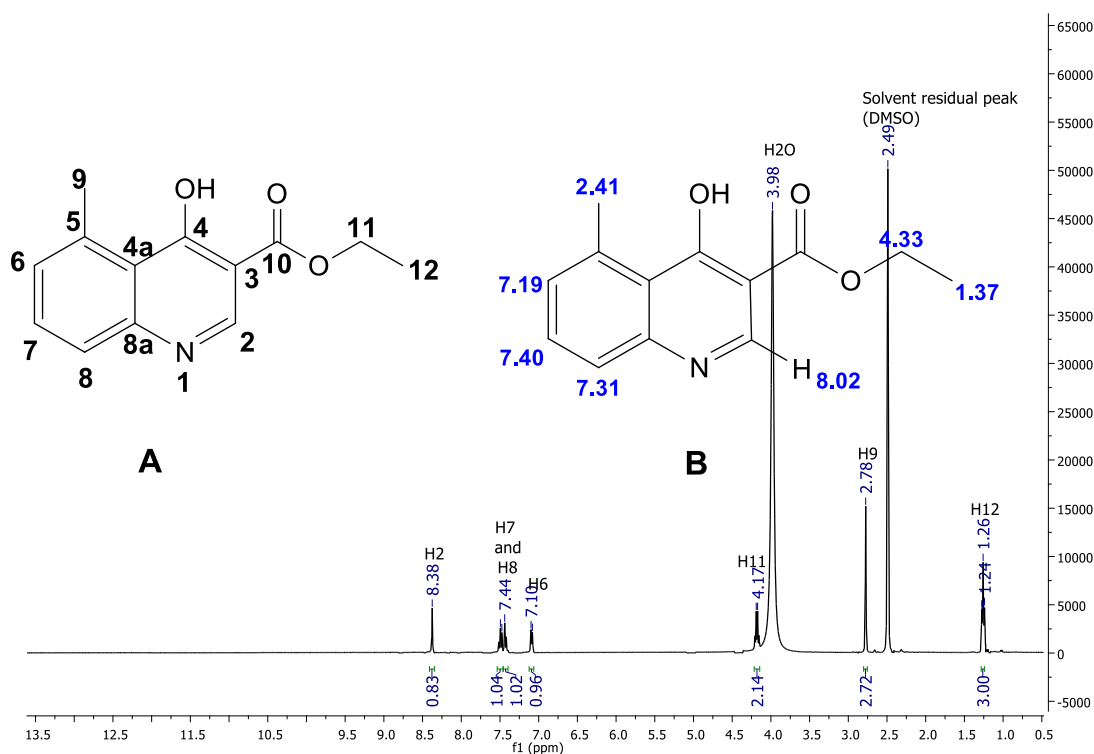


**Figure S19** -  $^1\text{H-NMR}$  spectrum of ethyl 4-hydroxy-5-methylquinoline-3-carboxylate (**82b**) (400 MHz;  $\text{D}_6\text{-DMSO}$ ). Atoms identification (A) and predicted chemical shifts (ppm) for  $^1\text{H-NMR}$  (B), obtained using MestReNova software and considering the literature, are shown.<sup>205</sup>

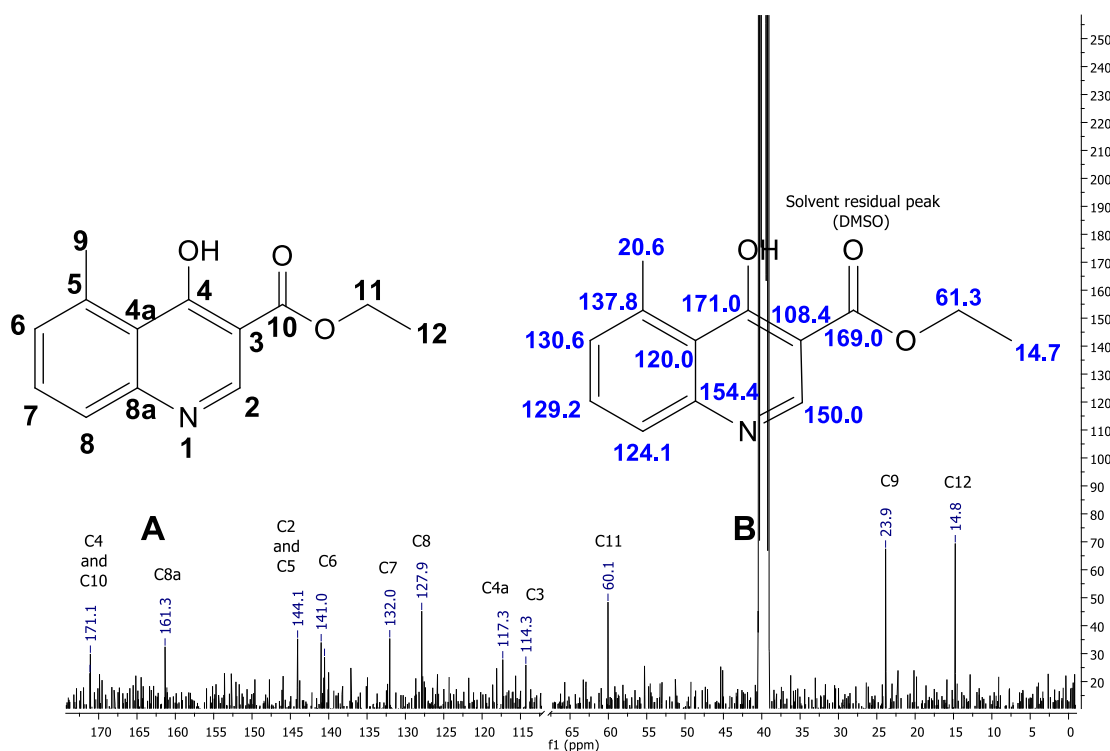


**Figure S20** -  $^{13}\text{C-NMR}$  spectrum of ethyl 4-hydroxy-5-methylquinoline-3-carboxylate (**82b**) (101 MHz;  $\text{D}_6\text{-DMSO}$ ). Atoms identification (A) and predicted chemical shifts (ppm) for  $^{13}\text{C-NMR}$  (B), obtained using MestReNova software, are shown.

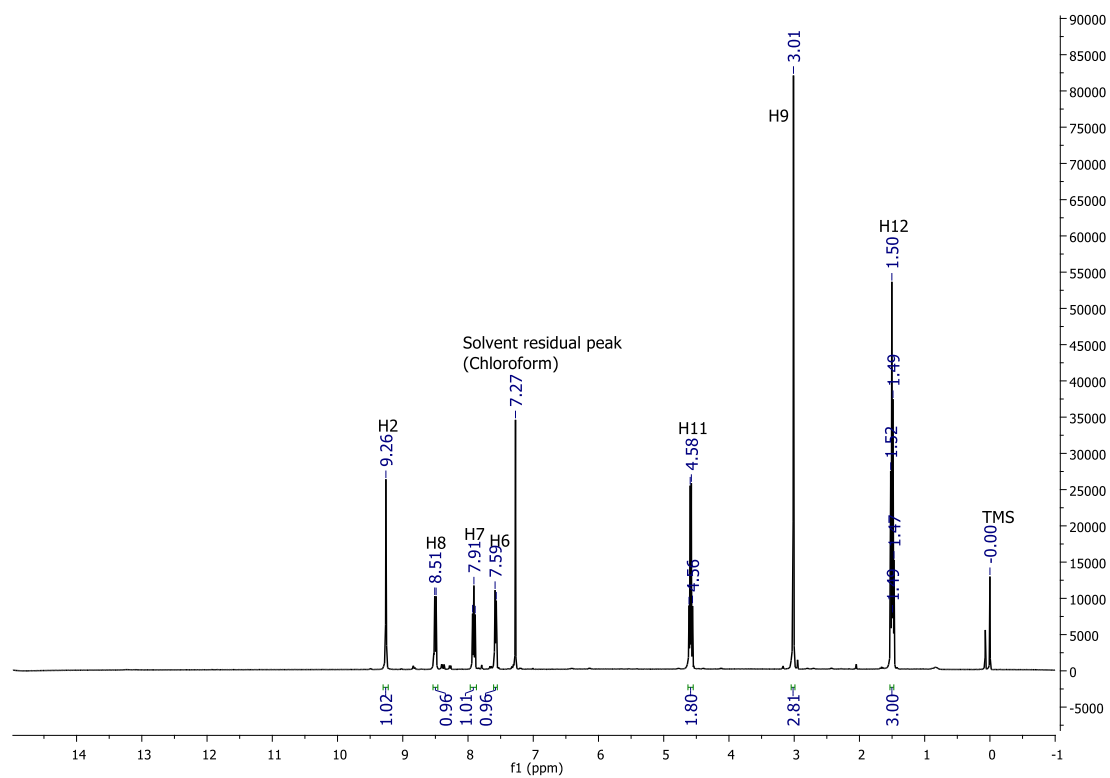


**Figure S21** - <sup>1</sup>H-NMR spectrum of ethyl 4-hydroxy-5-methylquinoline-3-carboxylate (**82b**) (400 MHz; D-Chloroform).

**Table S2** - Observed IR frequencies for **82b** in argon matrix (15 K) and B3LYP/6-311++G(d,p) calculated frequencies and IR intensities for conformers **82bI** and **82bII**. <sup>a</sup>

Observed (Ar matrix; 15 K)	Conformer I		Conformer II		Approximate Description <sup>b</sup>
	$\nu$	$I^{\text{IR}}$	$\nu$	$I^{\text{IR}}$	
<i>b</i>	3208	555	3209	560	vOH
3068	3132	8	3132	8	vCH $r_1$
3040	3109	19	3109	19	vCH $r_1$
3032	3100	4	3101	4	vCH $r_2$
	3094	9	3094	8	vCH $r_1$
2994	3051	34	3068	18	vCH <sub>3</sub> <i>as</i> et
	3043	23	3043	3	vCH <sub>3</sub> <i>as</i>
	3037	25	3043	28	vCH <sub>3</sub> <i>as</i> et
	3035	10	3035	10	vCH <sub>3</sub> <i>as</i>
	3026	1	3033	31	vCH <sub>2</sub> <i>as</i>
2943	2991	14	3010	23	vCH <sub>2</sub> <i>s</i>
	2977	22	2977	23	vCH <sub>3</sub> <i>s</i>
	2972	17	2970	18	vCH <sub>3</sub> <i>s</i> et
1669/ 1665	1651	337	1650	321	vC=O
1624/ 1616	1611	282	1611	289	vCC $r_2$ , $\delta$ COH
1607	1606	12	1606	6	vCC $r_1$
1596/ 1583/ 1573	1574	99	1574	97	vCC $r_1, r_2$
1504/ 1498	1496	84	1495	81	vCC $r_1, r_2$
1482	1485	6	1473	23	$\delta$ CH <sub>2</sub>
1468	1465	3	1465	19	$\delta$ CH <sub>3</sub> <i>as</i> et
	1465	17	1459	11	$\delta$ CH <sub>3</sub> <i>as</i>
1458	1453	8	1455	11	$\delta$ CH <sub>3</sub> <i>as</i> et
1451/ 1448	1450	8	1450	8	$\delta$ CH <sub>3</sub> <i>as</i>
1441	1443	31	1442	28	vCC $r_1, r_2$ , $\delta$ CH $r_1$
1427/ 1422	1424	68	1423	72	$\delta$ COH
1411	1406	25	1405	20	$\delta$ CH $r_2$
1406/ 1401	1400	73	1395	85	wCH <sub>2</sub>
1396	1392	12	1391	11	$\delta$ CH <sub>3</sub> <i>s</i>
1387/ 1382	1378	154	1377	140	$\delta$ CH <sub>3</sub> <i>s</i> et
	1370	26	1370	24	$\delta$ CH $r_1$
1357/ 1349	1348	149	1349	162	vCC $r_2$ , wCH <sub>2</sub>
1330/ 1320	1309	83	1310	76	vCC $r_1, r_2$
1283/ 1277	1271	424	1303	10	vCC(=O), $\delta$ CH $r_2$
	1269	1	1271	354	twCH <sub>2</sub>
1245	1258	16	1257	12	$\delta$ CH $r_1$
1229	1221	16	1219	8	vCC(H <sub>3</sub> ), vCC $r_2$
1208	1206	287	1204	269	vCN, vC-O
1162	1157	93	1169	43	$\delta$ CH $r_1$
1151	1149	4	1155	53	$\gamma$ CH <sub>3</sub> et, $\gamma$ CH <sub>2</sub>
1136/ 1132	1133	97	1125	124	vCC(=O), vC-O(H)
1117/ 1115/ 1108/ 1099	1107	13	1089	33	$\gamma$ CH <sub>3</sub> et
1085	1083	3	1081	2	vCC $r_1$ , $\gamma$ CH <sub>3</sub>
1041	1038	2	1038	2	$\gamma$ CH <sub>3</sub>
1040	1034	13	1034	13	$\gamma$ CH <sub>3</sub>
1031/ 1027/ 1021/ 1010	1013	89	1004	74	vCC et
n.obs.	978	1	979	1	$\gamma$ CH $r_1$
977/ 974	968	22	965	21	vCC $r_1$ , $\gamma$ CH <sub>3</sub>
950/ 949	941	7	943	7	$\gamma$ CH $r_2$
932	923	17	909	16	$\delta r_1, r_2$
899	896	0.3	897	0.3	$\gamma$ CH $r_1$
869	858	2	849	1	vOC et
842/ 839	825	108	828	105	$\tau$ OH
823	814	32	817	24	$\delta r_2$
813/ 810	806	12	807	15	$\gamma$ CH $r_1$
807	796	0.4	803	5	$\delta r_2$
804	795	5	782	16	$\gamma$ CH <sub>2</sub>
789	780	14	761	5	$\gamma$ CH $r_1$
769	754	12	754	12	vCC(=O)

## Appendix

676	}	670	0.1	670	0.2	$\delta_{r_1, r_2}$
		666	1	667	1	$\tau_{r_1}$
613		621	1	622	1	$\tau_{r_1}$
595		604	2	601	3	$\delta_{r_2}$
575		563	0.4	564	0.1	$\delta_{r_2}$
526		522	2	521	2	$\delta_{r_1}$
n.obs.		489	0.1	490	0.2	$\tau_{r_1}$
489		484	2	483	3	wC(CH <sub>3</sub> )
	}	472	1	476	1	$\tau_{r_1, r_2}$
		453	2	458	12	wC(C=O)O
		401	34	404	4	$\delta_{CC=O}$
		360	1	387	30	$\delta_{CCO}$
		334	1	356	0.1	$\delta_{CCC}$ et
		283	7	307	5	$\gamma_{C=O}$ , $\tau_{CH_3}$ et
		277	6	271	4	$\delta_{COC}$
		255	3	255	3	$\tau_{r_1, r_2}$ (butterfly)
n.i.		247	0.3	249	0.4	$\tau_{CH_3}$ et
		223	1	225	1	$\tau_{CH_3}$
		213	2	220	2	$\delta_{OCC}$ et
		192	0.04	190	0.03	$\tau_{r_1, r_2}$
		119	1	136	2	$\tau_{C-O}$
		113	0.1	113	0.1	$\tau_{C-O}$ et
		93	1	95	0.1	$\delta_{COC}$ , $\delta_{OCC}$ et
		71	0.2	73	0.2	$\tau_{r_2}$
		57	2	43	0.2	$\gamma_{C(C=O)O}$
		16	0.4	41	2	$\tau_{O-C}$ et

<sup>a</sup> Wavenumbers ( $\nu$ ) in  $\text{cm}^{-1}$ ; IR intensities ( $I^{\text{IR}}$ ) in  $\text{km mol}^{-1}$ . <sup>b</sup> Assignments and approximate descriptions are specific for conformer **I**;  $\nu$ , stretching;  $\delta$ , in-plane-bending;  $\gamma$ , out-of-plane rocking;  $\tau$ , torsion; w, wagging; tw, twisting;  $r_1$  and  $r_2$  refers to the benzene and heteroaromatic ring, respectively; et, ethyl group; *s*, symmetric; *as*, anti-symmetric; n.obs., non-observed; n.i., not investigated. <sup>b</sup> As it is common when the molecule contains a very strong intramolecular H-bond, the  $\nu\text{OH}$  band is very broad and difficult to distinguish from the baseline. Moreover, in the present case the spectral region when it is expected to occur is quite congested due to the presence of the bands due to the CH stretching modes and also those due to the stretching vibration of the co-deposited H-Cl (see experimental description). Under these circumstances, we let opened to investigation the precise assignment of this vibration.

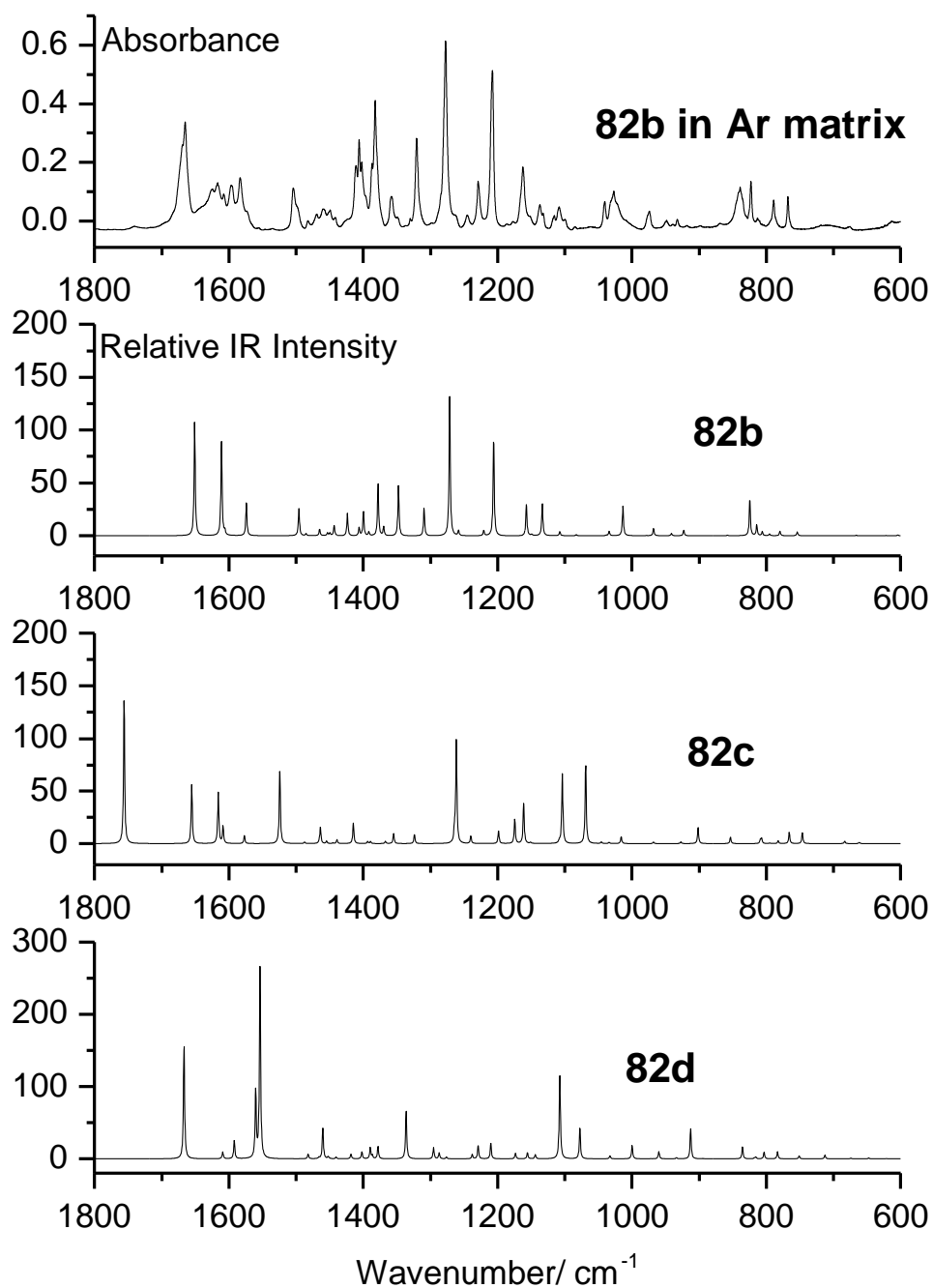


**Figure S22** - Comparison of the B3LYP/6-311++G(d,p) calculated IR spectra of the most stable conformers of **82b**, **82c** and **82d**, with the experimental IR spectrum of compound **82b**, obtained in argon matrix (15 K).